INVESTIGATING THE RELATIVE ADSORPTION OF POLYMERIC DEPRESSANTS ON PURE MINERALS

Sabatha Sanele Mhlanga

A thesis submitted to the Faculty of Engineering and the Built Environment at the University of Cape Town in fulfilment of the requirements for the degree of Master of Science in Chemical Engineering

DECLARATION

I declare that this thesis submitted for the degree of Master of Science in Chemical Engineering at the University of Cape Town is my own work and has not been submitted prior to this for any degree at this university or any other institution. I know the meaning of plagiarism and declare that all the work in the document except for that, which is properly acknowledged, is my own.

…….

Sabatha Sanele Mhlanga

ACKNOWLEDGEMENTS

I would like to acknowledge the following people who made it possible for me to complete this project:

- My supervisors, Dr. Belinda McFadzean and Professor Cyril O'Connor for their invaluable insights and guidance throughout this project. Dr. McFadzean for her constant support and encouragement through the challenging times in the course of project; and Prof. O'Connor whose leadership, humility and affirmation was inspiring.
- The Centre for Minerals Research (CMR), UCT, for funding this project
- Senmin for providing the depressants used in this study.
- Anglo American Research for providing some of the ore samples used in this study.
- Mrs. Christel Tiguely of the Geology Department, UCT, and Dr. Megan Becker for their assistance with microprobe experiments.
- Dr. Kirsten Corin for her assistance with XRD experiments.
- Mrs Jenny Wiese for her assistance in getting all the equipment that was needed to conduct all the experimental work.
- All the students and staff in the Centre for Minerals Research for the fruitful discussions during our Friday seminars, student research days and weekends away in Hermanus.
- Dr. Tshepo Maboke, Dr. Vuyo Soldati, Mr. Ntsabelo Ntsaluba, Mr. Patrick Kayongo, Mr. Lutho Sotashe, Mr. Samkelo Freemantle, Mr. Richard Migwalla and Mr. Monatumelo Mannya – you gentlemen are legends.
- My mentor, Mr. David Beattie
- My church His People Church-Baxter whose ethos of loving God, loving people and transforming society has been the biggest motivation in seeing this project through
- My family for their constant unconditional love, support and encouragement. To my mum and dad whose great example I follow.

- Finally, all glory and praise to God almighty whose amazing grace continues to lead me.

SYNOPSIS

The aim of this study was to investigate the relative adsorption of polymeric depressants on pure minerals. The minerals used were talc, pyroxene, plagioclase, chromite and chalcopyrite and the depressants used were guar gum and carboxymethyl cellulose (CMC). It was hypothesised at the beginning of this study that polymeric depressants adsorb preferentially onto different minerals because of the differences in the surface charge of the minerals which arise as a result of their different chemical structures. Zeta potential measurements were conducted to establish exactly what these differences in surface charge were and what role metal ions in solution played in modifying the mineral surface charge and therefore changing the adsorption characteristics.

Generally, the surface charge of each mineral became increasingly negative as pH increased in a buffered solution. At pH 9, plagioclase had the most negative surface charge, followed by talc, chromite and pyroxene whose surface charges were very similar at this pH. Chalcopyrite was found to have the least negative surface charge, possibly due to the effects of the presence of oxidation products. An acid/base theory proposed by Liu *et al.*, (2000), which describes an interaction between metal-hydroxyl species on the mineral surface and the hydroxyl groups on the polysaccharide, suggested that the strength of the interaction between mineral and depressant depended on the relative basicity of the metal-hydroxyl complexes on the mineral surface. In terms of this theory, chalcopyrite, whose surface was the least negative, had the most basic mineral surface, and plagioclase whose surface was the most negative, had the most acidic surface. Consequently, the strongest interaction was expected between chalcopyrite and depressant whereas that between plagioclase and depressant would be the weakest.

The presence of divalent calcium and magnesium ions in solution, as in the case of synthetic plant water (SPW) and a 10^{-2}M IS $Ca(NO_3)_2$ solution, resulted in a positive shift in the zeta potential. This was thought to have resulted from double layer compression.

A relative positive shift in the zeta potential was observed with the addition of guar which resulted in talc, chromite, pyroxene and chalcopyrite attaining a similar surface charge. The zeta potential of plagioclase remained relatively more negative compared to the other minerals. Plagioclase seemed to have the weakest interaction with guar. The addition of CMC in a buffered solution resulted in minimal change in the negative surface charge on each mineral, suggesting a minimal interaction between CMC and each of the minerals. However, the zeta potential on each mineral became less negative with the addition of CMC in a 10^{-2}M IS $Ca(NO_3)_2$ solution when compared to the buffered solution. This suggests that the adsorption of CMC is greatly enhanced by the presence of divalent ions in solution.

It was further hypothesised that depressants adsorb preferentially onto different minerals because there are differences in the equilibrium and kinetic adsorption characteristics of each mineral towards depressant molecules. A study of the kinetics of adsorption of guar and CMC onto each mineral at constant temperature showed that with guar, an adsorption density sufficient to achieve good depression was attained after two minutes for each mineral. The results obtained suggest that from an operational point of view depressant adsorption is not rate controlled.

Equilibrium studies were conducted to test which mineral had the highest affinity for polymer in a single mineral system. The adsorption isotherms displayed Langmuir behaviour. In a buffered solution, chalcopyrite had the highest affinity for guar, followed by talc and chromite, then pyroxene. Plagioclase had the lowest affinity for guar. This progression in the affinity for guar in buffer solution correlated closely with the differences observed in the surface charge of each mineral at pH 9. In terms of the acid/base interaction theory chalcopyrite had the most basic surface, hence the highest affinity for guar, and plagioclase, which had the most acidic surface, would have the weakest interaction with guar. The presence of ions solution had minimal effect on the maximum adsorption density of guar on all the minerals except for chalcopyrite, for which the adsorption density was slightly higher than that in buffer.

The adsorption of CMC showed a strong dependence on the presence of divalent ions in solution. This may be due to charge screening by Ca^{2+} ions within the CMC molecules in solution, which reduces the electrostatic repulsion between the CMC and the mineral surface (Burdukova *et al*., 2008). It has also been proposed that CMC assumes a coiled conformation in the presence of divalent calcium ions in solution, which results in a smaller area of adsorption per molecule on the mineral surface (Parolis *et al.*, 2008)

Microflotation experiments were conducted to evaluate the hydrophobicities of each mineral as a function of their relative affinity for depressant in a mixture of each mineral with talc. The recovery of a 2g talc sample in the size range +45-106μm in a microflotation cell sample served as a diagnostic of the extent to which depressant adsorbed onto a second mineral. Talc is hydrophobic and hence will float more readily in the relative absence of a depressant. This would indicate a preferential adsorption of the depressant onto the second mineral.

In the case of guar as a depressant, chalcopyrite as the second mineral was found to have the highest cumulative talc recovery as its total BET surface area was increased. This was followed by pyroxene, talc (-38μm) and chromite which had a similar cumulative talc recoveries. Plagioclase had the lowest cumulative talc recovery. These results represent a relative scale of preference of guar for the second mineral compared to talc and hence suggest that in a mixed mineral system chalcopyrite has the highest affinity for guar and plagioclase the lowest affinity. A similar progression in the maximum adsorption densities of guar was observed during the equilibrium adsorption experiments, again suggesting an acid/base interaction between guar and each mineral.

Microflotation experiments with CMC showed very little difference in talc recovery with increasing surface area for all added minerals when exposed to CMC. This suggests that there was little difference in mineral affinity towards CMC. It is possible that an acid/base interaction was not the dominant interaction between CMC and the minerals. It is possible that a coiled conformation of CMC due to presence of divalent calcium ions in solution may have resulted in the exposure of the hydrocarbon backbone of the CMC

which would favour hydrophobic interactions over acid-base complexation reactions. Hydrophobic interactions would be more non-specific than complexation reactions between the depressant hydroxyl groups and metal ions on the mineral surface.

TABLE OF CONTENTS

LIST OF FIGURES

LIST OF TABLES

GLOSSARY

ATR	Attenuated total internal reflection
BET	Brunauer, Emmet, Teller
BIC	Bushveld Igneous Complex
°C	Degrees Celsius
Ca^{2+}	Calcium ions
10^{-2}M IS Ca^{2+}	10^{-2} molar ionic strength calcium nitrate solution
CMC	Carboxymethyl cellulose
CMR	Centre for Minerals Research
c_i	Concentration of ions in solution
C_{eq}	Equilibrium concentration
DS	Degree of substitution
f(κa)	Henry function
FTIR	Fourier transform infrared spectroscopy
Finnfix700	CMC depressant
guar	Guar gum
I_{ads}	Adsorption density
IEP	Isoelectric point
I_{max}	Maximum adsorption density
IS	Ionic strength
K	Langmuir equilibrium constant
m^2	Metres squared
m^2/g	Metres squared per gram
mol/L	Moles per litre
mV	Millivolts
n	Number of moles per polymer adsorbed
N_A	Avogadro's number
$Na_2B_4O_7 \cdot 10H_2O$	Di-sodium tetraborate
-OH	Hydroxyl group
PGMs	Platinum group metals

PZC	Point of zero charge
R	Universal gas constant
Sendep369	Guar depressant
SPW	Synthetic plant water
std.dev	Standard deviation
std. error	Standard error
SIBX	Sodium isobutyl xanthate
T	Temperature
ToF-SIMS	Time of flight secondary ion mass spectroscopy
U_E	Electropheretic mobility
z_i	Valency of ion

ψ_o	Surface potential
ψ_δ	Stern plane potential
δ	Stern plane
ζ	Zeta potential (mV)
ε	Dielectric constant
η	Viscosity
μm	micron
σ°	Effective area occupied per adsorbed polymer molecule
ΔG_{ads}	Standard Gibbs free energy
θ	Fractional surface coverage (pseudo-monolayers)

1 INTRODUCTION

Froth flotation is used extensively in South Africa as the first concentration step in the recovery of platinum group metals (PGMs) from platinum bearing ores in the Bushveld Igneous Complex (BIC). Froth flotation is a process used to separate minerals suspended in liquids by their attachment to gas bubbles to provide selective levitation of the solid particles (Crozier, 1992). The flotation process relies on the differences in the mineral surface properties to maximise the recovery of valuable minerals to the concentrate, whilst minimising the recovery of silicate gangue, which constitutes the bulk of the ore.

However, this process is complicated by the presence of naturally floatable gangue minerals like talc in Merensky ore. Although talc is present in small quantities it has a disproportionate effect by enhancing froth stability and increasing the entrainment of other gangue minerals (Martinovic *et al*., 2005). This has negative effects on transportation and downstream smelting processes. Long chain polysaccharide depressants are frequently used in flotation to improve the grade of the concentrate by depressing naturally floatable gangue (Shortridge *et al*., 2000). Commonly used polysaccharide depressants in PGM flotation include carboxymethyl cellulose (CMC) and guar gum. The cost of depressants has been found in some cases to exceed the cost of other reagents in a concentrator. Consequently, it is important to try to understand the chemical interactions between depressant and mineral, in order to ensure their optimum use.

Extensive work has been done to elucidate the mechanisms involved in the adsorption of polymeric depressants onto talc. However, not much is known about the preferential adsorption of depressant in mixed mineral systems. Many studies have focused on equilibrium adsorption isotherms to explain the adsorption of depressants onto minerals, particularly talc. However this is an artificial environment in which the depressant is given enough time to adsorb to the mineral, thus the adsorption kinetics and competitive adsorption between different minerals are not considered. Furthermore, batch flotation

tests conducted by Wiese *et al., (*2008), found that at normal plant depressant concentrations very little depressant remains in solution. This suggests that minerals may be competing for depressant. It is not known to what extent depressant adsorbs onto one mineral relative to another, and whether some depressant adsorbs onto sulphide minerals resulting in a reduction in the recovery of value minerals.

This project focuses on investigating the relative adsorption of polymeric depressants viz. guar and CMC on pure minerals. These include silicate gangue minerals found in BIC ore namely talc, orthopyroxene, plagioclase feldspar; and chromite, a major gangue mineral component of UG2 ore. The adsorption of depressant onto chalcopyrite will also be investigated to test depressant adsorption on sulphides.

The following key questions address the objectives of the project:

1. What role do differences in the surface charge of each mineral play in preferential adsorption of depressant onto the mineral surface?
2. What role do metal ions in solution play in modifying the mineral surface charge, and therefore changing the adsorption characteristics?
3. Which mineral has the highest affinity for polymer in a single mineral system?
4. Which mineral has the highest rate of depressant adsorption in a single mineral system?
5. In a mixture of minerals, which mineral has the highest affinity for the polymer?

In addressing the research problem the following methods will be used:

- Zeta potential measurements will be conducted to determine the differences in mineral surface charge in the absence and the presence of ions in solution. The effect of the addition of depressant on the mineral surface charge will also be investigated.
- Kinetic adsorption studies will be conducted to test if depressant adsorption on each of the minerals is rate controlled. Equilibrium studies will be conducted to

quantify the adsorption densities of depressant on each mineral and compare the affinity of the mineral surfaces for polymer molecules

- Talc microflotation will be used as an indicator of selective depressant adsorption in mixed mineral systems.

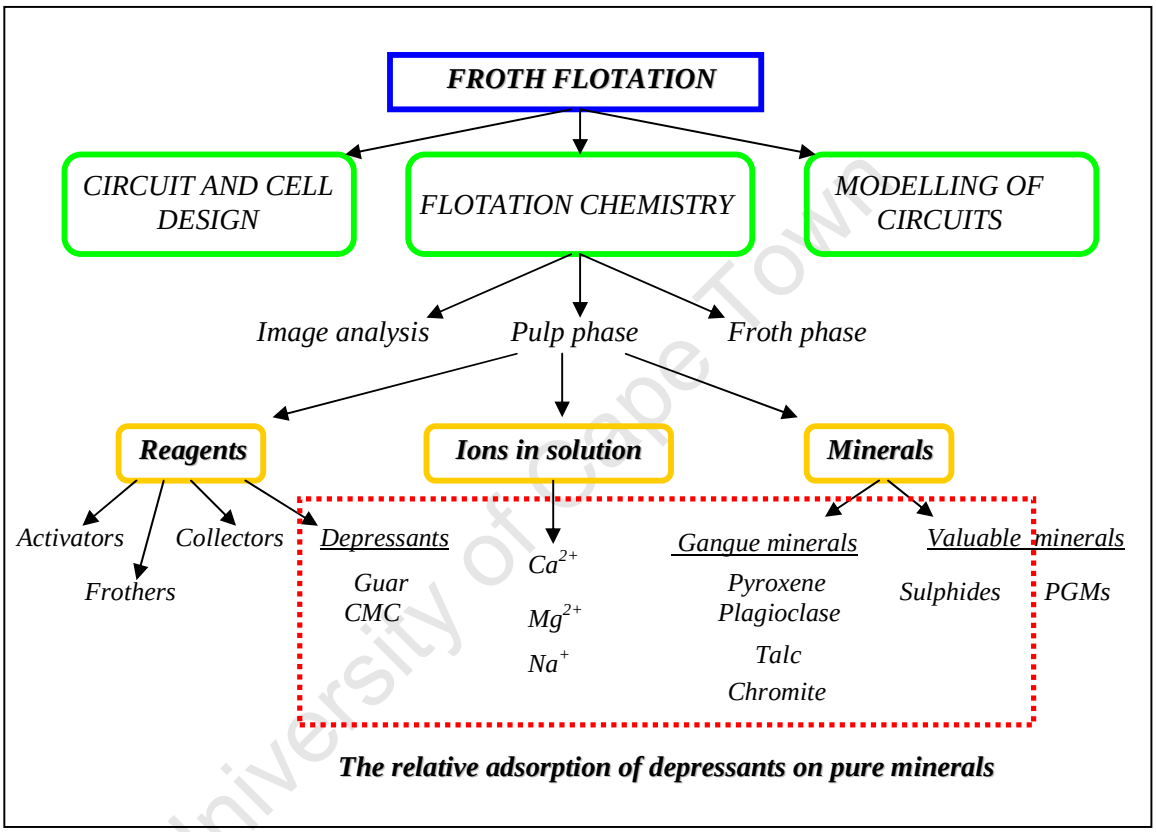

Figure 1.1: Schematic representation of the scope of this thesis: the red block encompasses the scope of this study

2 LITERATURE REVIEW

2.1 MINERALOGY OF MERENSKY ORE

The Bushveld Igneous Complex (BIC) is an extensive geological system, comprising various limbs in the Northwest and Limpopo Provinces of South Africa and with some evidence of its extension under surficial cover into Botswana (Lotter *et al.*, 2008) as shown in Figure 2.1. The Bushveld Complex crops out as three lobes, namely, the western, northern and eastern lobes (Barnes and Maier, 2002). The Bushveld Complex is the world's largest resource of platinum group elements (Platinum, Palladium, Ruthenium, Rhodium, Osmium and Iridium; referred to as PGEs), located in three main occurrences - the Merensky Reef, UG2 chromitite and Platreef (Wilson and Chunnett, 2006).

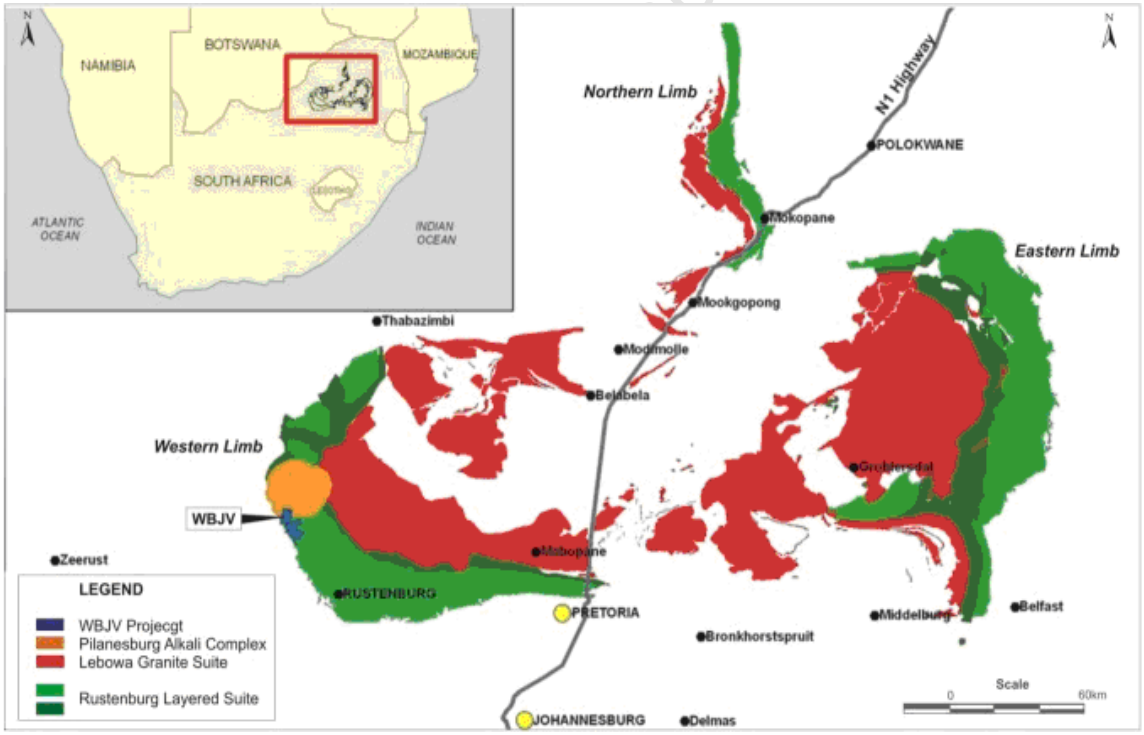

Figure 2.1: The Bushveld Igneous Complex (adapted from Minxcon, 2007)

Figure 2.2 shows a simplified stratiography of the BIC. The BIC is stratified into distinct zones with varying mineralogy, namely the Marginal Zone, Lower Zone, Critical Zone, Main Zone and the Upper Zone. The platinum bearing reefs (UG2 and Merensky) occur towards the top of the Critical zone (Barnes and Maier, 2002). The mining of Platinum Group Minerals (PGMs) in the Merensky Reef and UG2 is of major economic importance in South Africa. Associated with PGMs in the Merensky Reef are sulphides, however at a very low content of less than 1%, (Becker *et al.*, 2006). Predominant sulphide minerals are pentlandite, chalcopyrite and pyrrhotite (Malysiak *et al.*, 2004).

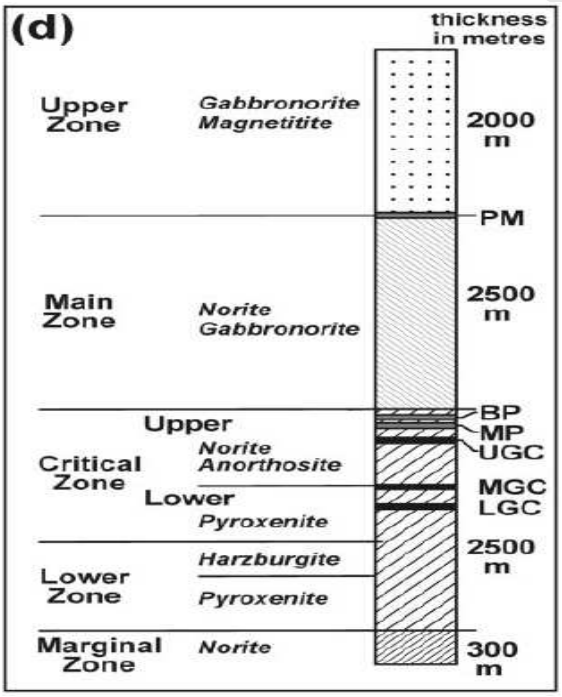

Figure 2.2: Simplified stratiography of the Bushveld Complex (adapted from Wilson and Chunnett, 2006)

Of particular interest in this study is the sulphide and gangue mineral content of the Merensky reef in the form of chalcopyrite, and silicates and chromite respectively. The primary silicate minerals of the Merensky reef are comprised of orthopyroxene, plagioclase, clinopyroxene and occasional olivine, and other hydrous silicate minerals (such as mica, talc and serpentine), some of which may be secondary in origin (Becker *et*

al., 2006). The mineralogy of talc, orthopyroxene, plagioclase, chromite and chalcopyrite, is considered in the following section

2.1.1 Talc

Talc ($Mg_3(Si_2O_5)_2(OH)_2$) is a magnesium-rich phyllosilicate mineral that occurs as a gangue component in many base metal sulphide ore deposits around the world (Burdukova *et al.*, 2007). Talc is a mineral of secondary origin formed by the alteration of magnesium silicates, such as olivine, pyroxenes and amphiboles (Hurlbut, 1941). Due to its natural floatability, talc readily enters the flotation concentrate, thus reducing its grade (Burdukova *et al.*, 2007). Although talc is present in small quantities it has a disproportionate effect by enhancing froth stability and increasing the entrainment of other gangue minerals (Martinovic *et al.* 2005). As a result, polysaccharide depressants have been used to depress talc by adsorbing onto the surface of talc, thus rendering it hydrophilic (Parolis *et al.*, 2008).

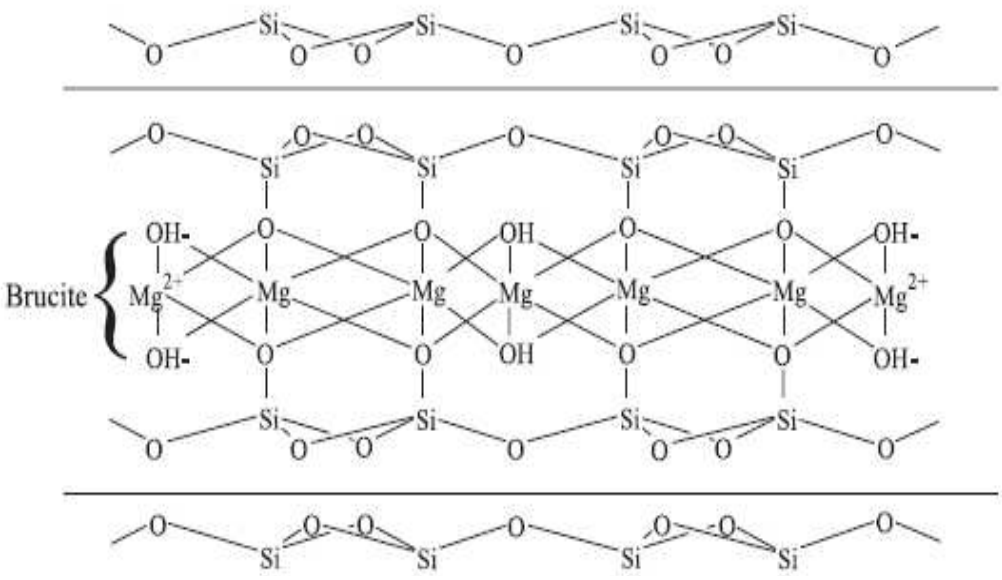

Figure 2.3: Schematic diagram showing the molecular structure of talc (adapted from Khraisheh et al., 2005)

Talc is a layered silicate mineral that consists of octahedral magnesium hydroxide complexes sandwiched between sheets of silicon–oxygen tetrahedra as shown in Figure 2.3. The layered talc sheets are held together by weak van de Waals forces (Burdukova *et al.*, 2007). The most significant feature of the talc surface is its heterogeneous nature, comprising of a hydrophobic face (-Si-O-Si-) and a hydrophilic edge (-MgOH and -SiOH groups) (Chiem *et al.*, 2006).

Typically, low levels of isomorphous substitution of silicon (Si) by aluminium (Al) or titanium (Ti), and magnesium (Mg) by iron (Fe) or aluminium (Al) occur in the talc lattice, leaving the face with a pH independent negative charge. This contrasts with the hydrophilic edges, consisting of -SiOH and -MgOH groups, whose amphoteric behaviour means that their charge is pH dependent. However, since the hydrophobic faces are the dominant surface, talc floats readily (Jenkins and Ralston, 1998).

2.1.2 Plagioclase

Feldspars owe their importance to the fact that they are the most abundant of all minerals. They are closely related in form and physical properties, but they fall into two subgroups namely, the potassium and barium feldspars which are monoclinic or very nearly monoclinic in symmetry; and the sodium and calcium feldspars (the plagioclases), which are triclinic (Berry and Mason, 1959).

The general formula for feldspars can be written as XZ_4O_8 in which X may be sodium (Na), potassium (K), calcium (Ca) and barium (Ba); and Z is Si and Al (Berry and Mason, 1959). Plagioclase feldspars form at elevated temperatures and are a complete solid solution series from pure albite (Ab), $NaAl_2Si_2O_8$, to pure anorthite (An), $CaAl_2Si_2O_8$ (Hurlbut, 1941; Klein , 2002). The structure of feldspars is a continuous three-dimensional network of SiO_4 and AlO_4 tetrahedra, with the positively charged sodium, potassium, calcium and barium situated in the interstices of the negatively charged network.

2.1.3 Pyroxene

Pyroxene is the most abundant mineral in the Merensky Reef, constituting about 60% of the reef by volume (O'Connor *et al.,* 2006). Pyroxenes are a group of minerals closely related in structure, physical properties, and chemical composition, although they crystallize in two different systems, orthorhombic and monoclinic (Berry and Mason, 1959). The chemical composition of pyroxenes can be expressed by the general formula $(Q, X, R)_2 Z_2 O_6$, in which Q, X, R, Z indicate elements having similar ionic radii and capable of replacing each other in the structure. In the pyroxenes, these elements may be:

- Q = Ca, Na
- X = Mg, Fe, Mn^{2+}, Li
- R = Al, Fe^{3+}, Ti
- Z = Si, Al (Berry and Mason, 1959; Klein, 2002)

The structure of pyroxene has SiO_4 tetrahedra linked together into a vertical chain. Each tetrahedron shares two oxygen atoms with those immediately above and below in the chain. These chains are joined together by means of cations (Martinovic, 2004). The chain silicate structure of pyroxenes offers much flexibility in the incorporation of various cations. The names of pyroxene minerals are primarily defined by their chemical composition. Figure 2.4 shows the chemical composition of various minerals comprised in the pyroxene group.

Orthopyroxene is a magnesium-rich ferro-magnesian inosilicate containing approximately 27–35% magnesium oxide (MgO) (Deer *et al.,* 1963). Orthopyroxene is the generic name given to minerals with a composition intermediate to the magnesium-rich end-member enstatite ($Mg_2Si_2O_6$) and iron-rich end-member ferrosilite ($Fe_2Si_2O_6$) of the pyroxene mineral group (Lotter *et al.,* 2008) represented at the base of the triangle as seen in Figure 2.4. Orthopyroxene crystals are orthorhombic in structure, hence the "ortho" prefix.

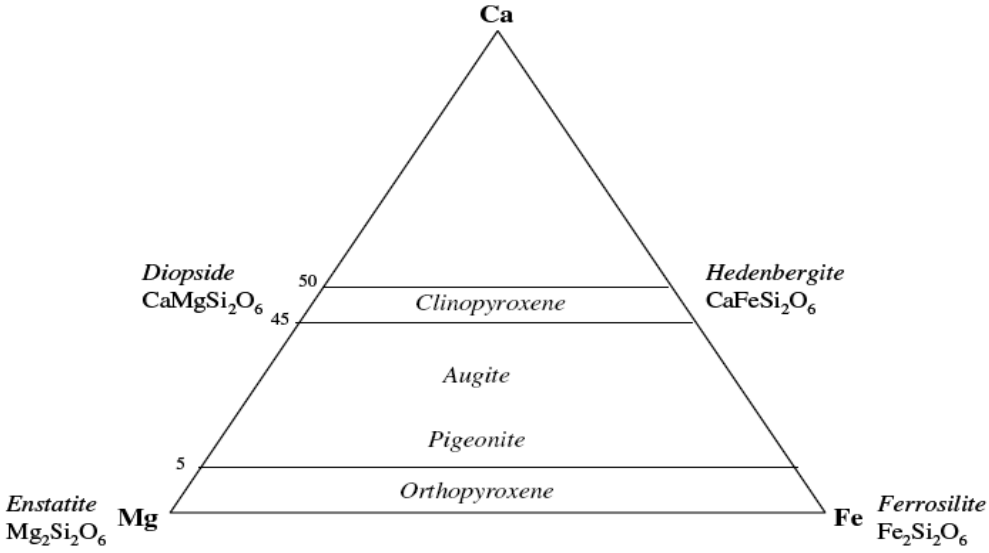

Figure 2.4: Chemical composition of the various minerals comprising the pyroxene group of silicates (Lotter et al, 2008)

A study done by Becker *et al*., (2009) has shown there to be an association between orthopyroxene and talc in Merensky ore. The manifestation of this association is in the form of partial talc rims surrounding orthopyroxene particles. The association of talc and pyroxene within Merensky ore is not entirely unexpected given that talc is an alteration product of anhydrous magnesium silicate minerals (Hurlbut, 1941; Becker *et al.*, 2009). This association was also confirmed by Lotter *et al.*, (2008) who showed that in the case of talc rimming, the composite particle flotation effect dominates and imparts naturally floating characteristics to the composite particle. Figure 2.5 shows a photomicrograph image of a thin section from a Bushveld Merensky sample adapted from Lotter *et al.*, (2008). Talc rimming features are annotated around orthopyroxene (opx) on the boundary between orthopyroxene cumulate crystals and a sulphide from the Merensky Reef. Other minerals present include lathes of biotite (bio) as well as euhedral chromite (chr) crystals.

Figure 2.5: A photomicrograph image showing a thin section from a Merensky ore sample (Lotter et al., 2008)

According to Fuerstenau and Fuerstenau (1982), when pyroxene and amphibole chain silicates are ground, an increasing number of Si-O bonds are broken, which leads to a progressively pH dependant negative surface. The surfaces of these minerals are not only hydrophilic but are also certain to be strongly anisotropic depending on the face to edge ratio. Along the backbone of the mineral, the silica chains carry a fixed negative charge, compensated for by any residual cations at the lattice surface, and the ends of the chains consist of broken Si-O bonds.

2.1.4 Chromite

The UG2 is a platinum group element (PGE) bearing reef from the Bushveld Igneous Complex, currently being beneficiated by flotation. Chromite is one of the main gangue constituents of UG2 ore, making up to 60% by mass of the ore (Wesseldijk *et al.*, 1999). Modal analysis of ore samples from the Merensky reef by Wiese *et al.*, (2008) also showed chromites to be present in Merensky ore at low concentrations.

Chromites are part of the spinel group of minerals. Spinel structures are usually described as double oxides AB_2X_4 in where;

- A is one or more divalent metals - magnesium (Mg), iron (Fe), zinc (Zn), manganese (Mn), and nickel (Ni),
- B is one or more trivalent metal- aluminium (Al), iron (Fe), chromium (Cr), manganese (Mn), or titanium (Ti^4), and
- X is oxygen (O) (Berry and Mason, 1959)

The composition of chromites is strongly influenced by the mineralogy of the host rock (Hulbert and von Gruenewaldt, 1985). Chromites approximate the composition $(Mg,Fe)Cr_2O_4$, with formula units per unit cell. The Cr_2O_3 content of most analyzed chromites extends from 30-60% in pure ferrochromite, and about 80% in magnesiochromite.

2.1.5 Chalcopyrite

The Merensky Reef is also exploited for its nickel (Ni) and copper (Cu), hosted by the sulphides pentlandite and chalcopyrite (Lotter *et al.*, 2008). However, the combined sulphide grade of the ore is typically less than 1% (Bradshaw *et al.*, 2005). The general formula for sulphides is given as X_mZ_n , in which X represents the metallic elements and Z the non-metallic element. The general order of listing of the various minerals is in a decreasing ratio of X:Z (Klein, 2002). Pentlandite $(Fe,Ni)_9S_8$ is exploited as a source of Ni and is nearly always associated with pyrrhotite. Pentlandite analyses show an iron to nickel ratio of 1:1, but varying somewhat (Berry and Mason, 1959). Chalcopyrite ($CuFeS_2$) is the most widespread copper mineral, and one of the most important sources of the metal. Chalcopyrite has a structure that can be derived from the sphalerite structure by regularly substituting copper (Cu) and iron (Fe) ions for zinc (Zn) in sphalerite (Klein, 2002)

The flotation and separation of sulphide minerals can be detrimentally affected by the oxidation of the surface of these minerals. The surface oxidation products consist mainly

of metal hydroxides and sulfur-oxy species, either adsorbed in thin layers or precipitated from solution as colloidal particles (Clarke *et al.*, 1995). The accepted mechanism for the initial oxidation stage of sulfide minerals involves the migration of the metal from the outermost layers to the surface followed by its dissolution in acidic solutions, while in alkaline solutions a layer of metal hydroxide is formed above the sulfur-rich mineral surface. The sulfur-rich surface consists of a metal-deficient sulfide lattice, polysulfide or elemental sulfur depending on the extent of oxidation (Fullston, 1999). The following reactions in acidic and alkaline conditions were proposed by Buckley and Woods (1984), with $x \approx 1$ for the outermost layers and with the ferric hydroxide covering the sulfur-rich lattice.

$$CuFeS_2 + \tfrac{3}{4} xO_2 + \tfrac{3}{2} xH_2O \rightarrow CuFe_{1-x}S_2 + xFe(OH)_3 \qquad (2.1)$$

$$CuFeS_2 \rightarrow CuFe_{1-x}S_2 + 2xe^- \qquad (2.2)$$

2.2 BASIC PRINCIPLES OF FROTH FLOTATION

Froth flotation is a physico-chemical separation process which relies on the differences in mineral surface properties to maximise the recovery of valuable minerals, whilst minimising the recovery of gangue to the concentrate. It is based on imparting a hydrophobic nature to the valuable minerals and rendering the gangue hydrophilic (Dalvie, 2001). After treatment with reagents, such differences in the surface properties between minerals within the flotation pulp become apparent. For flotation to occur, an air bubble must be able to attach itself to a particle and lift it to the water surface (Wills, 1997), as illustrated in Figure 2.6

There are two distinct zones in the flotation process namely, the pulp phase in which mineral recovery occurs, and the froth phase, in which concentrated material is separated from the bulk (Martinovic *et al.*, 2005). In the pulp phase it is important to create the necessary environment, both physical and chemical, to promote bubble-particle collision, successful attachment of the valuable hydrophobic particles and the transport of these

mineral-laden bubbles to the froth phase. At the same time, the unwanted gangue minerals should be hydrophilic and remain unattached after collision and therefore not be transported to the froth phase by "true flotation". Material can either reach the concentrate through true flotation or entrainment (Bradshaw *et al.*, 2005). Entrainment is unselective and results in unwanted gangue reporting to concentrate.

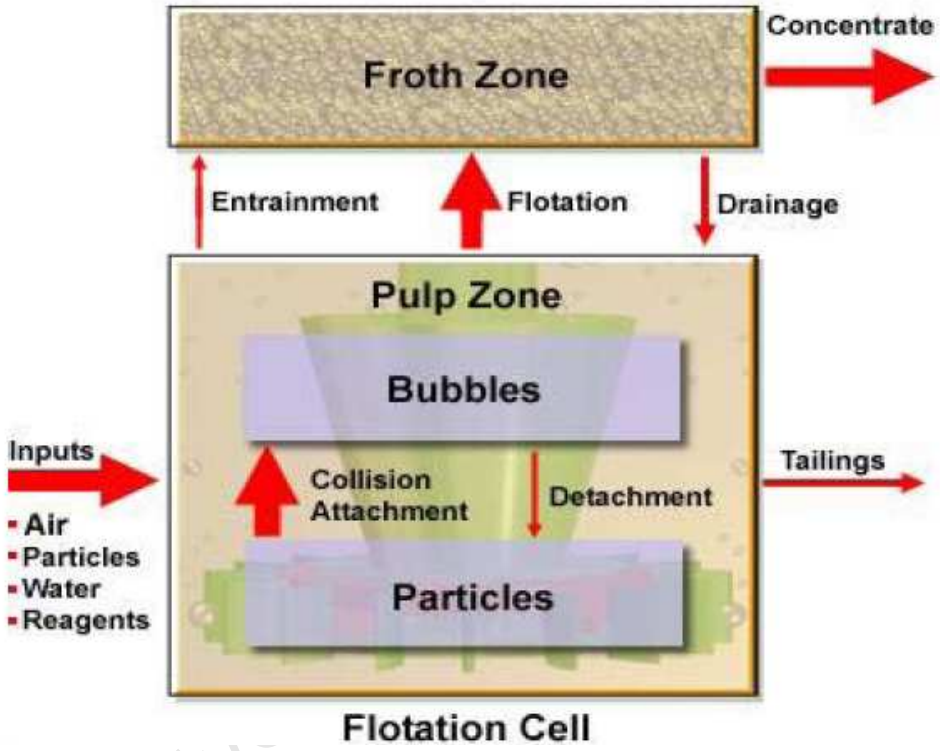

Figure 2.6: Schematic representation of froth flotation (adapted from Bradshaw, 2009)

2.2.1 Flotation reagents

Reagents are added to perform specific roles to manipulate the pulp chemistry and enhance the differences in mineral surface hydrophobicity to facilitate separation (Bradshaw *et al.*, 2005). Reagents used in flotation include collectors, frothers, and modifiers as stated by Pearse (2005) and Lovell (1982) in their reviews of reagents used in flotation.

2.2.1.1 Collectors

These are reagents that render the valuable mineral hydrophobic. They are usually surface active compounds, although many of them are not surface active at the water-air interface. They comprise of a polar functional group, hydrophilic in character through which they attach to the mineral, and a non-polar hydrophobic portion though which they attach the bubble. The hydrophobic tail is usually a hydrocarbon, but fluorocarbon and silane tails have been investigated (Lovell, (1982); Fuerstenau (1982)). A variety of collectors are available, and are classified on the basis of composition and whether they exist as cations, anions or molecular species in solution (Fuerstanau, 1982).

Alkyl xanthates are by far the largest volume reagents used in sulphide flotation. The next largest group of collectors are the dithiophosphates. Many other specialised sulphydryl (thiol) collectors have been developed. In many cases a combination of two sulphide collectors, a xanthate and a dithiophosphate for example, give optimum grade and recovery efficiency for a particular circuit (Pearse, 2005).

2.2.1.2 Frothers

Frothers are surface active, usually non-ionic molecules whose function in the flotation system is to provide a large air-water interface of sufficient stability to ensure that a particle will not fall back into the flotation pulp before it can be removed (Lovell, 1982). Frothers are neutral molecules consisting of a medium chain length hydrocarbon entity and a polar group(s) entity. This gives the molecule dual affinity to water and air. The hydrophobic contribution is not as strong as in collectors. The polar groups of frothers are always hydroxyls, usually in the form of alcohol or glycol (Pearse, 2005).

2.2.1.3 Modifiers

Modifiers include activators, depressants and pH modifiers. Activators enhance collector attachment to the valuable mineral, and pH modifiers modify the pH of the pulp so that the optimum conditions for collection, activation or depression are achieved (Lovell, 1982). Depressants inhibit the flotation of unwanted gangue minerals by enhancing the hydrophilic character of the gangue. A detailed description of polymeric depressants is given in Section 2.3.

2.3 POLYMERIC DEPRESSANTS

The function of a depressant is opposite to that of a collector. Its function is to inhibit flotation of a given mineral. This is achieved either by preventing collector from adsorbing onto an existing hydrophilic mineral, or by adsorbing onto a mildly hydrophobic or hydrophobic mineral and creating a hydrophilic surface (Bradshaw *et al.*, 2005). In the past inorganic depressants such as sodium cyanide, sodium dichromate, sulfur dioxide, arsenic trioxide, phosphorous pentasulphide have been used (Liu *et al.*, 2000). However these are toxic and harmful to the environment and have since been replaced by polymeric depressants which are derived from natural products.

Commonly used polymeric depressants in the recovery of PGMs in South Africa are carboxymethyl cellulose (CMC) and guar gum. In a review of macromolecular depressants in sulphide flotation, Pugh (1989) showed that the wide range of macromolecular organic depressants broadly have the following similar features:

- A hydrocarbon backbone capable of adsorbing on hydrophobic mineral sites
- In most cases, large numbers of hydrophilic groups (often hydroxyls) distributed throughout the polymer capable of ionization or hydrogen bonding
- Strongly hydrated polar groups (i.e. SO_3^{2-}, PO_4^{3-}, COO^-, e.t.c.) also frequently distributed throughout the molecule

The adsorption mechanism of polymeric depressants onto the mineral surface is not well understood. The factors that affect the adsorption of polymeric depressants onto mineral surfaces, and different postulations by leading researchers in this field will be dealt with at a later stage. It is important to first understand the chemistry of each of the depressants in question.

2.3.1 Carboxymethylcellulose (CMC)

CMCs are anionic polysaccharides with molecular weights ranging from 10^3 to 10^6 Dalton (Burdukova, 2007). The CMC polymer is prepared by steeping cellulose in a sodium hydroxide solution. The alkaline cellulose is then esterified with sodium monochloroacetate to form sodium carboxymethyl cellulose and sodium chloride (Batdorf and Rossman, 1973) as shown by the reaction below (Dalvie, 2001):

$$(C_6H_{12}O_5)_n + NaOH + ClCH_2OONa \rightarrow (C_6H_9O_5CH_2COONa)_n + NaCl \qquad (2.3)$$

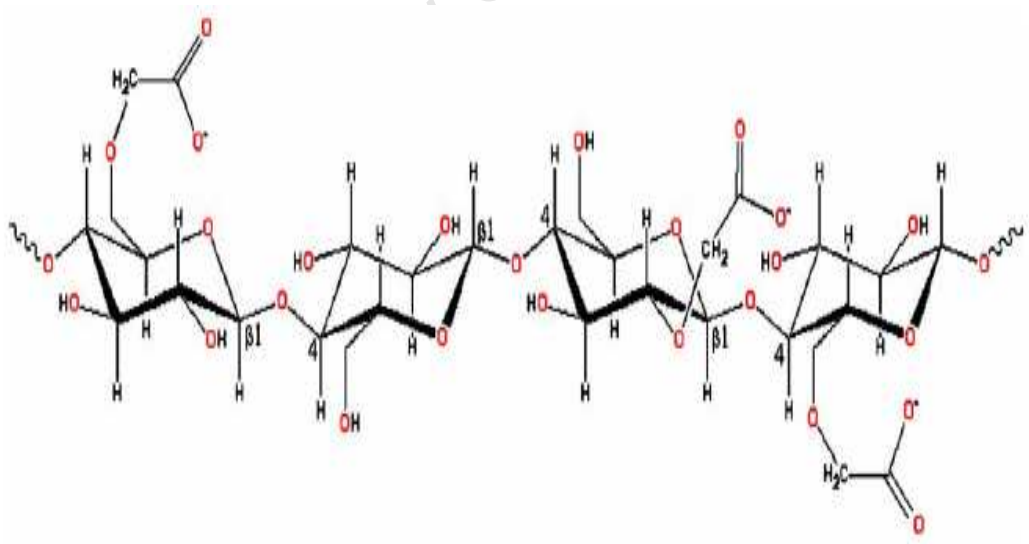

Figure 2.7: The molecular structure of CMC (adapted from Wang and Somasundaran, 2005)

Figure 2.7 shows the molecular structure of CMC. As can be seen, each hydroglucose unit of cellulose contains three hydroxyl groups. The ionic nature of the polymer is due to

the high degree of substitution of carboxylate groups along the chain (Martinovic, 2004). The degree of substitution (DS) refers to the extent of the reaction of these cellulose hydroxyls to form carboxylate derivatives and is defined as the number of hydroxyl groups in the anhydroglucose unit which have reacted. The highest theoretical DS is 3, but most commercial grades have DS values of about 0.7 to 0.8 (Pugh, 1989).

2.3.2 Guar gum

Guar gum is a natural nonionic polysaccharide with an average molecular weight of 100,000–2,000,000 (Wang *et al.*, 2005). Figure 2.8 shows two repeating units of guar gum. Each unit contains nine OH groups. These OH groups are available for hydrogen bonding of the guar gum molecule to mineral surfaces (Wang *et al.*, 2005).

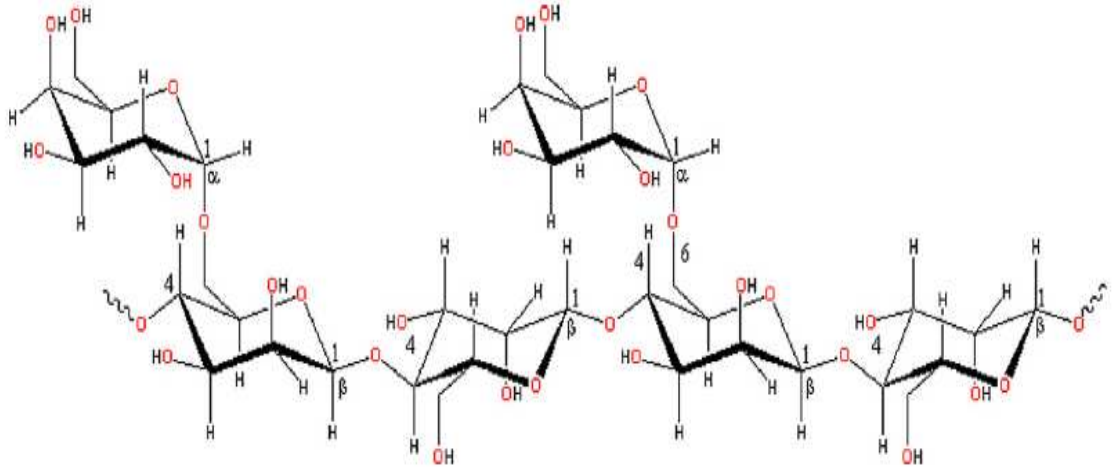

Figure 2.8: The molecular structure of guar (adapted from Wang and Somasundaran, 2007)

2.4 ADSORPTION MECHANISMS OF POLYMERIC DEPRESSANTS

Numerous studies have been conducted in trying to understand the mechanisms involved in the adsorption of polymeric depressants onto mineral surfaces, and the factors that affect this adsorption. The majority of these have focused on the adsorption of polymeric

depressants onto talc. In this section, a review of the current understanding of the adsorption mechanisms of polymers onto minerals is presented.

The adsorption of polymers at the solid–liquid interface is largely dependent on both the polymer solution chemistry and the solid surface properties of the system (Morris *et al.*, 2002) .The adsorption of macromolecular organic depressants from an aqueous solution to a mineral surface involves the replacement of water/mineral contact areas by depressant mineral contact areas and probably often also extensive changes in the hydration state of the depressant, i.e. replacement of water/depressant contact by depressant/depressant contacts in the adsorbed layer (Pugh, 1989).

Pugh (1989) further proposed that adsorption therefore is influenced by many different interactions such as:

1. Coulombic interaction between ionic groups on the surface and on the depressant
2. Replacement of water/hydrophobic contact areas by surface/depressant contacts
3. Hydrogen bonding or other specific interactions between the depressant and the surface (in competition with similar contacts with water)
4. The formation of energetically favourable structures of the adsorbed layer (e.g. hydrophobic interaction between hydrophobic segments of the depressant)
5. The solubility of the depressant in the aqueous medium surrounding the particles.

Despite the large number of studies that have been conducted, the mechanism of polysaccharide adsorption onto talc is not yet well understood. However, several postulations have been put forward.

2.4.1 Hydrogen bonding

Wang and Somasundaran, (2005); Wang *et al.*, (2005); Burdukova, (2007); Rath *et al.*, (1997); and Steenberg and Harris (1984) postulated hydrogen bonding to be the mechanism by which polymeric depressant molecules adsorb onto the mineral surface. In their study, Wang and Somasundaran, (2005) showed that urea (a hydrogen bond

breaker) reduced the adsorption of CMC on talc significantly. This result supported a mechanism involving hydrogen bonding rather than that of hydrophobic interactions. Their FTIR results provided data on spectral changes that are associated with hydrogen bonding between polysaccharides and the solid surface. The changes in the infra-red bands in the region of 1000-1080cm^{-1}, associated with the C-O stretch coupled to the C-C stretch and O-H deformation, were significant. In a similar study, Wang *et al.,* (2005) investigated the adsorption of guar gum at the solid-liquid interface using spectroscopic and allied techniques. In this study, hydrogen bonding was found to be the main mechanism responsible for the adsorption of guar gum onto talc.

2.4.2 Electrostatic interactions

Wang and Somasundaran, (2005) also found that the adsorption of CMC onto talc was affected by changes in pH and ionic strength. For example, as the pH increased, the charge on the CMC and the surface charge were altered, thereby decreasing the CMC adsorption onto talc. These results suggest that the electrostatic force plays an important role in the adsorption of CMC on talc. However, no such mechanism was found to act on the adsorption of guar gum onto talc (Wang *et al.,* 2005; Wang and Somasundaran, 2007).

2.4.3 Hydrophobic interactions

In an investigation of the adsorption mechanism of guar at the talc-aqueous solution interface, Jenkins and Ralston, (1998) found hydrophobic interactions to dominate the adsorption process, leading to the adsorption of guar onto hydrophobic sites, i.e. the talc ‘‘face’’. The adsorption isotherms of guar onto talc exhibited pseudo-Langmurian behaviour. From the classical Langmuir adsorption model, they were able to obtain the Langmuir adsorption equilibrium constant (K). This enabled the calculation of the standard Gibbs free energy of adsorption, ΔG_{ads} using the formula:

$$\Delta G_{ads} = -R \cdot T \cdot \ln(K) \qquad (2.4)$$

T is the absolute temperature in Kelvin and R is the universal gas constant. The contribution of electrostatic interactions to the ΔG_{ads} was estimated, and it was found that the free energy of adsorption due to electrostatics (ΔG_{el}) was less than 10% of the ΔG_{ads}. These results indicated that an electrostatic mechanism was not the driving force which governs the thermodynamics of non-ionic guar adsorption at the talc–aqueous solution interface (Jenkins and Ralston, 1998).

Furthermore, it was suggested that the adsorption of guar at the talc-solution interface was strongly dominated by adsorption onto the hydrophobic talc face. Adsorption onto the hydrophilic talc edge appeared to occur, but to a limited extent. This was also confirmed by Beattie *et al.,* (2006) in an in situ ATR–FTIR study of polyacrylamide adsorption at the talc surface. Adsorption isotherms and kinetic spectra showed no shifts in the spectral peaks of the polymer upon adsorption, suggesting that hydrophobic interactions between the hydrocarbon polymer backbone and the hydrophobic face of talc were the dominant binding mechanism.

These findings are in contrast to those obtained by Wang and Somasundaran, (2005); Wang *et al.,* (2005) and Wang *et al.*, (2007), in which they specifically found no evidence for hydrophobic interactions in the adsorption of both CMC and guar onto talc using pyrene-labelled CMC in fluorescence spectroscopy tests.

2.4.4 The acid/base hypothesis

Liu *et al.,* (2000) and Laskowski *et al.,* (2007) proposed that natural polysaccharides, such as starches, dextrins and guar gums that are widely used in mineral flotation adsorb through the interaction with mineral surface metal-hydroxylated species as shown in Figure 2.9. According to this theory, the hydroxyl groups on mineral surfaces can either donate or accept a proton, thus behaving as a Brønsted acid or Brønsted base. The reaction mechanism proposed between the hydroxyl groups in polysaccharides and the mineral surface metal hydroxyls is shown schematically in Figure 2.9.

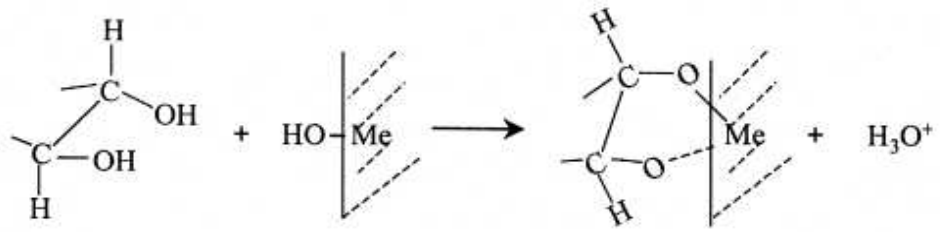

Figure 2.9: Schematic representation of the interaction of the polysaccharide molecules and metal-hydroxylated species on the mineral surface (Liu et al., 2000)

The extent of the acid/base interaction probably determines whether the adsorption is hydrogen bonding or chemical complexation. If it is assumed that a given polysaccharide behaves as an acid with a fixed acidity scale, then the degree of basicity of an adsorption substrate (such as a mineral surface) will dictate the intensity of the polysaccharide–mineral interaction. The higher the basicity, the stronger will be the interaction, and vice versa. It follows that at the "strong interaction" end, the acid–base interaction may manifest itself as a strong chemical interaction, whereas at the "weak interaction" end it is manifested as a hydrogen bond (Laskowski *et al.,* 2007).

If the acid/base interaction hypothesis as discussed is valid, polysaccharide adsorption will depend on the valence states, ionic radii and coordination numbers of the metal ions on the mineral surfaces. These characteristics contribute to the basicity of the surface hydroxyl groups, which then dictate the interaction with natural polysaccharides (Liu *et al.,* 2000).

2.5 THE ELECTRICAL DOUBLE LAYER

An electrical double layer is a system in which there exists a separation of electrical charge at an interface; that is, there is a layer of positive charge and a layer of negative charge, with the whole system being electrically neutral (Fuerstenau, 1982). A schematic representation of the electrical double layer at the mineral-water interface is shown in Figure 2.10. The figure shows the charge on the solid surface and the diffuse layer of

counter ions extending out into the aqueous phase and the drop in potential across the double layer. The closest distance of approach of counter ions to the surface (δ) is called the Stern plane. The surface potential is ψ_0 and at the Stern plane the potential is $\psi_{\delta,}$. The potential drops to zero in the bulk of the solution (Rao, 2004, Fuerstenau and Pradip, 2005).

When a particle migrates in an electric field, the layer of liquid immediately adjacent to the particle moves with the same velocity as the particle. The actual distance from the surface at which the relative motion sets in between the stationary layer and the mobile fluid is referred to as the surface of shear. It occurs within the double layer, at a location usually taken as equivalent to the Stern surface as the surface of shear. The potential at the surface of shear is defined as the zeta potential, ζ (mV). It is presumed to be close to the Stern potential, ψ_δ, in magnitude and obviously lower than the surface potential, ψ_0 (Rao, 2004).

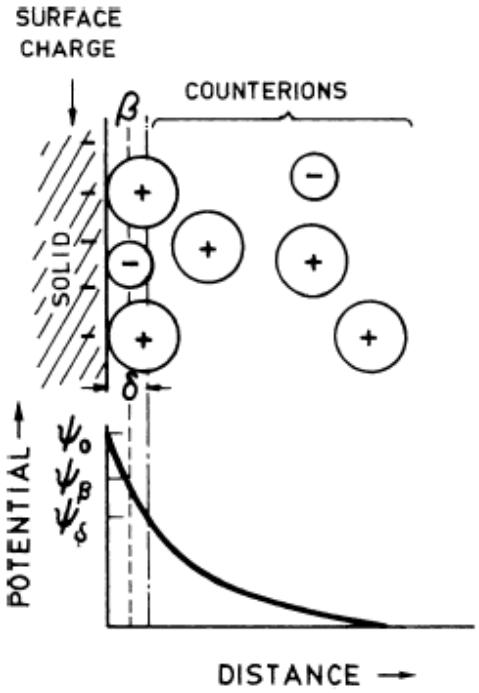

Figure 2.10: Schematic representation of the electrical double layer at the mineral-water interface (adapted from Fuerstanau and Pradip, 2005)

Since adsorption phenomena at mineral-water interfaces are controlled in most cases by the electrical double layer, an understanding of the factors responsible for the charge on the mineral surface, and the behaviour of ions that adsorb as counter-ions to maintain electro-neutrality, is crucial (Fuerstenau, 1982).

Electrokinetic studies by Rath *et al.*, (1997) investigated the variation in zeta potential of talc particles as a function of pH in the absence and presence of different concentrations of dextrin. In the absence of dextrin, the zeta potential of talc was negative in the entire pH range investigated. This finding was also confirmed by Morris *et al.*, (2002), who found that for pH values higher than 2, the zeta potential of talc is negative and increases in magnitude with pH. In terms of the effect of ions in solution on the zeta potential, Martinovic (2004) showed that Ca^{2+} ions adsorbed strongly on pyroxene, chromite, talc, and quartz, compared to K^{+} ions, causing a change in the zeta potential, particularly at alkaline values. It is important to note that the adsorption of Ca^{2+} ions on the mineral surfaces has the potential to mask the surface charge of each mineral resulting in non-selective adsorption of depressant onto the mineral surface.

2.6 ADSORPTION SELECTIVITY OF POLYMERIC DEPRESSANTS IN MIXED MINERAL SYSTEMS

As can be seen in the information presented above, extensive work has been done in trying to understand the mechanisms involved in the adsorption of polymeric depressants onto talc. However, not much is known about the selectivity of these depressants in mixed mineral systems. Many studies by researchers like Wang and Somasundaran, (2005); Lui *et al.*, (2006); Chiem *et al.*, (2006); Khraisheh *et al.*, (2005); Cuba-Cheim et al., (2008); and Morris *et al*., (2002) have focussed on the equilibrium adsorption isotherms to explain the adsorption of depressants onto minerals, particularly talc. However this is an artificial environment in which the depressant is given enough time to adsorb to the mineral, thus kinetics are not considered, and competitive adsorption between different minerals is not considered.

Furthermore, laboratory batch flotation tests conducted using guar and CMC by Wiese *et al.,* 2008 showed that at plant depressant dosages of up to 300g/ton very little depressant remained in solution. This suggests that the minerals were under conditions of competitive adsorption. Work conducted by Smeink *et al.,* (2004) investigated the use of ToF-SIMS to investigate the preferential adsorption of Depramin, a cellulose based depressant on a PGM ore sample. Their work was based upon developing the method as such, rather than relating flotation performances to differences in reagent distributions. The preferential adsorption of depressant onto one mineral relative to another in mixed mineral systems remains an area in flotation research which is not well understood.

2.7 RESEARCH OBJECTIVES, KEY QUESTIONS AND HYPOTHESIS

The overall objective of this work is to investigate the relative adsorption of polymeric depressants onto pure minerals. Pure minerals used in this investigation are chalcopyrite and gangue minerals typically found in Merensky and UG2 ore which include talc, pyroxene, plagioclase and chromite.

The following key questions are addressed in this work:

6. What role do differences in the surface charge of each mineral play in the relative adsorption of depressants onto the mineral surface?
7. What role do metal ions in solution play in modifying the mineral surface charge, and therefore changing the adsorption characteristics?
8. Which mineral has the highest affinity for polymer in a single mineral system?
9. Which mineral has the highest rate of depressant adsorption in a single mineral system?
10. In a mixture of minerals, which mineral has the highest affinity for the polymer?

The following hypothesis is put forward:

Depressants adsorb preferentially onto different minerals because:

- There are differences in mineral surface charge arising from the differences in their chemical structures
- There are differences in the equilibrium and kinetic adsorption characteristics of each mineral towards depressant molecules.

3 EXPERIMENTAL METHODS

3.1 MINERALS

3.1.1 Sample preparation

Minerals used in this investigation were talc, plagioclase, pyroxene, chromite and chalcopyrite. Talc and chalcopyrite were obtained from Wards Natural Science Establishment. Plagioclase and pyroxene were hand-picked from plagioclase and pyroxene rich Merensky ores, respectively, supplied by Anglo American Research. UG2 chromite was also supplied by Anglo American Research. These minerals were ground using a ring pulveriser to 100 percent passing 25μm for zeta potential experiments, and 100 percent passing 38μm for all adsorption and microflotation studies. Furthermore, a -106 + 53 micron talc sample was prepared for microflotation experiments. Chalcopyrite was stored in a freezer to minimise oxidation.

3.1.2 Mineral characterisation

The surface area of each mineral in each size class was determined using the BET method. This is shown in Table 3.1.

Table 3.1: BET surface area of each mineral in each size class

Mineral	**BET surface area (m^2/g)**		
	-25μm	**-38μm**	**+53 -106μm**
Talc	10.7	13.8	2.43
Plagioclase	1.24	1.23	-
Pyroxene	2.26	1.28	-
Chromite	0.81	0.86	-
Chalcopyrite	0.94	1.06	-

X-ray diffraction (XRD) was used to determine the relative purity of each mineral. Powder XRD spectra were obtained by using a Bruker D8 Advance powder

diffractometer with Vantec detector and fixed divergence and receiving slits with Co-Kα radiation. The phases were identified using Bruker Topas 4.1 software and the relative phase amounts (weight %) were estimated using the Rietveld method. Furthermore, electron microprobe experiments were carried out on each mineral to determine the elemental composition. Microprobe experiments conducted using the Electron Microprobe GEOL-JXA 8100 provided by the Geology Department, UCT. Thin sections of each mineral were carbon coated, then subjected to a probe current of 20A, and an accelerating voltage of 15kV. Measurements were done on two spots per slide.

3.2 REAGENTS

3.2.1 Matrix solutions

Deionised Millipore water was used to prepare di-sodium tetraborate (10^{-3}M $Na_2B_4O_7{\cdot}10H_2O$, IS=3 $x10^{-3}$ M), calcium nitrate ($Ca(NO_3)_2$, $3.3x10^{-3}$M, IS = 10^{-2}M) solution and synthetic plant water (IS = $2x10^{-2}$ M). The ionic strength of each solution was calculated using Equation 3.1, where μ is the ionic strength (mol/L), c_i is the concentration of the ion (mole/L) and z_i is the valency of the ion.

$$\mu = \frac{1}{2}\sum c_i \cdot z_i^2 \qquad (3.1)$$

Di-sodium tetraborate was chosen because of its buffering capacity. These solutions were used as background electrolytes for all zeta potential, adsorption and microflotation experiments. Hydrochloric acid (HCl) and sodium hydroxide (NaOH) were used for pH adjustment. Furthermore, dilute HCl (0.01M) was used to acid wash oxidised species on chalcopyrite. Fresh $Na_2B_4O_7{\cdot}10H_2O$ buffer and 10^{-2}M IS Ca^{2+} solution were prepared daily and SPW was prepared in 10L batches. All the above mentioned reagents were analytical grade reagent.

3.2.2 Synthetic plant water (SPW)

De-ionised water was modified by the addition of various chemical salts of analytical grade quality (Table 3.3) to produce synthetic plant water with an ionic strength of

2 x10^{-2} M. The synthetic plant water contained similar amounts of key ions found typically in circuit water as shown in Tables 3.2 and 3.3 (Malysiak, 2003; Wiese, 2009). This standard SPW recipe is used for all batch flotation tests at the Centre for Minerals Research (CMR), UCT.

Table 3.2: Synthetic plant water composition

Ions present	Ca^{2+}	Mg^{2+}	Na^{+}	Cl^{-}	SO_4^{2-}	NO_3^{2-}	CO_3^{2-}	TDS
Concentration (ppm)	80	70	153	287	240	176	17	1023

Table 3.3: Synthetic plant water recipe

Chemical compound	**Formula**	**Mass per litre (g/L)**
Magnesium sulphate	$MgSO_4 \cdot 7H_2O$	0.615
Magnesium nitrate	$Mg(NO_3) \cdot 6H_2O$	0.107
Calcium nitrate	$Ca(NO_2)_2 \cdot 4H_2O$	0.236
Calcium chloride	$CaCl_2$	0.111
Sodium chloride	NaCl	0.356
Sodium carbonate	Na_2CO_3	0.030

3.2.3 Depressants

Depressants used in this investigation were guar gum (Sendep 369) and CMC (Finnfix 700) supplied by Senmin. These were characterised in the Polymer Characterisation Lab, CMR, UCT as shown in Table 3.4. Depressant stock solutions (1000mg/L) were prepared by weighing out the required amount of dry depressant on an active content basis (see Appendix 3). Solvent was added and then left overnight on a magnetic stirrer to hydrate the dry depressant. All depressant stock solutions were stored in a fridge to prevent their degradation. Fresh stock solutions were prepared every five days.

Table 3.4: Depressant characterization

Depressant	**Molecular weight**	**Purity (%)**	**Insolubles (%)**	**Moisture content (%)**
Sendep 369	279500	88.1	7.56	9.04
Finnfix 700	425798	97.8	0	8.70

3.3 ZETA POTENTIAL MEASUREMENTS

In flotation studies, the most sought after electrokinetic quantity is the zeta potential. As previously mentioned, the development of a net charge at the particle surface affects the distribution of ions surrounding the interfacial regions. This results in an increased concentration of counterions close to the surface. The potential that exists at the boundary is known as the zeta potential (Malvern Instruments, 2005). By measuring the electrophoretic mobility, and hence the zeta potential over a range of pH under specified conditions, the isoelectric point of the mineral can be determined.

3.3.1 Theory

When an electric field is applied across an electrolyte, charged particles suspended in the electrolyte are attracted towards the electrode of opposite charge as depicted in Figure 3.1

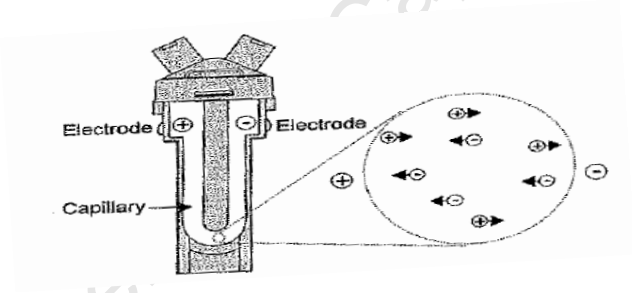

Figure 3.1: The movement of particles in a folded capillary cell (adapted from Malvern Instruments, 2005)

Viscous forces acting on the particles tend to oppose this movement. When equilibrium is reached between these two opposing forces, the particles move with constant velocity. The velocity of the particles is dependant on the strength of the electric field, the dielectric constant, the viscosity of the medium and the zeta potential. The velocity of a particle is referred to as the electrophoretic mobility (Malvern Instruments, 2005; Hunter, 2001; Rao, 2004). The zeta potential of the particle can be calculated from the electrophoretic mobility by the application of the Henry equation:

$$U_E = \frac{2 \cdot \varepsilon \cdot \zeta \cdot f(\kappa a)}{3 \cdot \eta} \qquad (3.2)$$

In this equation, U_E is the electrophoretic mobility, ζ is the zeta potential, ε is the dielectric constant, *f(κa)* is the Henry function and η is the viscosity. Electrophoretic determinations of the zeta potential are commonly made in aqueous media and moderate electrolyte concentration where *f(κa)* in this case is 1.5. This is referred to as the Smoluchowski equation.

$$U_E = \frac{\varepsilon \cdot \zeta}{\eta} \qquad (3.3)$$

3.3.2 Experimental programme

Zeta potential experiments were conducted using the Malvern Zeta Sizer Nano Series shown in Figure 3.2.

Figure 3.2: Malvern Zeta Sizer Nano series

Zeta potential measurements for each mineral were carried out in 10^{-3}M $Na_2B_4O_7 \cdot 10H_2O$, IS=3.3x10^{-3} buffered solution, 10^{-2}M IS $Ca(NO_3)_2$ solution and SPW as background electrolytes. Zeta potential measurements done in buffer alone were used as a reference case from which all other test conditions would be compared. SPW and 10^{-2}M IS Ca^{2+} solution were used to test the effect of the addition of ions in solution on the mineral surface charge. A 0.075g mineral sample was dispersed in 60ml of each

background electrolyte. The pH was adjusted using HCl and NaOH from pH 2 to 10 in buffer and SPW, and pH 8 to 10 in 10^{-2}M IS Ca^{2+} solution in the absence of depressant.

To test the effect of depressant addition on the zeta potential, depressant stock solutions were made such that the concentration was sufficient to give five pseudo-monolayers (see Appendix 3 for calculation). The required amount of dried depressant was weighed out and hydrated in each background electrolyte overnight. Fresh stock solutions were prepared every five days. The guar stock solution was filtered using 0.45μm Millipore filter paper to remove any insolubles in solution before each mineral was conditioned with depressant. A detailed experimental procedure is given in Appendix 4. Tables 3.5 and 3.6 give a detailed experimental matrix with all zeta potential tests done in triplicate in the absence of depressant, and in duplicate with depressant.

Table 3.5: Experimental matrix without depressant

Mineral	**Experimental conditions**					
	Buffer	**pH range**	**SPW**	**pH range**	**10^{-2}M IS Ca^{2+}**	**pH range**
Talc	x	2. - 10	x	2. - 10	x	8. - 10
Pyroxene	x	2. - 10	x	2. - 10	x	8. - 10
Plagioclase	x	2. - 10	x	2. - 10	x	8. - 10
Chromite	x	2. - 10	x	2. - 10	x	8. - 10
Chalcopyrite	x	2. - 10	x	2. - 10	x	8. - 10

Table 3.6: Experimental matrix with depressant

Mineral	**Experimental conditions**				
	Buffer + guar	**SPW + guar**	**CMC + buffer**	**CMC + 10^{-2}M IS Ca^{2+}**	**pH range**
Talc	x	x	x	x	8. - 10
Pyroxene	x	x	x	x	8. - 10
Plagioclase	x	x	x	x	8. - 10
Chalcopyrite	x	x	x	x	8. - 10
Chromite	x	x	x	x	8. - 10

3.4 ADSORPTION EXPERIMENTS

Adsorption studies were carried out in order to quantify and compare the amount of depressant in solution before and after exposure to each mineral. Equilibrium adsorption studies were conducted to quantify the relative adsorption of depressant on different minerals by comparing the maximum adsorption density of depressant on each mineral. Kinetic tests were conducted to investigate if depressant adsorption on different pure minerals was affected by the initial adsorption rates. All adsorption experiments were carried out at 25°C and pH 9 in the Ecobath shaker bath shown in Figure 3.3 at 140 revolutions per minute. Residual depressant in solution was determined by the du Bois phenol sulphuric method outlined in Section 3.4.1.

Figure 3.3: Ecobath shaker-bath

3.4.1 Kinetic studies

Kinetic tests were initially carried out over a 24 hour period for guar, and then reduced to 6 hours for CMC as it was found that equilibrium had been reached in that time. An initial depressant concentration of 100mg/L was maintained for all kinetic tests. This was done by measuring 10mL of depressant from a 1000mg/L stock solution into 100mL volumetric flasks, and diluting with SPW for guar and 10^{-2}M IS $Ca(NO_3)_2$ for CMC. A

mass of mineral sufficient to give $2m^2$ surface area was weighed into a conical flask for each mineral.

Each mineral was conditioned in depressant for 15s, 30s, 45s, 1min, 2 min, 5 min, 10 min, 20 min, 30 min, 1h , 2h, 4h , 6h and 24hrs in separate flasks in the shaker bath. After conditioning, the contents of each conical flask were immediately filtered under a vacuum using 0.45μm Millipore filter paper. The filtrate from each conditioning flask was analysed for residual depressant using the du Bois phenol sulphuric method (du Bois *et al.*, 1956) outlined below.

1. 1ml of each test solution was dispensed into glass test tubes
2. A blank was prepared by adding 1mL of matrix solution to a separate test tube
3. 1ml of 5 volume% phenol was added to each test tube
4. 5ml concentrated sulphuric acid was dispensed rapidly into the middle of the liquid surface in each test tube.
5. Each test tube was immediately placed on the vortex stirrer and stirred for 5 seconds. The reaction was allowed to run to equilibrium in a fume cupboard for 40 minutes (Wiese, 2009; Parolis *et al.*, 2005)
6. The absorbance of each solution was measured at 490nm in plastic cuvettes using a UV-VIS spectrophotometer

Calibration curves for each depressant were prepared as shown in Figure 3.4 and 3.5. All experiments were done in duplicate.

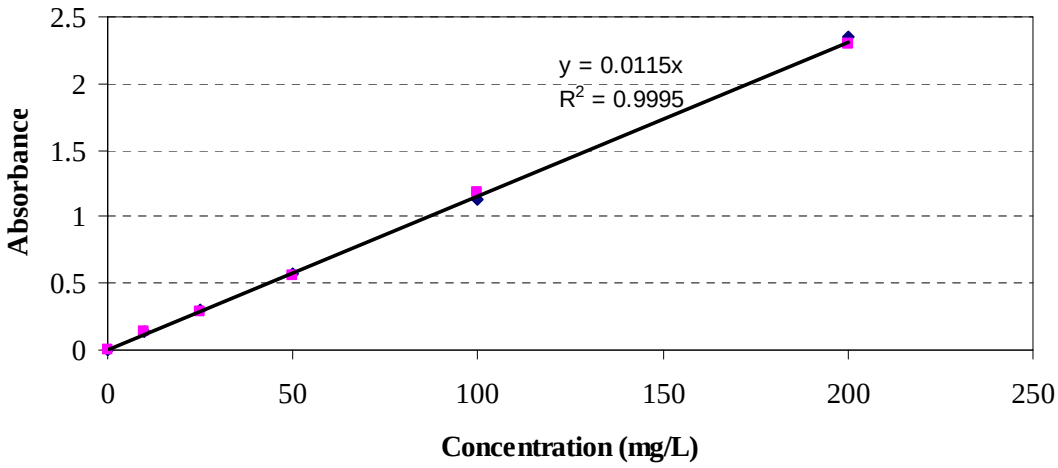

Figure 3.4: Guar calibration curve

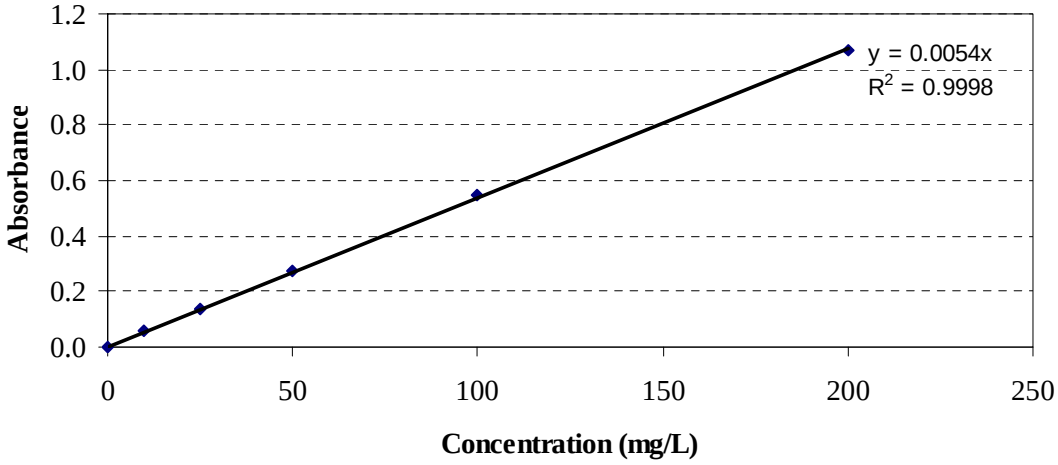

Figure 3.5: CMC calibration curve

3.4.2 Equilibrium studies

Equilibrium experiments were conducted by conditioning each mineral in depressant solution with different initial concentrations and allowing each experiment to run until it reached equilibrium. A mass of mineral sufficient to give $2m^2$ surface area was weighed into each of the twelve conical flasks. Depressant solutions of different initial

concentrations (10, 15, 20, 25, 30, 40, 50, 60, 70, 80, 90, 100mg/L) were prepared by pipetting different volumes of depressant from a 1000 mg/L stock solution, and diluting it with the required matrix solution in a 100ml volumetric flask. To test the effect of ions in solution on depressant adsorption characteristics of each mineral, adsorption experiments were conducted in buffer and SPW for guar and in buffer and 10^{-2}M IS Ca^{2+} solution for CMC at pH 9.

The $2m^2$ mineral sample was allowed to condition with the increasing concentrations of depressant for 4 hours in the shaker bath at 25°C. After conditioning, the contents of each flask were centrifuged for 10 minutes in a Hettich Zentrifugen Rotofix 32 at 5000 revolutions per minute. Analysis for residual depressant in solution using the du Bois phenol sulphuric method was then done on 1ml aliquots of supernatant liquid from each flask. All experiments were done in duplicate.

3.5 MICROFLOTATION EXPERIMENTS

The UCT Microflotation Cell was developed by Bradshaw and O'Connor (1996) to measure bubble loading in a microflotation cell. It has also been used extensively to investigate the hydrophobicity of pure and mixed mineral systems upon the addition of different reagents. In this investigation, the microflotation response of talc after conditioning in the presence of an added mineral at starvation concentrations of depressant, was used as a diagnostic of the extent to which depressant adsorbs onto one mineral relative to another.

3.5.1 Microflotation cell description

The cell consists of a conical tapered cylindrical tube with air introduced into the cell as the flotation gas via a syringe needle. Gas bubbles rise through the cell, passing through the pulp where collision between bubbles and talc particles occurs. The rising talc-loaded bubbles are deflected off the cone at the top off the column where they burst and any attached talc is collected as concentrate in the launder. After set times the needle was

removed and the particles in the launder were recovered as concentrate. An air flowrate of 7 ml/min was maintained throughout the experiments. The peristaltic pump flowrate was set to maintain a good particle suspension in the cell and kept constant throughout the experiments (Wesseldijk *et al.*, 1999; Bradshaw and O'Connor, 1996; Malysiak, 2003).

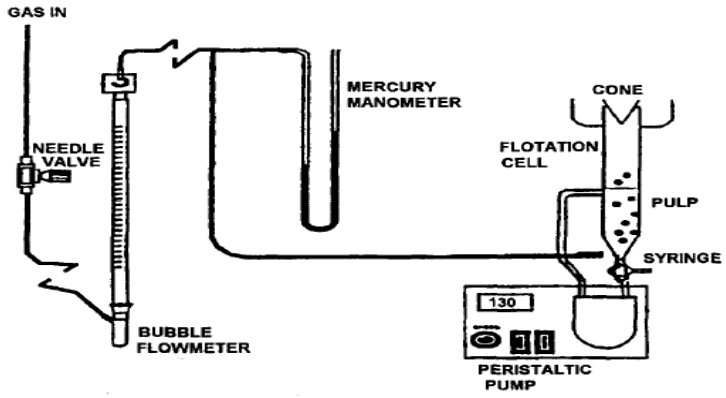

Figure 3.6: UCT Microflotation flow-through cell (adapted from Wesseldijk et al., 1999)

3.5.2 Experimental programme

Unlike the other minerals in question, talc is naturally hydrophobic and floats readily in the microflotation cell. A 2g sample of talc (+53-106μm, Total BET surface area = 4.86m^2) was conditioned in 350ml of 0.25 mg/L depressant solution for 10 minutes in a beaker. The depressant concentration was specially chosen by trial and error such that the talc sample was almost completely depressed, while leaving no residual depressant in solution. The mixture was sonicated in an ultra sonication bath to ensure good dispersion of the mixture and then transferred to the microflotation cell. SPW was then added to fill the rest of the column.

The microflotation experiment was initiated by inserting the needle at the bottom of the cell to introduce bubbles into the system. Concentrate was collected at 2, 6, 12 and 20 minutes. Tails were also collected at the end of each run. These samples were filtered and

then dried overnight in an oven. Each concentrate was weighed enabling the calculation of the recovery at each time period. This was done in duplicate and resulted in the "baseline" case.

In the following series of experiments, the 2g talc sample was then conditioned for 10 minutes in 350ml of 0.25mg/L depressant in the presence of a second mineral (chromite, plagioclase, pyroxene, chalcopyrite, talc) with a smaller size fraction (100% passing 38 μm). The mixture was then sonicated and the secondary mineral was sieved off. The 2g talc sample was then transferred from the sieve to the microflotation cell using SPW. Concentrate was collected at 2, 6, 12, and 20 minutes, and tails were collected at the end of each experiment. These samples were filtered, dried overnight and weighed to enable the calculation of the recovery.

The theory governing the analysis of these experiments is that, the 2g sample of talc would have a low recovery if it was conditioned alone at the given depressant concentration. This would result from a high adsorption density of depressant, thus a high depression of the talc sample. With the addition of a second mineral in the conditioning beaker, a decrease in the adsorption density of depressant on the talc sample was expected, resulting in a higher talc recovery in the microflotation cell. A higher talc recovery was expected in the microflotation cell as the BET surface area of the second mineral was increased. The BET surface area of the added mineral was increased from $2m^2$ to $4.86m^2$ to $6m^2$. A detailed matrix showing the amount of added mineral in the conditioning beaker is given in Table 3.7.

Table 3.7: Microflotation experimental matrix

	Guar in SPW			**CMC in 10^{-2} M IS $Ca(NO_3)_2$**		
	Mass of second mineral (g)			**Mass of second mineral (g)**		
BET surface area (m^2)	**2**	**4.86**	**6**	**2**	**4.86**	**6**
Chromite	2.321	5.637	6.963	2.321	5.637	6.963
Plagioclase	1.627	3.952	4.881	1.627	3.952	4.881
Pyroxene	1.558	3.785	4.674	1.558	3.785	4.674
Talc	0.145	0.352	0.435	0.145	0.352	0.435
Chalcopyrite	1.881	4.568	5.642	1.881	4.568	5.642

3.6 STATISTICAL TOOLS

All experiments in this section were either done in duplicate or triplicate. To quantify the variance in the data, the following statistical methods were used:

Suppose $y_1, y_2, y_3 \ldots y_i$ represent a sample, the sample mean is defined as:

$$\bar{y} = \frac{\sum_{i=1}^{n} y_i}{n} \tag{3.4}$$

where $\bar{y}$ is the sample mean, n is the number of observations. The sample variance is defined as:

$$S^2 = \frac{\sum_{i=1}^{n} (y_i - \bar{y})^2}{n-1} \tag{3.5}$$

These quantities are measures of the central tendencies and dispersion of the sample. The standard deviation defined in Equation 3.5 is also used as a measure of dispersion (Scheaffer and McClave, 1995).

$$S = \sqrt{S^2} \tag{3.6}$$

The standard error defined provides a confidence value of the sample mean. If S is the standard deviation of an individual observation, and there are n replicates, the standard error can be calculated as shown in Equation 3.7. The standard error will be represented as error bars on each figure in the results (Chapter 4)

$$s_{\bar{y}} = \frac{S}{\sqrt{n}} \tag{3.7}$$

4 RESULTS

4.1 MINERAL CHARACTERISATION

4.1.1 XRD Results

Table 4.1: XRD results - mineral components

Mineral sample	Source	Components	Abundance (%)
Talc	Balmat	Talc	71
		Quartz	29
Plagioclase	Merensky	Anorthite 65	100
Pyroxene	Merensky	Enstatite	83.5
		Diopside	13
		Talc	2.2
		Biotite	1.2
Chromite	UG2	Chromite	100
Chalcopyrite	Durango, Mexico	Chalcopyrite	100

Table 4.1 shows the XRD results for each mineral. This technique was used to quantify the components of each sample, thus giving an idea of its purity. The results show that chalcopyrite, chromite, and plagioclase were of high purity. Pyroxene showed a high percentage of enstatite (84%), and diopside (13%) which is the magnesium rich end-member of the clinopyroxene group. The pyroxene sample also contained some talc and biotite. Talc is an alteration product of orthopyroxene and has been found to form in rims on orthopyroxene particles. The talc sample was of relatively high purity with some quartz as an impurity.

4.1.2 Microprobe results

Table 4.2: Elemental composition of each mineral

Mineral	SiO_2	Na_2O	TiO_2	CaO	MgO	Cr_2O_3	S	Cu	FeO	Al_2O_3	MnO	K_2O	NiO	Total
Talc	62.2	0.08	0.03	0.01	31.6	0.06	-	-	0.07	0.13	0.058	-	-	94.2
Plagioclase	51.2	2.84	-	15.0	-	-	-	-	0.33	30.7	0.015	0.170	-	100
Pyroxene	53.3	0.03	0.16	1.80	29.3	0.47	-	-	13.1	1.25	0.303	-	-	99.9
Chromite	-	-	0.72	-	9.09	45.6	-	-	28.1	16.1	0.431	-	0.253	100
Chalcopyrite	-	-	-	-	-	-	35.1	34.2	30.7	-	-	-	-	99.9

Microprobe results as shown in Table 4.2 showed a high percentage of SiO_2 and MgO for talc which agree very well with literature (31.7% MgO and 63.5% SiO_2, (Klein, 2002). Trace amounts of TiO_2, CaO, Na_2O, Cr_2O_3, FeO, Al_2O_3 and MnO were found. The small amounts of Al or Ti may substitute for Si, and Fe may substitute for Mg (Klein, 2002). With plagioclase high percentages of SiO_2 (51.15%), CaO (14.9%) and Al_2O_3 (30.7%) were obtained. Trace amounts of FeO, MnO, Na_2O and K_2O were also found. Plagioclase feldspars form an essentially complete solution series which extend from pure albite ($NaAl_sSi_3O_8$) to pure anorthite ($CaAl_2Si_2O_8$). Considerable potassium may be present especially at the albite end of the series. End-member calculations show an $An_{84}Al_{16}$ (84% Anorthite and 16% Albite) combination in the plagioclase sample (Deer *et al.*, 1998).

Microprobe results for pyroxene showed a very high percentage of SiO_2 (51.15%) as expected for any silicate, and significant amounts of MgO (29.34%) and FeO (13.17%). Trace amounts of Na_2O, TiO_2, CaO, Cr_2O_3, Al_2O_3 and MnO. End-member calculations show $En_{69}Fe_{31}$ (69% Enstatite and 31% Ferrosilite) mix within the pyroxene sample. Chromite ($FeCr_2O_4$) was found to contain significant amounts of Cr_2O_3, FeO, Al_2O_3 and MgO as commonly reported in literature (Klein, 2002; Deer *et al.*, 1998).

4.2 ZETA POTENTIAL RESULTS

4.2.1 Method validation

Before carrying out zeta potential experiments on the full suite of minerals, six replicates of zeta potential tests were carried out on NY talc in a 10^{-3}M $Na_2B_4O_7 \cdot 10H_2O$,IS =$3.3x10^{-3}$ buffered solution. This was done firstly to ensure consistency between experiments, and thus reproducible results, and secondly, to validate the method against existing literature.

Table 4.3: Zeta potential of NY talc as a function of pH in 10^{-3}M $Na_2B_4O_7 \cdot 10H_2O$, IS =$3.3x10^{-3}$ M

pH	Zeta potential (mV)								
	Run 1	**Run 2**	**Run 3**	**Run 4**	**Run 5**	**Run 6**	**Mean**	**Std. dev.**	**Std. error**
4	-26.7	-23.2	-33.7	-17.5	-26.0	-26.8	-25.4	6.79	2.77
6	-32.5	-32.0	-33.1	-23.6	-31.0	-38.2	-30.4	4.50	1.84
8	-36.3	-34.9	-36.7	-38.1	-34.7	-45.8	-36.1	1.32	0.54
10	-41.3	-49.4	-51.0	-49.3	-46.9	-52.4	-47.6	4.37	1.78

Table 4.3 shows the zeta potential of talc at pH 4, 6, 8 and 10. The results showed slight deviations from the mean between run 3 and 4 at pH 4, run 4 and 5 at pH 6, run 6 at pH 8, and run 1 at pH 10. Although these deviations from the mean were observed, there seemed to be a good degree of reproducibility between replicates, as seen by the low standard error. This was generally the case for all tests in this section.

When compared to existing literature, the experimental results were acceptable as seen in Figure 4.1 which shows a comparison between experimental and literature results for the zeta potential of NY talc as a function of pH. Literature values were obtained from Fuerstenau and Huang (2003). Although literature and experimental values were obtained using different background electrolytes (10^{-2}M potassium nitrate - KNO_3 and 10^{-3}M $Na_2B_4O_7 \cdot 10H_2O$ respectively), there was a good correlation between the two data sets.

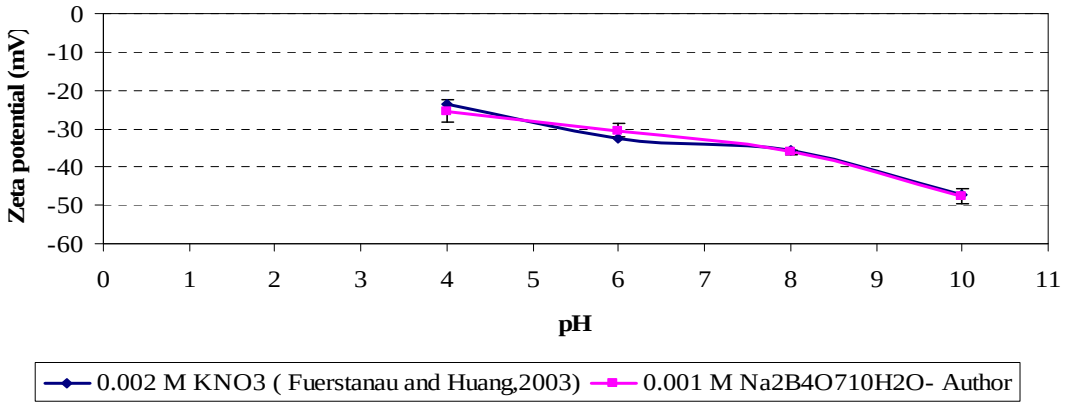

Figure 4.1: Comparison between experimental and literature results of the variation of the zeta potential of NY talc with varying pH

4.2.2 Variation of zeta potential of different pure minerals in a 10^{-3}M $Na_2B_4O_7 \cdot 10H_2O$, IS=3.3x10^{-3} M buffered solution and synthetic plant water (SPW)

The following results show the variation of the zeta potential with pH on pure minerals in 10^{-3}M $Na_2B_4O_7 \cdot 10H_2O$, IS=3.3x10^{-3} M buffer and SPW as matrix solutions. The zeta potential in buffer for each of the minerals was used as a reference case against which all other tests would be compared. The effect of the presence of ions in solution on the surface charge was tested by the use of SPW as a matrix solution.

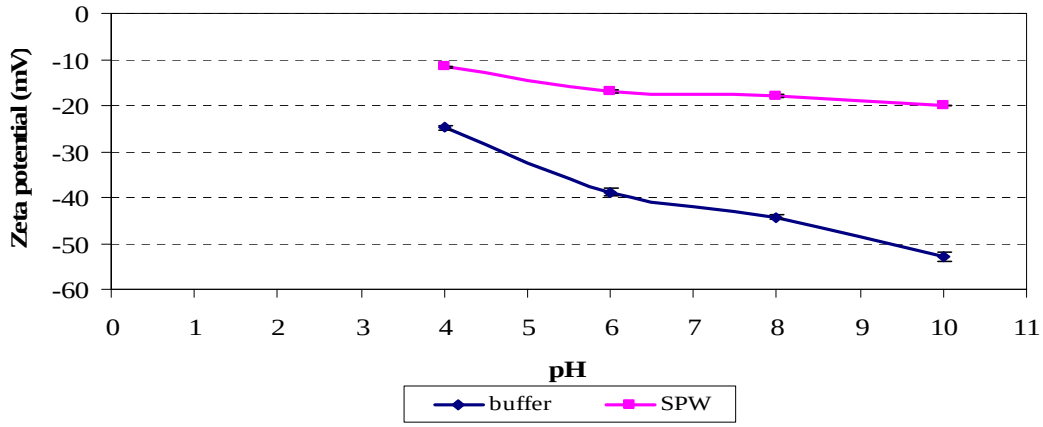

Figure 4.2: Zeta potential of talc as function of pH in 10^{-3}M $Na_2B_4O_7 \cdot 10H_2O$, IS=3.3x10^{-3} M buffered solution and SPW

Figure 4.2 shows the variation of zeta potential of NY talc with pH in buffered solution and SPW. In buffer, the zeta potential became more negative as pH increased from pH 4 to pH 10, indicating an increase in negative surface charge as pH was increased. As will be explained later, this probably reflects the surface charge on the basal planes of talc. In SPW, there was a significant positive shift in zeta potential as pH was increased from pH 4 to 10. This may be attributed to a masking effect by the ions in solution resulting in the compression of the electrical double layer.

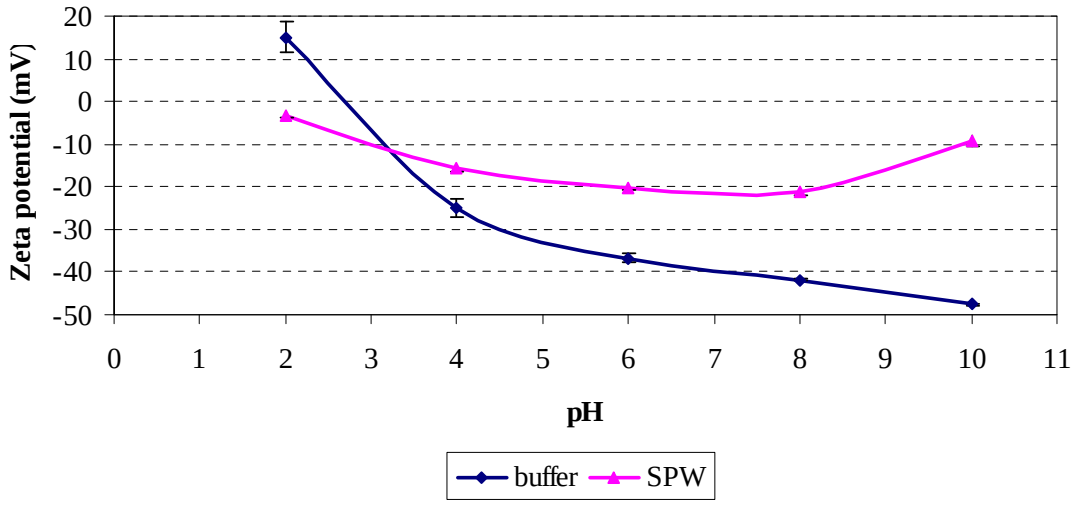

Figure 4.3: Zeta potential of pyroxene as a function of pH in 10^{-3}M $Na_2B_4O_7{\cdot}10H_2O$, IS=$3.3x10^{-3}$ M buffered solution and SPW

Figure 4.3 shows the zeta potential of pyroxene as a function of pH in 10^{-3}M $Na_2B_4O_7{\cdot}10H_2O$, IS =$3.3x10^{-3}$ buffered solution and in SPW. In buffered solution, the zeta potential was positive at pH 2, and become more negative as pH was increased from pH 2 to 10. The point of zero charge (PZC) was reached at approximately pH 3.2. Thereafter, the zeta potential became increasingly negative. This increasing negative charge as pH increased reflected a similar trend to that observed by Malysiak (2003), Malysiak *et al (*2002), when the same background electrolyte was used viz. 10^{-3}M $Na_2B_4O_7{\cdot}10H_2O$.

In SPW, a less negative zeta potential was observed as pH increased from pH 2 to 10. With the addition of ions in solution, the zeta potential became more negative at very

acidic conditions (pH 2), resulting in a lower PZC when compared to that in the buffer solution. However as the pH became more basic, the zeta potential became increasingly positive when compared to that observed in buffer. This effect is highlighted by the positive slope of the curve between pH 8 and 10.

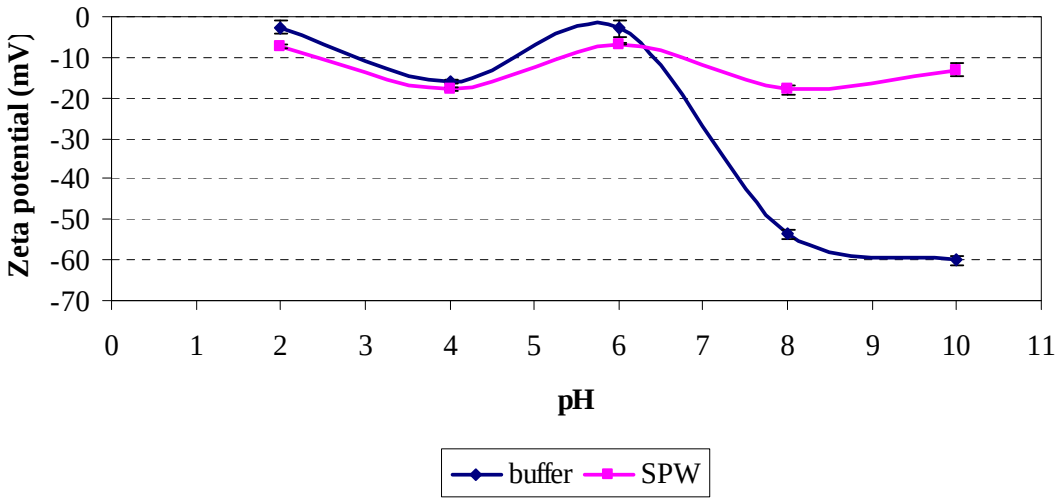

Figure 4.4: Zeta potential of plagioclase as a function of pH in 10^{-3}M $Na_2B_4O_7{\cdot}10H_2O$, IS =3.3x10^{-3} M buffer and SPW

Figure 4.4 shows the zeta potential of plagioclase as a function of pH in buffer and SPW. In buffered solution, the zeta potential became more negative as pH was increased. This was with the exception of a slight increase in the surface charge at approximately pH 6 in both buffer and SPW. As was observed by Gülgönül *et al.*, (2008), feldspar is negatively charged under most pH conditions, and the negativity increases with increasing pH. The PZC can be found by extrapolation to be around pH 1.5, which is in agreement with the previous studies (Gülgönül *et al.*, 2008; Fuerstenau and Fuerstenau, 1982; Rao and Forsberg, 1993).

The increase in the zeta potential at pH 6 was initially attributed to experimental error. However, repeat experiments carried out on subsequent days produced the same results, with good reproducibility, as observed by the very small error bars. This phenomena

deviates from electrokinetic studies carried out by other authors on feldspars as observed in Gülgönül *et al.,* (2007), Malysiak *et al*., (2002) and Karagüzel *et al.,* (2005).

In SPW, the same masking effect on the zeta potential resulting from the presence of ions in solution as shown in Figures 4.2-3 was seen with plagioclase. In very acidic conditions, i.e. at pH 2, the zeta potential in SPW was slightly more negative than that in buffer. The same "kink" in the curve was observed at pH 6. Between pH 8 and 10, the zeta potential became more positive as indicated by the positive slope between pH 8 and 10, probably caused by the interaction of the ions in solution and the mineral surface.

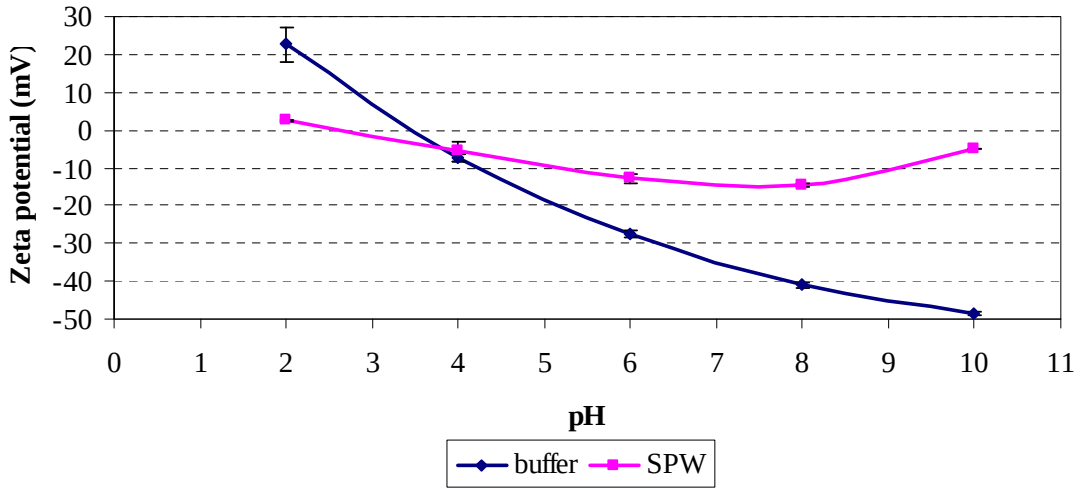

Figure 4.5: Zeta potential of chromite as a function of pH in 10^{-3}M $Na_2B_4O_7{\cdot}10H_2O$, IS=3.3x 10^{-3}M buffered solution and SPW

Figure 4.5 shows the zeta potential of chromite as a function of pH in buffered solution and SPW. In buffer, the results indicated a positive zeta potential at pH 2, which became more negative as pH increased to pH 10. A PZC was observed at approximately pH 3.5 which correlated well with other reported data (Wesseldijk *et al.*, 1999). A PZC as high as pH 6.5 has been reported by Palmer *et al.*, (1975). This highlights the differences in mineral composition in different ore samples. With the addition of ions in solution in

SPW, a decrease in the zeta potential at very acidic pH resulting in a lower PZC at about pH 2.6. When compared to that of buffer, the curve of SPW was significantly less negative, especially between pH 8 and 10.

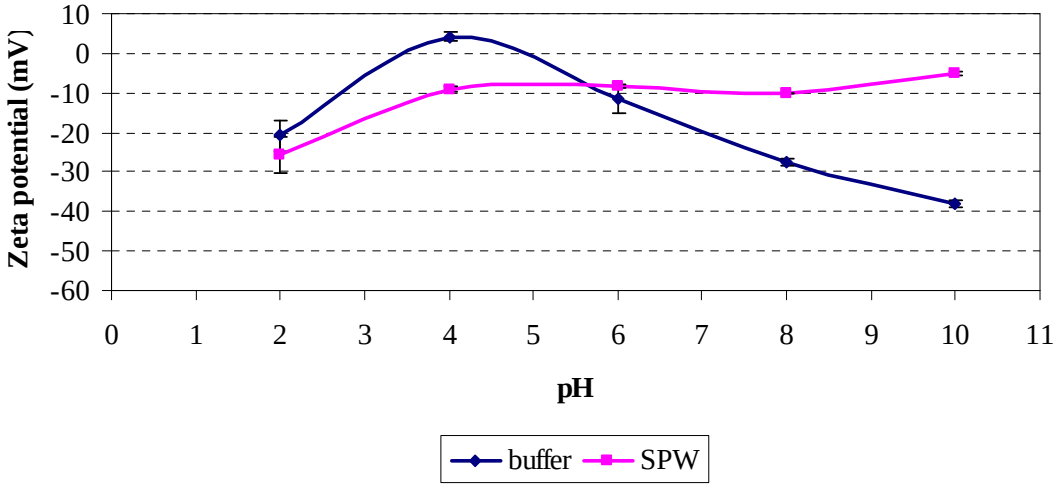

Figure 4.6: Zeta potential of chalcopyrite as a function of pH in 10^{-3}M $Na_2B_4O_7 \cdot 10H_2O$, IS =3.3x10^{-3} M buffer and SPW

Figure 4.6 shows the zeta potential of chalcopyrite as a function of pH in buffer and SPW. In buffered solution the zeta potential began at negative values at acidic pH, becoming more positive as the pH increased between pH 2 and 6. The PZC occurred at about pH 3.5 and pH 5, respectively. As the pH became more basic, the zeta potential became more negative. As was noted for the other minerals, the addition of SPW resulted in slightly less positive results at the acidic end of the range and less negative results at the basic end of the range.

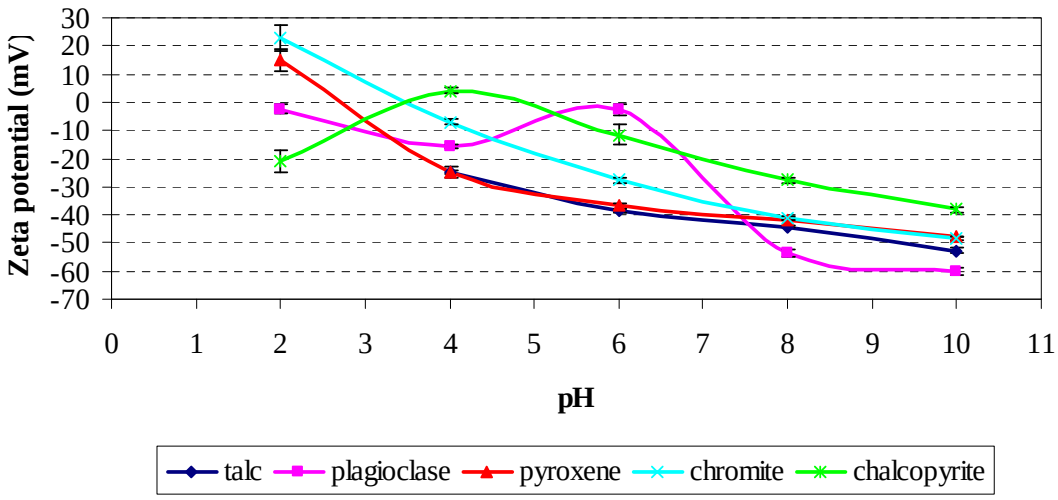

Figure 4.7: Zeta potential of all minerals as a function of pH in 10^{-3}M $Na_2B_4O_7 \cdot 10H_2O$, IS =3.3x10^{-3} M buffered solution

Figure 4.7 makes a comparison between the zeta potential as function of pH of all the pure minerals under investigation in buffered solution. The general trend observed was that the zeta potential became more negative as pH increased from pH 2 to 10. Of particular interest in this work, were the relative differences in zeta potential observed between pH 8 and 10 since this pH range encompasses plant operating pH i.e. pH 9 in sulphide and PGM concentrators in the Bushveld Complex.

Chalcopyrite had the most positive zeta potential, and plagioclase the most negative zeta potential between pH 8 and 10. Pyroxene and chromite had a similar zeta potential as observed by their curves which are superimposed on each other. Talc had a zeta potential which was similar to that of pyroxene and chromite. It is anticipated that these differences in surface charge may influence the adsorption characteristics of each mineral towards various polysaccharide depressant molecules.

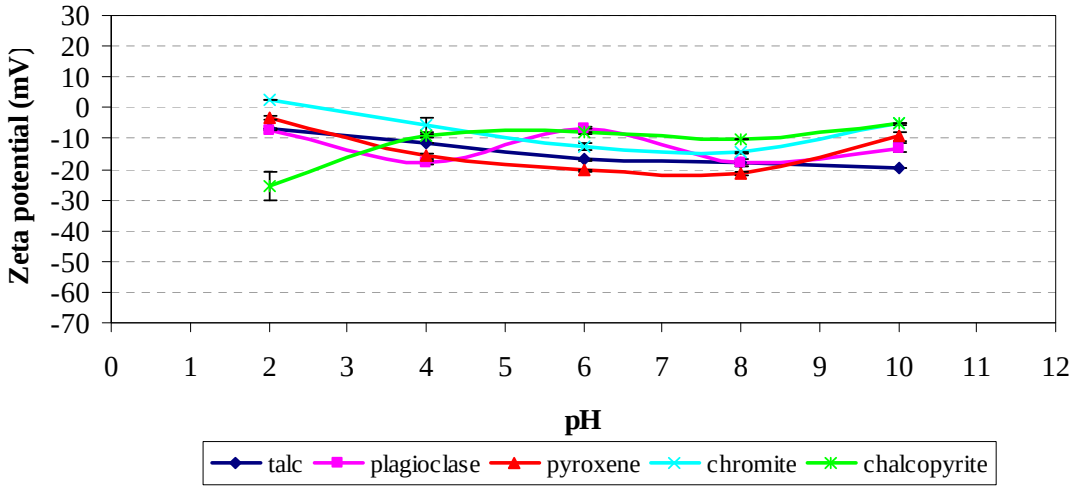

Figure 4.8: Zeta potential of all the minerals as a function of pH minerals in synthetic plant water

Figure 4.8 makes a comparison of the zeta potential as a function of pH for all minerals in SPW. This was shown in the same scale as Figure 4.8 to emphasize the effect of the addition of ions in solution in SPW. As previously mentioned, upon the addition of ions in solution in SPW, a masking effect on the zeta potential was observed. Under very acidic conditions chalcopyrite had the most negative zeta potential, and chromite the most positive. Talc, plagioclase and pyroxene had very similar zeta potential.

The differences in the zeta potential in SPW between pH 8 and 10 were not as great as they were in buffer solution in the same range. At pH 9, chalcopyrite and chromite, and pyroxene and plagioclase had similar zeta potentials. Talc had the most negative zeta potential. A summary of the results shown above is given in Table 4.4.

Table 4.4: Summary of the zeta potential of different minerals in 10^{-3}M $Na_2B_4O_7 \cdot 10H_2O$, IS=3.3x10^{-3}M buffer solution and SPW at pH 8 and pH 10

Mineral	Zeta potential (mV)			
	buffer		SPW	
	pH 8	pH 10	pH 8	pH 10
Talc	-44.3	-53.0	-18.1	-19.9
Plagioclase	-53.7	-60.1	-18.0	-13.1
Pyroxene	-41.8	-47.7	-21.3	-9.5
Chromite	-41.1	-48.4	-14.5	-4.9
Chalcopyrite	-27.7	-38.2	-10.3	-5.2

4.2.3 Variation of the zeta potential of different pure minerals between pH 8-10 with the addition of guar

The results in this section show the variation of the zeta potential on different pure minerals between pH 8 and 10 upon the addition of guar. As mentioned above, the reason this pH range was chosen was because plant operating pH (i.e. pH 9) in typical PGM concentrators in the Bushveld Complex falls within this range. Subsequent tests in this thesis were conducted at pH 9.

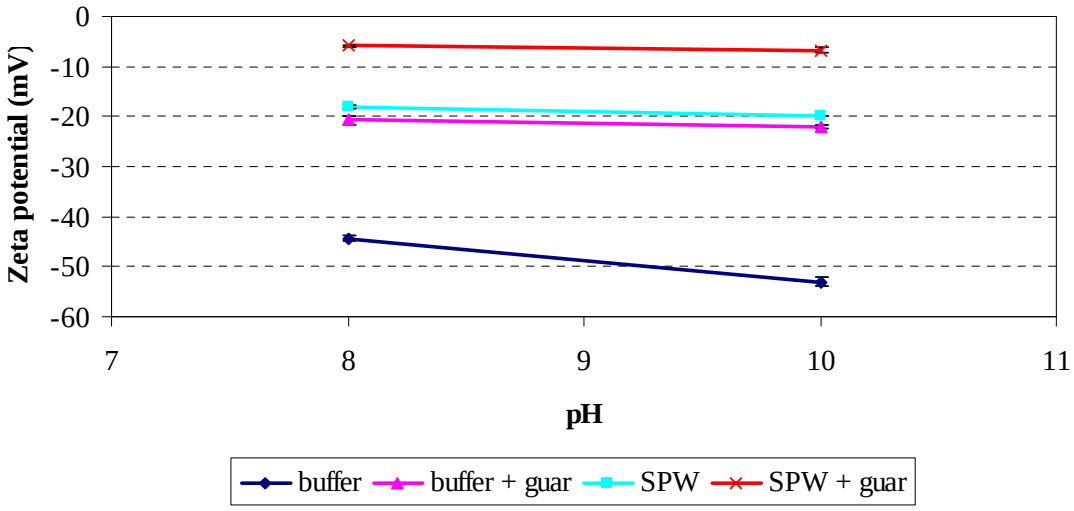

Figure 4.9: Variation of the zeta potential of talc between pH 8 and 10 with the addition of guar in 10^{-3}M $Na_2B_4O_7 \cdot 10H_2O$, IS=3.3x10^{-3} M buffered solution and SPW

Figure 4.9 shows the variation of the zeta potential of talc at pH 8 and 10 with the addition of guar in both buffer and SPW. In buffer solution the zeta potential of talc was very negative reaching a value of about -52 mV. Upon the addition of guar the zeta potential became more positive suggesting a change in the structure of the double layer due to the interaction of guar and the mineral surface which masks the charge. The zeta potential remained relatively constant in the given pH range upon the addition of guar (buffer + guar data). It is also interesting to note that the adsorption of guar onto talc in buffer had a similar effect on the zeta potential as adding ions in solution. This effect was seen by the similarity between the zeta potential of talc in SPW, and talc in buffer + guar.

In SPW, the addition of guar onto talc caused a positive shift in the zeta potential when compared to that of talc in SPW alone. However, this positive shift was not as significant when compared to that caused by the adsorption of guar onto talc in a buffer solution, highlighting the effect of ions in solution on the zeta potential. As the pH was increased from pH 8 to pH 10, the zeta potential of talc decreased slightly in SPW, but remained relatively constant upon the addition of guar.

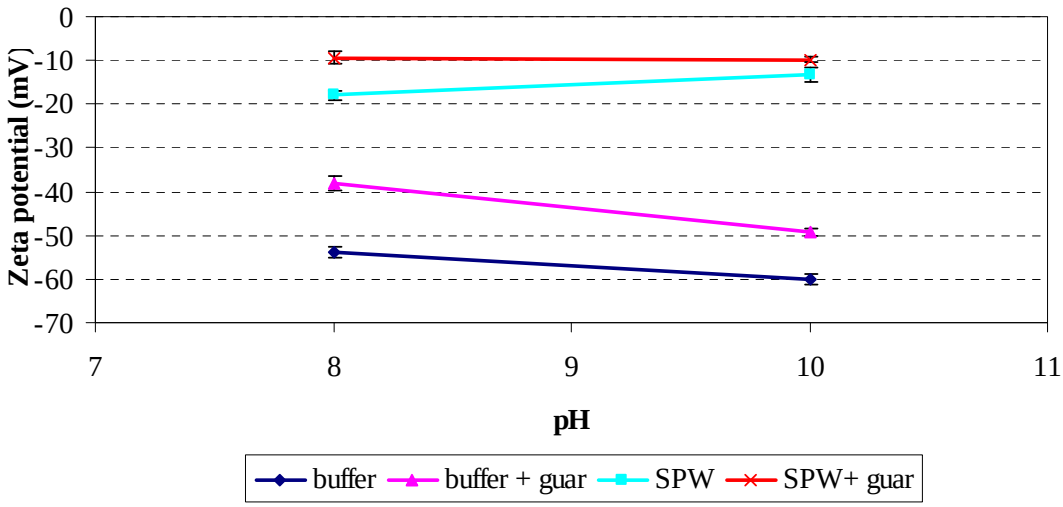

Figure 4.10: Variation of zeta potential of plagioclase between pH 8 and 10 with the addition of guar in 10^{-3}M $Na_2B_4O_7 \cdot 10H_2O$, IS =3.3x10^{-3} M buffer solution and SPW

Figure 4.10 shows the variation of the zeta potential of plagioclase between pH 8 and 10 in buffered solution and SPW respectively. In buffer, the zeta potential of plagioclase was very negative. Upon the addition of guar, there was a positive shift of about 10 mV around pH 9. This shift was not as significant as that observed when guar was added to talc in buffer. Furthermore, the adsorption of guar onto plagioclase did not have the same effect on the zeta potential as adding ions in solution, as was found with talc.

In SPW, there was a significant positive shift in the zeta potential of plagioclase when compared to that in buffer. When guar was added to plagioclase in SPW, there was a positive shift in zeta potential. This difference was more pronounced at pH 8, than at pH 10. As the zeta potential was increased between pH 8 and 10 in SPW, there was an increase in the zeta potential as shown by the positive slope of the SPW line. However, with the addition of guar in SPW, the zeta potential remained relatively constant. This again highlights the effect of the presence of ions in solution on the zeta potential of plagioclase at alkaline pH

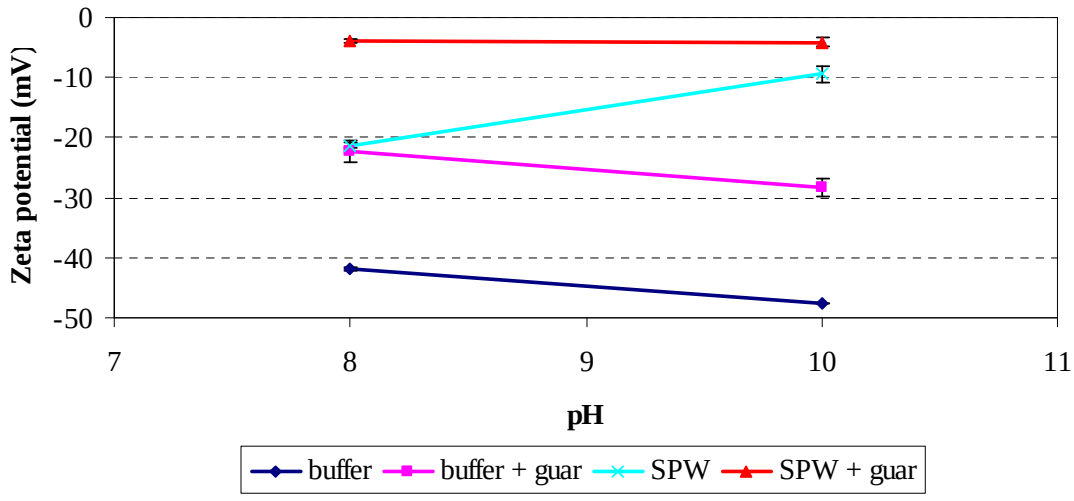

Figure 4.11: Variation of the zeta potential of pyroxene between pH 8 and 10 with the addition of guar in 10^{-3}M $Na_2B_4O_7 \cdot 10H_2O$, IS =3.3x10^{-3} M buffer solution and SPW

Figure 4.11 shows the variation of the zeta potential of pyroxene between pH 8 and 10 with the addition of guar. In buffer, the zeta potential of pyroxene was very negative,

reaching values of about -48 mV at pH 10. With the addition of guar, there was a significant positive shift of about 20 mV, with no change of slope between the buffer and the buffer + guar line. This again alludes to a change in the structure of the electrical double layer with the adsorption of guar on the mineral surface.

In SPW, the zeta potential of pyroxene became less negative when compared to that in buffer. The addition of guar had the same effect on the zeta potential of pyroxene at pH 8 as the addition of ions in solution. However as the pH become more basic, surface phenomena caused by the presence of ions in solution in SPW caused the zeta potential to increase, almost neutralising the surface charge. With addition of guar in SPW, the masking of the zeta potential was compounded, as seen by a further positive shift in the zeta potential at pH 8 almost approaching the PZC. However the adsorption of guar onto pyroxene in SPW had a lower masking effect on the zeta potential (from about -15 mV to -5 mV at pH 8) when compared to the adsorption of guar onto pyroxene in buffer (-41 mV to about -19 mV at pH 8).

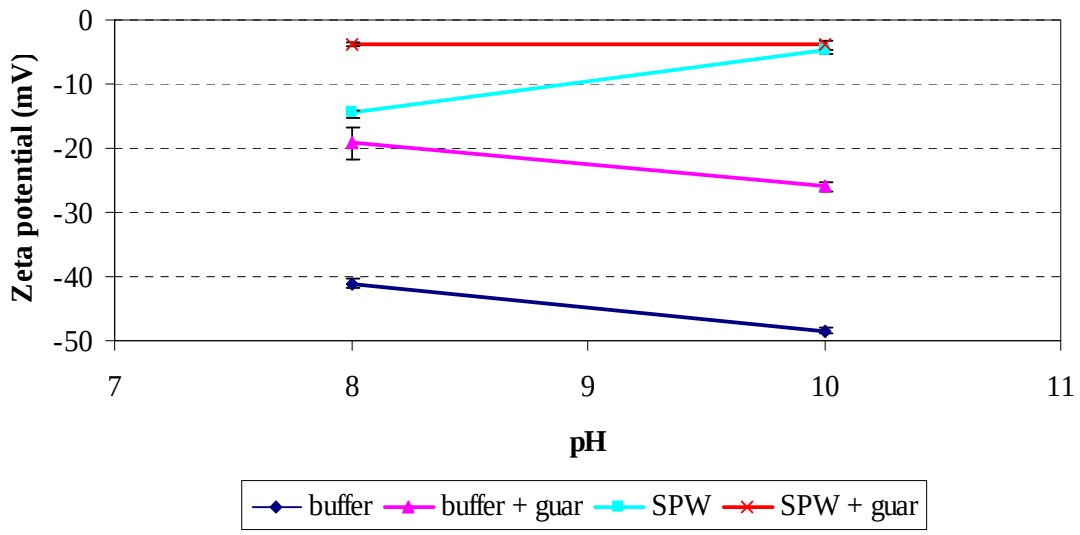

Figure 4.12: Variation of the zeta potential of chromite between pH 8 and 10 with the addition of guar in 10^{-3}M $Na_2B_4O_7 \cdot 10H_2O$, IS =3.3x10^{-3} M buffer solution and SPW

Figure 4.12 shows the variation of the zeta potential of chromite between pH 8 and 10 with the addition of guar in SPW and buffer. Similar trends in the zeta potential of chromite and pyroxene were observed. In buffer, the zeta potential of pyroxene was quite negative reaching values of up to -48 mV at pH 10. When guar was added onto chromite, the zeta potential became significantly less negative. Again, as was observed with pyroxene, the slope of the zeta potential of chromite in buffer was very similar to that of buffer + guar. Unlike talc and pyroxene, the addition of ions in solution in SPW did not have the same effect on the zeta potential as the addition of guar at pH 8. This was seen by the slight difference in the zeta potential at pH 8 in the buffer + guar and the SPW lines.

The addition of ions in solution in SPW caused a further positive increase in the zeta potential of chromite when compared to that in buffer. Furthermore with an increase in pH from pH 8 to 10, there was a further increase in the zeta potential as shown by the positive slope of the SPW line. When guar was added onto chromite in SPW, there was a further positive increase in the zeta potential at pH 8, almost neutralising the surface of chromite, compared to that in SPW alone. However, as the pH was increased from pH 8 to 10, the zeta potential remained relatively constant.

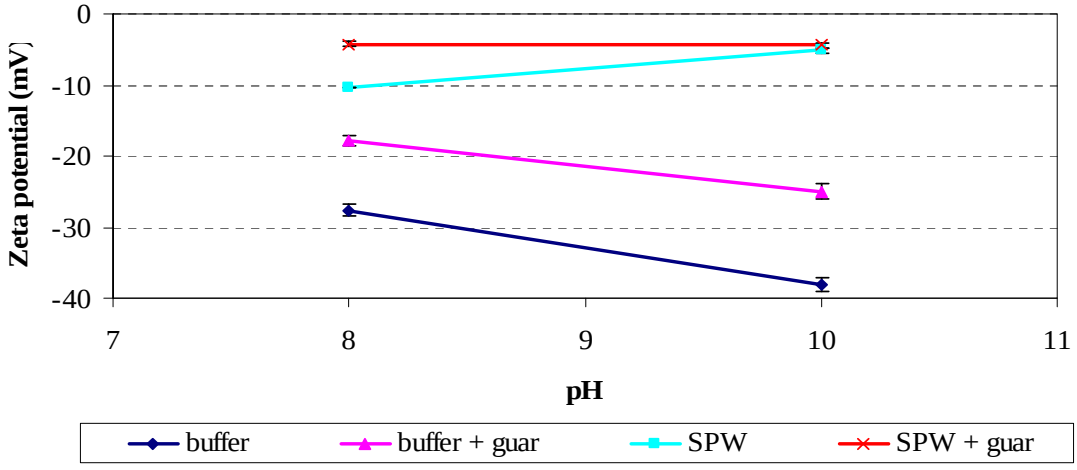

Figure 4.13: Variation of the zeta potential of chalcopyrite at pH 8 and 10 with the addition of guar in 10^{-3}M $Na_2B_4O_7 \cdot 10H_2O$, IS =3.3x10^{-3} M buffered solution and SPW

Figure 4.13 shows the variation of the zeta potential of chalcopyrite between pH 8 and 10 with the addition of guar in buffer and SPW. In buffer, the zeta potential was negative reaching -38 mV. However, as was noted in the previous section, chalcopyrite had the least negative zeta potential of all the minerals in buffer. When guar was adsorbed onto chalcopyrite, the zeta potential between pH 8 and 10 became less negative. When ions in solution in SPW were added, there was a further positive displacement of the zeta potential.

In SPW, the zeta potential of chalcopyrite increased as the pH increased between pH 8 and 10. This increase however was not as significant as was observed with pyroxene and chromite in the same pH range. When guar was added to chalcopyrite in SPW, there was a further masking of the zeta potential at pH 8. However, as pH was increased between pH 8 and 10, the zeta potential remained constant, suggesting a uniform charge on chalcopyrite regardless of an increase in pH after guar had adsorbed onto it.

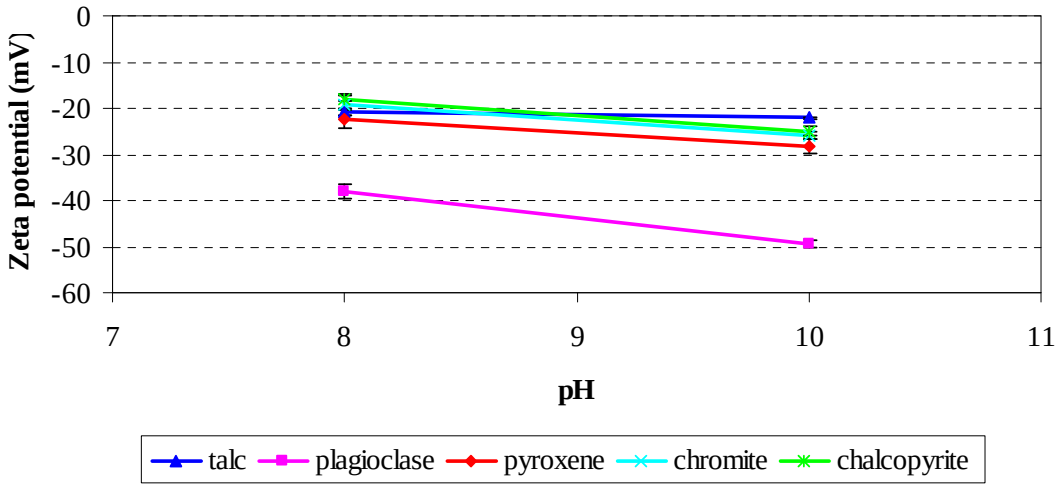

Figure 4.14: Variation of the zeta potential for all minerals between pH 8 and 10 with the addition of guar in 10^{-3}M $Na_2B_4O_7{\cdot}10H_2O$, IS =3.3x10^{-3} M buffered solution

Figure 4.14 makes a comparison of the zeta potential on the minerals between pH 8 and 10 with the addition of guar. In the given range, there was little difference in the zeta potential of talc, pyroxene, chromite and chalcopyrite when guar had adsorbed onto the

minerals in buffered solution. This suggests uniformity in the surface charge after the adsorption of guar onto the aforementioned minerals. Plagioclase however still remained very negative when compared to the rest of the minerals.

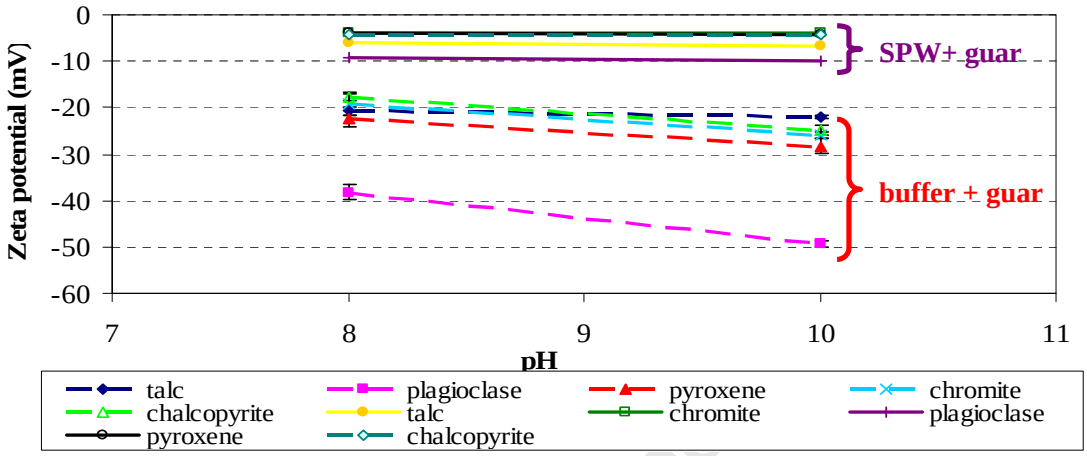

Figure 4.15: Variation of the zeta potential for all minerals between pH 8 and 10 with the addition of guar in SPW

Figure 4.15 makes a comparison of the variation of the zeta potential for all minerals between pH 8 and 10 with the addition of guar in buffer and SPW. The plot shows there to be very little difference in the zeta potential for all minerals in SPW. The values of pyroxene, chromite and chalcopyrite are superimposed on each other, showing that these minerals had a very similar zeta potential in the given pH range in SPW. Talc and plagioclase were slightly more negative than the other minerals in upon the addition of guar in SPW. A summary of the data presented in Figures 4.15 to 4.16 is given in Table 4.5.

Table 4.5: Summary of zeta potentials for all minerals at pH 8 and 10 in 10^{-3}M $Na_2B_4O_7{\cdot}10H_2O$, IS =3.3x10^{-3}M buffered solution and SPW after the addition of guar

Mineral	Zeta potential (mV)			
	buffer + guar		SPW + guar	
	pH 8	pH 10	pH 8	pH 10
Talc	-20.8	-22.0	-5.9	-6.7
Plagioclase	-38.2	-49.2	-9.4	-9.8
Pyroxene	-22.4	-28.3	-3.9	-4.1
Chromite	-19.2	-25.9	-3.9	-3.9
Chalcopyrite	-17.9	-25.0	-4.3	-4.4

4.2.4 Variation of the zeta potential of all pure minerals between pH 8 and 10 with the addition of CMC

The following results show the variation of the zeta potential of the minerals between pH 8 and 10 with the addition of CMC. The main reason for using CMC and guar was to compare the effects of charge on the depressant on its adsorption characteristics. In this section, instead of using SPW to investigate the effect of ions, 10^{-2}M IS $Ca(NO_3)_2$ was used as a matrix solution. Again these tests were conducted between pH 8, 9 and 10 because of the interest in what happens at pH 9.

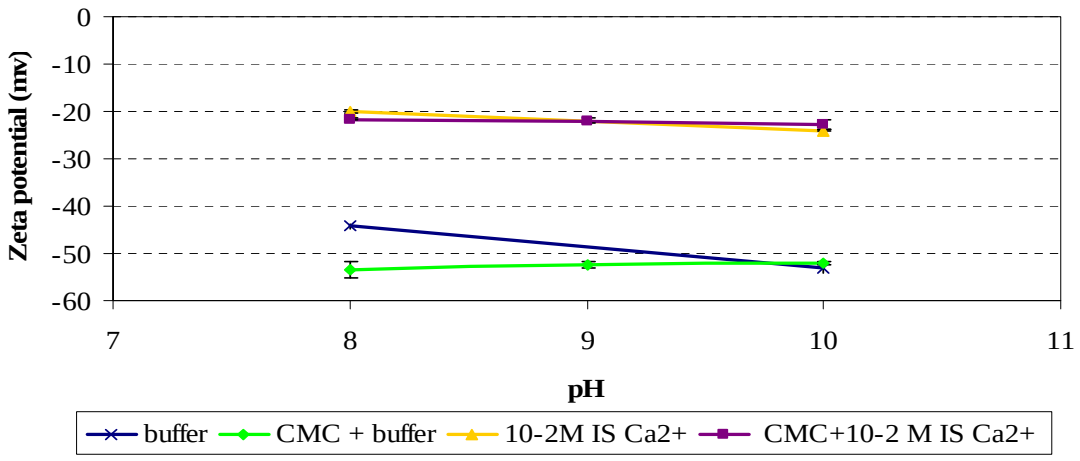

Figure 4.16: Variation of the zeta potential of talc between pH 8 and 10 in 10^{-3}M $Na_2B_4O_7{\cdot}10H_2O$, IS =3.3x10^{-3} M buffered solution and 10^{-2}M IS Ca^{2+} with the addition of CMC

Figure 4.16 shows the variation of the zeta potential of talc between pH 8 and 10 in buffered solution and in a 10^{-2}M IS Ca^{2+} solution with the addition of CMC. In buffer solution, the zeta potential of talc was negative, ranging from about -45 mV at pH 8 to -52 mV at pH 10. With the addition of CMC onto talc in buffer, the zeta potential became marginally more negative at pH 8. However, as the pH increased, there was an increase in the zeta potential of talc. At pH 10, the zeta potential of talc in buffer and, in the presence of CMC in buffer was the same. This result was quite different to that obtained for talc after the addition of guar in a buffer solution.

In a 10^{-2}M IS Ca^{2+} solution, the zeta potential of talc became more positive, when compared to that in buffer alone. A similar result was observed for the zeta potential of talc with SPW as a background electrolyte. With the addition of guar onto talc in SPW, there was a significant difference in the zeta potential when compared to the zeta potential in SPW alone. However, the addition of CMC onto talc in 10^{-2}M IS Ca^{2+} solution resulted in the same zeta potential as found in just with the 10^{-2}M IS Ca^{2+} alone.

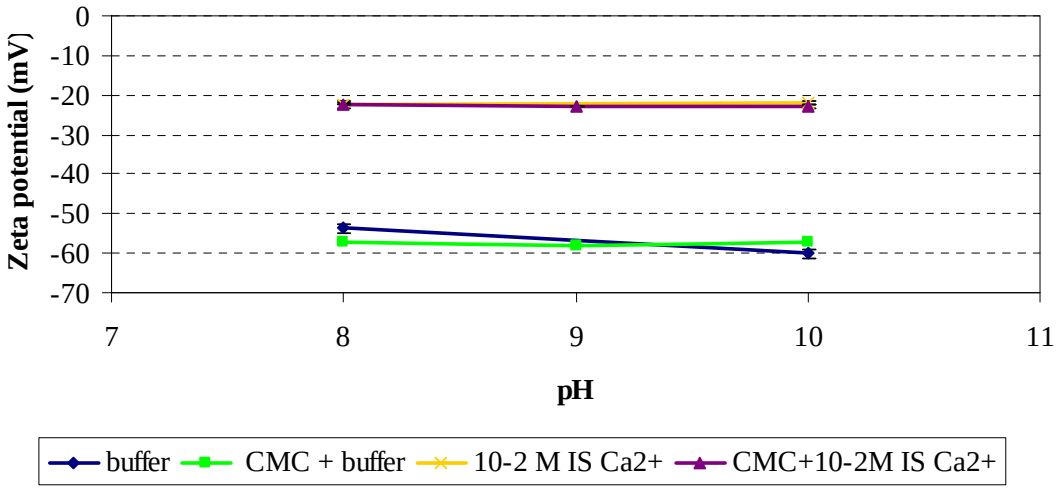

Figure 4.17: Variation of the zeta potential of plagioclase between pH 8 and 10 in 10^{-3}M $Na_2B_4O_7{\cdot}10H_2O$, IS =3.3x10^{-3} M and 10^{-2}M IS Ca^{2+} solution with the addition of CMC

Figure 4.17 shows the variation of the zeta potential of plagioclase between pH 8 and 10 with the addition of CMC. In buffered solution, the zeta potential of plagioclase was very negative ranging from about -52 mV at pH 8 to -60 mV at pH 10. The addition of CMC

in buffered solution seemed to have very little or no effect on the zeta potential of plagioclase. This again was different from the zeta potential of plagioclase as which saw a positive shift with the addition of guar in buffer.

When 10^{-2}M IS Ca^{2+} solution was used as a background electrolyte, a more positive zeta potential was observed. As pH increased from pH 8 to 10, the zeta potential of plagioclase 10^{-2}M IS Ca^{2+} solution remained relatively constant. When CMC was added to plagioclase in 10^{-2}M IS Ca^{2+} solution, there was no difference in the zeta potential compared to that in 10^{-2}M IS Ca^{2+} solution alone. This result was also different from what was observed after the addition of guar in SPW.

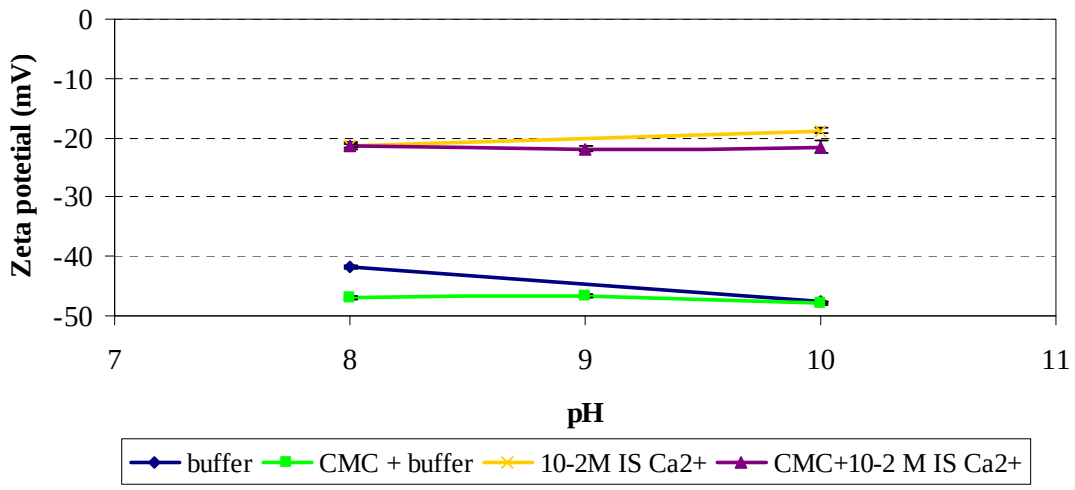

Figure 4.18: Variation of the zeta potential of pyroxene between pH 8 and 10 in 10^{-3}M $Na_2B_4O_7{\cdot}10H_2O$, IS =3.3x10^{-3} M buffer and 10^{-2}M IS Ca^{2+} solution with the addition of CMC

Figure 4.18 shows the variation of the zeta potential of pyroxene between pH 8 to 10 in buffered solution and 10^{-2}M IS Ca^{2+} solution. In buffer, the zeta potential of pyroxene was quite negative, ranging from about -41 mV to about -48 mV. With the addition of CMC to pyroxene in buffer, the zeta potential was similar to that in buffer alone. This again was different from what was observed when guar was added to pyroxene in a buffered solution where positive shift in the zeta potential observed.

An increase in the zeta potential of pyroxene was seen when a 10^{-2}M IS Ca^{2+} solution was used as a background electrolyte. The same effect was observed on the zeta potential of pyroxene when SPW was used as a background electrolyte. However, unlike the zeta potential of pyroxene in SPW which saw an increase in the zeta potential as the pH was increased from pH 8 to 10, the zeta potential of pyroxene remained relatively constant. With the addition of CMC onto plagioclase in 10^{-2}M IS Ca^{2+} solution no difference in the zeta potential was observed. This again differs from the increase in the zeta potential of pyroxene when guar was added to pyroxene in SPW.

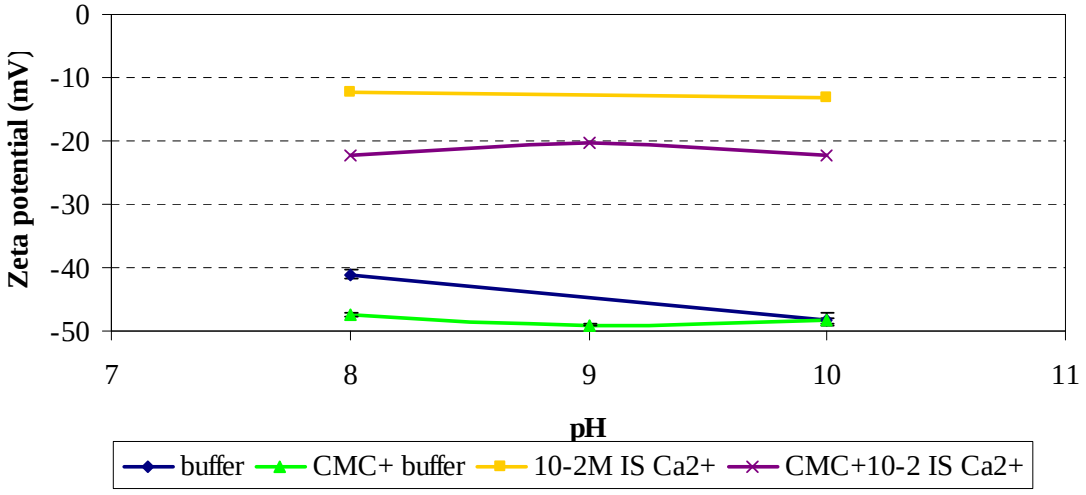

Figure 4.19: Variation of the zeta potential of chromite between pH 8 and 10 in 10^{-3}M $Na_2B_4O_7{\cdot}10H_2O$, IS =3.3x10^{-3} M buffered solution and 10^{-2}M IS Ca^{2+} solution with the addition of CMC

Figure 4.19 shows the variation of the zeta potential of chromite between pH 8 and 10 in buffer and 10^{-2}M IS Ca^{2+} solution with the addition of CMC. As with other minerals, the zeta potential of chromite in buffer was very negative, ranging from about -40 mV at pH 8 to about -48 mV at pH 10. With the addition of CMC onto chromite in buffer, the zeta potential decreased to about -48 mV at pH 8 and remained relatively constant as the pH is increased to pH 10. The addition of CMC in 10^{-2}M IS Ca^{2+} solution caused a positive shift in the zeta potential of chromite when compared that in a buffer solution. However, the zeta potential of chromite with the addition of CMC was less than that in 10^{-2}M IS Ca^{2+} alone.

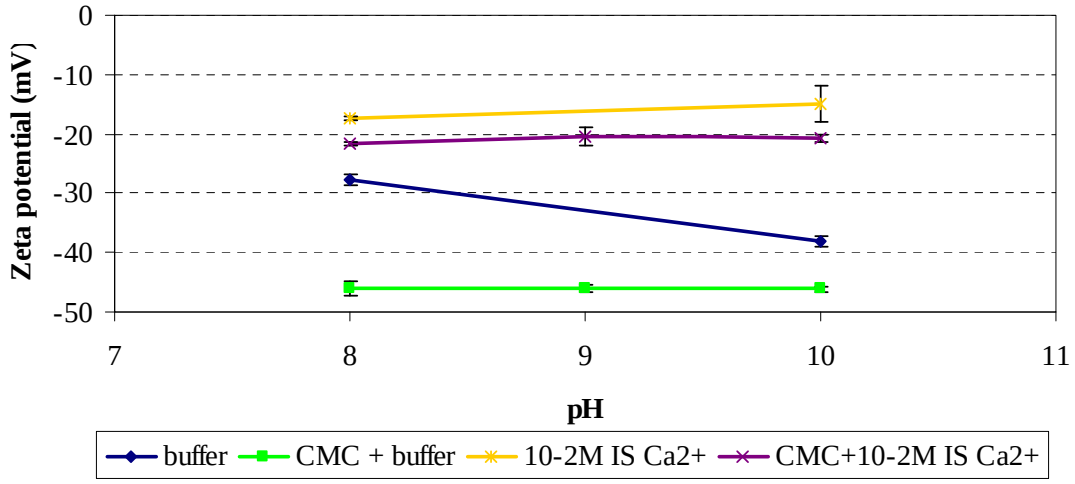

Figure 4.20: Variation of the zeta potential of chalcopyrite between pH 8 and 10 in 10^{-3}M $Na_2B_4O_7{\cdot}10H_2O$, IS =3.3x10^{-3} M buffer and 10^{-2}M IS Ca^{2+} solution with the addition of CMC

Figure 4.20 shows the variation of the zeta potential of chalcopyrite between pH 8 and 10 in buffer and 10^{-2}M IS Ca^{2+} solution. As was noted in the preceding section, chalcopyrite had the least negative zeta potential in buffer when compared to the other pure minerals. Its zeta potential ranged from about -29 mV at pH 8 to about -39 mV at pH 10. Unlike the positive increase in the zeta potential observed with addition of guar to chalcopyrite, there was a noticeable decrease in the zeta potential of chalcopyrite with the addition of CMC. As the pH was increased the zeta potential remained relatively constant..

When a 10^{-2}M IS Ca^{2+} solution was used as a background electrolyte, a positive shift in the zeta potential of chalcopyrite was observed. As pH increased from pH 8 to 10, a slight positive shift in the zeta potential was observed, but not to the same extent as was observed with an increase in pH in SPW. With the addition of CMC onto chalcopyrite, a slight decrease in the zeta potential of chalcopyrite was observed. This differed from the masking of the zeta potential of chalcopyrite observed with the addition of guar in SPW.

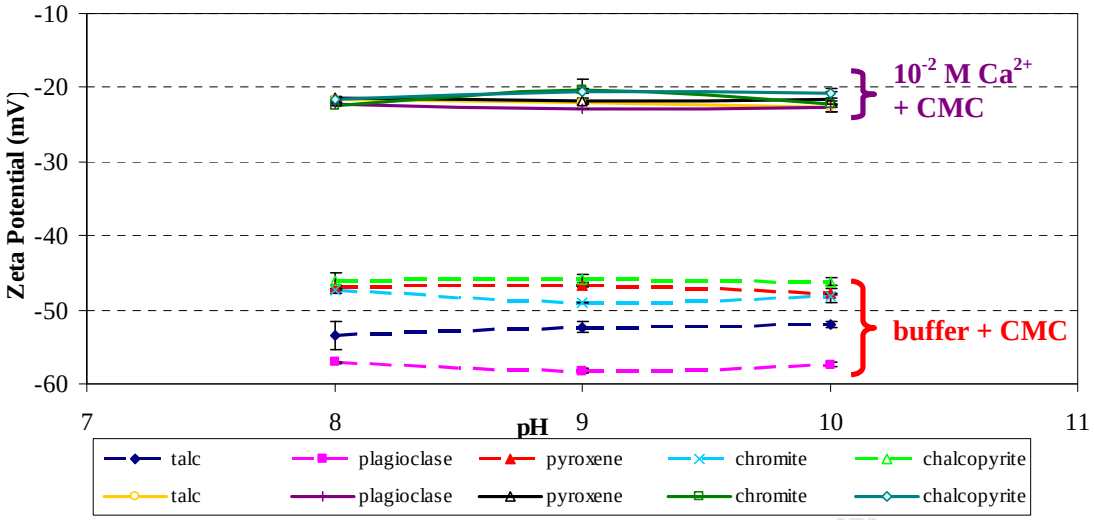

Figure 4.21: Variation of the zeta potential for all minerals between pH 8 and 10 in 10^{-3}M $Na_2B_4O_7{\cdot}10H_2O$, IS =3.3x10^{-3} M buffer solution and 10^{-2}M IS Ca^{2+} with the addition of CMC

Figure 4.21 makes a comparison on the variation of the zeta potential for all the minerals between pH 8 and 10 in buffer and 10^{-2}M IS Ca^{2+} solution. Upon the addition of CMC in buffer, plagioclase had the most negative zeta potential, followed by talc. Chromite, pyroxene and chalcopyrite had a similar zeta potential with the addition of CMC in buffer. These values were more negative when compared to the zeta potential of each of the minerals after the addition of guar in buffer. Although plagioclase had a negative zeta potential with the addition of guar in buffer, it was not as negative as that observed with the addition of CMC in buffer.

All the minerals showed a similar zeta potential after the addition of CMC in 10^{-2}M IS Ca^{2+} solution. All the results were between -20 and -23 mV, which was a very small range, highlighting the masking effect of the divalent Ca^{2+} ions. A summary of these results is given in Table 4.6.

Table 4.6: A summary of the zeta potential for all minerals between pH 8 and 10 in 10^{-3}M $Na_2B_4O_7 \cdot 10H_2O$, IS =3.3x10^{-3} M buffered solution and 10^{-2}M IS Ca^{2+} solution with the addition of CMC

Mineral	Zeta potential (mV)					
	Buffer + CMC			10^{-2}M IS Ca^{2+} + CMC		
	pH 8	pH 9	pH 10	pH 8	pH 9	pH 10
Talc	-53.5	-52.4	-52.0	-21.6	-22.0	-22.7
Plagioclase	-57.1	-58.3	-57.4	-22.2	-22.9	-22.8
Pyroxene	-46.9	-46.6	-47.9	-21.4	-21.9	-21.5
Chromite	-47.4	-49.0	-48.2	-22.4	-20.4	-22.2
Chalcopyrite	-46.1	-46.0	-46.2	-21.7	-20.5	-20.7

4.3 STUDIES OF THE KINETICS OF ADSORPTION OF GUAR AND CMC

The following results show the rate of adsorption of guar and CMC onto different minerals in SPW and 10^{-2} M IS Ca^{2+} respectively. All the experiments were carried out at pH 9 to simulate plant operation pH at 25°C.

4.3.1 Adsorption of guar in SPW

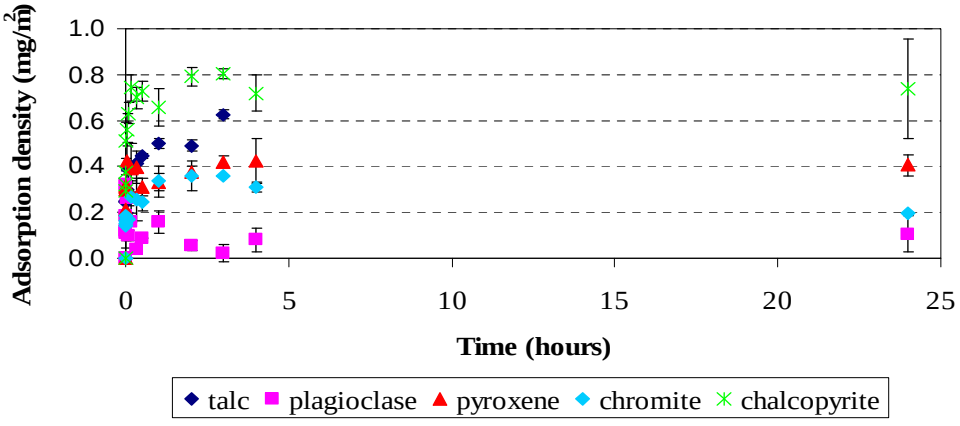

Figure 4.22: The adsorption of guar over 24 hours in SPW (T=25°C)

Figure 4.22 shows the rate of adsorption of guar at 25°C on all pure minerals in SPW over a 24 hour period. The plot shows that there was a rapid adsorption over the first few minutes and little further after the first hour. This is well illustrated when the scale of the Figure 4.22 is compressed to 1 hour as shown in Figure 4.23.

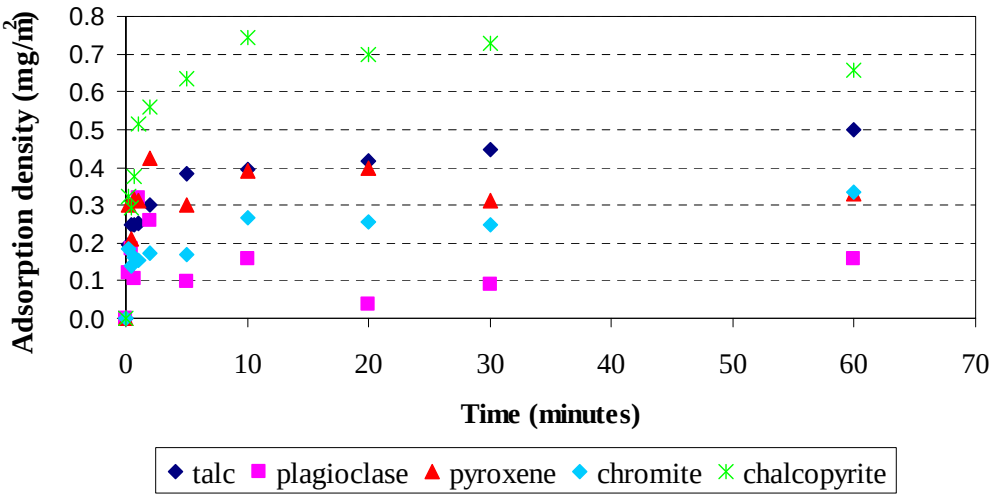

Figure 4.23: The adsorption of guar over the first 60 minutes in SPW (T=25°C)

Figure 4.23 shows the adsorption of guar on all minerals over the first hour. The highest rate of adsorption happened in the first five minutes for all the minerals. Although there seemed to be a similar affinity for guar on all the minerals, different maximum adsorption densities of guar are reached by each mineral. These remained relatively constant after the first 30 minutes, at which time equilibrium seemed to have been reached. Chalcopyrite had the highest adsorption density followed by talc, pyroxene and chromite, which had similar adsorption densities at equilibrium. Plagioclase had the lowest maximum adsorption density of the minerals.

To get an idea of the initial rate of adsorption, the scale of Figure 4.23 was decreased to the first 5 minutes as shown in Figure 4.24. An attempt was made to fit a first order kinetic model to the data, but this was poor due to scatter in the data. Although the data

points showed scatter, chalcopyrite seemed to have the highest initial rate of adsorption. The rate of adsorption tapered off quickly to values close to the maximum adsorption density.

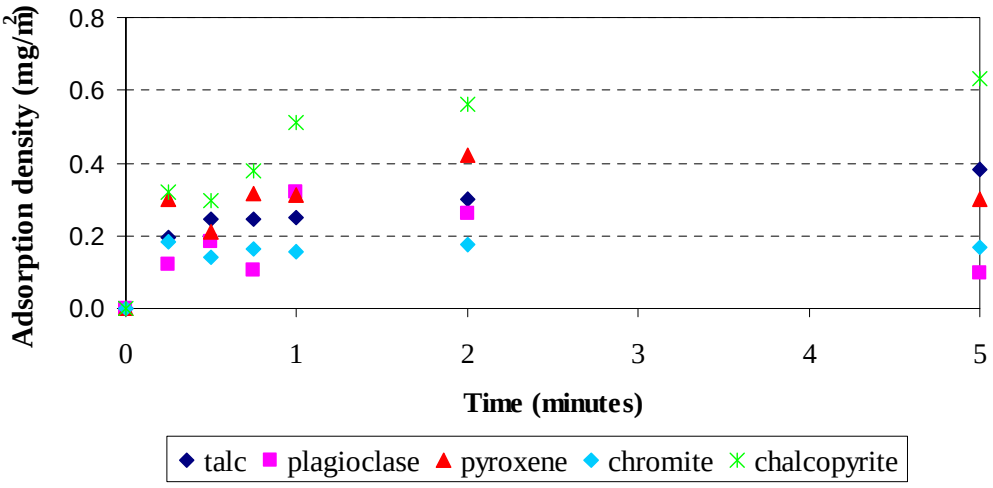

Figure 4.24: Initial adsorption of guar on all minerals in the first five minutes in SPW

4.3.2 Adsorption of CMC

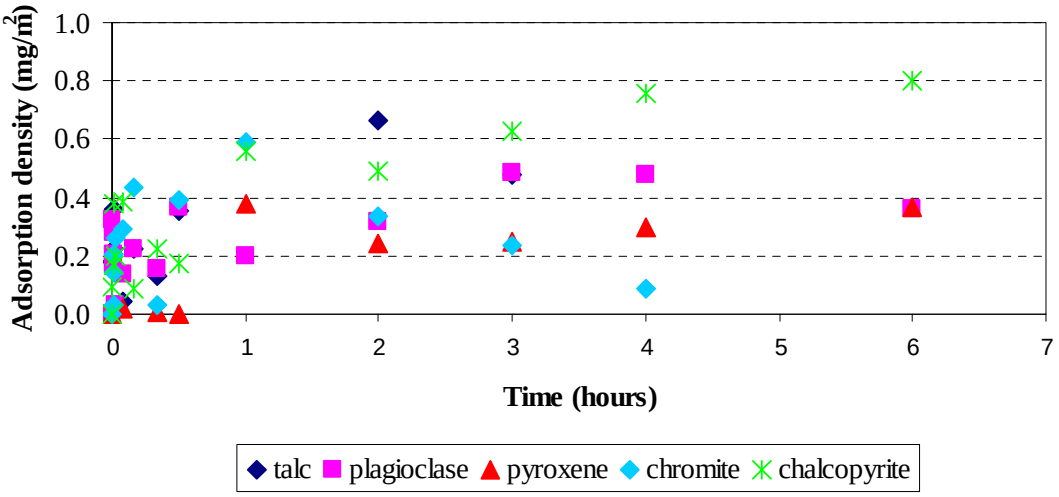

Figure 4.25: The adsorption of CMC over 6 hours in 10^{-2}M IS Ca^{2+} (T=25°C)

Figure 4.25 shows the rate of adsorption of CMC on the minerals over 6 hours in 10^{-2}M IS Ca^{2+} at 25°C. A calcium solution was used in this case because results in the SPW showed considerable scatter with no specific trends. The plot showed that, the highest adsorption seemed to happen in the first 30 minutes and then a plateau in the maximum adsorption density was reached. The data showed considerable scatter in the case of plagioclase, talc and chromite. When the scale of Figure 4.25 is decreased to the first hour, a better view of the isotherms was observed.

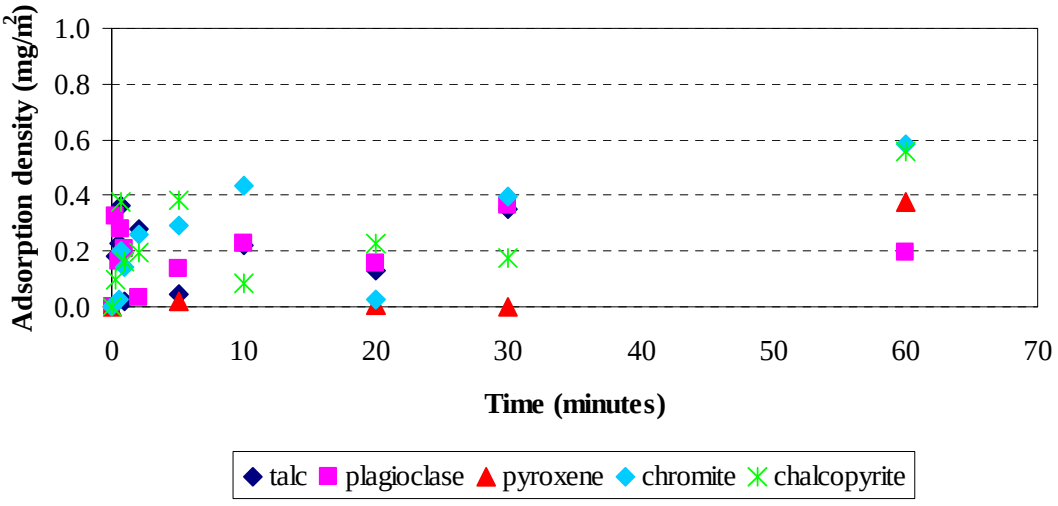

Figure 4.26: The adsorption of CMC on all minerals over the first 60 minutes in 10^{-2}M IS Ca^{2+}

Figure 4.26 shows the adsorption of CMC in 10^{-2}M IS Ca^{2+} over the first 60 minutes. The plot shows that the highest rate of CMC adsorption seemed to happen in the first 5 minutes for talc, chromite, plagioclase and chalcopyrite. Pyroxene showed very little or no adsorption until the 60th minute. Different maximum adsorption densities of CMC are attained on each mineral. Plagioclase had the lowest adsorption density in this time interval.

4.4 EQUILIBRIUM ADSORPTION ISOTHERMS

The results in this section show equilibrium adsorption isotherms for guar and CMC on all the minerals after an equilibrium time of 4 hours. All the tests were carried out at 25°C and pH 9. For each depressant a comparison was made on the maximum adsorption density on each of the minerals in buffered solution and SPW. Furthermore, the effect of the charge on the depressant on its adsorption was investigated by carrying out the adsorption studies using guar and CMC.

4.4.1 Adsorption isotherms – guar

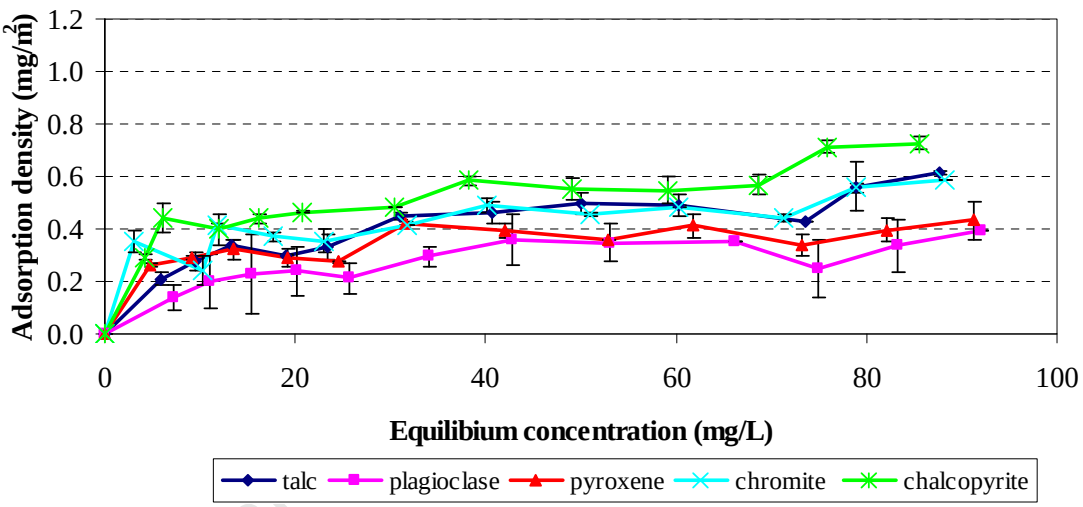

Figure 4.27: Adsorption density of guar on each mineral as a function of equilibrium concentration in 10^{-3}M $Na_2B_4O_7 \cdot 10H_2O$, IS =3.3x10^{-3} M buffered solution at pH 9, T=25°C

Figure 4.27 shows the adsorption density of guar on each mineral as a function of equilibrium concentration in buffered solution. The shape of each of the curves exhibits Langmuir behaviour. A common feature of this type of adsorption is an initial region concave to the concentration axis, and eventually reaching a plateau. Further adsorption above the plateau leads to the formation of a second plateau (Rao, 2004). Each of the isotherms above showed an initial region of increase in the adsorption density until a certain concentration was reached where the adsorption density reached a plateau. This

adsorption model was modelled using Equation 4.1 where: C_{eq} is the equilibrium concentration, I_{ads} is the adsorption density, I_{max} is the maximum adsorption density and K is the Langmuir equilibruim constant (Beattie *et al.*, 2005, Chiem *et al.*, 2006, Hunter, 2001).

$$\frac{C_{eq}}{I_{ads}} = \frac{1}{I_{\max} \cdot K} + \frac{C_{eq}}{I_{\max}} \qquad (4.1)$$

The maximum adsorption densities of guar on each of the minerals provided a method of quantifying the amount of depressant adsorbed onto each mineral and thus forming a basis from which the extent of adsorption of guar on each of the minerals could be compared. The isotherms showed that in buffer, chalcopyrite had the highest adsorption density. This was followed by talc and chromite whose isotherms were almost identical, showing that these minerals reached similar maximum adsorption densities. Pyroxene plateaued at an adsorption density slightly less than talc and chromite. Plagioclase showed the lowest adsorption density of all the minerals. One of the difficulties experienced in using this method was the inherent error resulting in poor reproducibility for some of the minerals. This was highlighted by the relatively large error bars on the plagioclase isotherm.

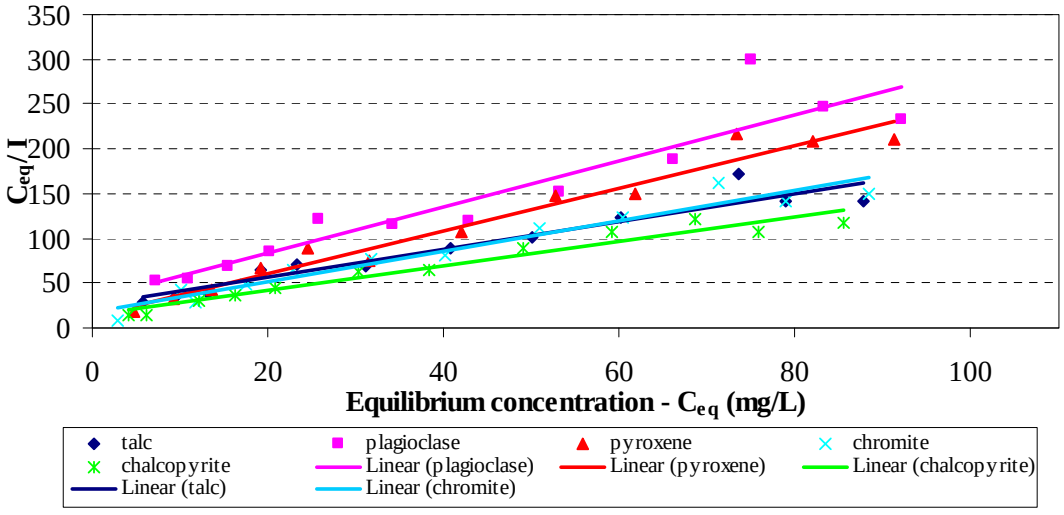

Figure 4.28: Evaluation of Langmuir equilibrium constants for guar onto each mineral

Figure 4.28 shows an analysis of the data using Langmuir theory to test if the isotherms for each mineral conformed to Langmuir behaviour and to evaluate the equilibrium constants of guar onto each of the minerals. For Langmuir adsorption isotherms, a plot of the C_{eq}/I_{ads} versus the equilibrium concentration (C_{eq}) from Equation 4.1 should yield a straight line from which the K and I_{max} can be determined from the slope and the intercept respectively. It has been proposed that the equilibrium constant (K) can be considered to represent the affinity of a polymer for a particular surface [Jenkins and Ralston, 1998; Rath *et al.*, 2000; Rath *et al.*, 2001; Morris *et al*., (2002); Wang and Somasundaran, 2005; Cheim *et al.*, 2006].

Figure 4.28 showed that all the minerals exhibit Langmuir behaviour. This was seen by the generally good regression coefficients except for plagioclase. Table 4.6 shows similarity between the calculated **(**$I_{max\text{-}calculated}$**)** and theoretical **(**$I_{max\text{-}experimental}$**)** values of the maximum adsorption density for talc, chromite chalcopyrite and pyroxene. With plagioclase however, these differ significantly, probably as a result of the poor regression on its data set. Pyroxene has the highest K, followed by chromite, then chalcopyrite, plagioclase and then talc.

Table 4.7: Experimental and calculated maximum adsorption density and Langmuir affinity constants for guar on each mineral in 10^{-3}*M* $Na_2B_4O_7{\cdot}10H_2O$*, IS =3.3x*10^{-3} *M buffered solution*

Mineral	$\mathbf{I_{max\text{-}calculated}}$ **(mg/m^2)**	$\mathbf{I_{max\text{-}experimental}}$ **(mg/m^2)**	**K**
Talc	0.63	0.62	0.064
Plagioclase	0.39	0.43	0.081
Pyroxene	0.42	0.43	0.172
Chromite	0.59	0.59	0.099
Chalcopyrite	0.73	0.73	0.097

Figure 4.29 shows the fractional surface coverage (θ) of guar on each mineral. This was found using the Equation 4.2 (Morris *et al.*, 2002), where σ^o is the effective area occupied per adsorbed polymer molecule, θ is the fractional surface coverage, N_A is Avogadro's number, n is the number of moles of polymer adsorbed, and A is the mineral surface area.

$$\sigma^o = \frac{\theta \cdot A}{n \cdot N_A} \qquad (4.2)$$

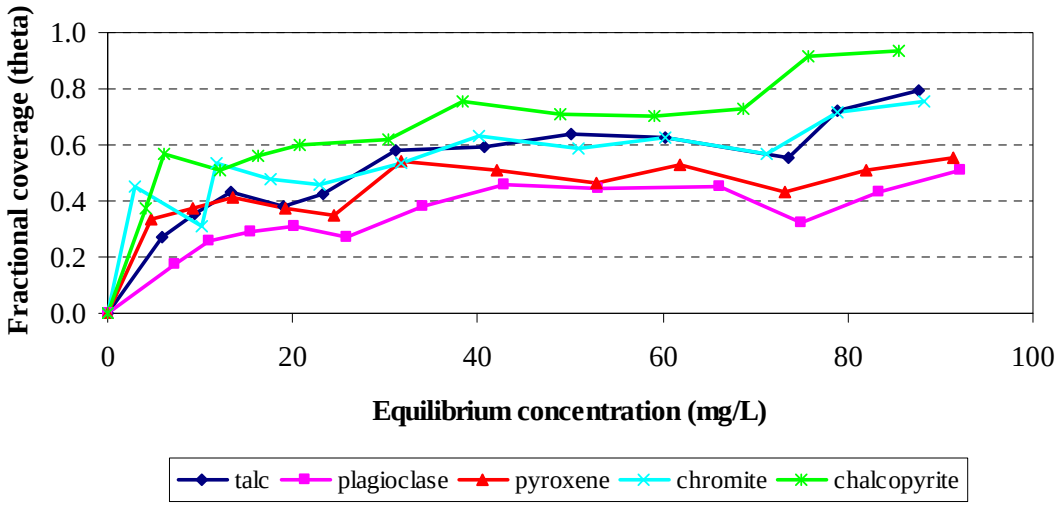

Figure 4.29: Fractional coverage of guar as a function of equilibrium concentration on each mineral in 10^{-3}M $Na_2B_4O_7 \cdot 10H_2O$, IS =3.3x10^{-3} M buffered solution

As expected, the fractional coverage (θ) followed the same trend as the isotherms of each mineral since θ was calculated from the adsorption density. From the graph, chalcopyrite had the highest θ which approached pseudo-monolayer coverage, followed by talc and chromite whose curves were superimposed on each other. This was followed by pyroxene and then plagioclase. These results are summarised in Table 4.8. Although the systems were at equilibrium, pseudo-monolayer coverage was not attained for any mineral.

Table 4.8: Summary of the fractional coverage of guar on each mineral in buffer:

Mineral	**Max. fractional coverage - θ**
Talc	0.79
Plagioclase	0.51
Pyroxene	0.56
Chromite	0.75
Chalcopyrite	0.94

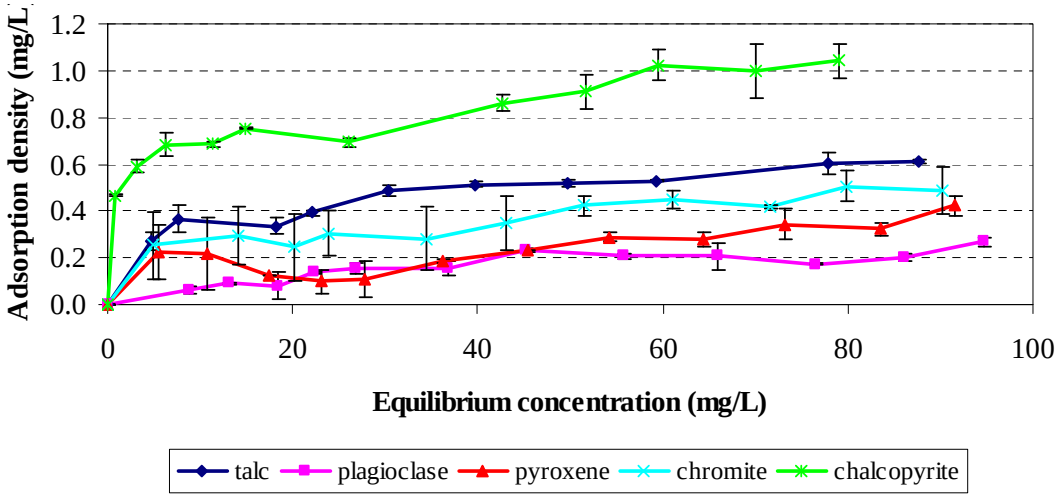

Figure 4.30: Adsorption density of guar on each mineral as a function of equilibrium concentration in SPW at pH 9, T=25°C

Figure 4.30 shows the adsorption density of guar as a function of equilibrium concentration in SPW. As was observed in Figure 4.27 to 4.28, the adsorption isotherms exhibit typical Langmuir adsorption behaviour. This was seen by an initial increase in the adsorption density with an increase in the equilibrium concentration until a certain point where a plateau in the adsorption density was reached. Different maximum adsorption densities of guar were attained on each mineral. The results showed a similar trend in the maximum adsorption density of guar on the minerals in SPW as was found in buffer. Chalcopyrite had the highest maximum adsorption density, followed by talc then, chromite, then pyroxene and plagioclase had the lowest adsorption density.

Figure 4.31 shows plots of C_{eq}/I as a function C_{eq} to test if the adsorption isotherms followed Langmuir behaviour. The plots yielded straight lines showing the good regression coefficients except with pyroxene. For pyroxene, this may be due to the effect of two seemingly outlier points between 20 and 30 minutes. This confirms Langmuir behaviour.

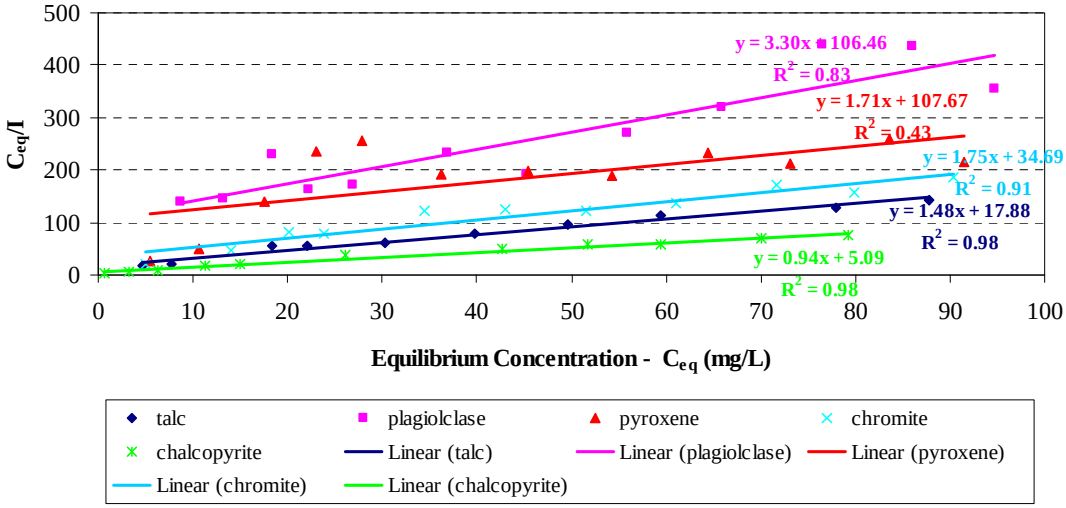

Figure 4.31: Evaluation of Langmuir affinity constants for guar onto each mineral

Table 4.9: Experimental and calculated maximum adsorption density and Langmuir affinity constants for guar on each mineral in SPW

Mineral	$I_{max\text{-}calculated}$ (mg/m^2)	$I_{max\text{-}experimental}$ (mg/m^2)	K
Talc	0.61	0.60	0.139
Plagioclase	0.27	0.27	0.031
Pyroxene	0.42	0.42	0.016
Chromite	0.49	0.49	0.050
Chalcopyrite	1.04	1.04	0.145

Table 4.9 above compares the experimental and calculated values of the I_{max}, and evaluates the equilibrium constant of guar onto each mineral. The calculated and experimental of the I_{max} were the same. In this case, the equilibrium constants (K) followed the same order as the maximum adsorption density where chalcopyrite showed the highest K, followed by talc, and then chromite. Plagioclase had a higher value for K than pyroxene.

Figure 4.32 shows the fractional coverage of guar onto each mineral in SPW. Again the curves followed the same trend as its corresponding isotherms since the fractional coverage is a function of the adsorption density. In this case pseudo-monolayer coverage was attained by chalcopyrite (1.34).

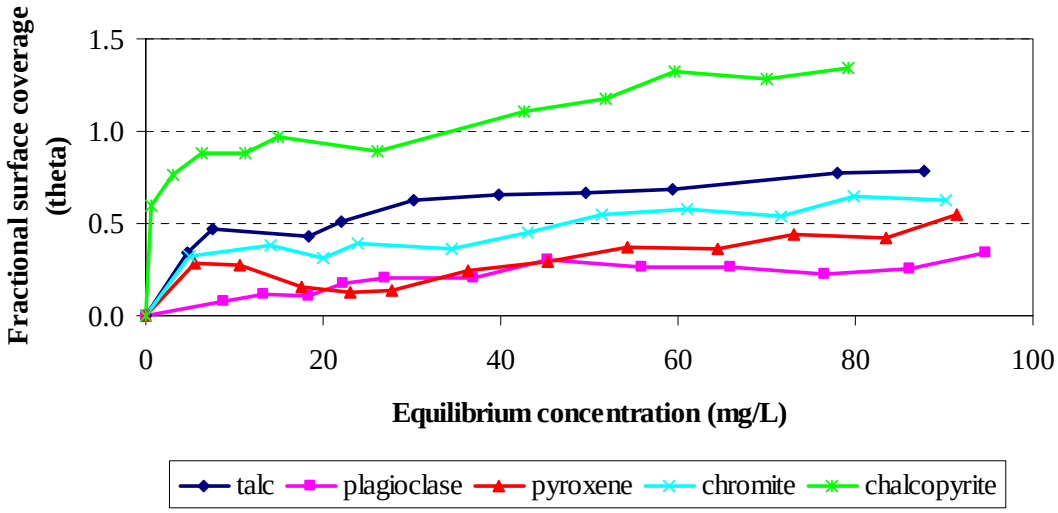

Figure 4.32: Fractional coverage of guar as a function of equilibrium concentration on each mineral in SPW

Table 4.10: Summary of the maximum adsorption density, the equilibrium constant and the maximum fractional coverage of guar on each mineral in buffer and SPW

Mineral	Max. adsorption density (mg/m^2)		Equilibrium constant - K		Max. fractional coverage	
	buffer	SPW	buffer	SPW	buffer	SPW
Talc	0.616	0.613	0.064	0.139	0.79	0.79
Plagioclase	0.396	0.267	0.081	0.031	0.51	0.34
Pyroxene	0.434	0.424	0.172	0.016	0.56	0.55
Chromite	0.586	0.486	0.099	0.050	0.75	0.62
Chalcopyrite	0.727	1.042	0.097	0.145	0.94	1.34

Table 4.10 summarises the maximum adsorption density, the equilibrium constants and the maximum fractional coverage of guar onto each of the minerals in buffer and SPW. When the adsorption densities of guar onto the minerals in buffer and SPW were compared, the results showed an increase in the adsorption density of chalcopyrite. The adsorption density of talc and pyroxene in buffer and SPW remained relatively similar within experimental error. A decrease was seen in the adsorption density of guar onto plagioclase and chromite.

4.4.2 Adsorption isotherms – CMC

This section presents the equilibrium adsorption isotherms of CMC onto the pure minerals in buffer and 10^{-2}M IS $Ca(NO_3)_2$. Initial experiments in this section were carried out in SPW. However this resulted in considerable scatter in the data. As a result, it was decided upon to use 10^{-2}M IS $Ca(NO_3)_2$ solution to study the effect of ions in solution on the adsorption of CMC onto the different pure minerals. This resulted in relatively more stable data.

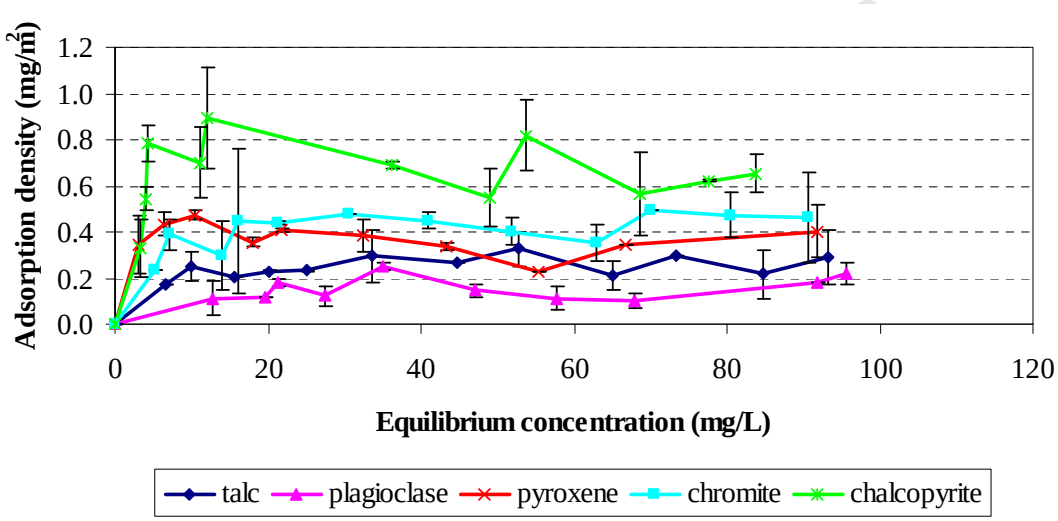

Figure 4.33: Adsorption density of CMC on each mineral as a function of equilibrium concentration in 10^{-2}M IS Ca^{2+} solution, pH 9, T=25°C

In buffered solution, no adsorption of CMC was observed (raw data presented in Appendix 7). Figure 4.33 shows the adsorption density of CMC on each mineral as a function of equilibrium concentration in 10^{-2}M IS Ca^{2+}. The isotherms showed an initial increase in the adsorption density as the concentration was increased. A plateau in the adsorption density was eventually reached. This is typical of Langmuir behaviour. Different maximum adsorption densities of CMC were eventually reached on each mineral. The plot shows that chalcopyrite had the highest adsorption density, followed by chromite, pyroxene, and talc. Plagioclase had the lowest adsorption density. Although good reproducibility was found with the residual concentration of CMC from which the

residual mass at equilibrium was calculated, the adsorption densities showed considerable scatter.

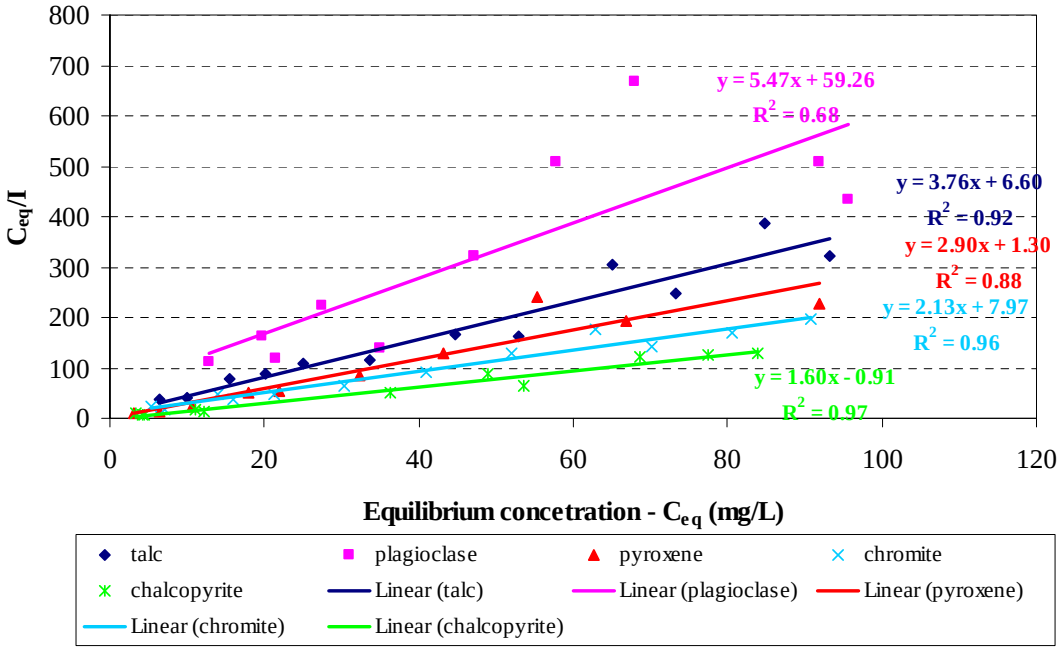

Figure 4.34: Evaluation of Langmuir equibrium constants for CMC onto each mineral

Figure 4.34 shows a plot of C_{eq}/I against C_{eq} which was used to confirm Langmuir behaviour of the system, and evaluate the Langmuir equilibrium constants of CMC on each mineral. Straight lines with reasonably good regression coefficients were obtained, except for plagioclase. The results presented a reasonable confirmation of an adherence to Langmuir behaviour. A summary of the calculated and experimental adsorption density and the Langmuir equilibrium constant is given in Table 4.11. The results show that there was similarity between the calculated and experimental adsorption densities.

Furthermore the fractional coverage is shown on Table 4.11 and on Figure 4.35. The fractional coverage follows the same trend for each isotherm, which was expected since θ was calculated from the adsorption density. Chalcopyrite had the highest fractional coverage (0.84 pseudo-monolayer), followed by chromite, then pyroxene, talc and lastly

plagioclase with θ = 0.28. The fractional coverage results showed that one pseudo-monolayer was not reached at equilibrium in the given range of concentrations.

Table 4.11: A summary of the calculated and experimental maximum adsorption density, the Langmuir equilibrium constant and the fractional coverage for CMC on all the minerals in 10^{-2}M IS Ca^{2+}

Mineral	$I_{max\text{-}cal}$ (mg/m^2)	$I_{max\text{-}exp}$ (mg/m^2)	K	θ
Talc	0.27	0.29	0.57	0.37
Plagioclase	0.18	0.22	0.09	0.28
Pyroxene	0.34	0.40	2.23	0.52
Chromite	0.43	0.46	0.29	0.59
Chalcopyrite	0.63	0.65	-1.76	0.84

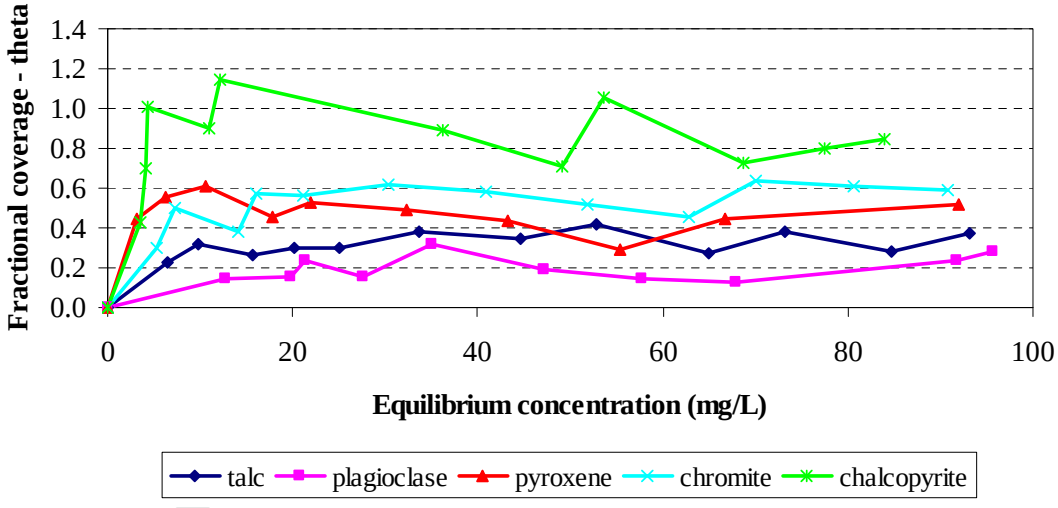

Figure 4.35: Fractional coverage of CMC as a function of equilibrium concentration on each mineral in 10^{-2}M IS $Ca(NO_3)_2$ solution

4.5 MICRFLOTATION RESULTS

The depressants used in this study, viz. guar and CMC, are used in flotation systems to render the minerals hydrophilic so that as little as possible reports to the concentrate. Microflotation is an excellent method to evaluate the effectiveness of such reagents since they will result in the mineral particles not adsorbing onto bubbles in such a cell and will not be collected in the concentrate. Hence the reduction in recovery of a mineral in a microflotation system is really a test of the extent to which the mineral has been rendered hydrophilic after addition of a depressant

The following results show the microflotation response of talc as a measure of preferential depressant adsorption. As outlined in the experimental section (cf. Section 3.5), the basis of the experiment was to measure what fraction of a 2g talc sample (+53-106μm) was recovered from the microflotation cell after it had been conditioned in depressant in the presence of another mineral of a smaller size class (100% passing 38 μm) which in this study was, respectively, chromite, pyroxene, plagioclase, talc and chalcopyrite.

Of particular interest was the comparison of the percent cumulative talc recovery as the BET surface area of the second mineral in the conditioning vessel was increased. The extent to which talc was recovered relative to the amount recovered in the absence of the second mineral served as a diagnostic of the extent to which depressant preferentially adsorbed onto the second mineral.

4.5.1 Microflotation tests in 0.25 mg/L guar in SPW

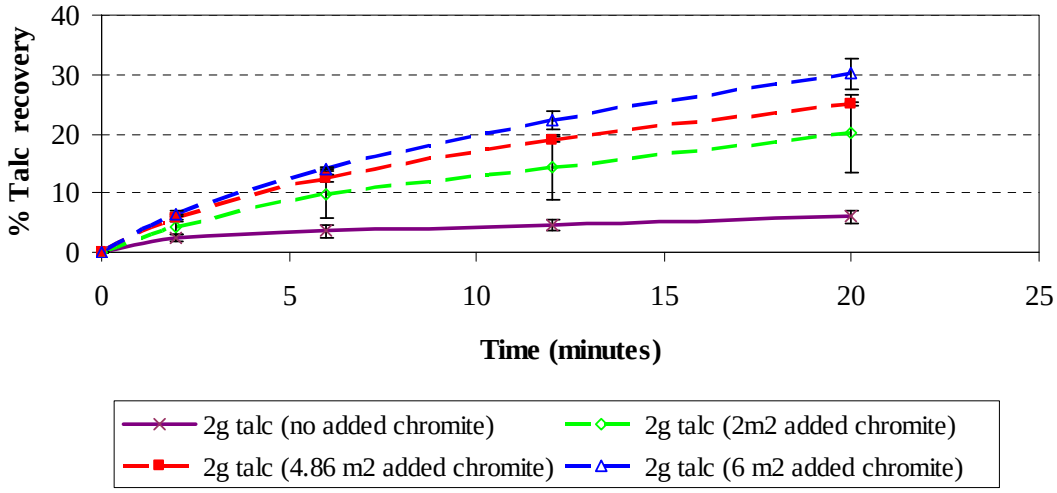

Figure 4.36: Talc recovery curves in 0.25 mg/L guar with chromite as a second mineral

Figure 4.36 shows the percent talc recovery curves when chromite as a second mineral. The total BET surface area of the 2g talc sample was 4.86$m^{2.}$ The 2g talc (no added chromite) recovery curve acted as a reference case from which the effect of increasing the mass, and hence the surface area, of the added minerals could be compared. As can be seen the cumulative talc recovery in the reference case is only 6% after 20 minutes. When 2m^2 of chromite was added the talc recovery increased to 20%. A further increase in the surface area of added chromite, resulted in a further increase in talc recovery indicating that guar was preferentially adsorbing onto chromite rather than talc.

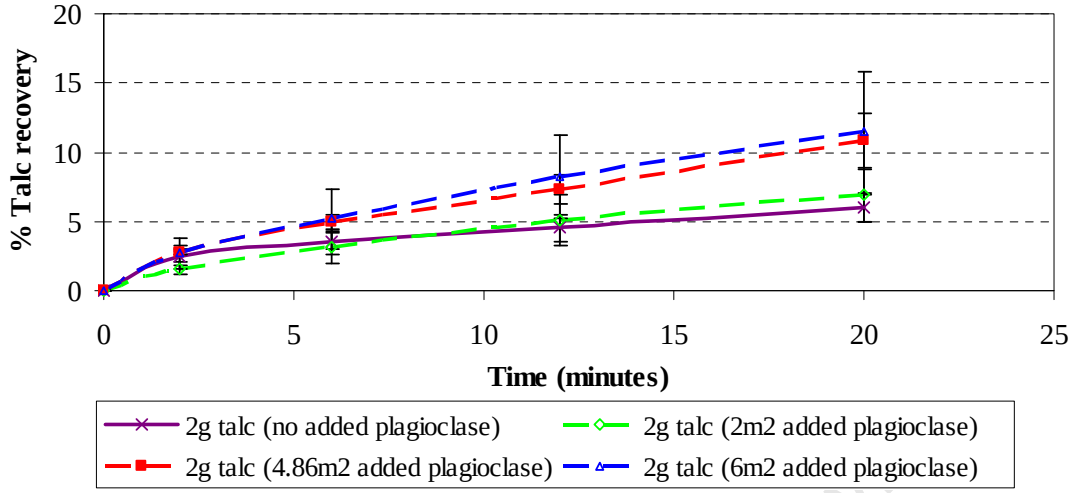

Figure 4.37: Talc recovery curves in 0.25 mg/L guar with plagioclase as the second mineral

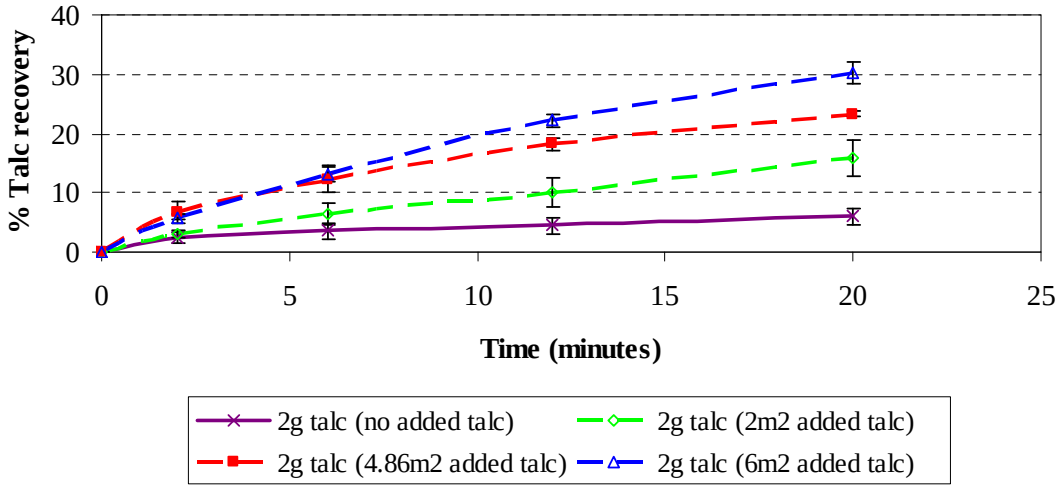

Figure 4.38: Talc recovery curves in 0.25 mg/L guar with talc as the second mineral

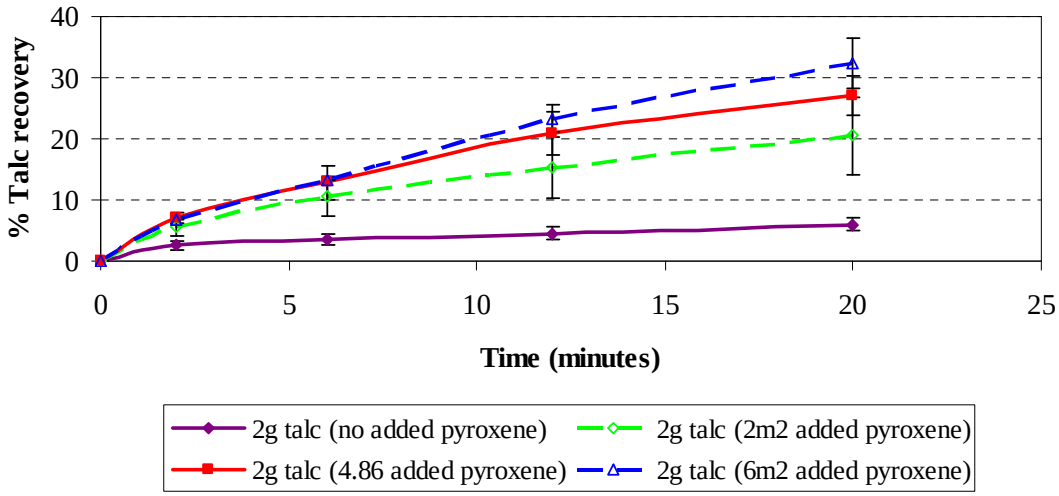

Figure 4.39: Talc recovery curves in 0.25 mg/L guar with pyroxene as the second mineral

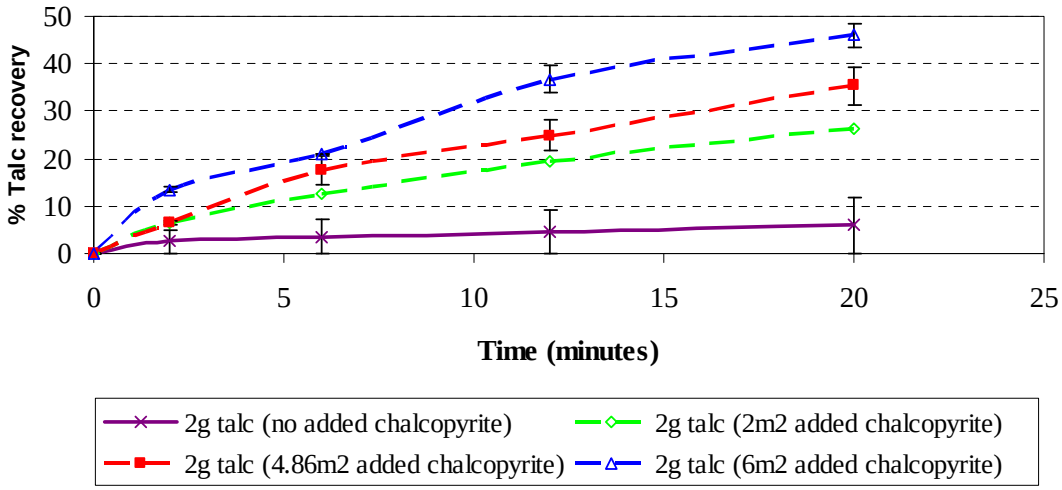

Figure 4.40: Talc recovery curves in 0.25 mg/L guar with chalcopyrite as the second mineral

Figures 4.37 to 4.40 show the results obtained when other minerals were added to talc in a similar manner. Each figure indicates the percentage talc recovery increased as the BET surface area of the second mineral was increased. In each case an increase in the BET surface area of the second mineral resulted in an increase in the talc recovery relative to the reference case (no added mineral). In Figure 4.41 a comparison is made of the

percentage cumulative talc recovery as a function of the total BET surface area of each added mineral.

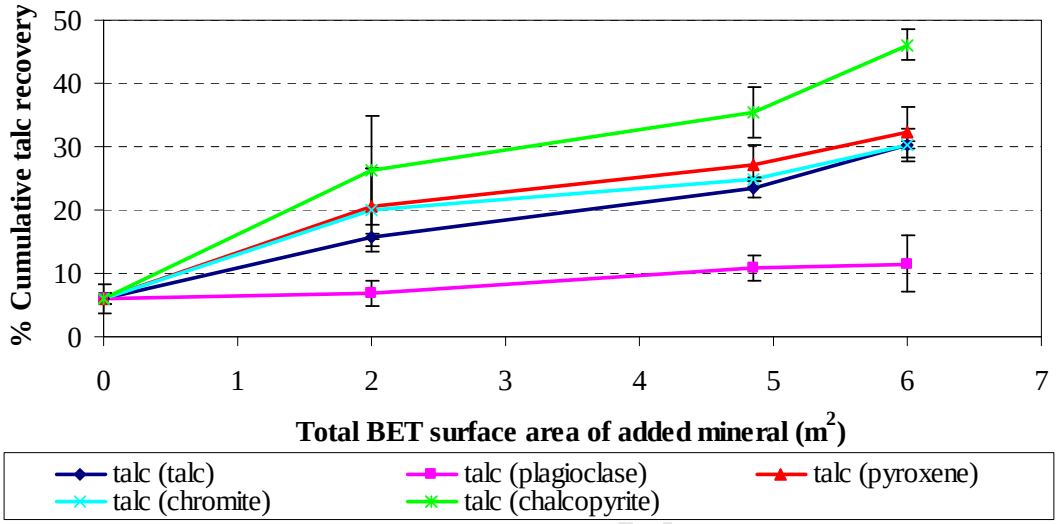

Figure 4.41: Cumulative talc recovery (%) as a function of total BET surface area of second mineral in 0.25 mg/L guar in SPW

Figure 4.41 shows the percentage cumulative talc recovery as a function of the total BET surface area of second mineral. The graph shows that with an increase in the total BET surface area; there was an increase in the percent cumulative talc recovery. The extent to which this increased was different depending on the particular mineral added. The graph shows that when chalcopyrite was the second mineral, it resulted in the highest cumulative talc recovery, indicating that it had the greatest competitive affinity for depressant relative to talc.

The sequence in this regard was then pyroxene, chromite and talc itself, whose cumulative recoveries were virtually the same with $6m^2$ of added mineral. In the case of talc added to talc, it has been explained in the Experimental section (cf. Section 3.5.2) that the added talc was in the -38µm fraction as opposed to the reference material which was in the -106+53µm fraction. Plagioclase had the lowest cumulative talc recovery of all the minerals. The higher the cumulative talc recovery the higher the adsorption density of guar on the second mineral as the total BET surface area of the second mineral was

increased. It is also interesting to note that the cumulative talc recovery follows a similar trend as the adsorption density of guar on each of the minerals in the equilibrium studies. These results are summarised in Table 4.12.

Table 4.12: Cumulative talc recovery as a function of the BET surface area of the second mineral

Mineral	**% Cumulative talc recovery**			
BET surface area of second mineral (m^2)	**0**	**2**	**4.86**	**6**
Talc	6.0	15.8	23.3	30.2
Plagioclase	6.0	6.90	10.8	11.5
Pyroxene	6.0	20.5	27.0	32.3
Chromite	6.0	20.1	24.9	30.2
Chalcopyrtie	6.0	26.3	35.5	46.1

4.5.2 Microflotation tests in 0.25 mg/L CMC in SPW

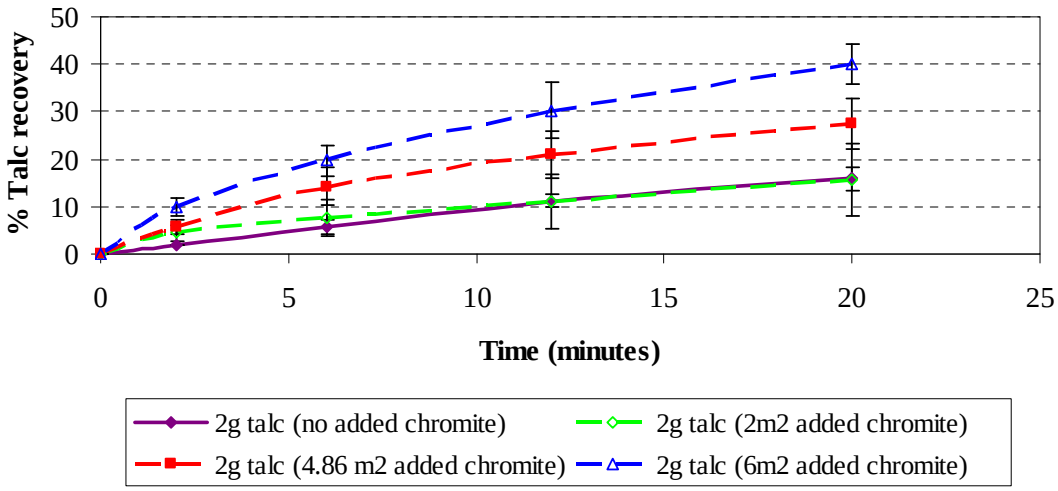

Figure 4.42: Talc recovery curves in 0.25 mg/L CMC with chromite as a second mineral

Figure 4.42 shows the result of a similar study to that outlined in Section 4.5.1 but using CMC instead of guar. In this plot the second mineral was chromite. With no added chromite, a talc recovery of 15% was reached at 20 minutes. This was the reference case for CMC. When chromite was added in increasing increments of total surface area, there

was an increase in the talc recovery. This trend in talc recovery was also observed in Figures 4.43 to 4.46, as the total surface area of the second mineral is increased.

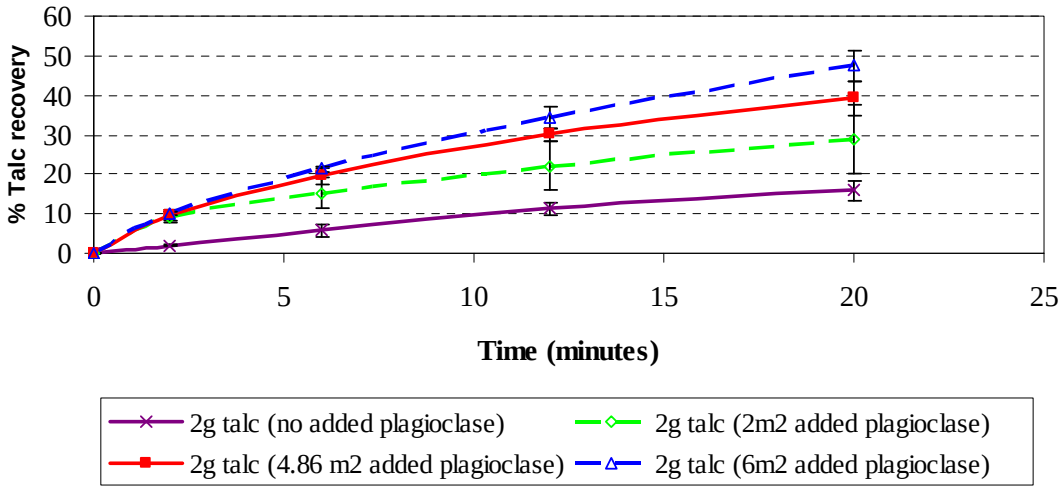

Figure 4.43: Talc recovery curves in 0.25 mg/L CMC with plagioclase as the second mineral

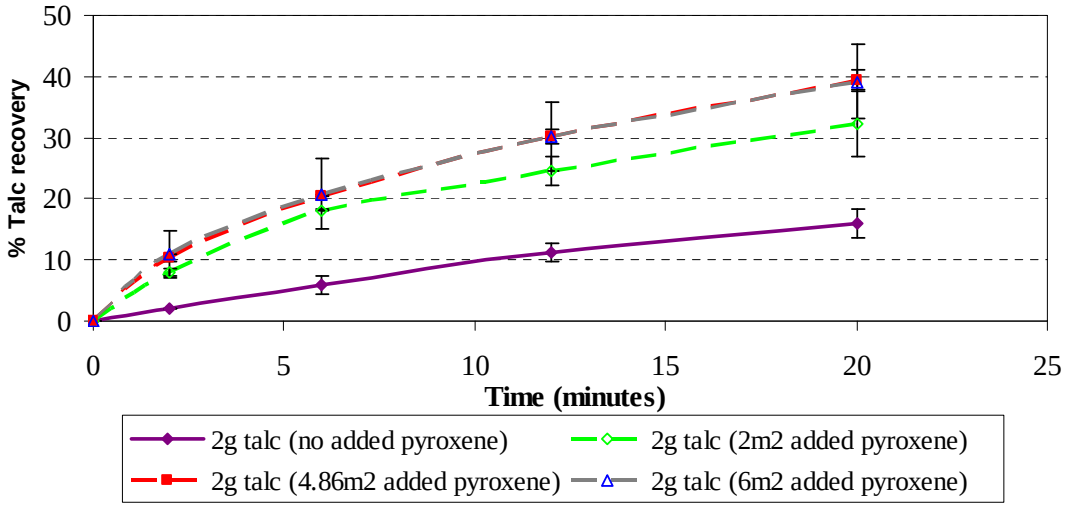

Figure 4.44: Talc recovery curves in 0.25 mg/L CMC with pyroxene as the second mineral

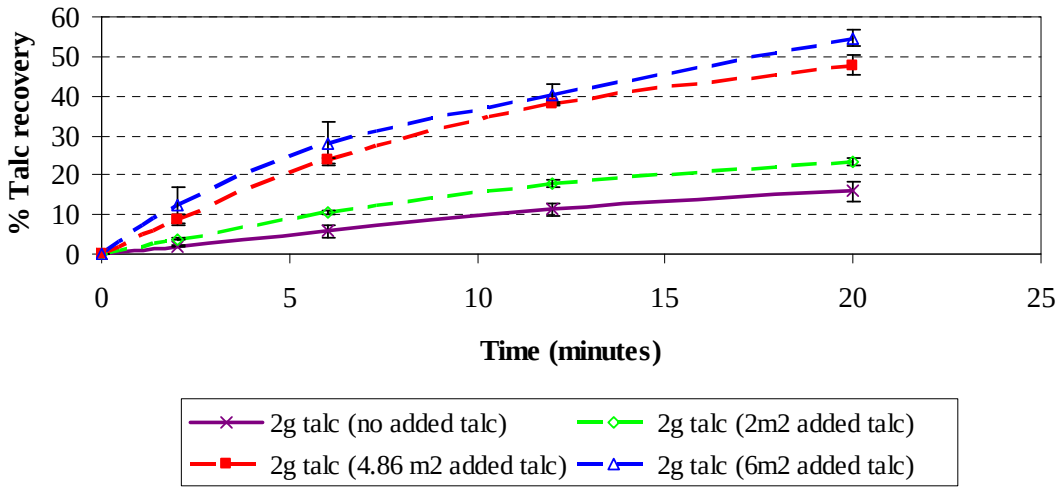

Figure 4.45: Talc recovery curves in 0.25 mg/L CMC with talc as the second mineral

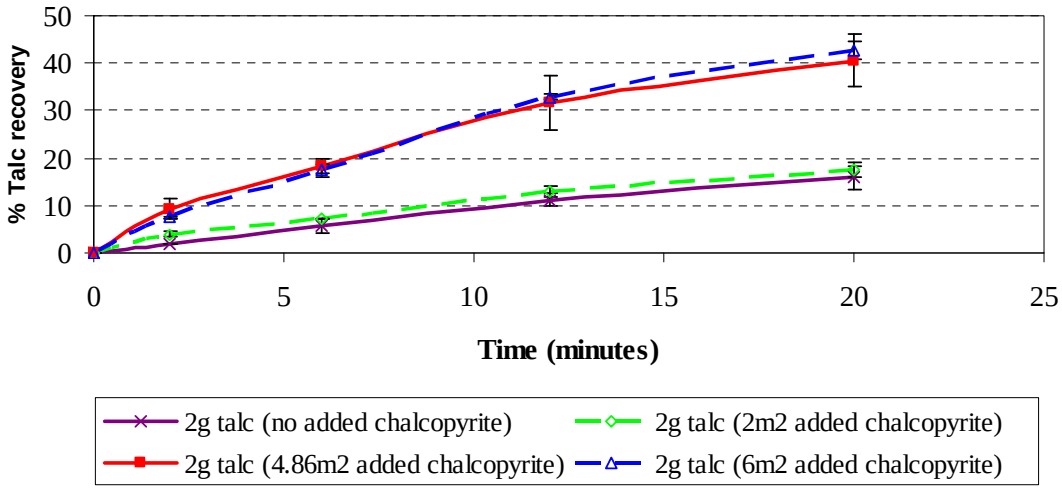

Figure 4.46: Talc recovery curves in 0.25mg/L with chalcopyrite as the second mineral

Figure 4.47 shows a plot of the cumulative talc recovery as a function of total BET surface area of the second mineral. The curves show an increase in the cumulative talc recovery as the total BET surface area of the second mineral was increased. The cumulative talc recovery of pyroxene remained relatively constant between 4.86 and 6m^2.

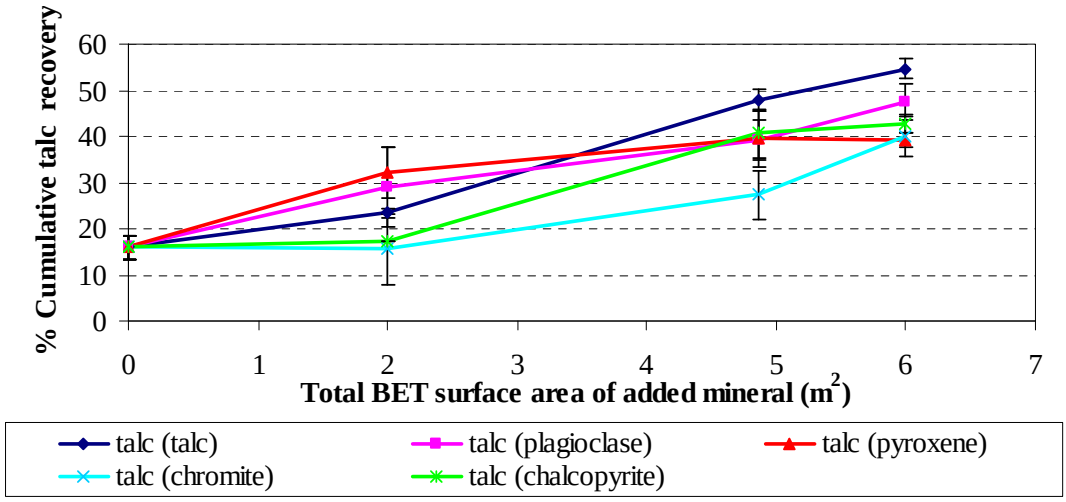

Figure 4.47: Cumulative talc recovery (%) as a function of total BET surface area of the second mineral in 0.25 mg/L CMC

Figure 4.47 shows that with $2m^2$ of second mineral, talc, plagioclase and pyroxene had similar cumulative percent talc recoveries. Chromite and chalcopyrite had the lowest talc recovery at this total BET surface area. As the surface area of the second mineral was increased to 4.86 m^2, pyroxene, plagioclase and chalcopyrite had virtually the same cumulative talc recoveries. Chromite, again, had the lowest cumulative percent talc recovery and talc had the highest cumulative talc recovery at this total BET value of added mineral. It should be emphasized again that the added talc was of a smaller particle size distribution to the 2g sample. As the total BET surface area of added minerals was increased to $6m^2$, chromite and chalcopyrite had a similar cumulative talc recovery. Talc (as an added mineral) has the highest cumulative talc recovery. The cumulative talc recovery of pyroxene remained relatively constant between 4.86 and $6m^2$

Table 4.13: Summary of the cumulative talc recovery as function of the total BET surface area of the second mineral after conditioning in guar and CMC

Mineral	% Cumulative talc recovery							
BET surface area second mineral (m^2)	Guar				CMC			
	0	2	4.86	6	0	2	4.86	6
Talc	6.0	15.8	23.3	30.2	15.9	23.4	47.9	54.7
Plagioclase	6.0	6.9	10.8	11.5	15.9	28.9	39.3	47.6
Pyroxene	6.0	20.5	27.0	32.3	15.9	26.2	40.6	29.4
Chromite	6.0	20.1	24.9	30.2	15.9	15.5	27.4	40.0
Chalcopyrite	6.0	26.3	35.5	46.1	15.9	17.4	40.6	42.9

Table 4.13 summarizes the cumulative talc recovery as a function of the total BET surface area of the second mineral after conditioning in guar and CMC. The table shows that higher cumulative talc recoveries were obtained when conditioning was done in CMC compared to guar. This suggests that CMC had a lower depressant action. In the case of guar, plagioclase showed little competitive adsorption relative to talc whereas chalcopyrite showed the greatest competitive adsorption. In the case of CMC chromite showed the lowest extent of competitive adsorption relative to talc whereas the added talc, which was a finer particle size material, showing the greatest competitive affinity for CMC relative to the coarser talc which was the reference material.

4.6 THE ADSOPTION OF GUAR ONTO CHALCOPYRITE IN THE PRESENCE OF COLLECTOR – AN EXPLORATORY INVESTIGATION

The adsorption studies and microflotation experiments of guar showed chalcopyrite to have the highest affinity for guar when compared to the other minerals as shown in Figures 4.27 and 4.30; and Figure 4.41 respectively. In PGM flotation, one aims at maximizing sulphide recovery since PGMs are associated with sulphides. These results raised the question of whether the high relative adsorption of guar onto chalcopyrite compared to the other minerals would have been the same had collector been present.. To test this, an equilibrium adsorption study of guar onto chalcopyrite in the presence of sodium isobutyl xanthate in buffer at 25°C was conducted. Chalcopyrite was conditioned in a concentration of SIBX sufficient to give one pseudo-monolayer coverage for 10

minutes, and thereafter in guar for an equilibrium time of 4 hours. The results of this experiment are presented in Figure 4.48.

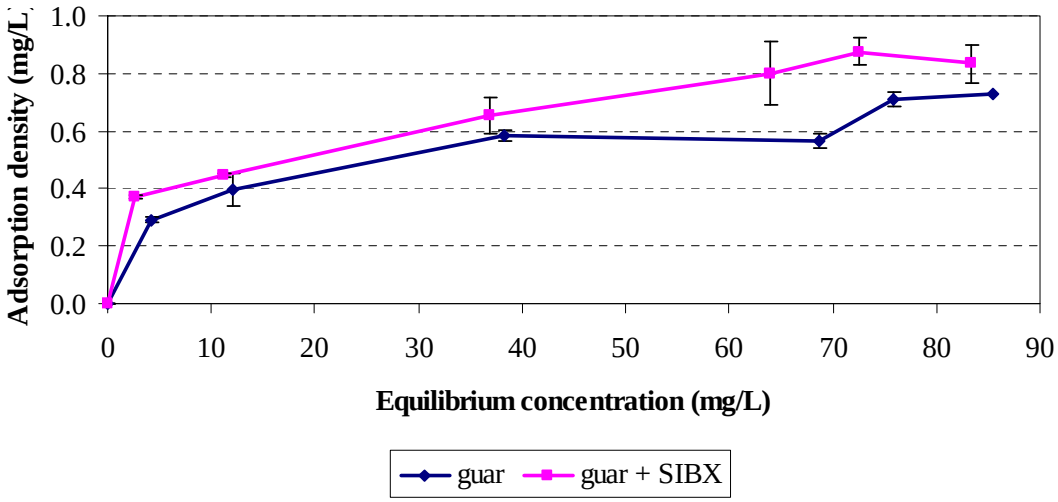

Figure 4.48: Adsorption density of guar as a function of equilibrium concentration on chalcopyrite in 10^{-3}M $Na_2B_4O_7{\cdot}10H_2O$, IS =3.3x10^{-3} M buffer with and without SIBX

Figure 4.48 shows the adsorption density of guar as a function of equilibrium concentration on chalcopyrite in buffer with and without SIBX. In the absence of SIBX, a maximum adsorption density of 0.73 mg/m^2 was attained. With the addition of SIBX, an increase in the adsorption density of guar was observed. A maximum adsorption of 0.83 mg/m^2 was attained.

5 DISCUSSION

In this section, a detailed discussion of the results on the nature of the mineral surface charge i.e. zeta potential of the minerals, where the zeta potential was determined in either a buffered solution or synthetic plant water (SPW) will be presented. Zeta potential results for each mineral in buffer presented a reference case against which the surface charge determined after the addition of ions in solution, and the addition of depressant on each mineral could be compared. A reference to the acid/base hypothesis presented by Liu *et al.*, (2000) will be made to provide a basis to interpret differences in surface charge. These mechanistic properties will also be used to interpret the differences in the adsorption characteristics of each depressant on each mineral.

The kinetic and equilibrium adsorption results will be discussed to determine firstly whether the adsorption of depressant onto mineral was rate controlled, and secondly, to quantify the differences in the adsorption densities of depressant on each mineral using Langmuir isotherms. Finally the results obtained in a microflotation study of the floatability of the minerals after being treated by depressant in the presence of other minerals will be discussed.

5.1 MINERAL SURFACE CHARGE

5.1.1 Mineral surface charge in buffer

It was postulated that depressants adsorb preferentially onto different minerals because there are differences in the mineral surface charge arising from the differences in the chemical structure of each mineral. A detailed description of the chemical structure of each mineral was given in the literature review (c.f. Section 2.1.1 to 2.1.5). Zeta potential measurements were conducted and were assumed to be indicative of the mineral surface charge. The effect of the presence of ions in solution, the adsorption of polymer (guar and CMC), and the charge of the respective polymer was investigated.

5.1.1.4 Silicates – Talc, plagioclase and pyroxene

Figures 4.2 to 4.4 showed the zeta potential of talc, pyroxene and plagioclase as a function of pH in buffer and SPW. The zeta potential in buffer for each mineral served as a reference case against which all other tests would be compared. For most of these minerals, the zeta potential became more negative as pH increased from pH 2 to 10, indicating a negatively charged surface at pH greater than pH 2 for talc and plagioclase, and pH greater than pH 3 for pyroxene. With plagioclase, a relative positive shift in the zeta potential was observed at pH 6, thereafter becoming more negative as the pH was increased to pH 10. The extent to which the mineral surface became negatively charged differed from mineral to mineral depending on its chemical structure.

Fuerstenau and Fuerstenau (1982) showed that, generally, for silicate minerals where the surface cation (or metal oxide) is insoluble, such metal cations will remain at the surface and participate in surface reactions. The formation of an electrical double layer at the surface between such a silicate mineral and an aqueous medium has long been considered to be controlled by broken –Si-O and –M-O bonds at the surface of the mineral as represented schematically below:

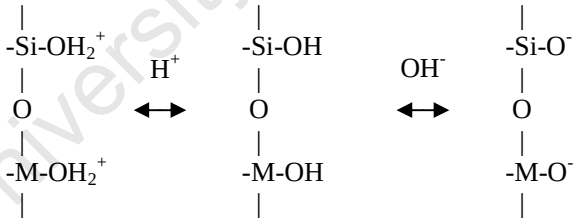

Figure 5.1: Schematic representation of the dissociation of silicates (Fuerstenau and Furstenau, 1982)

Figure 5.1 suggests that the surface charge character of each mineral mainly depends on the amount of dissociated silanol groups as a function of pH. Thus increasing the pH leads to an increase in the negative centres, resulting in a negative surface charge.

Talc showed a decrease in the zeta potential as pH increased from pH 4 to 10, indicating an increasingly negative surface charge with an increase in pH. As previously mentioned,

talc is slightly different from the other minerals in that its structure consists of edges and planes. Talc edges are considered to possess a negative charge which results from breaking ionic and covalent bonds in the brucite layer (Burdokova *et al.,* 2007). Furthermore, Alvarez-Silva *et al.,* (2010), and Fuerstenau and Pradip (2005) proposed that due to the highly polar nature of the talc edges because of the rupture of covalent or ionic bonds, the zeta potential of the edge plane exhibits strong pH dependence.

Johnson *et al.,* (2000) proposed that for anisotropic phyllosilicate minerals, the surface charge distribution can be broken down into the basal plane and edge contribution. The basal plane is typified by a negative zeta potential over a wide range of pH, whose PZC occurs at about pH 2.5, while the edge contribution is typified by a positive zeta potential at pH values less than pH 6 and negative zeta potential after pH 7 as shown in Figure 5.2. The presence of negative charge on the talc basal planes has also been reported by others [Fuerstenau and Huang, 2003; and Burdukova *et al.,* 2007]. On this basis the zeta potential results obtained in this study suggest that in the talc sample used, the ratio of basal planes to edges was high, resulting in the characteristic basal planes negative charge distribution.

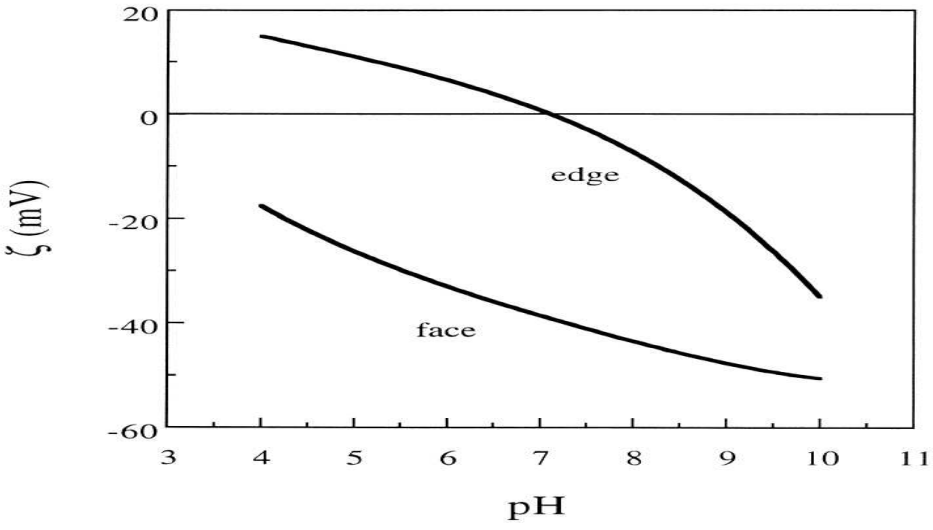

Figure 5.2: The zeta potential properties of the edge and face surfaces of kaolin (Johnson et al., 2000)

Zeta potential results of pyroxene in a buffered solution showed an increasingly negative surface charge with an increase in pH as previously observed by other researchers e.g. Malysiak (2003). According to Fuerstenau and Fuerstenau (1982), when pyroxene and amphibole chain silicates are ground, an increasing number of Si-O bonds are broken, resulting in an increase in the negative character of the surface with an increase in pH.

The PZC of plagioclase occurred at pH ≈ 2, which agrees very closely with Fuerstenau and Fuerstenau (1982) who found a PZC of pH 1.9 for albite, and pH 2 for anorthite. As previously mentioned albite ($NaAl_2Si_2O_8$) and anorthite ($CaAl_2Si_2O_8$) are the sodium rich and calcium rich end-members of plagioclase feldspars respectively (c.f. Section 2.1.2). At pH 6 a sudden increase in the zeta potential was observed. This sudden positive shift is in contrast to observations made by researchers like Demir *et al.,* (2001); Demir *et al*., (2003); Malysiak *et al.,* (2002); Karagüzel *et al.,* (2005) and Gülgönül *et al*., (2008) who found an increasingly negative zeta potential for plagioclase feldspars with an increase in pH. XRD results in Table 4.1 showed the plagioclase sample to contain 100% Anorthite 65 (i.e 65% of anorthite and 35% albite). These results suggest that the presence of contaminants in the plagioclase sample was minimal. Microprobe results showed that there was a significant amount of CaO (14.96%) in the plagioclase sample (Table 4.2). Dissolution of the calcium ions into the solution and subsequent hydrolysation and reprecipitation may account for the observed zeta potential reversal in the same way that Laskowski *et al.,* (1997) observed a surface coating of hydrolysed copper ion on sphalerite. The plagioclase sample contained about 30.2% of Al_2O_3. The PZC of Al_2O_3 has been reported by Parks (1967) to be at about pH 5. This may also offer an alternative explanation for the sudden positive shift between pH 4 and 6.

5.1.1.5 Oxides – chromite

Between pH 2 and 4 the zeta potential of chromite was positive and became progressively more negative as the pH increased from pH 6 to pH 10. A PZC of about pH 3.5 was observed which is similar to PZC values for chromite reported previously by Wesseldijk *et al.,* (1999); Sysilä *et al.,* (1996) and Martinovic *et al.,* (2005). In the case of oxide

minerals like chromite, H^+ and OH^- ions are the principal potential determining ions. By their interaction with water, surface hydroxyls are produced. Their dissociation produces the surface charge as described by Yopps and Fuerstenau, (1964); Fuerstenau and Fuerstenau, (1982) and Rao, (2004) as follows:

$$MOH_{surf} \rightleftharpoons MO^-_{surf} + H^+(aq) \quad (5.1)$$

$$MOH_{surf} + H^+(aq) \rightleftharpoons MOH_2^+{}_{surf} \quad (5.2)$$

Upon the immersion of an oxide mineral into an aqueous solution, the hydroxyl-covered surface, MOH_{surf}, can either donate a proton to the solution to form a negative surface site, MO^-_{surf}, or it can adsorb an extra proton to form a substituted surface hydronium ion (Yopps and Fuerstenau, 1964; Fuerstenau and Fuerstenau 1982). The above equations indicate that the positive site, $MOH_2^+{}_{surf}$, is favoured at high H^+ concentration (i.e. at pH < 3.5) while the negative site, MO^-, is favoured at low H^+ concentration (in this case at pH > 3.5). The distribution of these three kinds of sites shown in Equations 5.1 and 5.2, viz. MOH_{surf} , MO^- and $MOH_2^+{}_{surf}$, determines the charge on the oxide surface which in turn depends on the pH of the solution and the chemical structure of the oxide.

An alternative mechanism proposed by Parks and de Bruyn (1962) involves partial dissolution of oxide and the formation of surface hydroxyl species in solution, followed by the adsorption of these hydroxyl species onto the surface:

$$M_2O_3(s) + 3H_2O \rightleftharpoons 2M(OH)_3(aq) \quad (5.3)$$

$$M(OH)_3 \rightleftharpoons M(OH)^{3-m}(aq) + (3-m)OH^-(aq) \quad (5.4)$$

$$M(OH)_m^{3-m}(aq) \rightleftharpoons M(OH)_m^{3-m}{}_{surf} \quad (5.5)$$

The formation of surface charge by any mechanism, or by direct adsorption of hydrogen or hydroxyl ions, results in an equivalent change in pH of the solution. Under very acidic conditions, i.e. at pH 2, chromite exhibited a positive surface charge, indicating the presence of the positive $M(OH)_2^+{}_{surf}$ at high H^+ concentration. As the pH increased, the

surface charge became increasingly negative indicating the presence of the MO^- negative site which is favored at low H^+ concentration.

5.1.1.6 Sulphides - chalcopyrite

The zeta potential results for chalcopyrite in a buffered solution observed in Figure 4.6 showed a reversal in the zeta potential between pH 2 and 6, where the zeta potential moved from -21 mV at pH 2 and became more positive reaching 4.2 mV at pH 4. Two PZCs at pH 3.5 and pH 5 were attained, after which the zeta potential became more negative as pH was increased from pH 6 to pH 10. This reversal in the zeta potential may have resulted from the effects of oxidation on surface charge

Previous zeta potential studies on the effects on oxidation of sulphide minerals conducted by Fairthorne *et al.,* (1998); Fullston *et al.,* (1999) and He *et al.,* (2006) have indicated that the zeta potential of non-oxidised sulfide minerals is negative and comparable to that of elemental sulfur or to a sulfide mineral with a sulfur-rich surface. Upon oxidation, the sulfide mineral surface becomes increasingly covered with metal oxide and hydroxide species and the zeta potential versus pH curves of these sulfide minerals become less negative and even positive. According to Clarke *et al.,* (1995), the surface oxidation products on sulphides mainly consists of metal hydroxides and sulphur-oxy species, either adsorbed in thin layers or precipitated from solution as colloidal particles.

The copper speciation diagram adapted from Wesseldijk *et al.,* (1999) shown in Figure 5.3 shows the presence of $Cu(OH)_2(s)$ species in the pH range 6 to 11, and $Cu(OH)_2(aq)$ species between pH 3 to 11. The presence of these species in solution and on the chalcopyrite surface may be responsible for the observed charge reversal between pH 2 and 6.

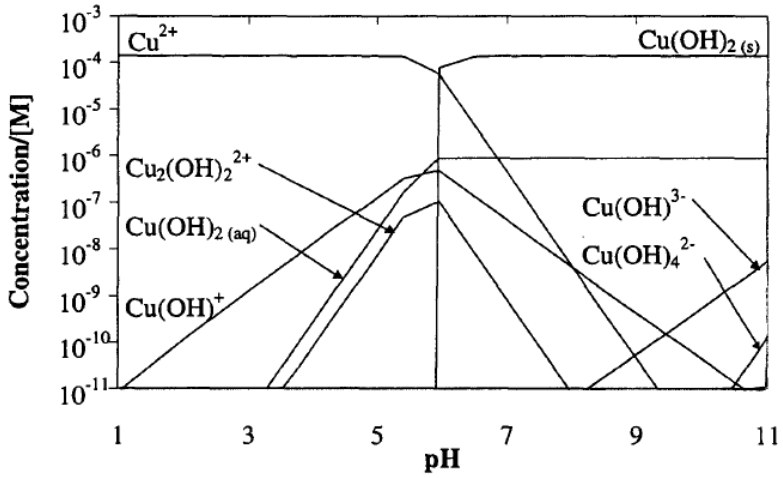

Figure 5.3: Speciation diagram for 1.4x10^{-2} M total copper (generated by MINTEQA2 for copper sulphate at 25°C) (Wesseldijk et al 1999)

Generally, the surface charge of each mineral became increasingly negative with an increase in pH in a buffered solution (Figure 4.7). At pH 9 which is of particular interest in this work, since sulphide concentrators in the Bushveld complex typically operate at this pH, there were differences in the observed zeta potential of each mineral as summarized in Table 5.1. Plagioclase had the most negative surface charge, followed by talc, chromite and pyroxene whose surface charges were very similar at this pH. Chalcopyrite was found to have the most positive surface charge due to the presence of hydroxyl species on its surface and in solution. It is anticipated that these differences in surface charge will affect the way in which depressant interacts with each mineral surface.

Table 5.1: Summary of the zeta potential of each mineral at pH 9 and the PZC in buffer

Mineral	**Zeta potential (mV)**		**PZC_{buffer} pH**
	buffer	**SPW**	
Talc	-48	-19	2
Plagioclase	-60	-16	1.8
Pyroxene	-44	-15	2.7
Chromite	-44	-10	3.5
Chalcopyrite	-33	-8	3.5 and 5

5.1.2 Mineral surface charge in synthetic plant water (SPW)

A significant positive shift in the zeta potential of each mineral was observed when measured in the presence of SPW compared to that in a buffer solution (Figures 4.2 to 4.6). In SPW, there was high concentration of calcium and magnesium ions. Figures 5.4 and 5.5 show speciation diagrams for $1x10^{-6}$ M Ca^{2+} and Mg^{2+} respectively. The speciation diagrams show that calcium and magnesium exist as divalent ions in solution between pH 2 and 10. Burdukova *et al.,* (2007) proposed that divalent Ca^{2+} ions tend not to adsorb onto the mineral surface, as such a process is thermodynamically unfavourable since they exist as ions in solution between pH 8 and 10. However Ca^{2+} hydrolysis products, namely $CaOH^{+}$ and $Ca(OH)_2(s)$, adsorb strongly. The adsorption of ions increases with the increasing amount of hydroxyl complexes (e.g. $CaOH^{+}$) at pH greater than pH 10 when these species are formed (Ahmed and Van Cleave (1965); James (1981); Burdukova *et al.,* (2008)). This however falls outside the scope of this investigation since all tests using SPW were conducted between pH 2 and 10.

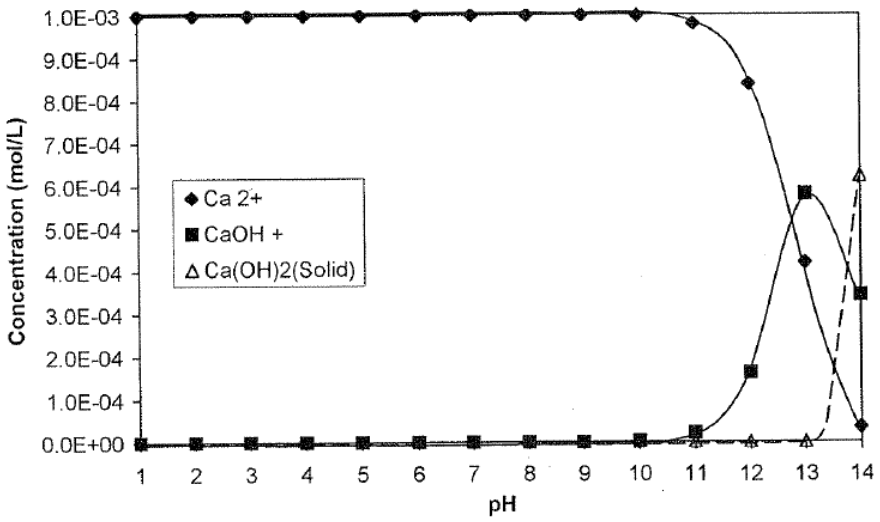

Figure 5.4: Speciation diagram for $1x10^{-6}$M Ca^{2+} (Rao, 2004)

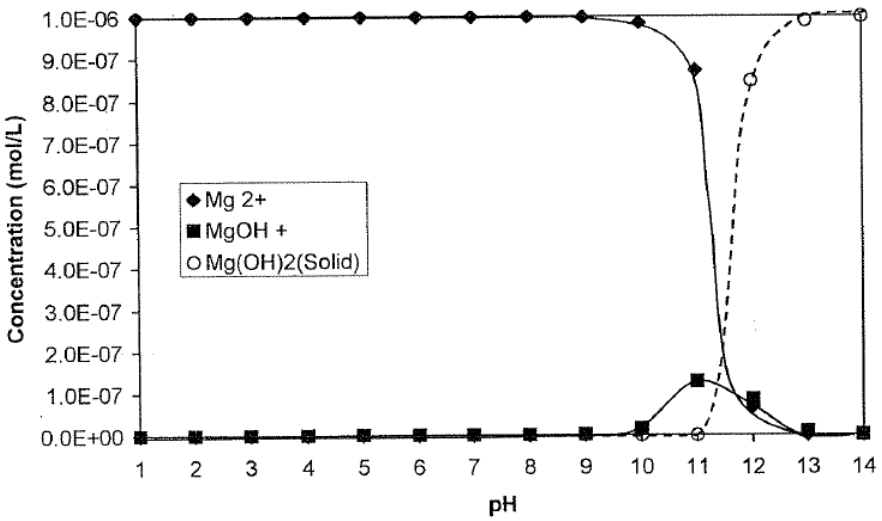

Figure 5.5: Speciation diagram for $1x10^{-6}$M Mg^{2+} (Rao, 2004)

Since calcium and magnesium only exist as divalent ions in solution between pH 2-10, they are thought to behave as indifferent electrolytes. Indifferent electrolytes do not alter the surface charge as they do not pass between solution phase and solid, but since they occur in the diffuse layer, they change the zeta potential (Rao, 2004). At high concentrations of indifferent electrolytes the double layer collapses and the zeta potential approaches zero even though the surface of the mineral is still charged. This is called "double layer compression'. It suggests that the Stern plane moves inwards. The variation of potential with distance from the mineral surface is compressed, resulting in a decrease in the zeta potential. The effect of indifferent ions increases with the valence and charge of the cations relative to the zeta potential of the solid (cf. Figure 5.6) and, with the valence of the anions when the zeta potential is positive. Double layer compression provides a possible explanation to the observed positive shift in the zeta potential of each mineral in the presence of ions found in SPW.

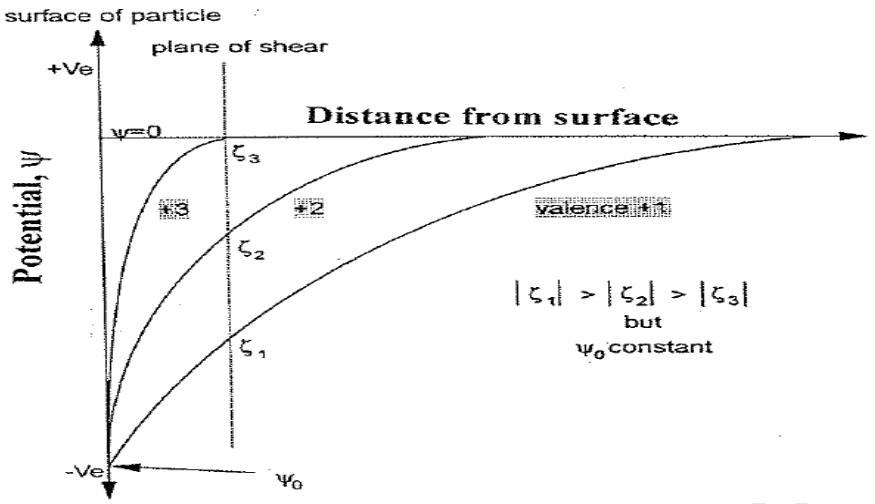

Figure 5.6: Double layer compression by indifferent electrolytes (Rao, 2004)

5.1.3 The effect of the adsorption of polymer on the mineral surface charge

Figures 4.9 to 4.13 show the effects of the addition of guar on the surface charge of each mineral. In these figures a comparison is made between the zeta potential of each mineral with and without guar in a buffer solution, and the zeta potential of each mineral with and without guar in SPW between pH 8 and 10.

5.1.3.1 Guar in buffer

Ma and Pawlik (2005) investigated the effect of cesium, potassium, sodium, and lithium cations on the adsorption of natural guar gum onto quartz. The role of these ions was analyzed in terms of their water structure-making or breaking capabilities. In the presence of structure makers (Na^+, Li^+) the polymer adsorption density did not change compared to the adsorption levels observed in distilled water. On the basis of these observations it was reasonable to assume that Na^+ ions in buffer did not affect the adsorption of polymer on the mineral surface.

In Figure 4.14 a comparison is made on the zeta potential of each mineral relative to each other after the addition of guar in buffer between pH 8 and 10. Generally, for each mineral the zeta potential became less negative with the addition of guar in buffer solution when compared that in just buffer solution alone. A similar positive shift in the zeta potential with the addition of guar on different mineral systems were obtained by other researchers e.g. Rath *et al*., (1997), Rath and Subramanian (1997); Wang *et al.*, (2005); Bicak *et al.*, (2007); Liu *et al*., (2006); Cuba-Chiem *et al.*, (2006), Jenkins and Ralston (1998) and Kaggwa *et al.*, (2005).

Although most of these authors investigated the effect of guar addition onto talc, their findings can be extended to each of the minerals used in this investigation. Rath *et al*, (1997) who investigated the adsorption of guar gum onto biotite mica, Wang *et al*., (2005) who investigated the adsorption mechanism of guar gum onto talc, and Bicak *et al.*, (2007) who investigated the adsorption of guar gum and CMC on pyrite, found that the addition of different concentrations of guar correspondingly reduced a negative zeta potential (i.e. the zeta potential became more positive) in proportion to the concentration of added guar. Brooks and Seaman (1972) who investigated the effect of neutral polymers on the electrokinetic potential of biological cells and other charged particles also found that the electrokinetic potentials of such systems become relatively more positive in the presence of neutral polymers.

Since the polymer appears to merely reduce the zeta potential and not change the PZC, the primary effect of the macromolecule seems to be to shift the slipping plane (or plane of shear) further away from the interface (Rath *et al.*, 1997). This suggests an increased thickness of the polymer layer within the electrical double layer with increasing guar concentration (Rath *et al.*, 1997; Wang *et al.*, 2005; Bicak *et al.*, 2007). According to Jenkins and Ralston (1998), guar was found to adsorb in a very flat conformation, with a high degree of segments (>75%) present at the talc–aqueous solution interface as trains, a conformation in which the majority of the polymer is in contact with the surface as illustrated in Figure 5.7. Jenkins and Ralston (1998), showed that the calculated adsorbed layer thickness, determined by microelectrophoresis, supported the hypothesis that the

mannose backbone of the guar chain adsorbs to the talc surface, leaving the pendant galactose groups protruding into the bulk solution.

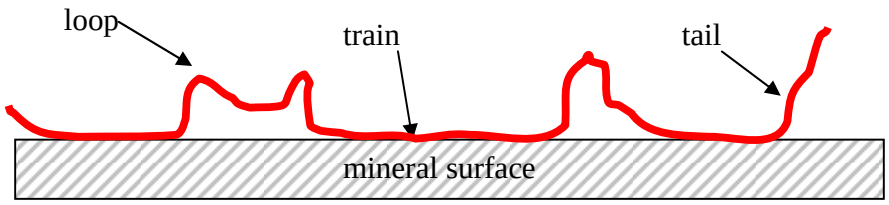

Figure 5.7: A schematic representation of the adsorption conformation of polymer on the mineral surface in the form of loops, trains and tails

Talc, pyroxene, chromite and chalcopyrite were found to posses a similar surface charge relative to each other with the addition of guar. This similarity in surface charge gives little indication on the relative differences in the adsorption density of guar on the mineral surface given that a uniform concentration was used when conditioning each mineral. This similarity does however give an indication of the degree of interaction between guar and each of the aforementioned minerals, in that the adsorption of guar onto the mineral surface caused a significant positive shift in the zeta potential. Plagioclase, however, remained significantly negative when compared to the other minerals, reaching a zeta potential of -49mV at pH10 when compared to -29mV to -22 mV attained by pyroxene, chromite, chalcopyrite and talc at pH 10. The fact that in the case of plagioclase the addition of guar caused virtually no change in the zeta potential suggests that plagioclase had the weakest interaction with guar.

5.1.3.2 Guar in SPW

In SPW, the zeta potential of each mineral became less negative with the addition of guar. The positive shift in the zeta potential for most of the minerals with the addition of guar in SPW was not as significant as was noted in buffer solution. The minerals attained a similar surface charge with the addition of guar (-4mV for pyroxene, chromite and chalcopyrite, and -6mV for talc). Plagioclase however still remained the most negative of

the minerals (-10mV) with the adsorption of guar in SPW. Given that standard error for these measurements was less than 1mV, this difference in the case of plagioclase was significant. The decrease in the negative surface charge shows a change in the surface properties of each mineral due the adsorption of guar on each mineral. With respect to the role of cations, Bicak, *et al.* (2007) has shown that the adsorption of guar onto pyrite was not affected by the addition of divalent Ca^{2+} ions. This factor is dealt with in detail Section 5.2.2.1.

5.1.3.3 CMC in buffer and 10^{-2}M IS Ca^{2+} solution

In buffer, the addition of CMC produced very little change in the zeta potential of each mineral (cf. Figure 4.16 to 4.20). The surface charge was virtually the same as it was in buffer alone. This suggests that very little or no interaction between CMC and the mineral surface took place in buffer. However with addition of calcium ions a positive shift in the zeta potential of each mineral was observed. The zeta potential trends of talc, plagioclase, and pyroxene with addition of CMC in 10^{-2}M IS Ca^{2+} solution were almost identical to those in 10^{-2}M IS Ca^{2+} solution alone as summarised in Table 5.2. Only in the case of chromite and chalcopyrite were slight differences observed in the zeta potential between the addition of CMC in 10^{-2}M IS Ca^{2+} solution and just 10^{-2}M IS Ca^{2+} solution alone. The observed similarity between the zeta potential of each mineral with or without CMC in 10^{-2}M IS Ca^{2+} solution suggests that the charge on CMC molecules may have been rendered neutral by the reaction with the calcium ions the bulk solution. This is dealt with in further detail in Section 5.2.2.2 which deals with the adsorption of CMC onto each mineral in 10^{-2}M IS Ca^{2+} solution.

Table 5.2: Summary of the zeta potential results for each mineral in buffer, buffer + CMC, 10^{-2} M IS Ca^{2+} solution and 10^{-2} M IS Ca^{2+} solution + CMC at pH 9

Mineral	Zeta potential (mV) at pH 9			
	buffer	**buffer + CMC**	**10^{-2} M IS Ca^{2+}**	**10^{-2} M IS Ca^{2+} + CMC**
Talc	-48.0	-52.4	-22.0	-22.0
Plagioclase	-60.0	-58.3	23.0	-22.9
Pyroxene	-44.0	-46.6	-20.0	-21.9
Chromite	-44.0	-49.0	-13.0	-20.4
Chalcopyrite	-33.0	-46.0	-17.0	-20.5

5.1.3.4 Comparison of the differences in mineral surface charge with the addition of guar and CMC

The results obtained above give an indication of the differences in the adsorption characteristics of guar, a neutral polymer, and CMC, which is negatively charged. Interactions between the mineral surface and depressant are observed with guar in both buffer and SPW, suggesting that the presence of divalent (Mg^{2+} and Ca^{2+}) ions in solution had little effect on the adsorption of guar. However, the interaction of CMC and the mineral surface seemed to be dependent on the presence of divalent ions in solution (c.f. Figure 4.16 to 4.21). It was observed that the surface charge on the minerals in buffer with the addition of CMC was similar to that obtained in buffer alone. As previously explained, this suggests that very little or no interaction between CMC and the mineral surface took place in buffer. With the addition of CMC in 10^{-2}M IS Ca^{2+} solution, the surface charge on each mineral became less negative. The presence of Ca^{2+} ions in solution has been found by Rao, (2004); Parolis *et al.*, (2005); Parolis *et al.*, (2008); Burdukova *et al.*, (2007) to greatly enhance the adsorption of CMC onto mineral sites . This is discussed in detail in Section 5.5.

5.1.4 Acid/base hypothesis

In order to discuss the significance of the zeta potential results it is necessary to present review of Liu and Laskowski's acid/base hypothesis. In a series of papers by Liu *et al.*, [Liu and Laskowski, 1989; Liu *et al.,* 2000; Liu *et al.,* 2006; Laskowski *et al.,* 2007] proposed that polysaccharides are adsorbed on mineral surfaces through interactions with the adsorption centers on mineral surfaces that are in the form of hydroxylated metallic sites. A direct consequence of the interaction of natural polysaccharides with the metal-hydroxylated species is that the interaction, and thus adsorption, is strongly dependent on pH. According to this theory, the interaction is an acid/base interaction.

According to this theory, the hydroxyl groups on mineral surfaces can either donate or accept a proton, thus behaving as a Brønsted acid or Brønsted base. The Brønsted acidity or basicity depends on the metal atom to which the hydroxyl group(s) is attached. If the metal atom is relatively more electron attracting, e.g. a small metal atom with a high positive valence, the proton will be less strongly held to the oxygen, and will be more labile, thus the acidity of the hydroxyl groups will be higher. The converse is true for a basic surface. The reaction mechanism proposed between the hydroxyl groups in polysaccharides and the mineral surface metal hydroxyls as shown schematically in Figure 5.8.

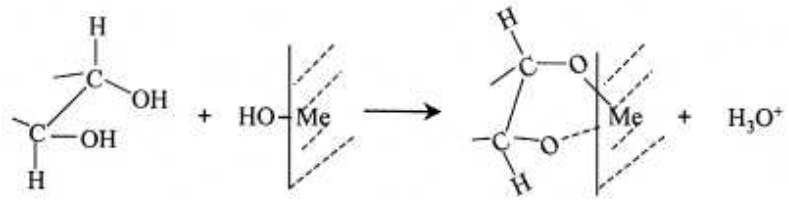

Figure 5.8: Schematic representation of the interaction polysaccharide molecules with the mineral surface (Liu et al., 2000)

Figure 5.8 suggests that the mineral surfaces donate an –OH group, and each of the two hydroxyl groups in the polysaccharide donate a proton to form the five-membered polysaccharide–metal ring complex. That is, the mineral surface metal-hydroxylated

species would behave as a Brønsted base during the interactions with polysaccharides. The stronger the basicity, the stronger will be the interaction with the polysaccharides.

Furthermore, Liu *et al.,* (2000) and Konan *et al.,* (2007) proposed that for a solid oxide, the PZC is an indication of the acidity or basicity of surface hydroxyl groups. A high PZC indicates a basic surface and a low PZC indicates an acidic surface.

In light of this, the zeta potential results for each mineral showed varying degrees of acidity/basicity. In a buffered solution, chalcopyrite had the least negative surface charge at pH 9 (-33 mV) and had the highest PZCs, viz. pH 3.5 and pH 5. Consequently, by the acid/base theory proposed by Lui *et al.,* (2000), chalcopyrite had the ability to readily donate –OH groups and to accept two protons from polysaccharide molecules, thus acting as a Brønsted base.

Plagioclase had the most negative surface charge of -60mV at pH 9 in buffer. Plagioclase is an alumino-silicate and the PZCs of Al_2O_3 and SiO_2 are quite low (5 and 1.8 as reported in Parks (1967)) indicating a high acidity of the surface hydroxyl groups. Trends in the periodic table show aluminium and silicon to posses a high electronegativity and small atomic radii (Sielberberg, 2002). As a result, it is thus expected that these metal-hydxolyated species will posses a strong Brønsted acidity. It is expected that the plagioclase will have the weakest interaction with the polysaccharide depressant.

The oxides of magnesium as found in talc and enstatite ($Mg_2Si_2O_6$, magnesium rich end member of pyroxene), and chromium as found in chromite have high PZCs (7 and 12 respectively) (Parks 1967). Consequently, due to the Brønsted basicity of the metal hydroxyl species, a strong interaction between polysaccharide and metal hydroxyl species for these minerals was expected. On the basis of surface charge, and in terms of the acid/base theory, chalcopyrite was the most basic, followed by talc, pyroxene and chromite which have similar surface charges. Plagioclase was the most acidic of these minerals due to its high eletronegativity. There is a good correlation between the surface charge and the depressant adsorption density on each mineral as observed in Figure 4.29

and Figure 4.31. This is discussed in detail in Section 5.3. It is noted however that the acid/base interactions do not necessarily explain whether the adsorption is through hydrogen bonding or through chemical complexation (Liu *et al.*, 2000).

5.2 ADSORPTION STUDIES

In this section the kinetics of adsorption of guar at constant temperature onto each of the minerals in synthetic plant water (SPW) is discussed. Furthermore, a discussion on the adsorption isotherms of guar and CMC in buffered solution, SPW and 10^{-2}M IS $Ca(NO_3)_2$ solution is presented.

5.2.1 Kinetic studies

For both guar and CMC, the rate of adsorption at constant temperature showed that the highest rate of depressant adsorption occurred in the first five minutes (c.f. Figure 4.23 and 4.26 respectively). After this the adsorption densities began to plateau at different values for each mineral. In the case of guar the highest initial rate (in the range of 0 to 2 minutes) of adsorption occurred with chalcopyrite. Talc, pyroxene, plagioclase and chromite had similar initial rates of adsorption. Although some scatter was observed in the CMC data (c.f. Figure 4.26), qualitatively, one observes a high rate of adsorption within the first 5 minutes for all the minerals except pyroxene. Equilibrium was reached within the first 30 minutes except again for pyroxene. These observations are similar to those made by Rath and Subramanian (1997) in a study of the adsorption of guar gum onto biotite mica in that equilibrium was attained within the first 30 minutes.

It was postulated that under conditions of competitive adsorption, different rates of depressant adsorption of one mineral over others would result in the preferential adsorption of depressant onto one mineral relative to another. However, the results obtained suggest that kinetics do not seem to be a strong factor affecting the preferential adsorption of depressant. In the microflotation experiments when a 2g talc sample (BET area = 4.86m^2, +45-106μm) was conditioned under starvation depressant concentrations

(0.25mg/L of guar which is equivalent to 0.88g/t ore), a surface coverage of 0.023 pseudo-monolayers was achieved. This was sufficient to achieve good depression of the talc sample resulting in a 3.2% talc recovery at 2 minutes and 6% talc recovery after 20 minutes. When this is compared to the fractional surface coverage of guar on each mineral at 2 minutes in the kinetic studies, the surface coverage was one order of magnitude greater than that obtained in the microflotation experiments as summarised in Table 5.3. This suggests that sufficient coverage was obtained after 2 minutes to achieve depression. Typically the residence time of ore in flotation cell is about 20 to 30 minutes. This allows for sufficient contact time between depressant and the ore.

Table 5.3: Summary of the fractional coverage of guar on each mineral after 2 minutes

Mineral	**Adsorption density (mg/m^2)**	**Surface coverage – θ pseudo-monolayers**
Talc	0.251	0.32
Plagioclase	0.261	0.34
Pyroxene	0.423	0.54
Chromite	0.174	0.22
Chalcopyrite	0.561	0.72

5.2.2 Equilibrium studies

Equilibrium studies provided a basis from which the adsorption density of depressant onto each mineral could be quantified. The effect of the presence of divalent ions in solution was tested by conducting the adsorption studies in buffer and SPW for guar ,and in buffer and 10^{-2}M IS $Ca(NO_3)_2$ solution for CMC. The effect of charge on the depressant was tested by comparing adsorption densities of guar and CMC on each mineral.

5.2.2.1 Adsorption isotherms – guar

Figures 4.27 and 4.30 showed the adsorption densities of guar on each mineral as a function of equilibrium concentration in buffer and SPW respectively. As expected the

adsorption isotherms for each mineral showed an increase in the adsorption density of guar as the concentration was increased. Each of the isotherms exhibited typical Langmuir behaviour, characterised by an initial increase in the adsorption density until a plateau was reached. Different maximum adsorption densities of guar were reached on each mineral in buffer. Chalcopyrite attained the highest maximum adsorption density, followed by talc and chromite whose isotherms were similar, followed by pyroxene and then plagioclase.

It is interesting to note that the trend in the differences in adsorption densities in buffer and in SPW correlate closely with the differences observed in the surface charge of each mineral at pH 9 in buffer as summarised in Table 5.4.

Table 5.4: Summary of the zeta potential, maximum adsorption densities, affinity constant (K) and the fractional coverage of guar in buffer and SPW

Mineral	**Zeta potential at pH 9 (mV)**		**Max. adsorption density (mg/m^2)**		**Equilibrium constant - K**		**Fractional surface coverage - θ**	
	buffer	**SPW**	**buffer**	**SPW**	**buffer**	**SPW**	**buffer**	**SPW**
Talc	-48	-19	0.62	0.60	0.064	0.139	0.79	0.79
Plagioclase	-60	-16	0.43	0.27	0.081	0.031	0.51	0.34
Pyroxene	-44	-15	0.43	0.42	0.172	0.016	0.56	0.55
Chromite	-44	-10	0.59	0.49	0.099	0.050	0.75	0.62
Chalcopyrite	-33	-8	0.73	1.04	0.097	0.145	0.94	1.34

As previously stated, guar is a neutral molecule. On the basis of its charge, one would expect it have an unselective or uniform depressant action on all the minerals. However, marked differences in the adsorption density of guar on each of the minerals were observed. Laskowski *et al.*, (2007) proposed that natural polysaccharides such as starch, dextrin and guar gum in general adsorb strongly on basic metal oxides (Pb, Ni, Ca, Mg, e.t.c.), and weakly on acidic metal oxides/hydroxides. Zeta potential results showed that chalcopyrite had relatively the most positive surface charge, and hence the most basic surface, and plagioclase had the most negative surface, and hence the most acidic surface. Consequently, it is expected that in terms of the acid/base hypothesis chalcopyrite would have the strongest interaction with guar, and plagioclase the weakest. The interaction is

between the metal hydroxyl species, and the hydroxyl groups on the polysaccharide. Talc, pyroxene and chromite were found to have similar surface charges, higher than plagioclase but lower than chalcopyrite. None of the minerals attained pseudo-monolayer coverage even though the system was at equilibrium.

In SPW, a similar progression in the maximum adsorption density of guar on each mineral is observed as was found in buffered solution. Chalcopyrite was found to have the highest adsorption density followed by talc, then chromite, then pyroxene and then plagioclase as shown in Figure 4.30, and summarised in Table 5.4. It was observed that, in the presence of calcium and magnesium ions in solution, there was an increase in the adsorption density of guar onto chalcopyrite, resulting in a fractional coverage of about 1.34 pseudo-monolayers. The adsorption density of guar onto talc, pyroxene and chromite, the adsorption density of guar remained relatively constant in SPW and there was a decrease observed for plagioclase.

The effect of the presence of divalent ions in solution on the adsorption densities obtained for talc, pyroxene and chromite in buffer and SPW relate closely with work done by Bicak, *et al.* (2007), who showed that the adsorption of guar onto pyrite was unaffected by the presence of calcium ions in solution. They also found that microflotation tests showed that addition of calcium ions promoted pyrite flotation in the absence of depressants but did not affect adsorption of guar gum. The addition of guar considerably decreased pyrite floatability, irrespective of the presence of calcium ions. A number of researchers [Jenkins and Ralston, 1998; Wang, *et al.* 2005; Wang and Somasundaran, 2007] have also found the adsorption of guar onto talc to be unaffected by ionic strength.

As previously mentioned, the adsorption isotherms obtained seemed to conform to the Langmuir adsorption model.

$$\frac{C_{eq}}{I_{ads}} = \frac{1}{I_{\max}} + \frac{C_{eq}}{I_{\max}} \qquad (5.6)$$

When the C_{eq}/I_{ads} (the equilibrium concentration/adsorption density) was plotted against the reciprocal of the equilibrium concentration ($1/C_{eq}$), this yielded straight lines with

good regression coefficients. This enabled the calculation of the Langmuir equilibrium constant (K) as reported in Tables 4.7 and 4.9. It has been proposed that the equilibrium constant can be considered to represent the affinity of a polymer for a particular surface [Jenkins and Ralston, 1998; Rath *et al.*, 2000; Rath *et al.*, 2001; Morris *et al.*, (2002); Wang and Somasundaran, 2005; Cheim *et al.*, 2006]. In SPW, chalcopyrite had the highest equilibrium constant, followed by talc and then chromite. Plagioclase however had a higher equilibrium constant than pyroxene. The equilibrium constants suggest that the mineral surfaces have different affinities for depressant which might not necessarily be reflected by the maximum adsorption densities due to availability of active sites on the mineral surface. In other words, plagioclase for example may contain a few highly energetic surface sites, which results in a strong affinity constant. However, these few sites are quickly used up and the maximum adsorption density remains low.

In the flotation of PGMs one aims at maximizing sulphide recovery, since PGMs are associated with sulphides. Hence, the goal is to render sulphide particles hydrophobic. It was interesting to note in this investigation that chalcopyrite had the highest adsorption density of guar when compared to other minerals in both buffer and SPW. This raised the question of whether this resulted from the absence of collector in the system, thus allowing a high adsorption of guar, or would a similar result be obtained if collector molecules were pre-adsorbed as in normal plant operations. To test this, chalcopyrite was conditioned in sodium isobutyl xanthate (SIBX) for 10 minutes in buffer solution at a concentration high enough ensure one pseudo-monolayer coverage. Guar was then added, and the mixture was allowed an equilibrium time of 4 hours. Figure 4.48 showed the result obtained in this exploratory experiment.

The results showed that the adsorption density of guar onto chalcopyrite in fact increased slightly in the presence of collector. Similar results were obtained by Rath *et al.*, (2001) who found that an increase in the concentration of ethyl xanthate resulted in an increase in the adsorption density of guar gum onto chalcopyrite, and conversely, an increase in the concentration of guar resulted in an increase in the adsorption density of ethyl xanthate onto chalcopyrite. They proposed that this mutual enhancement of adsorption by

guar gum and xanthate is suggestive of an association between them. Such a mechanism with the xanthate held inside the guar gum can also explain the observed enhanced adsorption of xanthate at the chalcopyrite-solution interface in the presence of guar gum without rendering the chalcopyrite surface hydrophobic. Thus, these researchers proposed that the wrapping of xanthate by guar gum could explain the loss of hydrophobicity of the chalcopyrite surface leading to its depression (Rath *et al.,* 2001).

Although the results shown in Figure 4.48 were preliminary, they raise the question of whether a similar increase in the adsorption density of guar onto chalcopyrite would be obtained at large dosages of xanthate; and if this high guar adsorption density on chalcopyrite affects the copper grade in existing sulphide concentrators. The question of synergistic or antagonistic interactions between sulphides onto which xanthate reaction products such as dixanthogen has adsorbed and guar depressant is clearly an important subject for further research.

5.2.2.2 Adsorption isotherms – CMC

Very little or no adsorption was observed in the case of CMC in buffer solution (see Appendix 7 for raw data). However, in 10^{-2}M IS $Ca(NO_3)_2$ solution, the adsorption of CMC onto each mineral increased significantly. Similar observations were made in the zeta potential measurements in the presence of CMC which saw very little or no change in the negative surface charge of each mineral upon the addition of CMC in buffer. However, in 10^{-2} M IS $Ca^{2+,}$ solution, a significant decrease in the negative zeta potential was observed in the presence of CMC, suggesting an increased interaction between CMC and the mineral surface.

Extensive work has been done by Parolis *et al.,* (2008) to elucidate the mechanisms of CMC adsorption onto talc. They observed that the adsorption of CMC onto talc was irreversible in the presence of calcium ions. Furthermore, it has also been reported that higher adsorption densities of CMC were obtained in the presence of divalent Mg^{2+} and Ca^{2+} ions [Parolis *et al.,* 2005; Parolis *et al.,* 2008; Khraisheh *et al.,* 2005; Wiese *et al.,*

2008; and Burdukova *et al.*, 2008]. This can be ascribed to the greater effectiveness of charge screening by the Ca^{2+} ions within the CMC molecules in solution, which reduces the electrostatic repulsion between the CMC and talc. In an in-situ particle film ATR-FTIR study of CMC adsorption on talc, Cuba-Chiem *et al.*, (2008) proposed that the polymer binds to the surface of talc through a chemical mechanism involving a bidentate chelating bond between the carboxyl groups and the talc surface, presumably through magnesium sites. They further proposed that the effect of calcium ions was more likely to be in the role of charge neutralisation of carboxyl groups, facilitating adsorption through a reduction in the electrostatic repulsion of CMC from the edge of the particles.

Furthermore, it has been reported by various researchers [Hoodgendam *et al.*, 1998; Morris *et al.*, 2002; Parolis *et al.*, 2008] that the presence of Ca^{2+} ions in solution leads to a more tightly coiled conformation of CMC molecules. This results in a smaller area of adsorption per molecule on the talc surface. It is also interesting to note that the differences in the adsorption densities of CMC onto each mineral correlates closely to the differences in surface charge observed in a buffered solution. This is summarised in Table 5.5.

Table 5.5: Summary of the zeta potential at pH 9 and maximum adsorption densities of CMC in buffer and 10^{-2}M IS $Ca(NO_3)_2$

Mineral	**Zeta potential at pH 9 (mV)**		**Max. adsorption density (mg/m^2)**
	buffer	**10^{-2}M IS Ca^{2+}**	**10^{-2}M IS Ca^{2+}**
Talc	-48	-20	0.29
Plagioclase	-60	-22	0.22
Pyroxene	-44	-20	0.40
Chromite	-44	-14	0.46
Chalcopyrite	-33	-16	0.65

These differences in the adsorption density are suggestive of the acidic or basic properties of each mineral. Chalcopyrite which was found to have the most basic surface still has the highest adsorption, and plagioclase which was found to have the most acidic surface has the lowest adsorption density of CMC. This is consistent with the theory on acid/base

interaction. The effect of the charge on the polymer is highlighted by the equilibrium adsorption results. Unlike guar where adsorption took place in the absence and the presence of ions in solution, CMC adsorption was highly dependent on the presence of divalent ions.

5.3 MICROFLOTATION RESULTS

The microflotation response of a 2g talc sample (+53-106μm) was used as an indicator of the preferential adsorption of depressant in a mixed mineral system. As previously explained, the recovery of the 2g talc sample in a microflotation cell served as a diagnostic of the extent to which depressant adsorbed onto a second mineral. It should also be noted that microflotation is essentially an indication of the extent to which a particle is able to attach to a bubble and rise as far as the pulp-froth interface. In this sense it does not indicate what would occur in a normal flotation cell in which the froth phase is known to play such a key role.

When the 2g talc sample was conditioned alone at a depressant concentration of 0.25 mg/L, it yielded a recovery of about 6 %. However, when the talc sample was intimately mixed with a second mineral with total surface areas between $2m^2$ or equivalent to that of the 2g talc sample ($4.86m^2$) or $6m^2$ of the second mineral, the depressant competitively adsorbs onto the two different mineral samples. Hence with the addition of a second mineral, and given a constant amount of depressant being added, as in the case of the pure talc, the adsorption density on the 2g talc sample was decreased and consequently resulted in a relatively higher recovery. As the surface area of the added mineral was increased, an even higher talc recovery would be expected due to a relative decrease in the depressant adsorption density onto talc. These results were shown in Figures 4.36 to 4.40 for guar and Figures 4.42 to 4.46 for CMC.

5.3.1 Microflotation tests in 0.25mg/L guar in SPW

Figures 4.36 to 4.40 show the percent talc recovery as a function of time for guar for the various cases of mixtures with the second mineral. For each curve, an increase in the talc recovery with time was observed with an increase in the amount of the second mineral were mixed with the talc. In other words, as the amount, and hence the BET surface area of the second mineral was increased, an increase in the percent recovery of talc was observed. The observed increase in talc flotation resulted from the decrease in the adsorption density of the guar onto talc in the presence of a second mineral. The extent to which talc recovery increased after conditioning in the presence of an added mineral reflected the relative preference of the depressant for the second mineral.

Figure 4.41 showed the percent cumulative talc recovery as a function of the BET surface area of the added mineral. The graph shows that the highest percentage cumulative talc recovery was observed with chalcopyrite as the second mineral, followed by pyroxene, talc (-38μm) and chromite which had similar cumulative talc recoveries. Plagioclase had the lowest cumulative talc recovery. These results represent a relative scale of preference of guar for the second mineral compared to talc and hence suggest that in a mixed mineral system chalcopyrite has the highest affinity for guar and plagioclase the lowest affinity.

The trend observed above correlates closely with the differences in surface charge obtained in zeta potential measurements and the differences in the adsorption densities obtained from the equilibrium adsorption studies. According to the results, guar adsorbs preferentially onto chalcopyrite, then talc, pyroxene and chromite, then plagioclase under conditions of starvation depressant concentrations. From these results it is reasonable to conclude that the zeta potentials of minerals give an indication of their relative preferential adsorption of guar.

According to Lotter, *et al.,* (2008) and Becker, *et al.,* (2009) orthopyroxene is by far the greatest diluent in PGM concentrate. Lotter, *et al.,* (2008) and Becker, *et al.,* (2009)

reported that, on closer examination, orthopyroxene particles show a surface association to talc. These composite orthopyroxene particles with partial talc rims are thought to be one of the main contributors to the occurrence of naturally floatable gangue (NFG) in the Merensky Reef ore. In light of this association between talc and orthopyryoxene, the use of a depressant that adsorbs preferentially onto pyroxene and talc, as shown in the adsorption and microflotation studies is crucial in reducing the recovery of such NFG.

The microflotation results above coupled with adsorption and zeta potential data provide a possible explanation for results obtained by Becker, *et al*. (2009) in their mineralogical characterization of concentrates obtained from batch flotation tests of Impala Merensky Reef ore with and without guar addition. A significant decrease in the recovery of orthopyroxene and talc was observed with the addition of guar. With plagioclase, however, an increase in recovery was observed with the addition of guar. This suggested that guar preferentially adsorbs onto talc and pyroxene relative to plagioclase as observed in the microflotation results. Since plagioclase had the least basic surface, its interaction with guar would be expected to be very weak.

5.3.2 *Microflotation tests in 0.25mg/L CMC in SPW*

The percent cumulative talc recovery in CMC gave results which were quite different from those obtained in the case of guar. The results showed that talc (as an added mineral) had the highest cumulative talc recovery. At 4.86m^2 of added mineral, plagioclase, pyroxene and chalcopyrite had a similar talc recovery, and chromite had the lowest talc recovery. This trend changed at 6m^2 of added mineral, showing a similar talc recovery for plagioclase, pyroxene, chromite and chalcopyrite. This similarity in talc recovery suggests that at starvation CMC concentrations, the adsorption of CMC was not selective. Unlike guar, these microflotation results did not show any strong relationship with the equilibrium adsorption isotherms.

Moreover, the percentage talc recovery in the absence of added mineral was higher in the case of CMC (15.9%) compared to guar (6%). This suggests that greater depression was achieved with guar than CMC suggesting that guar is a stronger depressant than CMC.

Table 5.6 compares the rate of change of the percent cumulative talc recovery with increasing total BET surface area of added mineral in guar and CMC as determined from the slope of the percent cumulative talc recovery of each mineral for each depressant (c.f. Figures 4.41 and 4.47). The higher the slope, the higher the rate of talc recovery with increasing surface area of added mineral, thus a high affinity for depressant of the mineral in question.

Table 5.6: Summary of the rate of change of the percent cumulative talc recovery with increasing total BET surface area of added mineral (from Figures 4.42 and 4.47).

Mineral	**Guar**	**CMC**
Talc	3.78	6.80
Plagioclase	0.99	4.97
Pyroxene	4.06	4.67
Chromite	3.66	3.87
Chalcopyrite	6.09	4.47

Table 5.6 shows that plagioclase and chalcopyrite had virtually the same slopes for CMC, suggesting no difference in the selectivity of these minerals towards CMC. However, the same minerals showed large differences in slope when exposed to guar, which suggested that they were respectively the least and the most selective for guar. Taking into account error bars in Figure 4.47, there was very little difference between the rates of change of talc recovery with increasing surface area for all added minerals when exposed to CMC. This suggests that there was little difference in mineral affinity towards CMC.

It is worth mentioning that microflotation tests in CMC were not consistent with differences observed in surface charge from zeta potential measurements and adsorption densities. This inconsistency rejects, in the case of CMC, the hypothesis that differences in mineral surface charge will affect the selective binding of the depressant molecules. A modification of the mineral surface chemistry that resulted in non-selective adsorption of

the CMC molecules may be responsible for the observed behaviour. However this may be discounted on the grounds that any mineral surface modification would be occurring equally for the minerals whether they interacted with CMC or guar. It is also possible that an acid-base interaction via carboxyl and hydroxyl groups on the CMC molecules with metal hydroxyl species on the mineral surface may not be the only dominant adsorption mechanism for CMC, since differences in the surface acidity/basicity seem not to result in different affinities for the CMC between the different minerals.

It has been found that the adsorption of divalent Ca^{2+} ions onto a talc surface was almost negligible in the absence of CMC but increased dramatically with the adsorption of CMC (Burdukova *et al*, 2008). This indicates that Ca^{2+} ions interact with the carboxylate groups on the CMC and are co-adsorbed with the CMC. According to Cuba-Chiem *et al.*, (2008) the effect of calcium ions is likely to play a role of charge neutralisation of carboxyl groups, thus facilitating adsorption through a reduction in the electrostatic repulsion of CMC from the negatively charged mineral surface. Cuba-Chiem *et al.*, (2008) further proposed that due to the multivalent nature of calcium, it is possible that the ions facilitate attractive intramolecular electrostatic interaction, which would affect the polymer conformation in solution and in the adsorbed state. This interaction will change the conformation of the CMC from that of a relaxed polymer chain to a coiled globular form (Ueno *et al*, 2007). It is possible that this conformational change results in the exposure of the hydrocarbon backbone of the CMC and favours hydrophobic interactions over acid-base complexation reactions. Hydrophobic interactions would be more non-specific than complexation reactions between the depressant hydroxyl groups and metal ions on the mineral surface.

6 CONCLUSIONS

The aim of this study was to investigate the adsorption characteristics of polymeric depressants on pure minerals. The minerals used were talc, pyroxene, plagioclase, chromite and chalcopyrite and the depressants used were guar gum and carboxymethyl cellulose (CMC).

It was hypothesised at the beginning of this study that polymeric depressants adsorb preferentially onto different minerals because of the differences in surface charge of the minerals which arise as a result of their different chemical structures. Zeta potential measurements were conducted to investigate what role such differences in the surface charge of each mineral play in determining the nature of adsorption of depressant onto the mineral surface, and what role metal ions in solution play in modifying the mineral surface charge and therefore changing the adsorption characteristics.

Generally, the surface charge of each mineral became increasingly negative as pH increased in a buffered solution. At pH 9, plagioclase had the most negative surface charge, followed by talc, chromite and pyroxene whose surface charges were very similar at this pH. Chalcopyrite was found to have the least negative surface charge possibly due to the effects of the presence of oxidation products. An acid/base theory proposed by Liu *et al.*, (2000), which describes an interaction between metal-hydroxyl species on the mineral surface and the hydroxyl groups on the polysaccharide, suggested that the strength of the interaction between mineral and depressant depended on the relative basicity of the metal-hydroxyl complexes on the mineral surface. In terms of this theory, chalcopyrite, whose surface was the least negative, was the most basic, and plagioclase which was the least negative, would be the most acidic. Consequently, the strongest interaction was expected between chalcopyrite and depressant whereas that between plagioclase and depressant would be the weakest.

The presence of divalent calcium and magnesium ions in solution resulted in a positive shift in the zeta potential. This was thought to have resulted from double layer

compression since it has been proposed that indifferent electrolytes do not directly alter the surface charge as they do not pass between solutions and solid, but since they occur in the diffuse layer, they may change the zeta potential (Rao, 2004).

A relative positive shift in the zeta potential was observed with the addition of guar which resulted in talc, chromite, pyroxene and chalcopyrite attaining a similar surface charge. The zeta potential of plagioclase remained relatively more negative compared to the other minerals. A similarity in the zeta potential at pH 9 gave little indication of the differences in the adsorption density of guar on each mineral. These zeta potentials did however give an indication of the degree of the interaction between guar and each of the minerals. With this in mind, plagioclase seemed to have the weakest interaction with guar. The addition of CMC in a buffered solution resulted in a minimal change in the negative surface charge on each mineral, suggesting minimal interaction between CMC and each of the minerals. However, the zeta potential on each mineral became less negative with the addition of CMC in a 10^{-2} M IS $Ca(NO_3)_2$ solution when compared to the buffered solution. This suggests that the adsorption of CMC is greatly enhanced by the presence of divalent ions in solution. The surface charge on each mineral in a 10^{-2} M IS $Ca(NO_3)_2$ solution with and without CMC present was the same. This similarity in surface charge may have resulted from a reduction in the negative charge on CMC due to the presence of the divalent ions solution.

It was further hypothesised that depressants adsorb preferentially onto different minerals because there are differences in the equilibrium and kinetic adsorption characteristics of each mineral towards depressant molecules. A study of the kinetics of adsorption of guar and CMC onto each mineral at constant temperature was conducted to test which mineral had the highest rate of depressant adsorption in a single mineral system. For both CMC and guar the maximum adsorption happened in the first five minutes on all the minerals. With guar, an adsorption density sufficient to achieve good depression was attained after only two minutes for each mineral. The results obtained suggest that from an operational point of view depressant adsorption is not rate controlled. Equilibrium was attained within the 30 minutes for all the minerals.

Equilibrium studies were conducted to test which mineral had the highest affinity for polymer in a single mineral system. The effect of the presence of ions in solution on depressant adsorption was tested by conducting the adsorption experiments in SPW for guar, and in a 10^{-2}M IS $Ca(NO_3)_2$ solution for CMC. The adsorption isotherms displayed Langmuir behaviour. In a buffered solution, chalcopyrite had the highest affinity for guar, followed by talc and chromite, then pyroxene. Plagioclase had the lowest affinity for guar. This progression in the affinity for guar in a buffered solution correlated closely with the differences observed in the surface charge of each mineral at pH 9. These observations were consistent with the acid/base interaction theory in terms of which chalcopyrite with the most basic surface would have the highest affinity for guar, and plagioclase, which had the most acidic surface, would have the weakest interaction with guar.

The presence of ions solution had a minimal effect on the maximum adsorption density of guar on all the minerals except for chalcopyrite, for which the adsorption density was slightly higher than that in buffer. The adsorption of CMC showed a strong dependence on the presence of divalent ions in solution. This may be due to the greater effectiveness of charge screening by the Ca^{2+} ions within the CMC molecules in solution, which reduces the electrostatic repulsion between the CMC and the mineral surface (Burdukova *et al.,* 2008). Another factor which may explain this observation is that it has also been proposed that CMC assumes a coiled conformation in the presence of divalent calcium ions in solution, which results in a smaller area of adsorption per molecule on the mineral surface (Parolis *et al.*, 2008)

Microflotation experiments were conducted to evaluate the hydrophobicities of each mineral as a function of their relative affinity for the depressant in a mixture of each mineral with talc. The recovery of a 2g talc sample in the size range +53-106μm in a microflotation cell served as a diagnostic of the extent to which depressant adsorbed onto the second mineral. Talc is hydrophobic and hence will float more readily in the relative absence of a depressant. This would indicate a preferential adsorption of the depressant

onto the added mineral. Chalcopyrite as an added mineral was found to have the highest cumulative talc recovery as its total BET surface area was increased. This was followed by pyroxene, talc (-38μm) and chromite, which had similar cumulative talc recoveries. Plagioclase had the lowest cumulative talc recovery. These results represent a relative scale of preference of guar for the second mineral compared to talc and hence suggest that in a mixed mineral system chalcopyrite has the highest affinity for guar and plagioclase the lowest affinity. A similar progression in the maximum adsorption densities of guar was observed, again validating an acid/base interaction between guar and each mineral.

Microflotation experiments with CMC showed very little difference in talc recovery with increasing surface area between the added minerals when exposed to CMC. This suggests that there was little difference in mineral affinity towards CMC at starvation dosages and under conditions of competitive adsorption. It is possible that an acid/base interaction is not the only dominant interaction between CMC and the minerals. A coiled CMC conformation, due to presence of divalent calcium ions in solution, may result in the exposure of the hydrocarbon backbone of CMC which would favour hydrophobic interactions over acid-base complexation reactions. Hydrophobic interactions would be more non-specific than complexation reactions between the depressant hydroxyl groups and metal ions on the mineral surface.

An exploratory experiment in which guar was adsorbed onto chalcopyrite, pretreated with a collector (SIBX) showed an increase in the adsorption density of guar in the presence of SIBX when compared to that in buffer alone. Rath *et al.*, (2001) proposed that this mutual enhancement of adsorption by guar gum and xanthate is suggestive of an association between them. Although these tests were preliminary, they raise the question of whether a similar increase in the adsorption density of guar onto chalcopyrite would be obtained at large dosages of xanthate and whether this high guar adsorption density on chalcopyrite affects the copper grade in existing sulphide concentrators. The question of synergistic or antagonistic interactions between sulphides onto which xanthate reaction

products such as dixanthogen has adsorbed and guar depressant is clearly an important subject for further research.

An investigation into the relative hydrophobicities of each of the minerals used in this project in the presence of collector by determining contact angles also presents an opportunity for an extension of this work. Further work could also be done in trying to understand the specific interactions occurring between CMC and each of the minerals. This would aid in optimizing the depression of naturally floating gangue.

REFERENCES

Ahmed, S.M., Van Cleave, A.B., 1965. Adsorption and flotation studies with quartz. Part I, Adsorption of calcium, hydrogen and hydroxyl ions on quartz. Canadian Journal of Chemical Engineering, vol. 43, pp.23–65.

Alvarez-Silva, M., Finch, J.A., Mirnezami, M., Uribe-Salas, A., 2010, The point of zero charge of phyllosilicate minerals using the Mular–Roberts titration technique, Minerals Engineering vol 23, pp.383–389

Batdorf, J.B., Rossan, J.M., 1973, Industrial Gums, ed. Whistler, R.L., Academic Press, New York

Barnes, S., Maier, W.D., 2002, Platinum-group Elements and Microstructures of Normal Merensky Reef from Impala Platinum Mines, Bushveld Complex, Journal of Petrology, vol. 43, pp.103-128

Beattie, A.D., Huynh, L., Kaggwa, G.B., Ralston, J., 2006, Influence of adsorbed polysaccharides and polyacrylamides on talc flotation, International Journal of Mineral Processing, vol.78, pp.238– 249

Becker, M., Harris, P., Wiese, J., Bradshaw, D.J., 2006, The use of quantitative mineralogical data to interpret the behaviour of gangue minerals in the flotation of Merensky ores, In: MEI Conference on Automated Mineralogy, Brisbane, July 2006

Becker, M., Bradshaw, D.J, Harris, P.J., Wiese, J. G., 2009, Mineralogical characterization of naturally floatable gangue in Merensky Reef ore flotation, International Journal of Mineral Processing, vol. 93, pp.246–255

Berry, L.G., Mason, B., 1959, Mineralogy-concepts, Descriptions, W.H. Freeman and Company, San Francisco, California, U.S.A., pp.299-461

Bicak, O., Bradshaw, D.J., Ekmekci, Z., Harris, P.J., 2007, Adsorption of guar gum and CMC on pyrite, Minerals Engineering, vol. 20, pp.996–1002

Bogusz, E., Brienne, S.R., Butler, I., Finch, J.A., Rao, S.R., 1997, Metal ions and dextrin adsorption on pyrite, Minerals Engineering. vol. 10, pp.441–445.

Buckley, A.N. and Woods, R., 1984, An x-ray photoelectron spectroscopic study of the oxidation of chalcopyrite, Aust. J. Chem., vol. 37, pp.2403–2413

Bradshaw, D.J., O'Connor, C.T., 1996, Measurement of the sub-process of bubble loading in flotation, Minerals Engineering, vol. 9, no. 4, pp.443-448

Bradshaw, D., 2009, Introduction to minerals processing and assessment of flotation performance, Lecture 7, Process Mineralogy Course, University of Cape Town, Cape Town, South Africa.

Bradshaw, D.J., Oostendorp, B., Harris, P.J., 2005, Development of methodologies to improve the assessment of reagent behaviour in flotation with particular reference to collectors and depressants, Minerals Engineering, vol. 18, pp.239 – 246

Brooks, D.E., Seaman, F.G.V., 1972, The effect of neutral polymers on the electrokinetic potential of cells and charged particles, Journal of Colloid and interface Science, vol.44, no3, pp.671 - 683

Burdukova, E., 2007, Surface properties of New York talc as a function of pH, polymer adsorption and electrolyte concentration, PhD Thesis, Department of Chemical Engineering, Faculty of Engineering and Built Environment, University of Cape Town, Cape Town

Burdukova, E., Becker, M., Bradshaw, D.J., Laskowski, J.S., 2007, Presence of negative charge on the basal planes of New York talc, Journal of Colloid and Interface Science, vol. 315, pp.337-342.

Burdukova, E.,, Bradshaw, D.J., Laskowski, J.S., Smeink R.G., Prins, F.E.,Van Leerdam, G.C., 2008, Effect of calcium ions on the adsorption of CMC onto the basal planes of New York talc – A ToF-SIMS study, Minerals Engineering, vol. 21, pp.1020–1025

Chiem, L.T., Huynh, L., Ralston, J. Beattie, D.A., 2006, An in situ ATR–FTIR study of polyacrylamide adsorption at the talc surface, Journal of Colloid and Interface Science, vol. 297, pp.54-61

Clarke, P., Fornasiero, D., Raslton, J., Smart, C., 1995, A study in the removal of oxidation products from sulfide minerals, Minerals Engineering, vol. 8, no. 11, pp.1347-1357,

Crozier, D. R., 1992, Flotation: Theory, Reagents and Ore Testing, Pergamon Press, Chap. 1-3

Cuba-Chiem, L.T., Huynh, L., Beattie, D.A., Ralston, J., 2008, In situ particle film ATR-FTIR studies of CMC adsorption on talc: The effect of ionic strength and multivalent metal ions Minerals Engineering, vol.21, pp.1013–1019

Dalvie M., 2001, The effect of polysaccharides and inorganic dispersants on the surface characteristics of talc and the effect on flotation performance of a Merensky ore, MSc Thesis, Department of Chemical Engineering, Faculty of Engineering and the Built Environment, University of Cape Town

Davidson, E.A., 1967, Carbohydrate Chemistry, Holt, Rinehart and Winston, New York.

Deer, W.A., Howie, R.A., Zussman, J., 1963, Rock-forming minerals chain silicates, vol. 2. Longmans, pp.1–41.

Deer, A.W., Howie, A.R., Zussman J., 1998, An introduction to the rock-forming minerals, 2nd edition, Longman, Essex, England, pp.683-685

Demir, C., Abramov, A. A., Celik, M. S., 2001, Flotation separation of Na- feldspar from K-feldspar by monovalent salts, Minerals Engineering, vol. 14, no. 1, pp.733-740,

Demir, C., Bentli, I., Gülgönül, I., Çelik, M.S., 2003, Effects of bivalent salts on the flotation separation of Na-feldspar from K-feldspar, Minerals Engineering, vol.16, pp.551–554

DuBois, M., Gilles, K. A., Hamilton, J. K., Rebers, P. A., Smith, F., 1956, Colorimetric Method for Determination of Sugars and Related Substances, Analytical Chemistry, vol. 28, no 3, pp.350-356

Fairthorne, G., Fornasiero, D., Ralston, J., 1997, Effect of oxidation on the collectorless flotation of chalcopyrite, International Journal of Mineral Processing, vol. 49, pp.31–48

Fairthorne, G., Brinen, J.S.,, Fornasiero, D., Nagaraj, D.R., Ralston, J., 1998, Spectroscopic and electrokinetic study of the adsorption of butyl ethoxycarbonyl thiourea on chalcopyrite, International Journal of Mineral Processing, vol. 54, pp.147–163

Fuerstenau, D.W., 1982, Mineral-water interfaces and the electrical double layer, In: King, R.P., ed, 1982, Principles of Flotation, South African Institute of Mining and Metallurgy, Johannesburg, South Africa

Fuerstenau, D.W., Fuerstenau, M.C., 1982. Principles of flotation. In: King, R.P. (ed.), The Oxide and Silicate Minerals, Principles of Flotation, South African Institute of Mining and Metallurgy.Johannesburg, South Africa, pp. 109–157

Fuerstanau, D.W., Huang, P., 2003, Interfacial phenomena involved in talc flotation, conference proceedings, 23rd Interantional Minerals Processing Congress, Cape Town, Document Transformation Technologies

Fuerstenau, D.W., Pradip, 2005, Zeta potentials in the flotation of oxide and silicate minerals, Advances in Colloid and Interface Science, vol. 26, pp114–1159,

Fullston, D, Fornasiero, D., Ralston, D., 1999, Zeta potential study of the oxidation of copper sulfide minerals, Colloids and Surfaces, vol. 146, pp. 113-129

Gülgönül, I., Çelik, M.S., Karagüzel, C., 2008, Surface vs. bulk analyses of various feldspars and their significance to flotation, International Journal of Mineral Processing, vol. 86, no. 1-4, pp. 68-74.

Hulbert, L.J., von Gruenewaldt, G., 1985, Textural and compositional features of chromite in the Lower and Critical Zones of the Bushveld Complex south of Potgietersrus, Economic Geology, vol. 80, pp.872-895

Hunter, J.R., 2001, Foundations of colloid science, Oxford University Press, Oxford

Hurlbut, C.S., 1941, Dana's Manual of Mineralogy, 15th ed, John Wiley & Sons, London, pp. 150-178, 270-354

He, S., Fornasiero, D., Skinner, W., 2006, Effect of oxidation potential and zinc sulphate on the separation of chalcopyrite from pyrite, International Journal of Mineral Processing, vol 80, pp. 169-176

Healy, T.W., Moignard, M.S., 1976. A review of electrokinetic studies of metal sulphides. In: Fuerstenau, M.C. (Ed.), Flotation, A.M. Gaudin Memorial. AIME, New York, Vol. 1, pp. 275–297

Hoogendam, C. W., de Keizer, A., Cohen Stuart, M. A., Bijsterbosch, B.H., Batelaan, J. G., van der Horst, P. M., 1998, Adsorption mechanisms of carboxymethyl cellulose on mineral surfaces, Langmuir,, vol.14, no.14, pp., 3825-3839

Kaggwa, B.K., Froebe, S., Huynh, L., Ralston, J., Bremmell, K., 2005, Morphology of Adsorbed Polymers and Solid Surface Wettability, Langmuir, vol. 21, pp.4695-4704

Karagüzel, C., Can, F.M., Çelik, M.S., Sönmez, E., 2005, Effect of electrolyte on surface free energy components of feldspar minerals using thin-layer wicking method, Journal of Colloid and Interface Science, vol. 285, pp. 192–200

Khraisheh, M., Holland, C., Creany, C., Harris, P., Parolis, L., 2005, Effect of molecular weight and concentration on the adsorption of CMC onto talc at different ionic strengths, International Journal of Mineral Processing, vol. 75, pp. 197-206.

James, R.O., 1981. Surface ionization and complexation at the colloid/aqueous electrolyte interface. In: Anderson, M.A., Rubin, A.J. (Eds.), Adsorption of Inorganics at the Solid–Liquid Interfaces. Ann Arbor Science, Ann-Arbor, MI.

James, R.O., Healy, T.W., 1972a. Adsorption of hydrolyzable metal ions at the oxide–water interface, III. A thermodynamic model of adsorption. Journal of Colloid and Interface Science 40, 65–81.

James, R.O., Healy, T.W., 1972b. Adsorption of hydrolyzable metal ions at the oxide–water Interface. I, Co(II) Adsorption on SiO2 and TiO2 as model systems. Journal of Colloid and Interface Science 40, 42–52.

Jenkins, P., Ralston. J., 1998, The adsorption of a polysaccharide at the talc–aqueous solution interface, Colloids and Surfaces : Physicochemical and Engineering Aspects vol. 139, p 27–40

Johnson, B.S., Franks, G.V., Scales, J.P., Boger, D.V., Healy, T.W., 2000,

Khraisheh, M., Holland, C., Creany, C., Harris, P., Parolis, L., 2005, Effect of molecular weight and concentration on the adsorption of CMC onto talc at different ionic strengths, International Journal of Mineral Processing, vol. 75, pp. 197-206

Klein, C, 2002, The Manual of Mineral Science, 22nd ed., John Wiley and Sons, New York, chapter 11

Konan, K.L., Ayrault, P., Bonnet, J.P., Peyratout, C., Smith, A., Jacquet, A., Magnoux, P., 2007, Surface properties of kaolin and illite suspensions in concentrated calcium hydroxide medium, Journal of Colloid and Interface Science, vol.307, pp101–108

Laskowski, J.S., Liu, Q., Zhan, Y., 1997, Sphalerite activation: flotation and electronic studies, Minerals Engineering, vol. 10, no. 8, pp. 78-802

Laskowski, J.S., Liu, Q., O'Connor, C.T. 2007, Current understanding of the mechanism of polysaccharide adsorption at the mineral / aqueous solution interface., International Journal of Mineral Processing, vol.84 pp. 59 – 68

Liu, Q., Laskowski, J.S., 1989, The role of metal hydroxides at mineral surfaces in dextrin adsorption: Studies on modified quartz samples, International Journal of Mineral Processing, vol. 26, pp.297-316

Liu, Q., Zhang, Y., Laskowski, J.S.. 2000, The adsorption of polysaccharides onto mineral surfaces: an acid/base interaction, International Journal of Mineral Processing, vol. 60, pp. 229-245

Liu, G., Feng, Q., Ou, L., Lu, Y., Zhang, G., 2006, Adsorption of polysaccharide onto talc, Minerals Engineering, vol. 19, pp. 147-153.

Lotter, N.O., Bradshaw, D.J., Becker, M., Parolis, L.A.S., Kormos, L.J., 2008, A discussion of the occurrence and undesirable flotation behaviour of orthopyroxene and talc in the processing of mafic deposits, Minerals Engineering, vol. 21, pp. 905-912.

Lovell, V.M., 1982, Industrial Flotation Reagents, In: King, R.P., ed, 1982, Principles of Flotation, South African Institute of Mining and Metallurgy, Johannesburg

Ma, X.,, Pawlik, M., 2005, Effect of alkali metal cations on adsorption of guar gum onto quartz, Journal of Colloid and Interface Science, vol. 289, pp48–55

Malysiak, V., 2003, Pentlandite-pyroxene and pentlandite-feldspar interactions and their effect on separation by flotation, PhD Thesis, Department of Chemical Engineering, University of Cape Town, Cape Town

Malysiak, V., Bradshaw, Coetzer, L.P., D.J., Gerson, A.R., O'Connor, C.T., Ralston, J., 2002, Pentlandite-feldsspar interactions and its effect on separation by flotation, International Journal of Minerals Processing, vol. 66, no 1-4, pp. 89-106

Malysiak, V., Shackleton, N.J., O'Connor, C.T., 2004, An investigation into the floatability of a pentlandite–pyroxene system, International Journal of Mineral Processing. vol 74, pp251– 262

Martinovic, J., Bradshaw, D.J., Harris, P.J., 2005, Investigation of surface properties of gangue minerals in platinum bearing ores, Journal of The South African Institute of Mining and Metallurgy, vol. 105, no. 5, pp. 349-356.

Malvern Instruments, 2005, Zetasizer Nano Series user manual, Worcestershire, England, pp 16.1-16.11

Minxcon, 2007, Platinum Group Metals: Location of the WBJV in the Bushveld Igneous Complex, [Online], Available: http://content.edgar-online.com/edgar_conv_img/2007/11/15/0001095052-07-000013_FIG1-070907.JPG, 29 April 2009

Morris, G. E., Fornasiero, D., Ralston, J., 2002, Polymer depressants at the talc–water interface: adsorption isotherm, microflotation and electrokinetic studies, International Journal of Mineral Processing, vol. 67, pp 211 – 227

O'Connor, C.T., Malysiak, V., Shackleton, N.J., 2006, The interaction of xanthates and amines with pyroxene activated by copper and nickel, Minerals Engineering, vol 19, 799–806

Palmer, B.R., Fuerstanau, M.C., Aplan, F.F., 1975, Mechanisms involved in the flotation of oxides and silicates with anionic collectors, Trans. AIME, pp258- 261

Parks, A.G., 1967, Aqueous surface chemistry of oxides and complex oxide minerals, isoelectric point and zero point of charge, Advanced Chemistry Series, vol, 67, pp 127-160

Parks, A.G., de Bruyn, L.P., 1962, The zero point of charge of oxides, Journal of Physical Chemistry, vol. 66, pp 967-973

Parolis, L.A.S., Groenmeyer, G.V., Harris, P.J., 2005. Equilibrium adsorption studies of polysaccharides on talc: the effect of molecular weight, charge and the influence of metal cations. Presented at SME Meeting, Denver, CO, USA.

Parolis, L.A.S., van der Merwe, R., van Leerdam, G.C., Prins, F.E., Smeink, R.G., 2007, The use of ToF-SIMS and microflotation to assess the reversibility of binding of CMC onto talc, Minerals Engineering, vol.20, pp. 970-978

Parolis, L.A.S., van der Merwe, R., Groenmeyer, G.V., Harris, P.J., 2008, The influence of metal cations on the behaviour of carboxymethyl celluloses as talc depressants, Colloids and Surfaces A: Physicochemical and Engineering Aspects, vol. 317, no. 1-3, pp. 109-115.

Pearse, M.J., 2005, An overview of the use of chemical reagents in mineral processing, Minerals Engineering, vol.18, pp.139–149

Pugh, R J, 1989, Macromolecular Organic Depressants in Sulphide Flotation--a Review. I. Principles, Types and Applications, International Journal of Mineral Processing. Vol. 25, pp. 101-129

Rath, R.K., Subramanian, S., 1997, Studies of guar gum onto biotite mica, Minerals Engineering, Vol. 10, No. 12, pp. 1405-1420

Rath, R.K., Subramanian, S., Laskowski, J.S., 1997. Adsorption of dextrin and guar gum onto talc. A comparative study. Langmuir, vol.13, pp 6260-6266

Rath, R.K., Subramanian, S., Pradeep. T., 2000, Surface chemical studies on pyrite in the presence of polysaccharide-based flotation depressants, Journal of Colloid and Interface Science, vol 229, pp 82–91

Rath, R.K., Subramanian, S., Sivanandam, V., Pradeep. T., 2001, Studies on the interactions of guar gum with chalcopyrite, Canadian Metallurgical Quarterly, vol 40, no 1, pp 1-12

Rao, K.H., Forsberg, K.S.E., 1993, Solution chemistry of mixed cationic/anionic collectors and flotation separation of feldspar from quartz, XVIII International Mineral Processing Congress, 23–28 May, pp. 837–844. Sydney, Australia.

Rao, R.S., 2004, Surface chemistry of froth flotation, Volume 1 Fundamentals, 2nd edition, Kluwer Academic/Plenum Publishers, New York

Rao, R.S., 2004, Surface chemistry of froth flotation: Volume 2 – Reagents and Mechanisms , 2nd edition, Kluwer Academic/Plenum Publishers, New York

Schaeffer, L.R., McClave, J.T., 1995, Probability and statistics for engineers, 4th edition, Duxbury Press, Belmont, California, U.S.A

Shackleton, J.N., 2003, The role of complexing agents in the flotation of pentlandite-pyroxene mixtures, MSc Thesis, Department of Chemical Engineering, University of Cape Town, Cape Town

Shackleton, J.N., 2007, Surface characterisation and flotation behaviour of the platinum and alladium arsenide, telluride and sulphide mineral species, PhD Thesis, Department of Chemical Engineering, University of Cape Town, Cape Town

Shortridge, P.G., Harris, P.J., Bradshaw, D.J., Koopal, L.K. 2000 "The effect of chemical composition and molecular weight of polysaccharide depressants on the flotation of talc". International Journal of Mineral Processing, vol 59, pp 215 – 224

Silberberg, M.S., 2002, Chemistry: the molecular nature of matter and change, McGraw-Hill, New York

Smeink, R.G., Leerdam van, G.C., Mahy, J.W.G., 2005, Determination of preferential adsorption of Depramin on mineral surfaces by ToF-SIMS, Minerals Engineering, vol. 18, pp. 247–255

Steenberg, E., Harris, P.J., 1984, Adsorption of carboxymethylcellulose, guar gum, and starch onto talc, sulphides, oxides, and salt type minerals, Council for Mineral Technology, Ranburg, South Africa

Sysilä, S., Heiskanen, K., Laapas, H., Ruokenen, 1996, E., The effect of surface potential on the flotation of chromite, Minerals Engineering, vol. 9, no. 5, pp. 519-525, 1996

Ueno, T., Yokota, S., Kitaoka. T., Wariishi, H., 2007, Conformational changes in single carboxymethylcellulose chains on a highly oriented pyrolytic graphite surface under different salt conditions, Carbohydrate Research, vol 342, pp 954–960

Wang, J., Somasundaran, P., Nagaraj, D.R., 2005, Adsorption mechanism of guar gum at solid–liquid interfaces, Minerals Engineering, vol. 18, pp. 77-81.

Wang, J., Somasundaran, P., 2005, Adsorption and conformation of carboxymethyl cellulose at solid–liquid interfaces using spectroscopic, AFM and allied techniques, Journal of Colloid and Interface Science, vol. 291, pp. 75-83.

Wang, J., Somasundaran, V., 2007, Study of galactomannose interaction with solids using AFM, IR and allied techniques, Journal of Colloid and Interface Science, vol. 309 pp 373–383

Wesseldijk, Q, L., Bradshaw, D.J., Harris, P.J., Reuter, M.A., 1999, The flotation behaviour of chromite with respect to the beneficiation of UG2 ore, Minerals Engineering, vol. 12, no 10, pp 1177-1184

Wills, B.A., 1997, Mineral processing technology: an introduction to the practical aspects of ore treatment and mineral recovery, Butterworth-Heineman

Wilson, A., Chunnett, G., 2006, Trace Element and Platinum Group Element Distributions and the Genesis of the Merensky Reef, Western Bushveld Complex, South Africa, Journal of Petrology, vol. 47, pp. 2369-2403.

Wiese, G.J., 2009, investigating depressant behaviour in the flotation of selected Merensky ore, MSc Thesis, Department of Chemical Engineering, University of Cape Town. Cape Town

Wiese, J.G., Harris, P.J. and Bradshaw, D.J. 2008. The use of very low molecular weight polysaccharides as depressants in PGM flotation. Minerals Engineering, vol. 21, pp471-482

Yopps, J. A., Fuerstenau D.W., 1964, The zero point of charge of alpha-alumina, Journal of Colloid Science, vol. 19, pp61-71

APPENDICES

APPENDIX 1: XRD DIFFRACTOGRAMS FOR EACH MINERAL

Sabatha - talc

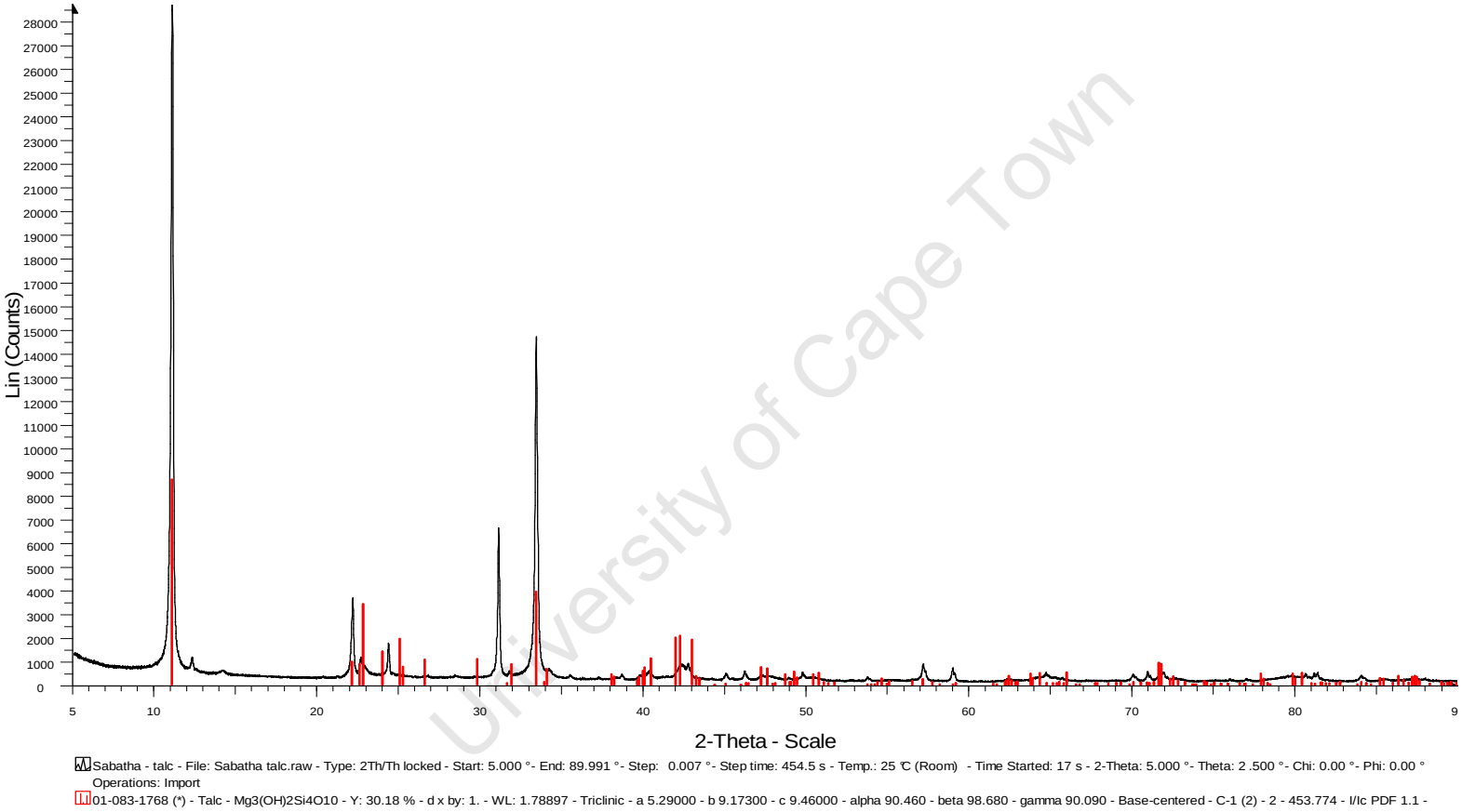

Sabatha Plag

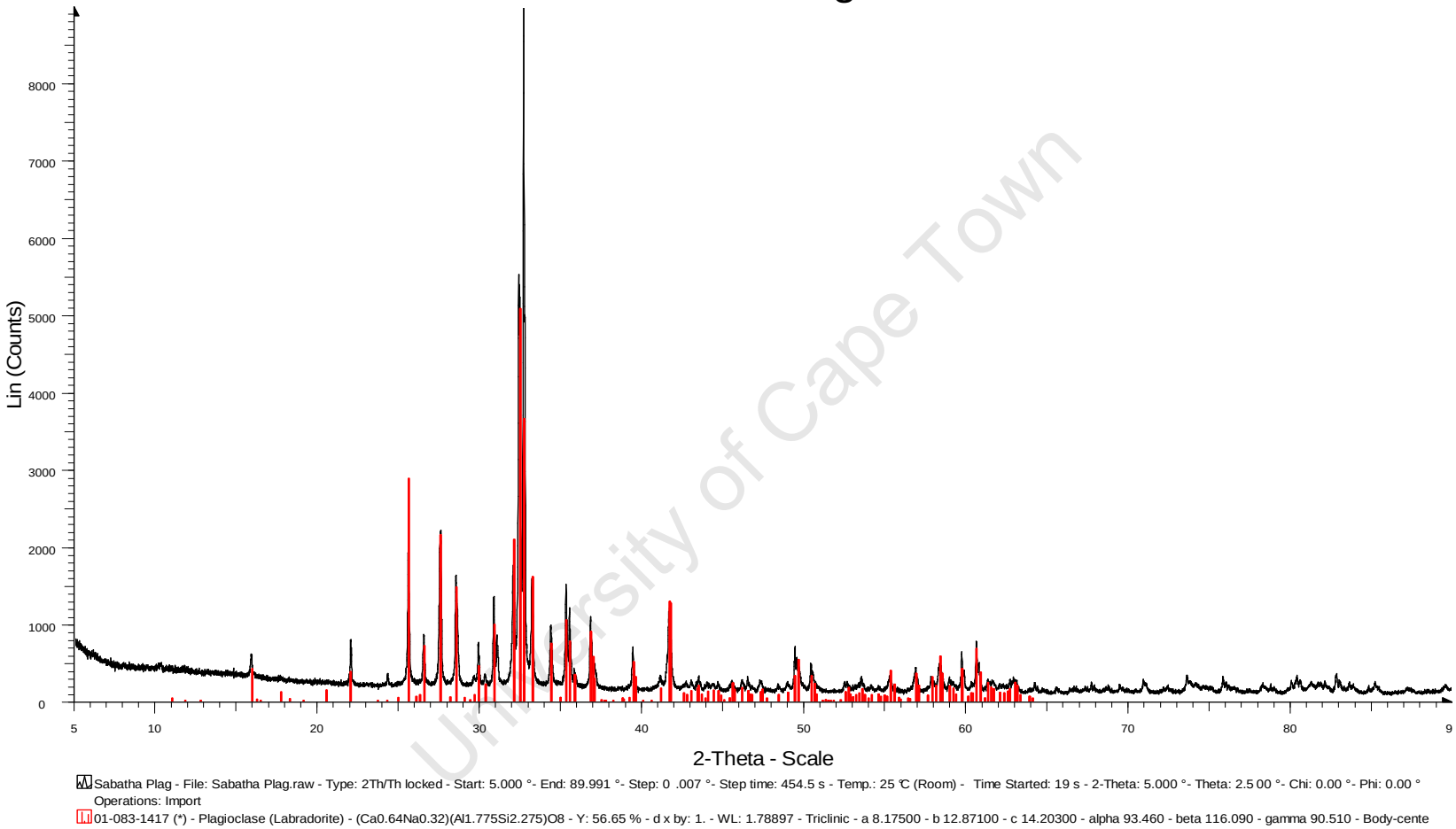

Sabathat - pyroxene

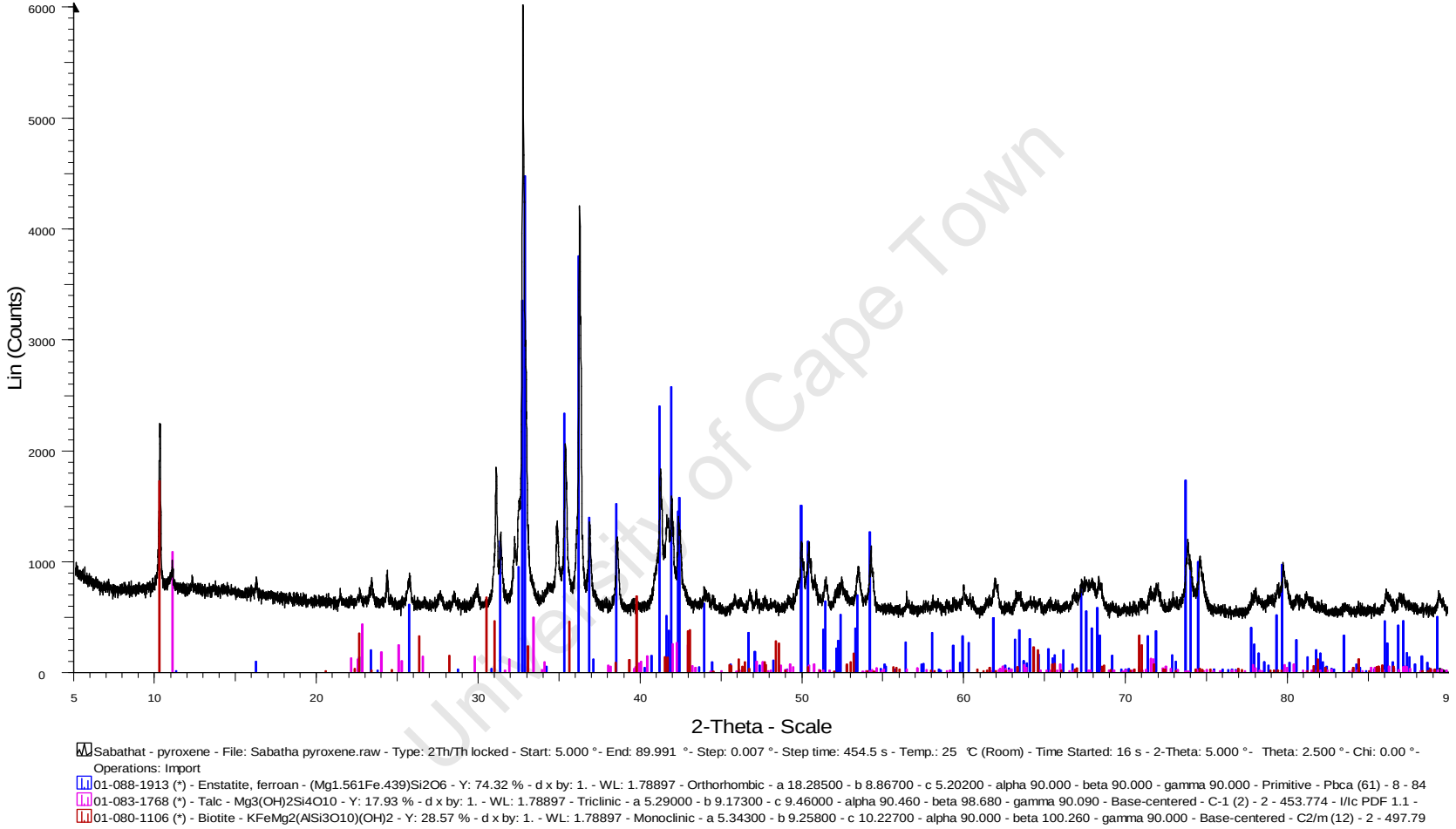

Sabathat - pyroxene - File: Sabatha pyroxene.raw - Type: 2Th/Th locked - Start: 5.000 °- End: 89.991 °- Step: 0.007 °- Step time: 454.5 s - Temp.: 25 °C (Room) - Time Started: 16 s - 2-Theta: 5.000 °- Theta: 2.500 °- Chi: 0.00 °- Operations: Import

01-088-1913 (*) - Enstatite, ferroan - (Mg1.561Fe.439)Si2O6 - Y: 74.32 % - d x by: 1. - WL: 1.78897 - Orthorhombic - a 18.28500 - b 8.86700 - c 5.20200 - alpha 90.000 - beta 90.000 - gamma 90.000 - Primitive - Pbca (61) - 8 - 84

01-083-1768 (*) - Talc - Mg3(OH)2Si4O10 - Y: 17.93 % - d x by: 1. - WL: 1.78897 - Triclinic - a 5.29000 - b 9.17300 - c 9.46000 - alpha 90.460 - beta 98.680 - gamma 90.090 - Base-centered - C-1 (2) - 2 - 453.774 - I/Ic PDF 1.1 -

01-080-1106 (*) - Biotite - KFeMg2(AlSi3O10)(OH)2 - Y: 28.57 % - d x by: 1. - WL: 1.78897 - Monoclinic - a 5.34300 - b 9.25800 - c 10.22700 - alpha 90.000 - beta 100.260 - gamma 90.000 - Base-centered - C2/m (12) - 2 - 497.79

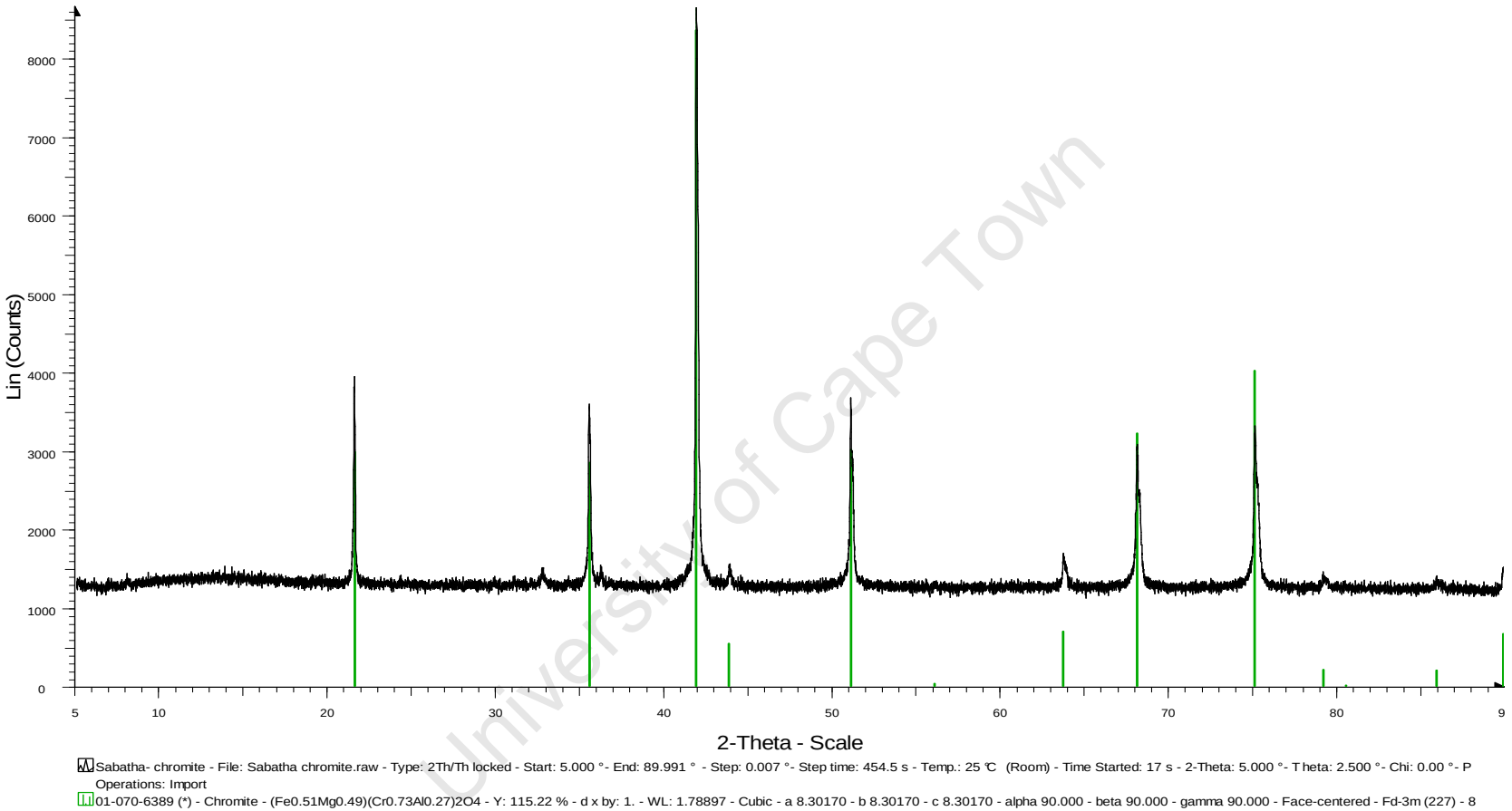

Sabatha Chalco

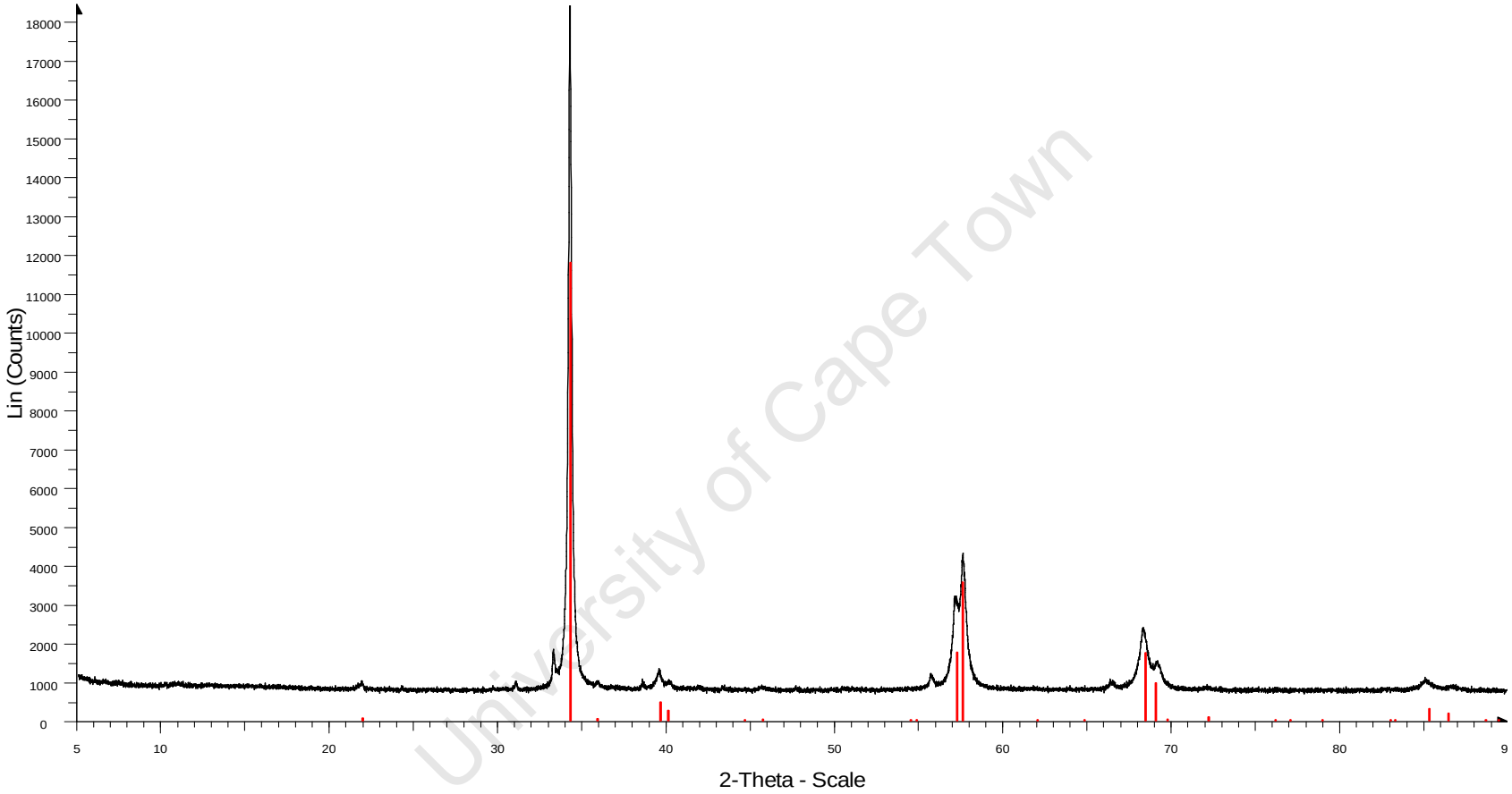

Sabatha Chalco - File: Sabatha Chalco.raw - Type: 2Th/Th locked - Start: 5.000 °- End: 89.991 °- Ste p: 0.007 °- Step time: 454.5 s - Temp.: 25 °C (Roo m) - Time Started: 17 s - 2-Theta: 5.000 °- Theta: 2.500 °- Chi: 0.00 °- Phi: 0
Operations: Import
01-073-9964 (*) - Chalcopyrite - CuFeS2 - Y: 64.03 % - d x by: 1. - WL: 1.78897 - Tetragonal - a 5.27700 - b 5.27700 - c 10.44100 - alpha 90.000 - beta 90.000 - gamma 90.000 - Body-centered - I-42d (122) - 4 - 290.748 - I/Ic PDF

APPENDIX 2: END-MEMBER CALCULATIONS FOR PLAGIOCLASE AND PYROXENE

Mineral	Na_2O	TiO_2	CaO	MgO	Cr_2O_3	FeO	Al_2O_3
plagioclase	2.840	-	14.96	-	-	0.331	30.68
pyroxene	0.034	0.16	1.80	29.34	0.468	13.17	1.250

All calculations derived from Deer *et al.*, (1998).

Plagioclase:

Albite ($NaAl_sSi_3O_8$):

$$NaAl_2Si_2O_3 = \frac{2.84}{2.84+14.96}\times 100 = 16\%$$

Anorthite ($CaAl_2Si_2O_8$):

$$CaAl_2Si_2O_3 = \frac{14.96}{2.84+14.96}\times 100 = 84\%$$

Pyroxene:

Enstatite ($Mg_2Si_2O_6$):

$$Mg_2Si_2O_6 = \frac{29.34}{29.34+13.17}\times 100 = 69\%$$

Ferrosilite ($Fe_2Si_2O_6$):

$$Fe_2Si_2O_6 = \frac{13{,}17}{29.34+13.17}\times 100 = 31\%$$

APPENDIX 3: PREPARATION OF DEPRESSANT STOCK SOLUTIONS

Depressant	Molecular weight	Purity (%)	% Insolubles	Moisture content (%)
Sendep 369	279500	88.1	7.56	9.04
Finnfix 700	425798	97.8	0	8.70

To calculate the amount of depressant needed for 5 pseudo-monolayer coverage (calculations done using Mathcad2001:

For guar on talc:

$A_{monomer} := 0.47$ $Mr_{molecule.guar} := 279500$ $Mr_{monomer.guar} := 220$

To find the area occupied by each molecule:

$$\sigma := \frac{A_{monomer} \cdot Mr_{molecule.guar}}{Mr_{monomer.guar} \cdot \left(1 \cdot 10^{9}\right)^{2}} = 5.971 \cdot 10^{-16} \quad m^2/molecule$$

where: $A_{monomer}$ is the area occupied by each monomer of guar, $Mr_{molecule\ guar}$ is the molecular mass of each molecule of guar, $Mr_{monomer\ guar}$ is the molecular weight of a monomer of guar

To find the moles of guar needed for 5 pseudo-monolayers:

$$n := \frac{A_{talc} \cdot \theta}{\sigma \cdot N_A}$$

where: n is the number of moles of depressant needed per gram of talc, A_{talc} is the BET surface area of talc, θ is the fractional coverage, σ is the area occupied per molecule of guar, N_A is Avogadro's number,

$A_{talc} := 10.712 m^2$ $N_A := 6.022 \cdot 10^{23}$ molecules/mol $m_{talc} := 0.075 g$ $V_{guar} := 0.06 L$

$n = 1.49 \times 10^{-7}$ mol/g_{talcr}

To find the mass concentration:

$$m_{conc} := \frac{n \cdot Mr_{molecule.guar} \cdot m_{talc}}{V_{guar}} = 0.052 \ g_{guar}/L$$

To find the actual mass of guar needed on an active content basis using the characterisation results:

$$m_{inactive} = m_{water} + m_{impure} + m_{insolubles}$$

where: m_{water} is the moisture content, m_{impure} is the impure mass, $m_{insolubles}$ is the mass of insolubles

$$m_{water} := 0.0904 \cdot m_{conc}$$

$$m_{dry} := m_{conc} - m_{water}$$

$$m_{inactive} := 0.0904 \cdot m_{conc} + (1 - 0.881) \cdot m_{dry} + 0.0756 \cdot m_{dry}$$

$$m_{inactive} = 0.014$$

$$m_{guar} := \left(m_{conc} + m_{inactive}\right)$$

$$m_{guar} = 0.066 \quad g/L$$

Thus the required mass concentration of guar is 66 mg/L

For CMC:

$$A_{monomer} := 0.47 \qquad Mr_{molecule.CMC} := 425795 \qquad Mr_{monomer.CMC} := 220$$

$$\sigma := \frac{A_{monomer} \cdot Mr_{molecule.CMC}}{Mr_{monomer.guar} \cdot \left(1 \cdot 10^{9}\right)^{2}} = 9.0965 \cdot 10^{-16}$$

To find the moles of guar needed for 5 pseudo-monolayers:

$$n := \frac{A_{talc} \cdot \theta}{\sigma \cdot N_A} = 9.777 \cdot 10^{-8} \ mol/g_{CMC}$$

To find the mass concentration:

$$m_{conc} := \frac{n \cdot Mr_{molecule.CMC} \cdot m_{talc}}{V_{guar}} = 0.052 \quad g_{guar}/L$$

$$m_{inactive} = m_{water} + m_{impure}$$

$$m_{water} := 0.087 \cdot m_{conc}$$

$$m_{dry} := m_{conc} - m_{water}$$

$$m_{inactive} := 0.0904 \cdot m_{conc} + (1 - 0.9782) \cdot m_{dry}$$

$$m_{inactive} = 5.74 \times 10^{-3}$$

$$m_{guar} := \left(m_{conc} + m_{inactive}\right)$$

$$m_{CMC} := \left(m_{conc} + m_{inactive}\right)$$

Actual mass of CMC required per L:

$m_{CMC} = 0.058\ g/L$

To calculate the amount of guar required to prepare a 1000mg/L stock solution using characterisation results:

$$m_{inactive} = m_{water} + m_{impure} + m_{insolubles}$$

$m_{water} := 0.0904 \cdot m_{conc}$

$m_{dry} := m_{conc} - m_{water}$

$m_{inactive} := 0.0904 \cdot m_{conc} + (1 - 0.881) \cdot m_{dry} + 0.0756 \cdot m_{dry}$

$m_{guar} := m_{conc} + m_{inactive}$

Thus the required mass of guar per litre

$m_{guar} = 1.267\ g/L$

To calculate the amount of CMC required to prepare 1000mg/L stock solution using characterisation results:

$$m_{inactive} = m_{water} + m_{impure}$$

$m_{water} := 0.087 \cdot m_{conc}$

$m_{dry} := m_{conc} - m_{water}$

$m_{inactive} := 0.0904 \cdot m_{conc} + (1 - 0.9782) \cdot m_{dry}$

$m_{CMC} := (m_{conc} + m_{inactive})$

Thus the required mass of CMC per litre:

$m_{CMC} = 1.11\ g/L$

APPENDIX 4: ZETA POTENTIAL EXPERIMENTAL PROCEDURE

A detailed zeta potential determination procedure used throughout the study is shown below. This procedure was used to ensure accuracy and reproducibility of zeta potential data (Malysiak 2003, Shackleton, 2003, Shackleton, 2007)

1. Weigh 0.375g of a mineral sample to 100% -25μm into a 500 cm^3 beaker
2. Add 300cm^3 10^{-2}M $Na_2B_4O_710H_2O$ solution or SPW or 10-2 IS $Ca(NO_3)_2$ solution
3. Stir well and split into 5 beaker (60 cm^3)
4. Adjust pH to 2, 4, 6, 8 and 10 with NaOH or HCl
5. Condition for 20 minutes on a magnetic stirrer ensuring that the pH remains constant
6. Pipette about 1 cm^3 of mineral dispersion into a folded capillary, ensuring that there are no bubbles in the cell
7. Place cell in the Zeta Sizer Nano Series to measure the electrophoretic mobility
8. Repeat 1-8 in depressant solution. With guar, filter solution using 0.45μm Millipore paper to remove any insolubles in solution

APPENDIX 5: ZETA POTENTIAL RAW DATA

\

Variation of the zeta potential as a function of pH in buffer:

Talc

pH	Zeta potential (mV)					
	run1	run 2	run 3	Average	Std. deviation	Std. error
4	-24.8	-26.4	-24.1	-25.1	1.18	0.83
6	-40.1	-39.8	-38.1	-39.3	1.08	0.76
8	-45.7	-44.8	-43.9	-44.8	0.90	0.64
10	-51.8	-52.8	-53.0	-52.5	0.64	0.45

Plagioclase

pH	Zeta potential (mV)					
	run1	run 2	run 3	Average	Std. deviation	Std. error
2	-4.73	0.18	-3.08	-2.54	2.50	1.76
4	-16.6	-15.3	-15.8	-15.9	0.64	0.45
6	-0.19	-5.9	-2.64	-2.90	2.85	2.02
8	-55.3	-54.1	-51.7	-53.7	1.83	1.29
10	-59.5	-58.8	-61.9	-60.1	1.59	1.12

Pyroxene

pH	Zeta potential (mV)					
	run1	run 2	run 3	Average	Std. deviation	Std. error
2	9.8	20.4	15.2	15.1	5.32	3.76
4	-25.6	-27.7	-21.6	-25.0	3.09	2.18
6	-35.5	-38.4	-36.4	-36.8	1.47	1.04
8	-42.1	-41.2	-41.9	-41.8	0.46	0.33
10	-47.7	-47.6	-47.8	-47.7	0.10	0.07

Chromite

pH	Zeta potential (mV)					
	run1	run 2	run 3	Average	Std. deviation	Std. error
2	16.1	22.6	29.3	22.7	6.60	4.67
4	-6.8	-8.7	-6.1	-7.2	1.33	0.94
6	-27.8	-28.8	-26.2	-27.6	1.31	0.93
8	-41.5	-40.0	-41.9	-41.1	0.98	0.69
10	-49.2	-47.8	-48.1	-48.4	0.74	0.53

Chalcopyrite

pH	Zeta potential (mV)					
	run1	run 2	run 3	Average	Std. deviation	Std. error
2	-14.80	-24.60	-23.20	-20.87	5.30	3.75
4	6.20	3.12	3.21	4.18	1.75	1.24
6	-7.47	-10.46	-17.20	-11.71	4.99	3.53
8	-26.77	-27.23	-29.07	-27.69	1.22	0.86
10	-36.97	-39.70	-37.83	-38.17	1.40	0.99

Variation of the zeta potential as a function of pH in SPW:

Talc

pH	Zeta potential (mV)				
	run1	run 2	Average	Std. deviation	Std. error
2	-6.6	-7.0	-6.8	0.27	0.19
4	-11.7	-11.7	-11.7	0.02	0.02
6	-17.2	-16.6	-16.9	0.38	0.27
8	-18.4	-17.8	-18.1	0.47	0.33
10	-19.9	-19.9	-19.9	0.02	0.02

Plagioclase

pH	Zeta potential (mV)				
	run1	run 2	Average	Std. deviation	Std. error
2	-6.9	-7.6	-7.3	0.55	0.39
4	-17.2	-18.5	-17.8	0.90	0.63
6	-7.0	-6.4	-6.7	0.42	0.30
8	-17.0	-19.0	-18.0	1.44	1.02
10	-11.4	-14.7	-13.1	2.33	1.65

Pyroxene

pH	Zeta potential (mV)				
	run1	run 2	Average	Std. deviation	Std. error
2	-3.8	-2.5	-3.1	0.89	0.63
4	-15.0	-16.6	-15.8	1.11	0.78
6	-20.6	-20.1	-20.3	0.38	0.27
8	-20.8	-21.8	-21.3	0.73	0.52
10	-8.2	-10.7	-9.5	1.81	1.28

Chromite

pH	Zeta potential (mV)				
	run1	run 2	Average	Std. deviation	Std. error
2	2.7	2.3	2.5	0.28	0.20
4	-3.1	-8.2	-5.6	3.61	2.55
6	-14.1	-11.6	-12.8	1.78	1.26
8	-14.8	-14.2	-14.5	0.42	0.30
10	-4.8	-4.9	-4.9	0.03	0.02

Chalcopyrite

pH	Zeta potential (mV)				
	run1	run 2	Average	Std. deviation	Std. error
2	-21.0	-30.2	-25.6	6.51	4.60
4	-8.5	-9.6	-9.0	0.82	0.58
6	-8.7	-7.9	-8.3	0.56	0.39
8	-10.3	-10.3	-10.3	0.00	0.00
10	-4.8	-5.5	-5.2	0.49	0.35

Variation of the zeta potential as a function of pH with the addition of guar in buffer:

Talc

pH	Zeta potential (mV)					
	run 1	run 2	run 3	Average	Std. Deviation	Std Error
8	-22.1	-20.4	-19.9	-20.8	1.2	0.82
10	-22.2	-22.3	-21.7	-22.0	0.3	0.24

Plagioclase

pH	Zeta potential (mV)					
	run 1	run 2	run 3	Average	Std. Deviation	Std Error
8	-37.3	-36.5	-40.7	-38.2	2.2	1.58
10	-49.9	-49.9	-48.0	-49.2	1.1	0.78

Pyroxene

pH	Zeta potential (mV)					
	run1	run2	run3	Average	Std. Deviation	Std Error
8	-24.7	-19.6	-22.8	-22.4	2.6	1.82
10	-30.9	-26.8	-27.2	-28.3	2.2	1.59

Chromite

pH	Zeta potential (mV)					
	run 1	run 2	run 3	Average	Std. Deviation	Std Error
8	-18.7	-22.9	-16.2	-19.2	3.4	2.38
10	-25.7	-27.0	-25.0	-25.9	1.0	0.72

Chalcopyrite

pH	Zeta potential (mV)					
	run 1	run 2	run 3	Average	Std. Deviation	Std Error
8	-18.4	-18.5	-16.8	-17.9	1.0	0.67
10	-23.6	-24.8	-26.5	-25.0	1.5	1.05

Variation of the zeta potential as a function of pH with the addition of guar in SPW:

Talc

pH	Zeta potential (mV)					
	run 1	run 2	run 3	Average	Std. Deviation	Std Error
8	-6.16	-5.57	-6.04	-5.92	0.31	0.22
10	-7.39	-5.92	-6.78	-6.70	0.74	0.52

Plagioclase

pH	Zeta potential (mV)					
	run 1	run 2	run 3	Average	Std. Deviation	Std Error
8	-7.34	-10.07	-10.75	-9.39	1.80	1.27
10	-9.82	-9.59	-9.89	-9.77	0.16	0.11

Pyroxene

pH	Zeta potential (mV)					
	run1	run2	run3	Average	Std. Deviation	Std Error
8	-3.54	-4.37	-3.88	-3.93	0.42	0.29
10	-4.10	-3.09	-5.18	-4.12	1.04	0.74

Chromite

pH	Zeta potential (mV)					
	run 1	run 2	run 3	Average	Std. Deviation	Std Error
8	-3.40	-4.45	-3.70	-3.85	0.54	0.38
10	-3.16	-3.34	-5.13	-3.88	1.09	0.77

Chalcopyrite

pH	Zeta potential (mV)					
	run 1	run 2	run 3	Average	Std. Deviation	Std Error
8	-4.81	-4.09	-3.92	-4.28	0.47	0.33
10	-4.05	-4.32	-4.93	-4.43	0.45	0.32

Variation of the zeta potential as a function of pH in 10^{-2} IS Ca $(NO_3)_2$ solution:

Talc

pH	Zeta potential (mV)				
	run1	run2	Average	Std. Deviation	Std. Error
8	-19.7	-20.4	-20.1	0.5	0.38
10	-23.9	-24.2	-24.0	0.2	0.13

Plagioclase

pH	Zeta potential (mV)				
	run1	run2	Average	Std. Deviation	Std. Error
8	-23.1	-21.3	-22.2	1.3	0.92
10	-22.5	-21.6	-22.1	0.6	0.43

Pyroxene

pH	Zeta potential (mV)				
	run1	run2	Average	Std. Deviation	Std. Error
8	-21.9	-20.6	-21.3	0.9	0.63
10	-19.2	-18.3	-18.8	0.6	0.45

Chromite

pH	Zeta potential (mV)				
	run1	run2	Average	Std. Deviation	Std Error
8	-11.5	-13.3	-12.4	1.3	0.92
10	-14.7	-11.3	-13.0	2.4	1.70

Chalcopyrite

pH	Zeta potential (mV)				
	run1	run2	Average	Std. Dev	Std Error
8	-17.1	-17.7	-17.4	0.4	0.28
10	-11.8	-18.1	-15.0	4.4	3.12

Variation of the zeta potential as a function of pH in with the addition of CMC in buffer:

Talc

pH	Zeta potential (mV)				
	run1	run2	Average	Std. Dev	Std Error
8	-51.6	-55.3	-53.5	2.6	1.83
9	-51.6	-53.1	-52.4	1.0	0.72
10	-51.6	-52.4	-52.0	0.5	0.37

Plagioclase

pH	Zeta potential (mV)				
	run1	run2	Average	Std. Dev	Std Error
8	-57.3	-57.0	-57.1	0.2	0.17
9	-58.6	-57.9	-58.3	0.5	0.33
10	-57.7	-57.0	-57.4	0.5	0.37

Pyroxene

pH	Zeta potential (mV)				
	run1	run2	Average	Std. Dev	Std Error
8	-46.6	-47.2	-46.9	0.4	0.28
9	-46.2	-47.0	-46.6	0.5	0.38
10	-48.0	-47.7	-47.9	0.2	0.17

Chromite

pH	Zeta potential (mV)				
	run1	run2	Average	Std. Dev	Std Error
8	-47.0	-47.8	-47.4	0.5	0.37
9	-48.9	-49.1	-49.0	0.1	0.08
10	-49.1	-47.2	-48.2	1.3	0.93

Chalcopyrite

pH	Zeta potential (mV)				
	run1	run2	Average	Std. Dev	Std Error
8	-47.3	-44.9	-46.1	1.7	1.18
9	-46.6	-45.3	-46.0	0.9	0.63
10	-46.7	-45.6	-46.2	0.8	0.55

Variation of the zeta potential as a function of pH in with the addition of CMC in 10^{-2} IS $Ca(NO_3)_2$ solution:

Talc

pH	Zeta potential (mV)				
	run1	run2	Average	Std. Dev	Rel.Std Error
8	-21.8	-21.4	-21.6	0.3	0.22
9	-21.8	-22.1	-22.0	0.3	0.18
10	-22.3	-23.2	-22.7	0.7	0.47

Plagioclase

pH	Zeta potential (mV)				
	run1	run2	Average	Std. Dev	Rel.Std Error
8	-22.3	-22.1	-22.2	0.1	0.08
9	-23.0	-22.9	-22.9	0.1	0.05
10	-23.2	-22.3	-22.8	0.7	0.48

Pyroxene

pH	Zeta potential (mV)				
	run1	run2	Average	Std. Dev	Rel.Std Error
8	-21.1	-21.6	-21.4	0.3	0.23
9	-22.3	-21.4	-21.9	0.6	0.43
10	-20.5	-22.6	-21.5	1.5	1.03

Chromite

pH	Zeta potential (mV)				
	run1	run2	Average	Std. Dev	Rel.Std Error
8	-22.5	-22.3	-22.4	0.1	0.08
9	-20.8	-20.1	-20.4	0.5	0.35
10	-22.5	-21.8	-22.2	0.5	0.35

Chalcopyrite

pH	Zeta potential (mV)				
	run1	run2	Average	Std. Dev	Rel.Std Error
8	-22.0	-21.4	-21.7	0.4	0.28
9	-18.9	-22.1	-20.5	2.3	1.60
10	-21.3	-20.1	-20.7	0.9	0.62

APPENDIX 6: ADSORPTION KINETICS RAW DATA

Talc – guar in SPW, pH 9, T = 25°C

Time (mins))	Initial depressant mass (mg)	Sample mass (g)	Mineral surface area (m^2)	Absorbance				Actual Absorbance	Residual Concentration (mg/L)	Residual mass (mg)	Amount adsorbed (mg/m^2)
				1	2	Average	Std. deviation				
0	10	0	0.0000						100		0
0.25	10	0.388	4.0031	1.063	1.062	1.063	0.001	1.063	92.4	9.24	0.190
0.5	10	0.3879	4.0020	1.025	1.041	1.033	0.011	1.033	89.8	8.98	0.254
0.75	10	0.3876	3.9989	1.031	1.077	1.054	0.033	1.054	91.7	9.17	0.209
1	10	0.3882	4.0051	1.037	1.036	1.037	0.001	1.037	90.1	9.01	0.246
2	10	0.3878	4.0010	1.048	1.027	1.038	0.015	1.038	90.2	9.02	0.245
5	10	0.3879	4.0020	1.034	1.016	1.025	0.013	1.025	89.1	8.91	0.272
10	10	0.3879	4.0020	0.95	0.987	0.969	0.026	0.969	84.2	8.42	0.394
20	10	0.3877	4.0000	0.948	0.969	0.959	0.015	0.959	83.3	8.33	0.416
30	10	0.3874	3.9969	1.013	0.982	0.998	0.022	0.998	86.7	8.67	0.332
60	10	0.3878	4.0010	0.943	0.969	0.956	0.018	0.956	83.1	8.31	0.422
120	10	0.3880	4.0031	0.922	0.956	0.939	0.024	0.939	81.7	8.17	0.458
180	10	0.3877	4.0000	0.917	0.943	0.930	0.018	0.930	80.9	8.09	0.478
240	10	0.3876	3.9989	0.94	0.932	0.936	0.006	0.936	81.4	8.14	0.465
1440	10	0.3882	4.0051	0.836	0.868	0.852	0.023	0.852	74.1	7.41	0.647

Time (min)	Initial depressant mass (mg)	Sample mass (g)	Mineral surface area (m^2)	Absorbance				Actual Absorbance	Residual Concentration (mg/L)	Residual mass (mg)	Amount adsorbed mg/m2
				1	2	Average	Std. deviation				
0	10	0	0.0000						100		0
0.25	10	0.3876	3.9989	1.064	1.053	1.059	0.008	1.059	92.0	9.20	0.199
0.5	10	0.3878	4.0010	1.055	1.026	1.041	0.021	1.041	90.5	9.05	0.238
1	10	0.3875	3.9979	1.025	1.049	1.037	0.017	1.037	90.2	9.02	0.246
2	10	0.3875	3.9979	1.025	1.039	1.032	0.010	1.032	89.7	8.97	0.257
5	10	0.3879	4.0020	0.991	1.006	0.999	0.011	0.999	86.8	8.68	0.329
10	10	0.3879	4.0020	0.967	0.989	0.978	0.016	0.978	85.0	8.50	0.374
20	10	0.3881	4.0041	0.975	0.982	0.979	0.005	0.979	85.1	8.51	0.372
60	10	0.3879	4.0020	0.94	0.983	0.962	0.030	0.962	83.6	8.36	0.410
120	10	0.3878	4.0010	0.956	0.944	0.950	0.008	0.950	82.6	8.26	0.435
180	10	0.3876	3.9989	0.901	0.92	0.911	0.013	0.911	79.2	7.92	0.521
240	10	0.3877	4.0000	0.933	0.893	0.913	0.028	0.913	79.4	7.94	0.515
1440	10	0.3878	4.0010	0.858	0.884	0.871	0.018	0.871	75.7	7.57	0.606

Plagioclase – guar in SPW, pH 9, T = 25°C

Time (mins)	Initial depressant mass (mg)	Sample mass (g)	Mineral surface area (m^2)	Absorbance				Actual Absorbance	Residual Concentration (mg/L)	Residual mass (mg)	Amount Adsorbed (mg/m^2)
				1	2	Average	Std. deviation				
0	10	0	0.0000						100		0
0.25	10	1.8961	1.9996	1.143	1.136	1.140	0.005	1.140	99.1	9.91	0.046
0.5	10	1.8964	1.9999	1.141	1.187	1.164	0.033	1.164	101.2	10.12	-0.061
0.75	10	1.8965	2.0000	1.136	1.163	1.150	0.019	1.150	100.0	10.00	0.002
1	10	1.8963	1.9998	1.127	1.182	1.155	0.039	1.155	100.4	10.04	-0.020
2	10	1.8966	2.0002	1.115	1.189	1.152	0.052	1.152	100.2	10.02	-0.009
5	10	1.8964	1.9999	1.112	1.153	1.133	0.029	1.133	98.5	9.85	0.076
10	10	1.8962	1.9997	1.147	1.193	1.170	0.033	1.170	101.7	10.17	-0.087
20	10	1.8961	1.9996	1.206	1.15	1.178	0.040	1.178	102.4	10.24	-0.122
30	10	1.8967	2.0003	1.175	1.232	1.204	0.040	1.204	104.7	10.47	-0.233
60	10	1.8970	2.0006	1.115	1.135	1.125	0.014	1.125	97.8	9.78	0.109
120	10	1.8962	1.9997	1.126	1.14	1.133	0.010	1.133	98.5	9.85	0.074
180	10	1.8964	1.9999	1.113	1.16	1.137	0.033	1.137	98.8	9.88	0.059
240	10	1.8969	2.0005	1.119	1.12	1.120	0.001	1.120	97.3	9.73	0.133
1440	10	1.8968	2.0004	1.094	1.121	1.108	0.019	1.108	96.3	9.63	0.185

Time (mins)	Initial depressant mass (mg)	Sample mass (g)	Mineral surface area (m^2)	Absorbance				Actual Absorbance	Residual Concentration (mg/L)	Residual mass (mg)	Amount Adsorbed (mg/m^2)
				1	2	Average	Std. deviation				
0	10	0	0.0000						100		0
0.25	10	1.8961	1.9996	1.109	1.100	1.105	0.006	1.105	96.0	9.60	0.198
0.5	10	1.8962	1.9997	1.100	1.116	1.108	0.011	1.108	96.3	9.63	0.183
0.75	10	1.8964	1.9999	1.075	1.128	1.102	0.037	1.102	95.8	9.58	0.211
1	10	1.9063	2.0104	1.076	1.076	1.076	0.000	1.076	93.6	9.36	0.320
2	10	1.8962	1.9997	1.086	1.094	1.090	0.006	1.090	94.8	9.48	0.261
5	10	1.8962	1.9997	1.085	1.159	1.122	0.052	1.122	97.6	9.76	0.122
10	10	1.8962	1.9997	1.096	1.132	1.114	0.025	1.114	96.9	9.69	0.157
20	10	1.8968	2.0004	1.134	1.148	1.141	0.010	1.141	99.2	9.92	0.039
30	10	1.8964	1.9999	1.113	1.146	1.130	0.023	1.130	98.2	9.82	0.089
60	10	1.8964	1.9999	1.079	1.127	1.103	0.034	1.103	95.9	9.59	0.204
120	10	1.8964	1.9999	1.138	1.148	1.143	0.007	1.143	99.4	9.94	0.030
180	10	1.8968	2.0004	1.153	1.155	1.154	0.001	1.154	100.3	10.03	-0.017
240	10	1.8962	1.9997	1.155	1.133	1.144	0.016	1.144	99.5	9.95	0.026
1440	10	1.8966	2.0002	1.094	1.194	1.144	0.071	1.144	99.5	9.95	0.026

Pyroxene – guar in SPW, pH 9, T = 25°C

Time (min)	Initial depressant mass (mg)	Sample mass (g)	Mineral surface area (m^2)	Absorbance				Actual Absorbance	Residual Concentration (mg/L)	Residual mass (mg)	Amount adsorbed (mg/m^2)
				1	2	Average	Std. deviation				
0	10	0	0.0000						100		0
0.25	10	1.1635	2.0004	1.078	1.079	1.079	0.001	1.079	93.8	9.38	0.311
0.5	10	1.1635	2.0004	1.104	1.141	1.123	0.026	1.123	97.6	9.76	0.120
0.75	10	1.1630	1.9995	1.065	1.084	1.075	0.013	1.075	93.4	9.34	0.328
1	10	1.1635	2.0004	1.049	1.097	1.073	0.034	1.073	93.3	9.33	0.335
2	10	1.1630	1.9995	1.048	1.019	1.034	0.021	1.034	89.9	8.99	0.507
5	10	1.1631	1.9997	1.113	1.081	1.097	0.023	1.097	95.4	9.54	0.230
10	10	1.1631	1.9997	1.044	1.027	1.036	0.012	1.036	90.0	9.00	0.498
20	10	1.1630	1.9995	1.032	1.052	1.042	0.014	1.042	90.6	9.06	0.470
30	10	1.1635	2.0004	1.064	1.075	1.070	0.008	1.070	93.0	9.30	0.350
60	10	1.1631	1.9997	1.06	1.07	1.065	0.007	1.065	92.6	9.26	0.370
120	10	1.1636	2.0006	1.025	1.114	1.070	0.063	1.070	93.0	9.30	0.350
180	10	1.1632	1.9999	1.072	1.023	1.048	0.035	1.048	91.1	9.11	0.446
240	10	1.1630	1.9995	0.98	1.08	1.030	0.071	1.030	89.6	8.96	0.522
1440	10	1.1634	2.0002	1.011	1.123	1.067	0.079	1.067	92.8	9.28	0.361

Time min)	Initial depressant mass (mg)	Sample mass (g)	Mineral surface area (m^2)	Absorbance				Actual Absorbance	Residual Concentration (mg/L)	Residual mass (mg)	Amount adsorbed (mg/m^2)
				1	2	Average	Std. deviation				
0	10	0	0.0000						100		0
0.25	10	1.1631	1.9997	1.081	1.086	1.084	0.004	1.084	94.2	9.42	0.289
0.5	10	1.1635	2.0004	1.097	1.065	1.081	0.023	1.081	94.0	9.40	0.300
0.75	10	1.1630	1.9995	1.082	1.078	1.080	0.003	1.080	93.9	9.39	0.304
1	10	1.1631	1.9997	1.073	1.095	1.084	0.016	1.084	94.3	9.43	0.287
2	10	1.1632	1.9999	1.073	1.071	1.072	0.001	1.072	93.2	9.32	0.339
5	10	1.1631	1.9997	1.047	1.082	1.065	0.025	1.065	92.6	9.26	0.372
10	10	1.1636	2.0006	1.079	1.089	1.084	0.007	1.084	94.3	9.43	0.287
20	10	1.1633	2.0001	1.048	1.103	1.076	0.039	1.076	93.5	9.35	0.324
30	10	1.1638	2.0009	1.066	1.109	1.088	0.030	1.088	94.6	9.46	0.272
60	10	1.1632	1.9999	1.08	1.085	1.083	0.004	1.083	94.1	9.41	0.293
120	10	1.1631	1.9997	1.072	1.043	1.058	0.021	1.058	92.0	9.20	0.402
180	10	1.1633	2.0001	1.065	1.053	1.059	0.008	1.059	92.1	9.21	0.396
240	10	1.1628	1.9992	1.087	1.064	1.076	0.016	1.076	93.5	9.35	0.324
1440	10	1.1632	1.9999	1.052	1.041	1.047	0.008	1.047	91.0	9.10	0.450

Chormite – guar in SPW, pH 9, T = 25°C

Time (min)	Initial depressant mass (mg)	Sample mass (g)	Mineral surface area (m^2)	Absorbance				Actual Absorbance	Residual Concentration (mg/L)	Residual mass (mg)	Amount adsorbed (mg/m^2)
				1	2	Average	Std. deviation				
0	10	0	0.0000						100		0
0.25	5	2.7038	2.0000	1.106	1.043	1.075	0.045	1.075	93.4	4.67	0.164
0.5	5	2.7036	1.9999	1.12	1.11	1.115	0.007	1.115	97.0	4.85	0.076
0.75	5	2.7036	1.9999	1.075	1.074	1.075	0.001	1.075	93.4	4.67	0.164
1	5	2.7037	1.9999	1.051	1.147	1.099	0.068	1.099	95.6	4.78	0.111
2	5	2.7035	1.9998	1.095	1.127	1.111	0.023	1.111	96.6	4.83	0.085
5	5	2.7041	2.0002	1.071	1.083	1.077	0.008	1.077	93.7	4.68	0.159
10	5	2.7035	1.9998	1.026	1.096	1.061	0.049	1.061	92.3	4.61	0.193
20	5	2.7036	1.9999	1.096	1.054	1.075	0.030	1.075	93.5	4.67	0.163
30	5	2.7042	2.0003	1.08	1.031	1.056	0.035	1.056	91.8	4.59	0.205
60	5	2.7034	1.9997	1.012	1.043	1.028	0.022	1.028	89.3	4.47	0.266
120	5	2.7036	1.9999	1.023	1.005	1.014	0.013	1.014	88.2	4.41	0.296
180	5	2.7038	2.0000	0.977	0.993	0.985	0.011	0.985	85.7	4.28	0.359
240	5	2.7037	1.9999	0.99	1.046	1.018	0.040	1.018	88.5	4.43	0.287
1440	5	2.7036	1.9999	1.006	1.115	1.061	0.077	1.061	92.2	4.61	0.195

Time (min	Initial depressant mass (mg)	Sample mass (g)	Mineral surface area (m^2)	Absorbance				Actual Absorbance	Residual Concentration (mg/L)	Residual mass (mg)	Amount adsorbed (mg/m^2)
				1	2	Average	Std. deviation				
0	5	0	0.0000						100		0
0.25	10	2.7037	1.9999	1.148	1.058	1.103	0.064	1.103	95.9	9.59	0.204
0.5	10	2.7036	1.9999	1.085	1.122	1.104	0.026	1.104	96.0	9.60	0.202
0.75	10	2.7040	2.0001	1.118	1.108	1.113	0.007	1.113	96.8	9.68	0.161
1	10	2.7041	2.0002	1.088	1.121	1.105	0.023	1.105	96.0	9.60	0.198
2	10	2.7040	2.0001	1.086	1.093	1.090	0.005	1.090	94.7	9.47	0.263
5	10	2.7041	1.9999	1.096	1.123	1.110	0.019	1.110	96.5	9.65	0.176
10	10	2.7037	2.0000	1.056	1.088	1.072	0.023	1.072	93.2	9.32	0.339
20	10	2.7038	2.0000	1.059	1.082	1.071	0.016	1.071	93.1	9.31	0.346
30	10	2.7038	2.0001	1.089	1.079	1.084	0.007	1.084	94.3	9.43	0.287
60	10	2.7039	1.9999	1.048	1.066	1.057	0.013	1.057	91.9	9.19	0.404
120	10	2.7037	1.9997	1.054	1.052	1.053	0.001	1.053	91.6	9.16	0.422
180	10	2.7034	1.9997	1.065	1.07	1.068	0.004	1.068	92.8	9.28	0.359
240	10	2.7034	1.9997	1.086	1.061	1.074	0.018	1.074	93.3	9.33	0.333

Chalcopyrite – guar in SPW, pH 9, T = 25°C

Time (min)	Initial depressant mass (mg)	Sample mass (g)	Mineral surface area (m^2)	Absorbance				Actual Absorbance	Residual Concentration (mg/L)	Residual mass (mg)	Amount adsorbed mg/m2
				1	2	Average	Std. deviation				
0	10	0	0.0000						100		0
0.25	10	1.8801	1.9993	1.069	1.113	1.091	0.031	1.091	94.9	9.49	0.257
0.5	10	1.8799	1.9991	1.036	1.088	1.062	0.037	1.062	92.3	9.23	0.383
0.75	10	1.8802	1.9994	1.087	1.045	1.066	0.030	1.066	92.7	9.27	0.365
1	10	1.8803	1.9995	0.995	1.032	1.014	0.026	1.014	88.1	8.81	0.594
2	10	1.8804	1.9996	1.012	0.998	1.005	0.010	1.005	87.4	8.74	0.631
5	10	1.8797	1.9989	1.028	1.002	1.015	0.018	1.015	88.3	8.83	0.587
10	10	1.8802	1.9994	0.938	0.994	0.966	0.040	0.966	84.0	8.40	0.800
20	10	1.8801	1.9993	0.995	1.004	1.000	0.006	1.000	86.9	8.69	0.655
30	10	1.8798	1.9990	0.999	0.986	0.993	0.009	0.993	86.3	8.63	0.685
60	10	1.8797	1.9989	1.002	1.034	1.018	0.023	1.018	88.5	8.85	0.574
120	10	1.8799	1.9991	0.971	0.983	0.977	0.008	0.977	85.0	8.50	0.753
180	10	1.8803	1.9995	0.995	0.946	0.971	0.035	0.971	84.4	8.44	0.781
240	10	1.8800	1.9992	0.988	0.945	0.967	0.030	0.967	84.0	8.40	0.798
1440	10	1.8800	1.9992	1.036	1.025	1.031	0.008	1.031	89.6	8.96	0.520

Time (min)	Initial depressant mass (mg)	Sample mass (g)	Mineral surface area (m^2)	Absorbance				Actual Absorbance	Residual Concentration (mg/L)	Residual mass (mg)	Amount adsorbed (mg/m^2)
				1	2	Average	Std. deviation				
0	10	0	0.0000						100		0
0.25	10	1.8801	1.9993	1.044	1.078	1.061	0.024	1.061	92.3	9.23	0.387
0.5	10	1.8801	1.9993	1.098	1.107	1.103	0.006	1.103	95.9	9.59	0.207
0.75	10	1.8804	1.9996	1.056	1.065	1.061	0.006	1.061	92.2	9.22	0.389
1	10	1.8804	1.9996	1.039	1.062	1.051	0.016	1.051	91.3	9.13	0.433
2	10	1.8798	1.9990	0.992	1.082	1.037	0.064	1.037	90.2	9.02	0.492
5	10	1.8800	1.9992	1.002	0.986	0.994	0.011	0.994	86.4	8.64	0.679
10	10	1.8798	1.9990	0.998	0.987	0.993	0.008	0.993	86.3	8.63	0.685
20	10	1.8800	1.9992	0.971	0.986	0.979	0.011	0.979	85.1	8.51	0.746
30	10	1.8803	1.9995	0.962	0.984	0.973	0.016	0.973	84.6	8.46	0.770
60	10	1.8803	1.9995	1.012	0.948	0.980	0.045	0.980	85.2	8.52	0.739
120	10	1.8804	1.9996	0.885	1.033	0.959	0.105	0.959	83.4	8.34	0.831
180	10	1.8803	1.9995	0.957	0.962	0.960	0.004	0.960	83.4	8.34	0.828
240	10	1.8797	1.9989	0.947	1.059	1.003	0.079	1.003	87.2	8.72	0.639
1440	10	1.8801	1.9993	0.918	0.943	0.931	0.018	0.931	80.9	8.09	0.955

Talc – CMC in SPW, pH 9, T = 25°C

Time (hours)	Initial depressant mass (mg)	Sample mass (g)	Mineral surface area (m^2)	Absorbance				Actual Absorbance	Residual Concentration (mg/L)	Residual mass (mg)	Amount adsorbed (mg/m^2)
				1	2	Average	Std. deviation				
0	10	0	0.0000	0.356	0.353	0.355	0.002	0.000	100	10.0	0
0.008	10	0.1453	2.0033	0.867	0.877	0.872	0.007	0.518	97.6	9.8	0.118
0.013	10	0.1452	2.0019	0.867	0.857	0.862	0.007	0.508	95.8	9.6	0.212
0.017	10	0.1449	1.9978	0.842	0.846	0.844	0.003	0.490	92.4	9.2	0.383
0.033	10	0.1451	2.0005	0.891	0.86	0.876	0.022	0.521	98.3	9.8	0.085
0.083	10	0.1451	2.0005	0.895	0.859	0.877	0.025	0.523	98.6	9.9	0.071
0.167	10	0.1451	2.0005	0.877	0.891	0.884	0.010	0.530	99.9	10.0	0.005
0.367	10	0.1452	2.0019	0.852	0.868	0.860	0.011	0.506	95.4	9.5	0.231
0.5	10	0.1451	2.0005	0.879	0.884	0.882	0.004	0.527	99.4	9.9	0.028
1	10	0.1451	2.0005	0.873	0.845	0.859	0.020	0.505	95.2	9.5	0.241
2	10	0.1450	1.9991	0.887	0.855	0.871	0.023	0.517	97.5	9.7	0.127
3	10	-0.1452	-2.0019	1.028	2.019	1.524	0.701	1.169	220.6	22.1	6.023
4	10	0.1451	2.0005	0.861	0.883	0.872	0.016	0.518	97.6	9.8	0.118
6	10	0.1450	1.9991	0.956	0.878	0.917	0.055	0.563	106.1	10.6	-0.307

Time (hours)	Initial depressant mass (mg)	Sample mass (g)	Mineral surface area (m^2)	Absorbance				Actual Absorbance	Residual Concentration (mg/L)	Residual mass (mg)	Amount adsorbed mg/m2
				1	2	Average	Std. deviation				
0	10	0.00	0.0000	0.356	0.353	0.355	0.002	0	100	100.0	0
0.008	10	0.1352	1.8640	0.881	0.839	0.860	0.030	0.5055	95.4	9.5	0.248
0.013	10	0.1451	2.0005	0.859	0.859	0.859	0.000	0.5045	95.2	9.5	0.241
0.017	10	0.1451	2.0005	0.857	0.84	0.849	0.012	0.494	93.2	9.3	0.340
0.033	10	0.1449	1.9978	0.884	0.896	0.890	0.008	0.5355	101.0	10.1	-0.052
0.083	10	0.1452	2.0019	0.844	0.822	0.833	0.016	0.4785	90.3	9.0	0.485
0.167	10	0.1452	2.0019	0.859	0.892	0.876	0.023	0.521	98.3	9.8	0.085
0.367	10	0.1452	2.0019	0.888	0.836	0.862	0.037	0.5075	95.8	9.6	0.212
0.5	10	0.1453	2.0033	0.86	0.86	0.860	0.000	0.5055	95.4	9.5	0.231
1	10	0.1452	2.0019	0.861	0.81	0.836	0.036	0.481	90.8	9.1	0.462
3	10	0.1451	2.0005	0.853	0.843	0.848	0.007	0.4935	93.1	9.3	0.344
4	10	0.1453	2.0033	0.723	0.789	0.756	0.047	0.4015	75.8	7.6	1.210
6	10	0.1351	1.8627	0.743	0.776	0.760	0.023	0.405	76.4	7.6	1.266

Plagioclase – CMC in SPW, pH 9, T = 25°C

Time (hours)	Initial depressant mass (mg)	Sample mass (g)	Mineral surface area (m^2)	Absorbance				Actual Absorbance	Residual Concentration (mg/L)	Residual mass (mg)	Amount adsorbed (mg/m^2)
				1	2	Average	Std. deviation				
				0.32	0.313	0.317	0.005	0.000			
0	10	0	0.0000	0.419	0.401	0.410	0.013	0.000	100	10.0	0
0.004	10	1.6270	2.0001	0.929	0.894	0.912	0.025	0.502	94.6	9.5	0.269
0.008	10	1.6272	2.0003	0.927	0.943	0.935	0.011	0.525	99.1	9.9	0.047
0.013	10	1.6273	2.0004	0.908	0.889	0.899	0.013	0.489	92.2	9.2	0.391
0.017	10	1.6271	2.0002	0.903	0.946	0.925	0.030	0.515	97.1	9.7	0.146
0.033	10	1.6266	1.9996	0.906	0.899	0.903	0.005	0.493	92.9	9.3	0.354
0.083	10	1.6271	2.0002	0.916	0.887	0.902	0.021	0.492	92.7	9.3	0.363
0.167	10	1.6269	1.9999	0.9	0.898	0.899	0.001	0.489	92.3	9.2	0.387
0.367	10	1.6270	2.0001	0.904	0.896	0.900	0.006	0.490	92.5	9.2	0.377
0.5	10	1.6267	1.9997	0.893	0.884	0.889	0.006	0.479	90.3	9.0	0.486
1	10	1.6267	1.9997	0.952	0.915	0.934	0.026	0.524	98.8	9.9	0.061
2	10	1.6272	2.0003	0.874	0.919	0.897	0.032	0.487	91.8	9.2	0.410
3	10	1.6267	1.9997	0.879	0.897	0.888	0.013	0.478	90.2	9.0	0.491
4	10	1.6269	1.9999	0.89	0.884	0.887	0.004	0.477	90.0	9.0	0.500
6	10	1.6269	1.9999	0.918	0.917	0.918	0.001	0.508	95.8	9.6	0.212

Time (hours)	Initial depressant mass (mg)	Sample mass (g)	Mineral surface area (m^2)	Absorbance				Actual Absorbance	Residual Concentration (mg/L)	Residual mass (mg)	Amount adsorbed (mg/m^2)
				1	2	Average	Std. deviation				
				0.32	0.313	0.317	0.005	0.000			
0	10	0	0.0000	0.419	0.401	0.410	0.013	0.000	100	10.0	0
0.004	10	1.6272	2.0003	0.908	0.892	0.900	0.011	0.490	92.5	9.2	0.377
0.008	10	1.6269	1.9999	0.905	0.915	0.910	0.007	0.500	94.3	9.4	0.283
0.013	10	1.6270	2.0001	0.938	0.906	0.922	0.023	0.512	96.6	9.7	0.170
0.017	10	1.6268	1.9998	0.918	0.905	0.912	0.009	0.502	94.6	9.5	0.269
0.033	10	1.6271	2.0002	0.989	0.953	0.971	0.025	0.561	105.8	10.6	-0.292
0.083	10	1.6269	1.9999	0.96	0.938	0.949	0.016	0.539	101.7	10.2	-0.085
0.167	10	1.6269	1.9999	0.943	0.923	0.933	0.014	0.523	98.7	9.9	0.066
0.367	10	1.6272	2.0003	0.98	0.915	0.948	0.046	0.538	101.4	10.1	-0.071
0.5	10	1.6268	1.9998	0.909	0.919	0.914	0.007	0.504	95.1	9.5	0.245
1	10	1.6269	1.9999	0.905	0.905	0.905	0.000	0.495	93.4	9.3	0.330
2	10	1.6270	2.0001	0.918	0.915	0.917	0.002	0.507	95.6	9.6	0.222
3	10	1.6200	1.9915	0.903	0.876	0.890	0.019	0.480	90.5	9.0	0.478
4	10	1.3359	1.6422	0.92	0.88	0.900	0.028	0.490	92.5	9.2	0.460
6	10	1.3360	1.6423	0.898	0.894	0.896	0.003	0.486	91.7	9.2	0.505

Pyroxene – CMC in SPW, pH 9, T = 25°C

Time (hours)	Initial depressant mass (mg)	Sample mass (g)	Mineral surface area (m^2)	Absorbance				Actual Absorbance	Residual Concentration (mg/L)	Residual mass (mg)	Amount adsorbed (mg/m^2)
				1	2	Average	Std. deviation				
0	10		0.0000	0.21875	0.216	0.218	0.002	0.000	100	10.0	0
0.004	10	0.9973	1.9998	0.769	0.793	0.781	0.017	0.564	106.3	10.6	-0.316
0.008	10	0.9974	2.0000	0.786	0.778	0.782	0.006	0.565	106.5	10.7	-0.325
0.013	10	0.9973	1.9998	0.741	0.770	0.756	0.021	0.538	101.5	10.2	-0.075
0.017	10	0.9975	2.0002	0.79	0.768	0.779	0.016	0.562	105.9	10.6	-0.297
0.033	10	0.9974	2.0000	0.767	0.775	0.771	0.006	0.554	104.4	10.4	-0.222
0.083	10	0.9974	2.0000	0.702	0.737	0.720	0.025	0.502	94.7	9.5	0.264
0.167	10	0.9973	1.9998	0.738	0.768	0.753	0.021	0.536	101.0	10.1	-0.052
0.367	10	0.9975	2.0002	0.76	0.778	0.769	0.013	0.552	104.1	10.4	-0.203
0.5	10	0.9975	2.0002	0.727	0.714	0.721	0.009	0.503	94.9	9.5	0.255
1	10	0.9973	1.9998	0.71	0.709	0.710	0.001	0.492	92.8	9.3	0.359
2	10	0.9974	2.0000	0.721	0.709	0.715	0.008	0.498	93.9	9.4	0.307
3	10	0.9976	2.0004	0.709	0.715	0.712	0.004	0.495	93.3	9.3	0.335
4	10	0.9975	2.0002	0.729	0.724	0.727	0.004	0.509	96.0	9.6	0.198
6	10	0.9975	2.0002	0.718	0.729	0.724	0.008	0.506	95.5	9.5	0.226

Time (hours)	Initial depressant mass (mg)	Sample mass (g)	Mineral surface area (m^2)	Absorbance				Actual Absorbance	Residual Concentration (mg/L)	Residual mass (mg)	Amount adsorbed (mg/m^2)
				1	2	Average	Std. deviation				
0	10	0	0.0000	0.219	0.219	0.218	0.002	0.000	100	10.0	0
0.004	10	0.9974	2.0000	0.818	0.755	0.787	0.045	0.569	107.4	10.7	-0.368
0.008	10	0.9972	1.9996	0.756	0.76	0.758	0.003	0.541	102.0	10.2	-0.099
0.013	10	0.9972	1.9996	0.796	0.766	0.781	0.021	0.564	106.3	10.6	-0.316
0.017	10	0.9973	1.9998	0.791	0.759	0.775	0.023	0.558	105.2	10.5	-0.259
0.033	10	0.9976	2.0004	0.758	0.788	0.773	0.021	0.556	104.8	10.5	-0.241
0.083	10	0.9974	2.0000	0.786	0.758	0.772	0.020	0.555	104.6	10.5	-0.231
0.167	10	0.9974	2.0000	0.748	0.775	0.762	0.019	0.544	102.6	10.3	-0.132
0.367	10	0.9975	2.0002	0.724	0.725	0.725	0.001	0.507	95.7	9.6	0.217
0.5	10	0.9975	2.0002	0.802	0.746	0.774	0.040	0.557	105.0	10.5	-0.250
1	10	0.9975	2.0002	0.7	0.71	0.705	0.007	0.488	92.0	9.2	0.401
2	10	0.9976	2.0004	0.742	0.716	0.729	0.018	0.512	96.5	9.7	0.174
3	10	0.9974	2.0000	0.756	0.704	0.730	0.037	0.513	96.7	9.7	0.165
4	10	0.9975	2.0002	0.696	0.714	0.705	0.013	0.488	92.0	9.2	0.401
6	10	0.9974	2.0000	0.687	0.701	0.694	0.010	0.477	89.9	9.0	0.505

Chromite – CMC in SPW, pH 9, T = 25°C

Time (hours)	Initial depressant mass (mg)	Sample mass (g)	Mineral surface area (m^2)	Absorbance				Actual Absorbance	Residual Concentration (mg/L)	Residual mass (mg)	Amount adsorbed (mg/m^2)
				1	2	Average	Std. deviation				
0	10	0	0.0000	0.321	0.333	0.327	0.008	0.000	100		0
0.008	10	2.3208	1.9998	0.832	0.812	0.822	0.014	0.495	93.4	9.3	0.330
0.013	10	2.3209	1.9999	0.889	0.84	0.865	0.035	0.538	101.4	10.1	-0.071
0.017	10	2.3209	1.9999	0.814	0.864	0.839	0.035	0.512	96.6	9.7	0.170
0.033	10	2.3210	2.0000	0.813	0.826	0.820	0.009	0.493	92.9	9.3	0.354
0.083	10	2.3210	2.0000	0.805	0.835	0.820	0.021	0.493	93.0	9.3	0.349
0.167	10	2.3212	2.0002	0.835	0.816	0.826	0.013	0.499	94.1	9.4	0.297
0.367	10	2.3208	1.9998	0.818	0.799	0.809	0.013	0.482	90.8	9.1	0.458
0.5	10	2.3209	1.9999	0.806	0.802	0.804	0.003	0.477	90.0	9.0	0.500
1	10	2.3210	2.0000	0.825	0.833	0.829	0.006	0.502	94.7	9.5	0.264
2	10	2.3211	2.0001	0.836	0.836	0.836	0.000	0.509	96.0	9.6	0.198
3	10	2.3210	2.0000	0.797	0.847	0.822	0.035	0.495	93.4	9.3	0.330
4	10	2.3210	2.0000	0.8	0.813	0.807	0.009	0.480	90.5	9.0	0.476

Time (hours)	Initial depressant mass (mg)	Sample mass(g)	Mineral surface area (m^2)	Absorbance				Actual Absorbance	Residual Concentration (mg/L)	Residual mass (mg)	Amount adsorbed (mg/m^2)
				1	2	Average	Std. deviation				
0	10	0	0.0000	0.322	0.333	0.328	0.008	0.000	100	10.0	0
0.008	10	2.3212	2.0002	0.853	0.805	0.829	0.034	0.502	94.6	9.5	0.269
0.013	10	2.3210	2.0000	0.843	0.822	0.833	0.015	0.505	95.3	9.5	0.236
0.017	10	2.321	2.0000	0.787	0.809	0.798	0.016	0.471	88.8	8.9	0.561
0.033	10	2.3209	1.9999	0.827	0.837	0.832	0.007	0.505	95.2	9.5	0.241
0.083	10	2.3209	1.9999	0.785	0.783	0.784	0.001	0.457	86.1	8.6	0.693
0.167	10	2.3209	2.0000	0.747	0.746	0.747	0.001	0.419	79.1	7.9	1.047
0.367	10	2.3210	2.0002	0.721	0.726	0.724	0.004	0.396	74.7	7.5	1.264
0.5	10	2.3212	2.0000	0.736	0.722	0.729	0.010	0.402	75.8	7.6	1.212
1	10	2.3210	2.0001	0.69	0.696	0.693	0.004	0.366	69.0	6.9	1.552
2	10	2.3211	2.0002	0.758	0.726	0.742	0.023	0.415	78.2	7.8	1.090
3	10	2.3212	2.0002	0.692	0.683	0.688	0.006	0.360	67.9	6.8	1.604
4	10	2.3210	2.0000	0.7	0.734	0.717	0.024	0.390	73.5	7.3	1.325

Chalcopyrite – CMC in SPW, pH 9, T = 25°C

Time (hours)	Initial depressant mass (mg)	Sample mass (g)	Mineral surface area (m^2)	Absorbance				Actual Absorbance	Residual Concentration (mg/L)	Residual mass (mg)	Amount adsorbed (mg/m^2)
				1	2	Average	Std. deviation				
0	10	0	0.0000	0.187	0.189	0.188	0.001	0.000	100	10.0	0
0.004	10	1.8809	2.0001	0.714	0.7	0.707	0.010	0.519	97.9	9.8	0.104
0.008	10	1.8810	2.0003	0.734	0.698	0.716	0.025	0.528	99.6	10.0	0.019
0.013	10	1.8810	2.0003	0.661	0.671	0.666	0.007	0.478	90.2	9.0	0.491
0.017	10	1.8805	1.9997	0.714	0.700	0.707	0.010	0.519	97.9	9.8	0.104
0.033	10	1.8810	2.0003	0.716	0.682	0.699	0.024	0.511	96.4	9.6	0.179
0.083	10	1.8808	2.0000	0.679	0.686	0.683	0.005	0.495	93.3	9.3	0.335
0.167	10	1.8808	2.0000	0.727	0.700	0.714	0.019	0.526	99.2	9.9	0.042
0.367	10	1.8810	2.0003	0.686	0.689	0.688	0.002	0.500	94.2	9.4	0.288
0.5	10	1.8808	2.0000	0.705	0.697	0.701	0.006	0.513	96.8	9.7	0.160
1	10	1.8807	1.9999	0.659	0.651	0.655	0.006	0.467	88.1	8.8	0.594
2	10	1.8808	2.0000	0.653	0.668	0.661	0.011	0.473	89.2	8.9	0.542
3	10	1.8810	2.0003	0.654	0.663	0.659	0.006	0.471	88.8	8.9	0.561
4	10	1.8807	1.9999	0.654	0.631	0.643	0.016	0.455	85.8	8.6	0.712
6	10	1.8808	2.0000	0.63	0.628	0.629	0.001	0.441	83.2	8.3	0.840

Time (hours)	Initial depressant mass (mg)	Sample mass (g)	Mineral surface area (m^2)	Absorbance				Actual Absorbance	Residual Concentration (mg/L)	Residual mass (mg)	Amount adsorbed (mg/m^2)
				1	2	Average	Std. deviation				
0	10	0	0.0000	0.187	0.189	0.188	0.001	0.000	100	10.0	0
0.004	10	1.8810	2.0003	0.727	0.691	0.709	0.025	0.521	98.3	9.8	0.085
0.008	10	1.8806	1.9998	0.731	0.723	0.727	0.006	0.539	101.7	10.2	-0.085
0.013	10	1.8807	1.9999	0.702	0.677	0.690	0.018	0.502	94.6	9.5	0.269
0.017	10	1.8808	2.0000	0.697	0.691	0.694	0.004	0.506	95.5	9.5	0.226
0.033	10	1.8809	2.0001	0.698	0.693	0.696	0.004	0.508	95.8	9.6	0.212
0.083	10	1.8806	1.9998	0.668	0.676	0.672	0.006	0.484	91.3	9.1	0.434
0.167	10	1.8810	2.0003	0.696	0.713	0.705	0.012	0.517	97.5	9.7	0.127
0.367	10	1.8808	2.0000	0.697	0.704	0.701	0.005	0.513	96.7	9.7	0.165
0.5	10	1.8810	2.0003	0.703	0.692	0.698	0.008	0.510	96.1	9.6	0.193
1	10	1.8810	2.0003	0.667	0.659	0.663	0.006	0.475	89.6	9.0	0.519
2	10	1.8809	2.0001	0.671	0.673	0.672	0.001	0.484	91.3	9.1	0.434
3	10	1.8810	2.0003	0.64	0.648	0.644	0.006	0.456	86.0	8.6	0.698
4	10	1.8810	2.0003	0.631	0.636	0.634	0.004	0.446	84.1	8.4	0.797
6	10	1.8809	2.0001	0.64	0.635	0.638	0.004	0.450	84.8	8.5	0.759

APPENDIX 7: EQUILIBRIUM ADSORPTION RAW DATA

Talc – guar in buffer, pH 9, T = 25°C

Initial depressant concentration (mg/L)	Initial depressant mass (mg)	Sample mass (g)	Mineral surface area (m^2)	Absorbance				Actual absorbance	Residual Concentration	Residual mass	Amount adsorbed
				1	2	Average	Std. deviation		(mg/L)	(mg)	mg/m^2
0	0	0	0	0	0	0.000	0.000	0.000	0.0	0.000	0.000
10	1.0	0.1937	1.9984	0.091	0.054	0.073	0.026	0.073	6.3	0.630	0.185
15	1.5	0.1940	2.0015	0.117	0.117	0.117	0.000	0.117	10.2	1.017	0.241
20	2.0	0.1940	2.0015	0.162	0.153	0.158	0.006	0.158	13.7	1.370	0.315
25	2.5	0.1937	1.9984	0.218	0.222	0.220	0.003	0.220	19.1	1.913	0.294
30	3.0	0.1936	1.9974	0.271	0.290	0.281	0.013	0.281	24.4	2.439	0.281
40	4.0	0.1936	1.9974	0.359	0.360	0.360	0.001	0.360	31.3	3.126	0.438
50	5.0	0.1939	2.0005	0.474	0.481	0.478	0.005	0.478	41.5	4.152	0.424
60	6.0	0.1938	1.9995	0.578	0.593	0.586	0.011	0.586	50.9	5.091	0.454
70	7.0	0.1942	2.0036	0.701	0.703	0.702	0.001	0.702	61.0	6.104	0.447
80	8.0	0.1941	2.0026	0.812	0.830	0.821	0.013	0.821	71.4	7.139	0.430
90	9.0	0.1936	1.9974	0.940	0.915	0.928	0.018	0.928	80.7	8.065	0.468
100	10.0	0.1935	1.9964	0.994	1.026	1.010	0.023	1.010	87.8	8.783	0.610

Initial depressant concentration (mg/L)	Initial depressant mass (mg)	Sample mass (g)	Mineral surface area (m^2)	Absorbance				Actual Absorbance	Residual Concentration (mg/L)	Residual mass (mg)	Amount adsorbed mg/m2
				1	2	Average	Std. deviation				
0	0	0	0	0	0	0.000	0.000	0.000	0.0	0.000	0.000
10	1.0	0.1939	2.0005	0.054	0.069	0.062	0.011	0.062	5.3	0.535	0.233
15	1.5	0.1937	1.9984	0.102	0.100	0.101	0.001	0.101	8.8	0.878	0.311
20	2.0	0.1934	1.9953	0.145	0.150	0.148	0.004	0.148	12.8	1.283	0.360
25	2.5	0.1936	1.9974	0.221	0.216	0.219	0.004	0.219	19.0	1.900	0.300
30	3.0	0.1942	2.0036	0.260	0.254	0.257	0.004	0.257	22.3	2.235	0.382
40	4.0	0.1936	1.9974	0..336	0.354	0.354	0.250	0.354	30.8	3.078	0.461
50	5.0	0.1938	1.9995	0.465	0.455	0.460	0.007	0.460	40.0	4.000	0.500
60	6.0	0.1941	2.0026	0.567	0.566	0.567	0.001	0.567	49.3	4.926	0.536
70	7.0	0.1939	2.0005	0.677	0.690	0.684	0.009	0.684	59.4	5.943	0.528
80	8.0	0.1939	2.0005	0.851	0.894	0.873	0.030	0.873	75.9	7.587	0.206
90	9.0	0.1938	1.9995	0.879	0.891	0.885	0.008	0.885	77.0	7.696	0.652
100	10.0	0.1936	1.9974	0.998	1.016	1.007	0.013	1.007	87.6	8.757	0.623

Plagioclase - guar in buffer, pH 9, T = 25°C

Initial depressant concentration (mg/L)	Initial depressant mass (mg)	Sample mass (g)	Mineral surface area (m^2)	Absorbance				Actual Absorbance	Residual Concentration (mg/L)	Residual mass (mg)	Amount adsorbed (mg/m^2)
				1	2	Average	Std. deviation				
0	0	0	0	0.122	0.122	0.122	0.000	0.000	0.0	0.000	0.000
10	1.0	1.2152	2.0002	0.212	0.209	0.211	0.002	0.089	8.2	0.819	0.090
15	1.5	1.2150	1.9999	0.262	0.264	0.263	0.001	0.141	13.1	1.306	0.097
20	2.0	1.2153	2.0004	0.321	0.323	0.322	0.001	0.200	18.5	1.852	0.074
25	2.5	1.2153	2.0004	0.366	0.355	0.361	0.008	0.239	22.1	2.208	0.146
30	3.0	1.2149	1.9997	0.413	0.412	0.413	0.001	0.291	26.9	2.690	0.155
40	4.0	1.2150	1.9999	0.496	0.501	0.499	0.004	0.377	34.9	3.486	0.257
50	5.0	1.2150	1.9999	0.601	0.61	0.606	0.006	0.484	44.8	4.477	0.262
60	6.0	1.2150	1.9999	0.717	0.703	0.710	0.010	0.588	54.4	5.444	0.278
70	7.0	1.2149	1.9997	0.788	0.816	0.802	0.020	0.680	63.0	6.296	0.352
80	8.0	1.2149	1.9997	0.912	0.904	0.908	0.006	0.786	72.8	7.278	0.361
90	9.0	1.2150	1.9999	1.016	0.984	1.000	0.023	0.878	81.3	8.130	0.435

Initial depressant concentration (mg/L)	Initial depressant mass (mg)	Sample mass (g)	Mineral surface area (m^2)	Absorbance				Actual Absorbance	Residual Concentration (mg/L)	Residual mass (mg)	Amount adsorbed mg/m^2
				1	2	Average	Std. deviation				
0	0	0	0	0.122	0.122	0.122	0.000	0.000	0.0	0.000	0.000
10	1.0	1.2150	1.9999	0.221	0.305	0.263	0.059	0.141	13.1	1.306	-0.076
15	1.5	1.2152	2.0002	0.323	0.282	0.303	0.029	0.181	16.7	1.671	-0.043
20	2.0	1.2153	2.0004	0.314	0.327	0.321	0.009	0.199	18.4	1.838	0.041
25	2.5	1.2149	1.9997	0.394	0.38	0.387	0.010	0.265	24.5	2.454	0.012
30	3.0	1.2153	2.0004	0.404	0.45	0.427	0.033	0.305	28.2	2.824	0.044
40	4.0	1.2149	1.9997	0.511	0.505	0.508	0.004	0.386	35.7	3.574	0.106
50	5.0	1.2152	2.0002	0.6	0.587	0.594	0.009	0.472	43.7	4.366	0.159
60	6.0	1.2150	1.9999	0.718	0.715	0.717	0.002	0.595	55.0	5.505	0.124
70	7.0	1.2151	2.0001	0.999	1.019	1.009	0.014	0.887	82.1	8.213	-0.303
80	8.0	1.2149	1.9997	0.922	0.889	0.906	0.023	0.784	72.5	7.255	0.186
90	9.0	1.2153	2.0004	0.833	0.803	0.818	0.021	0.696	64.4	6.444	0.639
100	10.0	1.2151	2.0001	1.088	1.072	1.080	0.011	0.958	88.7	8.870	0.282

Pyroxene - guar in buffer, pH 9, T = 25°C

Initial depressant concentration (mg/L)	Initial depressant mass (mg)	Sample mass (g)	Mineral surface area (m^2)	Absorbance				Actual Absorbance	Residual Concentration (mg/L)	Residual mass (mg)	Amount adsorbed (mg/m^2)
				1	2	Average	Std. deviation				
0	0	0	0	0	0	0.000	0.000	0.000	0.0	0.000	0.000
10	1.0	1.5582	2.0001	0.054	0.060	0.057	0.004	0.057	5.0	0.496	0.252
15	1.5	1.5578	1.9996	0.107	0.103	0.105	0.003	0.105	9.1	0.913	0.294
20	2.0	1.5581	2.0000	0.150	0.144	0.147	0.004	0.147	12.8	1.278	0.361
25	2.5	1.5581	2.0000	0.220	0.238	0.229	0.013	0.229	19.9	1.991	0.254
30	3.0	1.5580	1.9998	0.290	0.274	0.282	0.011	0.282	24.5	2.452	0.274
40	4.0	1.5579	1.9997	0.359	0.371	0.365	0.008	0.365	31.7	3.174	0.413
50	5.0	1.5578	1.9996	0.477	0.478	0.478	0.001	0.478	41.5	4.152	0.424
60	6.0	1.5579	1.9997	0.609	0.606	0.608	0.002	0.608	52.8	5.283	0.359
70	7.0	1.5579	1.9997	0.695	0.705	0.700	0.007	0.700	60.9	6.087	0.457
80	8.0	1.5580	1.9998	0.817	0.888	0.853	0.050	0.853	74.1	7.413	0.294
90	9.0	1.5580	1.9998	0.918	0.991	0.955	0.052	0.955	83.0	8.300	0.350
100	10.0	1.5579	1.9997	1.023	1.044	1.034	0.015	1.034	89.9	8.987	0.507

Initial depressant concentration (mg/L)	Initial depressant mass (mg)	Sample mass (g)	Mineral surface area (m^2)	Absorbance				Actual Absorbance	Residual Concentration (mg/L)	Residual mass (mg)	Amount adsorbed mg/m^2
				1	2	Average	Std. deviation				
0	0	0	0	0	0	0.000	0.000	0.000	0.0	0.000	0.000
10	1.0	1.5580	1.9998	0.054	0.052	0.053	0.001	0.053	4.6	0.461	0.270
15	1.5	1.5583	2.0002	0.102	0.112	0.107	0.007	0.107	9.3	0.930	0.285
20	2.0	1.5580	1.9998	0.167	0.163	0.165	0.003	0.165	14.3	1.435	0.283
25	2.5	1.5579	1.9997	0.207	0.218	0.213	0.008	0.213	18.5	1.848	0.326
30	3.0	1.5581	2.0000	0.271	0.294	0.283	0.016	0.283	24.6	2.457	0.272
40	4.0	1.5580	1.9998	0.364	0.360	0.362	0.003	0.362	31.5	3.148	0.426
50	5.0	1.5578	1.9996	0.475	0.506	0.491	0.022	0.491	42.7	4.265	0.367
60	6.0	1.5579	1.9997	0.602	0.613	0.608	0.008	0.608	52.8	5.283	0.359
70	7.0	1.5581	2.0000	0.729	0.713	0.721	0.011	0.721	62.7	6.270	0.365
80	8.0	1.5583	2.0002	0.819	0.845	0.832	0.018	0.832	72.3	7.235	0.383
90	9.0	1.5581	2.0000	0.920	0.947	0.934	0.019	0.934	81.2	8.117	0.441
100	10.0	1.5583	2.0002	1.074	1.060	1.067	0.010	1.067	92.8	9.278	0.361

Chromite - guar in buffer, pH 9, T = 25°C

Initial depressant concentration (mg/L)	Initial depressant mass (mg)	Sample mass (g)	Mineral surface area (m^2)	Absorbance				Actual Absorbance	Residual Concentration (mg/L)	Residual mass (mg)	Amount adsorbed mg/m2
				1	2	Average	Std. deviation				
0	0	0	0	0	0	0.000	0.000	0.000	0.0	0.000	0.000
10	1.0	2.3208	1.9998	0.046	0.041	0.044	0.004	0.044	3.8	0.378	0.311
15	1.5	2.3208	1.9998	0.102	0.108	0.105	0.004	0.105	9.1	0.913	0.294
20	2.0	2.3210	2.0000	0.137	0.135	0.136	0.001	0.136	11.8	1.183	0.409
25	2.5	2.3210	2.0000	0.211	0.203	0.207	0.006	0.207	18.0	1.800	0.350
30	3.0	2.3209	1.9999	0.281	0.267	0.274	0.010	0.274	23.8	2.383	0.309
40	4.0	2.3209	1.9999	0.355	0.375	0.365	0.014	0.365	31.7	3.174	0.413
50	5.0	2.3208	1.9998	0.467	0.445	0.456	0.016	0.456	39.7	3.965	0.517
60	6.0	2.3208	1.9998	0.589	0.585	0.587	0.003	0.587	51.0	5.104	0.448
70	7.0	2.3208	1.9998	0.696	0.690	0.693	0.004	0.693	60.3	6.026	0.487
80	8.0	2.3212	2.0002	0.827	0.805	0.816	0.016	0.816	71.0	7.096	0.452
90	9.0	2.3208	1.9998	0.914	0.907	0.911	0.005	0.911	79.2	7.917	0.541
100	10.0	2.3209	1.9999	1.021	1.010	1.016	0.008	1.016	88.3	8.830	0.585

Initial depressant concentration (mg/L)	Initial depressant mass (mg)	Sample mass (g)	Mineral surface area (m^2)	Absorbance				Actual Absorbance	Residual Concentration (mg/L)	Residual mass (mg)	Amount adsorbed (mg/m^2)
				1	2	Average	Std. deviation				
0	0	0	0	0	0	0.000	0.000	0.000	0.0	0.000	0.000
10	1.0	2.3210	2.0000	0.027	0.022	0.025	0.004	0.025	2.1	0.213	0.393
15	1.5	2.3211	2.0001	0.124	0.134	0.129	0.007	0.129	11.2	1.122	0.189
20	2.0	2.3210	2.0000	0.134	0.132	0.133	0.001	0.133	11.6	1.157	0.422
25	2.5	2.3210	2.0000	0.199	0.197	0.198	0.001	0.198	17.2	1.722	0.389
30	3.0	2.3212	2.0002	0.243	0.263	0.253	0.014	0.253	22.0	2.200	0.400
40	4.0	2.3212	2.0002	0.376	0.353	0.365	0.016	0.365	31.7	3.170	0.415
50	5.0	2.3211	2.0001	0.470	0.466	0.468	0.003	0.468	40.7	4.070	0.465
60	6.0	2.3213	2.0003	0.566	0.600	0.583	0.024	0.583	50.7	5.070	0.465
70	7.0	2.3213	2.0003	0.688	0.699	0.694	0.008	0.694	60.3	6.030	0.485
80	8.0	2.3210	2.0000	0.822	0.822	0.822	0.000	0.822	71.5	7.148	0.426
90	9.0	2.3213	2.0003	0.913	0.894	0.904	0.013	0.904	78.6	7.857	0.572
100	10.0	2.3214	2.0004	1.018	1.012	1.015	0.004	1.015	88.3	8.826	0.587

Chalcopyrite - guar in buffer, pH 9, T = 25°C

Initial depressant concentration (mg/L)	Initial depressant mass (mg)	Sample mass (g)	Mineral surface area (m^2)	Absorbance				Actual Absorbance	Residual Concentration (mg/L)	Residual mass (mg)	Amount adsorbed (mg/m^2)
				1	2	Average	Std. deviation				
0	0	0	0	0	0	0.000	0.000	0.000	0.0	0.000	0.000
10	1.0	1.8805	1.9997	0.049	0.043	0.046	0.004	0.046	4.0	0.400	0.300
15	1.5	1.8806	1.9998	0.056	0.060	0.058	0.003	0.058	5.0	0.504	0.498
20	2.0	1.8806	1.9998	0.166	0.137	0.152	0.021	0.152	13.2	1.317	0.341
25	2.5	1.8807	1.9999	0..184	0.191	0.191	0.135	0.191	16.6	1.661	0.420
30	3.0	1.8806	1.9998	0.247	0.232	0.240	0.011	0.240	20.8	2.083	0.459
40	4.0	1.8808	2.0000	0.358	0.340	0.349	0.013	0.349	30.3	3.035	0.483
50	5.0	1.8804	1.9996	0.461	0.428	0.445	0.023	0.445	38.7	3.865	0.567
60	6.0	1.8804	1.9996	0.580	0.566	0.573	0.010	0.573	49.8	4.983	0.509
70	7.0	1.8808	2.0000	0.688	0.695	0.692	0.005	0.692	60.1	6.013	0.493
80	8.0	1.8804	1.9996	0.767	0.795	0.781	0.020	0.781	67.9	6.791	0.604
90	9.0	1.8807	1.9999	0.855	0.877	0.866	0.016	0.866	75.3	7.530	0.735
100	10.0	1.8806	1.9998	0.989	0.988	0.989	0.001	0.989	86.0	8.596	0.702

Initial depressant concentration (mg/L)	Initial depressant mass (mg)	Sample mass (g)	Mineral surface area (m^2)	Absorbance				Actual Absorbance	Residual Concentration (mg/L)	Residual mass (mg)	Amount adsorbed (mg/m^2)
				1	2	Average	Std. deviation				
0	0	0	0	0	0	0.000	0.000	0.000	0.0	0.000	0.000
10	1.0	1.8804	1.9996	0.032	0.068	0.050	0.025	0.050	4.3	0.435	0.283
15	1.5	1.8805	1.9997	0.081	0.085	0.083	0.003	0.083	7.2	0.722	0.389
20	2.0	1.8804	1.9996	0.122	0.130	0.126	0.006	0.126	11.0	1.096	0.452
25	2.5	1.8806	1.9998	0.195	0.170	0.183	0.018	0.183	15.9	1.587	0.457
30	3.0	1.8808	2.0000	0.245	0.229	0.237	0.011	0.237	20.6	2.061	0.470
50	5.0	1.8806	1.9998	0.421	0.452	0.437	0.022	0.437	38.0	3.796	0.602
60	6.0	1.8808	2.0000	0.554	0.553	0.554	0.001	0.554	48.1	4.813	0.593
70	7.0	1.8803	1.9995	0.688	0.645	0.667	0.030	0.667	58.0	5.796	0.602
80	8.0	1.8804	1.9996	0.790	0.807	0.799	0.012	0.799	69.4	6.943	0.528
90	9.0	1.8804	1.9996	0.879	0.875	0.877	0.003	0.877	76.3	7.626	0.687
100	10.0	1.8807	1.9999	0.971	0.983	0.977	0.008	0.977	85.0	8.496	0.752

Chalcopyrite – guar + SIBX in buffer, pH 9 , T= 25°C

Initial depressant concentration (mg/L)	Initial depressant mass (mg)	Sample mass (g)	Mineral surface area (m^2)	Absorbance				Actual Absorbance	Residual Concentration (mg/L)	Residual mass (mg)	Amount adsorbed (mg/m^2)
				1	2	Average	Std. deviation				
0	0	0	0	0.185	0.196	0.191	0.008	0.000	0.0	0.000	0.000
10	1.0	1.8805	1.9997	0.229	0.215	0.222	0.010	0.032	2.7	0.274	0.363
20	2.0	1.8810	2.0003	0.317	0.317	0.317	0.000	0.127	11.0	1.100	0.450
50	5.0	1.8808	2.0000	0.636	0.624	0.630	0.008	0.440	38.2	3.822	0.589
80	8.0	1.8810	2.0003	0.903	0.899	0.901	0.003	0.711	61.8	6.178	0.911
90	9.0	1.8810	2.0003	1.017	1.008	1.013	0.006	0.822	71.5	7.148	0.926
100	10.0	1.8810	2.0003	1.162	1.105	1.134	0.040	0.943	82.0	8.200	0.900

Initial depressant concentration (mg/L)	Initial depressant mass (mg)	Sample mass (g)	Mineral surface area (m^2)	Absorbance				Actual Absorbance	Residual Concentration (mg/L)	Residual mass (mg)	Amount adsorbed (mg/m^2)
				1	2	Average	Std. deviation				
0	0	0	0	0.185	0.196	0.191	0.008	0.000		0.000	0.000
10	1.0	1.8808	2.0000	0.221	0.215	0.218	0.004	0.028	2.4	0.239	0.380
20	2.0	1.8808	2.0000	0.315	0.324	0.320	0.006	0.129	11.2	1.122	0.439
50	5.0	1.8809	2.0001	0.589	0.611	0.600	0.016	0.410	35.6	3.561	0.720
80	8.0	1.8811	2.0004	0.955	0.949	0.952	0.004	0.762	66.2	6.622	0.689
90	9.0	1.8807	1.9999	1.041	1.029	1.035	0.008	0.845	73.4	7.343	0.828
100	10.0	1.8807	1.9999	1.149	1.179	1.164	0.021	0.974	84.7	8.465	0.767

Talc – guar in SPW, pH 9, T = 25°C

Initial depressant concentration (mg/L)	Initial depressant mass (mg)	Sample mass (g)	Mineral surface area (m^2)	Absorbance				Actual Absorbance	Residual Concentration (mg/L)	Residual mass (mg)	Amount adsorbed mg/m2
				1	2	Average	Std. deviation				
0	0	0	0	0	0	0.000	0.000	0.000	0.0	0.000	0.000
10	1.0	0.1940	2.0015	0.030	0.059	0.045	0.021	0.045	3.9	0.387	0.306
15	1.5	0.1938	1.9995	0.067	0.083	0.075	0.011	0.075	6.5	0.652	0.424
20	2.0	0.1937	1.9984	0.074	0.100	0.087	0.018	0.087	7.6	0.757	0.622
25	2.5	0.1937	1.9984	0.183	0.221	0.202	0.027	0.202	17.6	1.757	0.372
30	3.0	0.1938	1.9995	0.243	0.261	0.252	0.013	0.252	21.9	2.191	0.404
40	4.0	0.1938	1.9995	0.339	0.345	0.342	0.004	0.342	29.7	2.974	0.513
50	5.0	0.1938	1.9995	0.471	0.437	0.454	0.024	0.454	39.5	3.948	0.526
60	6.0	0.1938	1.9995	0.574	0.575	0.575	0.001	0.575	50.0	4.996	0.502
70	7.0	0.1940	2.0015	0.667	0.698	0.683	0.022	0.683	59.3	5.935	0.532
80	8.0	0.1937	1.9984	0.743	0.750	0.747	0.005	0.747	64.9	6.491	0.755
90	9.0	0.1940	2.0015	0.883	0.930	0.907	0.033	0.907	78.8	7.883	0.558
100	10.0	0.1938	1.9995	0.979	1.043	1.011	0.045	1.011	87.9	8.791	0.605

Initial depressant concentration (mg/L)	Initial depressant mass (mg)	Sample mass (g)	Mineral surface area (m^2)	Absorbance				Actual Absorbance	Residual Concentration (mg/L)	Residual mass (mg)	Amount adsorbed (mg/m^2)
				1	2	Average	Std. deviation				
0	0	0	0	0	0	0.000	0.000	0.000	0.0	0.000	0.000
10	1.0	0.1940	2.0015	0.054	0.069	0.062	0.011	0.062	5.3	0.535	0.232
15	1.5	0.1938	1.9995	0.102	0.100	0.101	0.001	0.101	8.8	0.878	0.311
25	2.5	0.1937	1.9984	0.221	0.216	0.219	0.004	0.219	19.0	1.900	0.300
30	3.0	0.1938	1.9995	0.260	0.254	0.257	0.004	0.257	22.3	2.235	0.383
40	4.0	0.1938	1.9995	0..336	0.354	0.354	0.250	0.354	30.8	3.078	0.461
50	5.0	0.1938	1.9995	0.465	0.455	0.460	0.007	0.460	40.0	4.000	0.500
60	6.0	0.1938	1.9995	0.567	0.566	0.567	0.001	0.567	49.3	4.926	0.537
70	7.0	0.1940	2.0015	0.677	0.690	0.684	0.009	0.684	59.4	5.943	0.528
90	9.0	0.1940	2.0015	0.879	0.891	0.885	0.008	0.885	77.0	7.696	0.652
100	10.0	0.1938	1.9995	0.998	1.016	1.007	0.013	1.007	87.6	8.757	0.622

Plagioclase - guar in SPW, pH 9, T = 25°C

Initial depressant concentration (mg/L)	Initial depressant mass (mg)	Sample mass (g)	Mineral surface area (m^2)	Absorbance				Actual Absorbance	Residual Concentration (mg/L)	Residual mass (mg)	Amount adsorbed (mg/m^2)
				1	2	Average	Std. deviation				
0	0	0	0	0	0	0.000	0.000	0.000	0.0	0.000	0.000
10	1.0	1.6267	1.9997	0.116	0.092	0.104	0.017	0.104	9.0	0.904	0.048
15	1.5	1.6268	1.9998	0.167	0.139	0.153	0.020	0.153	13.3	1.330	0.085
20	2.0	1.6269	1.9999	0.196	0.201	0.199	0.004	0.199	17.3	1.726	0.137
25	2.5	1.6271	2.0002	0.264	0.250	0.257	0.010	0.257	22.3	2.235	0.133
30	3.0	1.6270	2.0001	0.312	0.296	0.304	0.011	0.304	26.4	2.643	0.178
40	4.0	1.6272	2.0003	0.419	0.414	0.417	0.004	0.417	36.2	3.622	0.189
50	5.0	1.6267	1.9997	0.526	0.518	0.522	0.006	0.522	45.4	4.539	0.230
60	6.0	1.6271	2.0002	0.654	0.636	0.645	0.013	0.645	56.1	5.609	0.196
70	7.0	1.6271	2.0002	0.786	0.755	0.771	0.022	0.771	67.0	6.700	0.150
80	8.0	1.6270	2.0001	0.883	0.879	0.881	0.003	0.881	76.6	7.661	0.170
90	9.0	1.6271	2.0002	0.994	0.992	0.993	0.001	0.993	86.3	8.635	0.183
100	10.0	1.6267	1.9997	1.102	1.067	1.085	0.025	1.085	94.3	9.430	0.285

Initial depressant concentration (mg/L)	Initial depressant mass (mg)	Sample mass (g)	Mineral surface area (m^2)	Absorbance				Actual Absorbance	Residual Concentration (mg/L)	Residual mass (mg)	Amount adsorbed (mg/m^2)
				1	2	Average	Std. deviation				
0	0	0	0	0	0	0.000	0.000	0.000	0.0	0.000	0.000
10	1.0	1.6273	2.0004	0.091	0.103	0.097	0.008	0.097	8.4	0.843	0.078
15	1.5	1.6270	2.0001	0.163	0.138	0.151	0.018	0.151	13.1	1.309	0.096
20	2.0	1.6269	1.9999	0.234	0.215	0.225	0.013	0.225	19.5	1.952	0.024
25	2.5	1.6273	2.0004	0.249	0.261	0.255	0.008	0.255	22.2	2.217	0.141
30	3.0	1.6268	1.9998	0.328	0.300	0.314	0.020	0.314	27.3	2.730	0.135
40	4.0	1.6272	2.0003	0.438	0.424	0.431	0.010	0.431	37.5	3.748	0.126
50	5.0	1.6267	1.9997	0.519	0.520	0.520	0.001	0.520	45.2	4.517	0.241
60	6.0	1.6270	2.0001	0.653	0.627	0.640	0.018	0.640	55.7	5.565	0.217
70	7.0	1.6272	2.0003	0.750	0.739	0.745	0.008	0.745	64.7	6.474	0.263
80	8.0	1.6269	1.9999	0.889	0.869	0.879	0.014	0.879	76.4	7.643	0.178
90	9.0	1.6271	2.0002	0.999	0.973	0.986	0.018	0.986	85.7	8.574	0.213
100	10.0	1.6268	1.9998	1.113	1.072	1.093	0.029	1.093	95.0	9.500	0.250

Pyroxene - guar in SPW, pH 9, T = 25°C

Initial depressant concentration (mg/L)	Initial depressant mass (mg)	Sample mass (g)	Mineral surface area (m^2)	Absorbance				Actual Absorbance	Residual Concentration (mg/L)	Residual mass (mg)	Amount adsorbed (mg/m2)
				1	2	Average	Std. deviation				
0	0	0	0	0	0	0.000	0.000	0.000	0.0	0.000	0.000
10	1.0	1.5581	2.0000	0.034	0.040	0.037	0.004	0.037	3.2	0.322	0.339
15	1.5	1.5579	1.9997	0.089	0.086	0.088	0.002	0.088	7.6	0.761	0.370
20	2.0	1.5580	1.9998	0.206	0.196	0.201	0.007	0.201	17.5	1.748	0.126
25	2.5	1.5582	2.0001	0..267	0.253	0.253	0.179	0.253	22.0	2.200	0.150
30	3.0	1.5581	2.0000	0.300	0.304	0.302	0.003	0.302	26.3	2.626	0.187
40	4.0	1.5580	1.9998	0.416	0.421	0.419	0.004	0.419	36.4	3.639	0.180
50	5.0	1.5583	2.0002	0.533	0.513	0.523	0.014	0.523	45.5	4.548	0.226
60	6.0	1.5583	2.0002	0.615	0.642	0.629	0.019	0.629	54.7	5.465	0.267
70	7.0	1.5579	1.9997	0.745	0.723	0.734	0.016	0.734	63.8	6.383	0.309
80	8.0	1.5580	1.9998	0.836	0.816	0.826	0.014	0.826	71.8	7.183	0.409
90	9.0	1.5579	1.9997	0.952	0.957	0.955	0.004	0.955	83.0	8.300	0.350
100	10.0	1.5581	2.0000	1.035	1.051	1.043	0.011	1.043	90.7	9.070	0.465

Initial depressant concentration (mg/L)	Initial depressant mass (mg)	Sample mass (g)	Mineral surface area (m^2)	Absorbance				Actual Absorbance	Residual Concentration (mg/L)	Residual mass (mg)	Amount adsorbed (mg/m^2)
				1	2	Average	Std. deviation				
0	0	0	0	0	0	0.000	0.000	0.000	0.0	0.000	0.000
10	1.0	1.5582	2.0001	0.096	0.085	0.091	0.008	0.091	7.9	0.787	0.107
15	1.5	1.5582	2.0001	0.160	0.156	0.158	0.003	0.158	13.7	1.374	0.063
20	2.0	1.5581	2.0000	0.183	0.220	0.202	0.026	0.202	17.5	1.752	0.124
25	2.5	1.5581	2.0000	0.284	0.270	0.277	0.010	0.277	24.1	2.409	0.046
30	3.0	1.5581	2.0000	0.325	0.351	0.338	0.018	0.338	29.4	2.939	0.030
40	4.0	1.5583	2.0002	0.415	0.415	0.415	0.000	0.415	36.1	3.609	0.196
50	5.0	1.5579	1.9997	0.514	0.528	0.521	0.010	0.521	45.3	4.530	0.235
60	6.0	1.5582	2.0001	0.621	0.617	0.619	0.003	0.619	53.8	5.383	0.309
70	7.0	1.5583	2.0002	0.751	0.745	0.748	0.004	0.748	65.0	6.504	0.248
80	8.0	1.5580	1.9998	0.841	0.872	0.857	0.022	0.857	74.5	7.448	0.276
90	9.0	1.5581	2.0000	0.960	0.973	0.967	0.009	0.967	84.0	8.404	0.298
100	10.0	1.5580	1.9998	1.082	1.042	1.062	0.028	1.062	92.3	9.235	0.383

Chromite - guar in SPW, pH 9, T = 25°C

Initial depressant concentration (mg/L)	Initial depressant mass (mg)	Sample mass (g)	Mineral surface area (m^2)	Absorbance				Actual Absorbance	Residual Concentration (mg/L)	Residual mass (mg)	Amount adsorbed (mg/m^2)
				1	2	Average	Std. deviation				
0	0	0	0	0	0	0.000	0.000	0.000	0.0	0.000	0.000
10	1.0	2.7038	2.0000	0.088	0.091	0.090	0.002	0.090	7.8	0.778	0.111
15	1.5	2.7039	2.0001	0.153	0.187	0.170	0.024	0.170	14.8	1.478	0.011
20	2.0	2.7037	1.9999	0.187	0.194	0.191	0.005	0.191	16.6	1.657	0.172
25	2.5	2.7038	2.0000	0.266	0.261	0.264	0.004	0.264	22.9	2.291	0.104
30	3.0	2.7040	2.0001	0.309	0.284	0.297	0.018	0.297	25.8	2.578	0.211
40	4.0	2.7037	1.9999	0.442	0.411	0.427	0.022	0.427	37.1	3.709	0.146
50	5.0	2.7035	1.9998	0.520	0.524	0.522	0.003	0.522	45.4	4.539	0.230
60	6.0	2.7037	1.9999	0.606	0.598	0.602	0.006	0.602	52.3	5.235	0.383
70	7.0	2.7040	2.0001	0.720	0.702	0.711	0.013	0.711	61.8	6.183	0.409
80	8.0	2.7037	1.9999	0.818	0.833	0.826	0.011	0.826	71.8	7.178	0.411
90	9.0	2.7038	2.0000	0.921	0.946	0.934	0.018	0.934	81.2	8.117	0.441
100	10.0	2.7040	2.0001	1.081	1.042	1.062	0.028	1.062	92.3	9.230	0.385

Initial depressant concentration (mg/L)	Initial depressant mass (mg)	Sample mass (g)	Mineral surface area (m^2)	Absorbance				Actual Absorbance	Residual Concentration (mg/L)	Residual mass (mg)	Amount adsorbed (mg/m^2)
				1	2	Average	Std. deviation				
0	0	0	0	0	0	0.000	0.000	0.000	0.0	0.000	0.000
10	1.0	2.3210	2.0000	0.027	0.022	0.025	0.004	0.025	2.1	0.213	0.393
20	2.0	2.3210	2.0000	0.134	0.132	0.133	0.001	0.133	11.6	1.157	0.422
25	2.5	2.3210	2.0000	0.199	0.197	0.198	0.001	0.198	17.2	1.722	0.389
30	3.0	2.3212	2.0002	0.243	0.263	0.253	0.014	0.253	22.0	2.200	0.400
40	4.0	2.3212	2.0002	0.376	0.353	0.365	0.016	0.365	31.7	3.170	0.415
50	5.0	2.3211	2.0001	0.470	0.466	0.468	0.003	0.468	40.7	4.070	0.465
60	6.0	2.3213	2.0003	0.566	0.600	0.583	0.024	0.583	50.7	5.070	0.465
70	7.0	2.3213	2.0003	0.688	0.699	0.694	0.008	0.694	60.3	6.030	0.485
80	8.0	2.3210	2.0000	0.822	0.822	0.822	0.000	0.822	71.5	7.148	0.426
90	9.0	2.3213	2.0003	0.913	0.894	0.904	0.013	0.904	78.6	7.857	0.572
100	10.0	2.3214	2.0004	1.018	1.012	1.015	0.004	1.015	88.3	8.826	0.587

Chalcopyrite - guar in SPW, pH 9, T = 25°C

Initial depressant concentration (mg/L)	Initial depressant mass (mg)	Sample mass (g)	Mineral surface area (m^2)	Absorbance				Actual Absorbance	Residual Concentration (mg/L)	Residual mass (mg)	Amount adsorbed (mg/m^2)
				1	2	Average	Std. deviation				
0	0	0	0	0	0	0.000	0.000	0.000	0.0	0.000	0.000
10	1.0	1.8811	2.0004	0.006	0.008	0.007	0.001	0.007	0.6	0.061	0.469
15	1.5	1.8812	2.0005	0.035	0.024	0.030	0.008	0.030	2.6	0.257	0.622
20	2.0	1.8811	2.0004	0.079	0.090	0.085	0.008	0.085	7.3	0.735	0.632
25	2.5	1.8811	2.0004	0.143	0.122	0.133	0.015	0.133	11.5	1.152	0.674
30	3.0	1.8810	2.0003	0.175	0.166	0.171	0.006	0.171	14.8	1.483	0.759
40	4.0	1.8809	2.0001	0.310	0.299	0.305	0.008	0.305	26.5	2.648	0.676
50	5.0	1.8811	2.0004	0.505	0.476	0.491	0.021	0.491	42.7	4.265	0.367
60	6.0	1.8812	2.0005	0.477	0.491	0.484	0.010	0.484	42.1	4.209	0.895
70	7.0	1.8811	2.0004	0.578	0.578	0.578	0.000	0.578	50.3	5.026	0.987
80	8.0	1.8808	2.0000	0.710	0.688	0.699	0.016	0.699	60.8	6.078	0.961
90	9.0	1.8811	2.0004	0.855	0.810	0.833	0.032	0.833	72.4	7.239	0.880
100	10.0	1.8811	2.0004	0.960	0.895	0.928	0.046	0.928	80.7	8.065	0.967

Initial depressant concentration (mg/L)	Initial depressant mass (mg)	Sample mass (g)	Mineral surface area (m^2)	Absorbance				Actual Absorbance	Residual Concentration (mg/L)	Residual mass (mg)	Amount adsorbed (mg/m^2)
				1	2	Average	Std. deviation				
0	0	0	0	0	0	0.000	0.000	0.000	0.0	0.000	0.000
10	1.0	1.8811	2.0004	0.014	0.004	0.009	0.007	0.009	0.8	0.078	0.461
15	1.5	1.8812	2.0005	0.066	0.020	0.043	0.033	0.043	3.7	0.374	0.563
20	2.0	1.8811	2.0004	0.059	0.064	0.062	0.004	0.062	5.3	0.535	0.732
25	2.5	1.8811	2.0004	0.128	0.125	0.127	0.002	0.127	11.0	1.100	0.700
30	3.0	1.8810	2.0003	0.175	0.170	0.173	0.004	0.173	15.0	1.500	0.750
40	4.0	1.8809	2.0001	0.291	0.300	0.296	0.006	0.296	25.7	2.570	0.715
60	6.0	1.8812	2.0005	0.487	0.511	0.499	0.017	0.499	43.4	4.339	0.830
70	7.0	1.8811	2.0004	0.643	0.582	0.613	0.043	0.613	53.3	5.326	0.837
80	8.0	1.8808	2.0000	0.676	0.663	0.670	0.009	0.670	58.2	5.822	1.089
90	9.0	1.8811	2.0004	0.776	0.781	0.779	0.004	0.779	67.7	6.770	1.115
100	10.0	1.8811	2.0004	0.891	0.895	0.893	0.003	0.893	77.7	7.765	1.117

Talc – CMC in 10^{-2} IS $Ca(NO_3)_2$, pH 9, T = 25°C

Initial depressant concentration (mg/L)	Initial depressant mass (mg)	Sample mass (g)	Mineral surface area (m^2)	Absorbance				Actual Absorbance	Residual Concentration (mg/L)	Residual mass (mg)	Amount adsorbed (mg/m^2)
				1	2	Average	Std. deviation				
0	0	0	0	0.214	0.209	0.212	0.004	0.000	0.0	0.000	0.000
10	1.00	0.1451	2.0005	0.251	0.241	0.246	0.007	0.035	6.5	0.651	0.174
15	1.50	0.1451	2.0005	0.271	0.271	0.271	0.000	0.060	11.2	1.123	0.189
20	2.00	0.1452	2.0019	0.315	0.321	0.318	0.004	0.107	20.1	2.009	-0.005
25	2.50	0.1449	1.9978	0.319	0.32	0.320	0.001	0.108	20.4	2.038	0.231
30	3.00	0.1452	2.0019	0.348	0.343	0.346	0.004	0.134	25.3	2.528	0.236
40	4.00	0.1451	2.0005	0.382	0.378	0.380	0.003	0.169	31.8	3.179	0.410
50	5.00	0.1452	2.0019	0.442	0.454	0.448	0.008	0.237	44.6	4.462	0.269
60	6.00	0.1452	2.0019	0.506	0.5	0.503	0.004	0.292	55.0	5.500	0.250
70	7.00	0.1452	2.0019	0.579	0.554	0.567	0.018	0.355	67.0	6.698	0.151
80	8.00	0.1453	2.0033	0.605	0.603	0.604	0.001	0.393	74.1	7.406	0.297
90	9.00	0.1451	2.0005	0.651	0.657	0.654	0.004	0.443	83.5	8.349	0.325
100	10.00	0.1449	1.9978	0.708	0.688	0.698	0.014	0.487	91.8	9.179	0.411

Initial depressant concentration (mg/L)	Initial depressant mass (mg)	Sample mass (g)	Mineral surface area (m^2)	Absorbance				Actual Absorbance	Residual Concentration (mg/L)	Residual mass (mg)	Amount adsorbed (mg/m^2)
				1	2	Average	Std. deviation				
0	0.00	0	0	0.214	0.209	0.212	0.004	0.000	0.0	0.000	0.000
10	0.98	0.1449	1.9978	0.237	0.264	0.301	0.019	0.090	16.9	1.689	-0.355
15	1.47	0.1450	1.9991	0.255	0.258	0.257	0.002	0.045	8.5	0.849	0.311
20	1.96	0.1449	1.9978	0.291	0.297	0.294	0.004	0.083	15.6	1.557	0.202
25	2.45	0.1451	2.0005	0.316	0.318	0.317	0.001	0.106	19.9	1.991	0.230
30	2.94	0.1451	2.0005	0.346	0.34	0.343	0.004	0.132	24.8	2.481	0.229
40	3.92	0.1452	2.0019	0.411	0.389	0.400	0.016	0.189	35.6	3.557	0.182
50	4.90	0.1449	1.9978	0.495	0.463	0.479	0.023	0.268	50.5	5.047	-0.074
60	5.88	0.1452	2.0019	0.487	0.474	0.481	0.009	0.269	50.8	5.075	0.402
70	6.86	0.1450	1.9991	0.551	0.541	0.546	0.007	0.335	63.1	6.311	0.274
80	7.84	0.1452	2.0019	0.599	0.592	0.596	0.005	0.384	72.5	7.245	0.297
90	8.82	0.1452	2.0019	0.673	0.661	0.667	0.008	0.456	85.9	8.594	0.113
100	9.80	0.1452	2.0019	0.715	0.711	0.713	0.003	0.502	94.6	9.462	0.169

Plagioclase – CMC in 10^{-2} IS $Ca(NO_3)_2$, pH 9, T = 25°C

Initial depressant concentration (mg/L)	Initial depressant mass (mg)	Sample mass (g)	Mineral surface area (m^2)	Absorbance				Actual Absorbance	Residual Concentration (mg/L)	Residual mass (mg)	Amount adsorbed (mg/m^2)
				1	2	Average	Std. deviation				
0	0	0	0	0.205	0.199	0.202	0.004	0.000	0.0	0.000	0.000
10	1.0	1.6271	2.0002		0.275	0.275		0.073	13.5	1.352	-0.176
15	1.5	1.6269	1.9999	0.286	0.272	0.279	0.010	0.077	14.3	1.426	0.037
20	2.0	1.6270	2.0001	0.303	0.291	0.297	0.008	0.095	17.6	1.759	0.120
25	2.5	1.6271	2.0002	0.332	0.299	0.316	0.023	0.114	21.0	2.102	0.199
30	3.0	1.6271	2.0002	0.361	0.35	0.356	0.008	0.154	28.4	2.843	0.079
40	4.0	1.6268	1.9998	0.393	0.392	0.393	0.001	0.191	35.3	3.528	0.236
50	5.0	1.6269	1.9999	0.446	0.461	0.454	0.011	0.252	46.6	4.657	0.171
60	6.0	1.6269	1.9999	0.522	0.516	0.519	0.004	0.317	58.7	5.870	0.065
70	7.0	1.6270	2.0001	0.559	0.586	0.573	0.019	0.371	68.6	6.861	0.069
80	8.0	1.6269	1.9999	0.637	0.625	0.631	0.008	0.429	79.4	7.944	0.028
90	9.0	1.6268	1.9998	0.663	0.674	0.669	0.008	0.467	86.4	8.639	0.181
100	10.0	1.6269	1.9999	0.718	0.708	0.713	0.007	0.511	94.6	9.463	0.269

Initial depressant concentration (mg/L)	Initial depressant mass (mg)	Sample mass (g)	Mineral surface area (m^2)	Absorbance				Actual Absorbance	Residual Concentration (mg/L)	Residual mass (mg)	Amount adsorbed (mg/m^2)
				1	2	Average	Std. deviation				
0	0	0	0	0.205	0.199	0.202	0.004	0.000	0.0	0.000	0.000
15	1.5	1.6268	1.9998	0.261	0.264	0.263	0.002	0.061	11.2	1.120	0.190
20	2.0	1.6269	1.9999	0.324	0.316	0.320	0.006	0.118	21.9	2.185	-0.093
25	2.5	1.6269	1.9999	0.324	0.315	0.320	0.006	0.118	21.8	2.176	0.162
30	3.0	1.6269	1.9999	0.346	0.346	0.346	0.000	0.144	26.7	2.667	0.167
40	4.0	1.6270	2.0001	0.391	0.388	0.390	0.002	0.188	34.7	3.472	0.264
50	5.0	1.6267	1.9997	0.459	0.459	0.459	0.000	0.257	47.6	4.759	0.120
60	6.0	1.6272	2.0003	0.498	0.519	0.509	0.015	0.307	56.8	5.676	0.162
70	7.0	1.6272	2.0003	0.564	0.567	0.566	0.002	0.364	67.3	6.731	0.134
90	9.0	1.6271	2.0002	0.723	0.731	0.727	0.006	0.525	97.2	9.722	-0.361
100	10.0	1.6268	1.9998	0.712	0.735	0.724	0.016	0.522	96.6	9.657	0.171

Pyroxene – CMC in 10^{-2} IS $Ca(NO_3)_2$, pH 9, T = 25°C

Initial depressant concentration (mg/L)	Initial depressant mass (mg)	Sample mass (g)	Mineral surface area (m^2)	Absorbance				Actual Absorbance	Residual Concentration (mg/L)	Residual mass (mg)	Amount adsorbed mg/m2
				1	2	Average	Std. deviation				
0	0	0	0	0.205	0.199	0.202	0.004	0.000	0.0	0.000	0.000
10	1.0	1.5581	2.0000	0.232	0.231	0.232	0.001	0.030	5.6	0.557	0.222
15	1.5	1.5580	1.9998	0.236	0.246	0.241	0.007	0.039	7.4	0.736	0.382
20	2.0	1.5581	2.0000	0.266	0.254	0.260	0.008	0.058	10.9	1.094	0.453
25	2.5	1.5580	1.9998	0.297	0.292	0.295	0.004	0.093	17.5	1.745	0.377
30	3.0	1.5582	2.0001	0.316	0.321	0.319	0.004	0.117	22.0	2.198	0.401
40	4.0	1.5579	1.9997	0.359	0.372	0.366	0.009	0.164	30.8	3.085	0.458
50	5.0	1.5581	2.0000	0.426	0.433	0.430	0.005	0.228	42.9	4.292	0.354
60	6.0	1.5581	2.0000	0.49	0.501	0.496	0.008	0.294	55.4	5.538	0.231
70	7.0	1.5583	2.0002	0.537	0.536	0.537	0.001	0.335	63.1	6.311	0.344
80	8.0	1.5583	2.0002	0.576	0.642	0.609	0.047	0.407	76.8	7.679	0.160
90	9.0	1.5580	1.9998	0.72	0.659	0.690	0.043	0.488	92.0	9.198	-0.099
100	10.0	1.5583	2.0002	0.671	0.683	0.677	0.008	0.475	89.6	8.962	0.519

Initial depressant concentration (mg/L)	Initial depressant mass (mg)	Sample mass (g)	Mineral surface area (m^2)	Absorbance				Actual Absorbance	Residual Concentration (mg/L)	Residual mass (mg)	Amount adsorbed (mg/m^2)
				1	2	Average	Std. deviation				
0	0	0	0	0.205	0.199	0.202	0.004	0.000	0.0	0.000	0.000
10	1.0	1.5579	1.9997	0.204	0.206	0.205	0.001	0.003	0.6	0.057	0.472
15	1.5	1.5581	2.0000	0.229	0.231	0.230	0.001	0.028	5.3	0.528	0.486
20	2.0	1.5581	2.0000	0.252	0.259	0.256	0.005	0.054	10.1	1.009	0.495
25	2.5	1.5582	2.0001	0.306	0.292	0.299	0.010	0.097	18.3	1.830	0.335
30	3.0	1.5579	1.9997	0.325	0.309	0.317	0.011	0.115	21.7	2.170	0.415
40	4.0	1.5583	2.0002	0.379	0.383	0.381	0.003	0.179	33.8	3.377	0.311
50	5.0	1.5583	2.0002	0.429	0.437	0.433	0.006	0.231	43.6	4.358	0.321
60	6.0	1.5580	1.9998	0.486	0.506	0.496	0.014	0.294	55.5	5.547	0.226
70	7.0	1.5579	1.9997	0.559	0.592	0.576	0.023	0.374	70.5	7.047	-0.024
100	10.0	1.5583	2.0002	0.71	0.693	0.702	0.012	0.500	94.2	9.425	0.288

Chromite – CMC in 10^{-2} IS $Ca(NO_3)_2$, pH 9, T = 25°C

Initial depressant concentration (mg/L)	Initial depressant mass (mg)	Sample mass (g)	Mineral surface area (m^2)	Absorbance				Actual Absorbance	Residual Concentration (mg/L)	Residual mass (mg)	Amount adsorbed (mg/m^2)
				1	2	Average	Std. deviation				
0	0	0	0	0.214	0.209	0.212	0.004	0.000	0.0	0.000	0.000
10	1.0	2.3209	1.9999	0.233	0.246	0.240	0.009	0.028	5.3	0.528	0.236
15	1.5	2.3212	2.0002	0.249	0.236	0.243	0.009	0.031	5.8	0.585	0.458
20	2.0	2.3210	2.0000	0.31	0.293	0.302	0.012	0.090	17.0	1.698	0.151
25	2.5	2.3208	1.9998	0.259	0.268	0.264	0.006	0.052	9.8	0.981	0.759
30	3.0	2.3212	2.0002	0.321	0.325	0.323	0.003	0.112	21.0	2.104	0.448
40	4.0	2.3211	2.0001	0.371	0.375	0.373	0.003	0.162	30.5	3.047	0.476
50	5.0	2.3211	2.0001	0.421	0.429	0.425	0.006	0.214	40.3	4.028	0.486
60	6.0	2.3211	2.0001	0.49	0.471	0.481	0.013	0.269	50.8	5.075	0.462
70	7.0	2.3210	2.0000	0.538	0.568	0.553	0.021	0.342	64.4	6.443	0.278
80	8.0	2.3211	2.0001	0.658	0.615	0.637	0.030	0.425	80.2	8.019	-0.009
90	9.0	2.3211	2.0001	0.621	0.635	0.628	0.010	0.417	78.6	7.858	0.571
100	10.0	2.3210	2.0000	0.71	0.716	0.713	0.004	0.502	94.6	9.462	0.269

Initial depressant concentration (mg/L)	Initial depressant mass (mg)	Sample mass (g)	Mineral surface area (m^2)	Absorbance				Actual Absorbance	Residual Concentration (mg/L)	Residual mass (mg)	Amount adsorbed (mg/m^2)
				1	2	Average	Std. deviation				
0	0	0	0	0.214	0.209	0.212	0.004	0.000	0.0	0.000	0.000
10	1.0	2.3212	2.0002			#DIV/0!	#DIV/0!	#DIV/0!	#DIV/0!	#DIV/0!	#DIV/0!
15	1.5	2.3212	2.0002	0.273	0.24	0.257	0.023	0.045	8.5	0.849	0.325
20	2.0	2.3213	2.0003	0.268	0.273	0.271	0.004	0.059	11.1	1.113	0.443
25	2.5	2.3212	2.0002	0.286	0.373	0.330	0.062	0.118	22.3	2.226	0.137
30	3.0	2.3209	1.9999	0.322	0.328	0.325	0.004	0.114	21.4	2.142	0.429
40	4.0	2.3213	2.0003	0.378	0.367	0.373	0.008	0.161	30.4	3.038	0.481
50	5.0	2.3210	2.0000	0.434	0.431	0.433	0.002	0.221	41.7	4.170	0.415
60	6.0	2.3209	1.9999	0.494	0.492	0.493	0.001	0.282	53.1	5.311	0.344
70	7.0	2.3213	2.0003	0.532	0.541	0.537	0.006	0.325	61.3	6.132	0.434
80	8.0	2.3208	1.9998	0.583	0.583	0.583	0.000	0.372	70.1	7.009	0.495
90	9.0	2.3213	2.0003	0.64	0.658	0.649	0.013	0.438	82.5	8.255	0.373
100	10.0	2.3209	1.9999	0.658	0.686	0.672	0.020	0.461	86.9	8.689	0.656

Chalcopyrite – CMC in 10^{-2} IS $Ca(NO_3)_2$, pH 9, T = 25°C

Initial depressant concentration (mg/L)	Initial depressant mass (mg)	Sample mass (g)	Mineral surface area (m^2)	Absorbance				Actual Absorbance	Residual Concentration (mg/L)	Residual mass (mg)	Amount adsorbed (mg/m^2)
				1	2	Average	Std. deviation				
0	0	0	0	0.205	0.199	0.202	0.004	0.000	0.0	0.000	0.000
10	1.0	1.8806	1.9998	0.208	0.206	0.207	0.001	0.005	0.9	0.093	0.454
15	1.5	1.8807	1.9999	0.217	0.22	0.219	0.002	0.017	3.1	0.306	0.597
20	2.0	1.8808	2.0000	0.234	0.234	0.234	0.000	0.032	5.9	0.593	0.704
25	2.5	1.8805	1.9997	0.283	0.273	0.278	0.007	0.076	14.1	1.407	0.546
30	3.0	1.8806	1.9998	0.29	0.292	0.291	0.001	0.089	16.5	1.648	0.676
40	4.0	1.8808	2.0000	0.326	0.328	0.327	0.001	0.125	23.1	2.315	0.843
50	5.0	1.8808	2.0000	0.406	0.386	0.396	0.014	0.194	35.9	3.593	0.704
60	6.0	1.8810	2.0003	0.442	0.465	0.454	0.016	0.252	46.6	4.657	0.671
70	7.0	1.8806	1.9998	0.529	0.487	0.508	0.030	0.306	56.7	5.667	0.667
80	8.0	1.8805	1.9997	0.545	0.562	0.554	0.012	0.352	65.1	6.509	0.745
90	9.0	1.8809	2.0001	0.605	0.636	0.621	0.022	0.419	77.5	7.750	0.625
100	10.0	2.8806	3.0632	0.639	0.656	0.648	0.012	0.446	82.5	8.250	0.571

Initial depressant concentration (mg/L)	Initial depressant mass (mg)	Sample mass (g)	Mineral surface area (m^2)	Absorbance				Actual Absorbance	Residual Concentration (mg/L)	Residual mass (mg)	Amount adsorbed (mg/m^2)
				1	2	Average	Std. deviation				
0	0	0	0	0.205	0.199	0.202	0.004	0.000	0.0	0.000	0.000
10	1.0	1.8807	1.9999	0.266	0.202	0.234	0.045	0.032	5.9	0.593	0.204
15	1.5	1.8807	1.9999	0.228	0.232	0.230	0.003	0.028	5.2	0.519	0.491
20	2.0	1.8811	2.0004	0.218	0.216	0.217	0.001	0.015	2.8	0.278	0.861
25	2.5	1.8810	2.0003	0.252	0.238	0.245	0.010	0.043	8.0	0.796	0.852
30	3.0	1.8806	1.9998		0.244	0.244		0.042	7.8	0.778	1.111
50	5.0	1.8810	2.0003	0.399		0.399		0.197	36.5	3.648	0.676
60	6.0	1.8811	2.0004	0.465	0.495	0.480	0.021	0.278	51.5	5.148	0.426
70	7.0	1.8808	2.0000	0.478	0.472	0.475	0.004	0.273	50.6	5.056	0.972
80	8.0	1.8808	2.0000	0.58	0.605	0.593	0.018	0.391	72.3	7.231	0.384
90	9.0	1.8808	2.0000	0.625	0.618	0.622	0.005	0.420	77.7	7.769	0.616
100	10.0	1.8808	2.0000	0.663	0.662	0.663	0.001	0.461	85.3	8.528	0.736

Talc - CMC in buffer, pH 9, T = 25°C

Initial depressant concentration (mg/L)	Initial depressant mass (mg)	Sample mass (g)	Mineral surface area (m^2)	Absorbance				Actual Absorbance	Residual Concentration (mg/L)	Residual mass (mg)	Amount adsorbed mg/m2
				1	2	Average	Std. deviation				
0	0	0	0	0.365	0.375	0.370	0.007	0.000	0.0	0.000	0.000
10	1.00	0.1450	1.9991	0.393	0.395	0.394	0.001	0.024	4.5	0.453	0.274
15	1.50	0.1451	2.0005	0.456	0.47	0.463	0.010	0.093	17.5	1.755	-0.127
20	2.00	0.1452	2.0019	0.493	0.482	0.488	0.008	0.118	22.2	2.217	-0.108
25	2.50	0.1451	2.0005	0.536	0.518	0.527	0.013	0.157	29.6	2.962	-0.231
30	3.00	0.1450	1.9991	0.546	0.544	0.545	0.001	0.175	33.0	3.302	-0.151
40	4.00	0.1452	2.0019	0.607	0.608	0.608	0.001	0.238	44.8	4.481	-0.240
50	5.00	0.1449	1.9978	0.657	0.677	0.667	0.014	0.297	56.0	5.604	-0.302
60	6.00	0.1452	2.0019	0.745	0.754	0.750	0.006	0.380	71.6	7.160	-0.580
70	7.00	0.1450	1.9991	0.793	0.787	0.790	0.004	0.420	79.2	7.925	-0.462
80	8.00	0.1451	2.0005	0.828	0.831	0.830	0.002	0.460	86.7	8.670	-0.335
90	9.00	0.1452	2.0019	0.877	0.848	0.863	0.021	0.493	92.9	9.292	-0.146
100	10.00	0.1452	2.0019	0.933		0.933		0.563	106.2	10.623	-0.311

Initial depressant concentration (mg/L)	Initial depressant mass (mg)	Sample mass (g)	Mineral surface area (m^2)	Absorbance				Actual Absorbance	Residual Concentration (mg/L)	Residual mass (mg)	Amount adsorbed ($mg/m2^{)}$
				1	2	Average	Std. deviation				
0	0.00	0	0	0.1	0.103	0.102	0.002	0.000	0.0	0.000	0.000
10	0.98	0.1449	1.9978	0.183	0.165	0.301	0.013	0.200	37.6	3.764	-1.394
15	1.47	0.1452	2.0019	0.196	0.19	0.193	0.004	0.092	17.3	1.726	-0.128
20	1.96	0.1451	2.0005	0.216	0.218	0.217	0.001	0.116	21.8	2.179	-0.110
25	2.45	0.1451	2.0005	0.237	0.242	0.240	0.004	0.138	26.0	2.604	-0.077
30	2.94	0.1452	2.0019	0.273	0.286	0.280	0.009	0.178	33.6	3.358	-0.209
40	3.92	0.1451	2.0005	0.34	0.34	0.340	0.000	0.239	45.0	4.500	-0.290
50	4.90	0.1450	1.9991	0.416	0.403	0.410	0.009	0.308	58.1	5.811	-0.456
60	5.88	0.1452	2.0019	0.443	0.444	0.444	0.001	0.342	64.5	6.453	-0.286
70	6.86	0.1449	1.9978	0.509	0.499	0.504	0.007	0.403	75.9	7.594	-0.368
80	7.84	0.1451	2.0005	0.549	0.563	0.556	0.010	0.455	85.8	8.575	-0.368
90	8.82	0.1449	1.9978	0.609	0.623	0.616	0.010	0.515	97.1	9.708	-0.444
100	9.80	0.1451	2.0005	0.68	0.629	0.655	0.036	0.553	104.3	10.434	-0.317

Plagioclase - CMC in buffer, pH 9, T = 25°C

Initial depressant concentration (mg/L)	Initial depressant mass (mg)	Sample mass (g)	Mineral surface area (m^2)	Absorbance				Actual Absorbance	Residual Concentration (mg/L)	Residual mass (mg)	Amount adsorbed (mg/m^2)
				1	2	Average	Std. deviation				
0	0	0	0	0.312	0.312	0.312	0.000	0.000	0.0	0.000	0.000
10	1.0	1.6271	2.0002	0.362	0.377	0.370	0.011	0.058	10.8	1.085	-0.042
15	1.5	1.6268	1.9998	0.431	0.403	0.417	0.020	0.105	19.8	1.981	-0.241
20	2.0	1.6269	1.9999	0.453	0.45	0.452	0.002	0.140	26.3	2.632	-0.316
25	2.5	1.6270	2.0001	0.478	0.478	0.478	0.000	0.166	31.3	3.132	-0.316
30	3.0	1.6267	1.9997	0.504	0.517	0.511	0.009	0.199	37.5	3.745	-0.373
40	4.0	1.6267	1.9997	0.565	0.556	0.561	0.006	0.249	46.9	4.689	-0.344
50	5.0	1.6269	1.9999	0.628	0.63	0.629	0.001	0.317	59.8	5.981	-0.491
60	6.0	1.6268	1.9998	0.695	0.674	0.685	0.015	0.373	70.3	7.028	-0.514
70	7.0	1.6271	2.0002	0.724	0.711	0.718	0.009	0.406	76.5	7.651	-0.325
80	8.0	1.6269	1.9999	0.79	0.792	0.791	0.001	0.479	90.4	9.038	-0.519
90	9.0	1.6272	2.0003	0.837	0.842	0.840	0.004	0.528	99.5	9.953	-0.476
100	10.0	1.6267	1.9997	0.891	0.88	0.886	0.008	0.574	108.2	10.821	-0.410

Initial depressant concentration (mg/L)	Initial depressant mass (mg)	Sample mass (g)	Mineral surface area (m^2)	Absorbance				Actual Absorbance	Residual Concentration (mg/L)	Residual mass (mg)	Amount adsorbed mg/m2
				1	2	Average	Std. deviation				
0	0	0	0	0.208	0.209	0.209	0.001	0.000	0.0	0.000	0.000
10	1.0	1.6268	1.9998	0.246	0.246	0.246	0.000	0.038	7.1	0.708	0.146
15	1.5	1.6269	1.9999	0.295	0.296	0.296	0.001	0.087	16.4	1.642	-0.071
20	2.0	1.6270	2.0001	0.319	0.314	0.317	0.004	0.108	20.4	2.038	-0.019
25	2.5	1.6269	1.9999	0.369	0.322	0.346	0.033	0.137	25.8	2.585	-0.042
30	3.0	1.6268	1.9998	0.355	0.367	0.361	0.008	0.153	28.8	2.877	0.061
40	4.0	1.6270	2.0001	0.423	0.426	0.425	0.002	0.216	40.8	4.075	-0.038
50	5.0	1.6268	1.9998	0.486	0.467	0.477	0.013	0.268	50.6	5.057	-0.028
60	6.0	1.6270	2.0001	0.52	0.524	0.522	0.003	0.314	59.2	5.915	0.042
70	7.0	1.6271	2.0002	0.581	0.598	0.590	0.012	0.381	71.9	7.189	-0.094
80	8.0	1.6268	1.9998	0.67	0.75	0.710	0.057	0.502	94.6	9.462	-0.731
90	9.0	1.6269	1.9999	0.694	0.689	0.692	0.004	0.483	91.1	9.113	-0.057
100	10.0	1.6268	1.9998	0.74	0.736	0.738	0.003	0.530	99.9	9.991	0.005

Pyroxene - CMC in buffer, pH 9, T = 25°C

Initial depressant concentration (mg/L)	Initial depressant mass (mg)	Sample mass (g)	Mineral surface area (m^2)	Absorbance				Actual Absorbance	Residual Concentration (mg/L)	Residual mass (mg)	Amount adsorbed (mg/m^2)
				1	2	Average	Std. deviation				
0	0	0	0	0.157	0.132	0.145	0.018	0.000	0.0	0.000	0.000
10	1.0	1.5582	2.0001	0.187	0.176	0.182	0.008	0.037	7.0	0.698	0.151
15	1.5	1.5579	1.9997	0.217	0.22	0.219	0.002	0.074	14.0	1.396	0.052
20	2.0	1.5578	1.9996	0.248	0.251	0.250	0.002	0.105	19.8	1.981	0.009
25	2.5	1.5580	1.9998	0.267	0.277	0.272	0.007	0.128	24.1	2.406	0.047
30	3.0	1.5580	1.9998	0.304	0.298	0.301	0.004	0.157	29.5	2.953	0.024
40	4.0	1.5578	1.9996	0.346	0.349	0.348	0.002	0.203	38.3	3.830	0.085
50	5.0	1.5579	1.9997	0.415	0.409	0.412	0.004	0.268	50.5	5.047	-0.024
60	6.0	1.5580	1.9998	0.461	0.46	0.461	0.001	0.316	59.6	5.962	0.019
70	7.0	1.5579	1.9997	0.518	0.518	0.518	0.000	0.374	70.5	7.047	-0.024
80	8.0	1.5580	1.9998	0.566	0.567	0.567	0.001	0.422	79.6	7.962	0.019
90	9.0	1.5582	2.0001	0.629	0.642	0.636	0.009	0.491	92.6	9.264	-0.132
100	10.0	1.5580	1.9998	0.697	0.702	0.700	0.004	0.555	104.7	10.472	-0.236

Initial depressant concentration (mg/L)	Initial depressant mass (mg)	Sample mass (g)	Mineral surface area (m^2)	Absorbance				Actual Absorbance	Residual Concentration (mg/L)	Residual mass (mg)	Amount adsorbed mg/m2
				1	2	Average	Std. deviation				
0	0	0	0	0.263	0.255	0.259	0.006	0.000	0.0	0.000	0.000
10	1.0	1.5583	2.0002	0.208	0.219	0.214	0.008	-0.046	-8.6	-0.858	0.929
15	1.5	1.5579	1.9997	0.263	0.255	0.259	0.006	0.000	0.0	0.000	0.750
20	2.0	1.5581	2.0000	0.331	0.303	0.317	0.020	0.058	10.9	1.094	0.453
25	2.5	1.5580	1.9998	0.498	0.352	0.425	0.103	0.166	31.3	3.132	-0.316
30	3.0	1.5579	1.9997	0.368	0.392	0.380	0.017	0.121	22.8	2.283	0.359
40	4.0	1.5580	1.9998	0.576	0.453	0.515	0.087	0.256	48.2	4.821	-0.410
50	5.0	1.5581	2.0000	0.46	0.497	0.479	0.026	0.220	41.4	4.142	0.429
60	6.0	1.5581	2.0000	0.571	0.531	0.551	0.028	0.292	55.1	5.509	0.245
70	7.0	1.5578	1.9996	0.528	0.626	0.577	0.069	0.318	60.0	6.000	0.500
80	8.0	1.5581	2.0000	0.857	0.818	0.838	0.028	0.579	109.2	10.915	-1.458
90	9.0	1.5582	2.0001	0.875	0.923	0.899	0.034	0.640	120.8	12.075	-1.538
100	10.0	1.5581	2.0000	0.984	0.973	0.979	0.008	0.720	135.8	13.575	-1.788

Chromite - CMC in buffer, pH 9, T = 25°C

Initial depressant concentration (mg/L)	Initial depressant mass (mg)	Sample mass (g)	Mineral surface area (m^2)	Absorbance				Actual Absorbance	Residual Concentration (mg/L)	Residual mass (mg)	Amount adsorbed (mg/m^2)
				1	2	Average	Std. deviation				
0	0	0	0	0.1	0.098	0.099	0.001	0.000	0.0	0.000	0.000
10	1.0	2.3211	2.0001	0.155	0.151	0.153	0.003	0.054	10.2	1.019	-0.009
15	1.5	2.3208	1.9998	0.188	0.188	0.188	0.000	0.089	16.8	1.679	-0.090
20	2.0	2.3212	2.0002	0.214	0.211	0.213	0.002	0.114	21.4	2.142	-0.071
25	2.5	2.3209	1.9999	0.243	0.233	0.238	0.007	0.139	26.2	2.623	-0.061
30	3.0	2.3209	1.9999	0.262	0.272	0.267	0.007	0.168	31.7	3.170	-0.085
40	4.0	2.3211	2.0001	0.322	0.332	0.327	0.007	0.228	43.0	4.302	-0.151
50	5.0	2.3210	2.0000	0.374	0.39	0.382	0.011	0.283	53.4	5.340	-0.170
60	6.0	2.3208	1.9998	0.447	0.448	0.448	0.001	0.349	65.8	6.575	-0.288
70	7.0	2.3212	2.0002	0.523	0.525	0.524	0.001	0.425	80.2	8.019	-0.509
80	8.0	2.3209	1.9999	0.573	0.582	0.578	0.006	0.479	90.3	9.028	-0.514
90	9.0	2.3210	2.0000	0.6	0.612	0.606	0.008	0.507	95.7	9.566	-0.283
100	10.0	2.3210	2.0000	0.628	0.667	0.648	0.028	0.549	103.5	10.349	-0.175

Initial depressant concentration (mg/L)	Initial depressant mass (mg)	Sample mass (g)	Mineral surface area (m^2)	Absorbance				Actual Absorbance	Residual Concentration (mg/L)	Residual mass (mg)	Amount adsorbed (mg/m^2)
				1	2	Average	Std. deviation				
0	0	0	0	0.1	0.095	0.098	0.004	0.000	0.0	0.000	0.000
10	1.0	2.3212	2.0002	0.141	0.138	0.140	0.002	0.042	7.9	0.792	0.104
15	1.5	2.3211	2.0001	0.168	0.175	0.172	0.005	0.074	14.0	1.396	0.052
20	2.0	2.3211	2.0001	0.185	0.185	0.185	0.000	0.088	16.5	1.651	0.175
25	2.5	2.3210	2.0000	0.23	0.221	0.226	0.006	0.128	24.2	2.415	0.042
30	3.0	2.3209	1.9999	0.246	0.248	0.247	0.001	0.150	28.2	2.821	0.090
40	4.0	2.3209	1.9999	0.319	0.313	0.316	0.004	0.219	41.2	4.123	-0.061
50	5.0	2.3210	2.0000	0.368	0.37	0.369	0.001	0.272	51.2	5.123	-0.061
60	6.0	2.3209	1.9999	0.416	0.42	0.418	0.003	0.321	60.5	6.047	-0.024
70	7.0	2.3209	1.9999	0.473	0.476	0.475	0.002	0.377	71.1	7.113	-0.057
80	8.0	2.3209	1.9999	0.531	0.518	0.525	0.009	0.427	80.6	8.057	-0.028
90	9.0	2.3210	2.0000	0.6	0.613	0.607	0.009	0.509	96.0	9.604	-0.302
100	10.0	2.3212	2.0002	0.644	0.648	0.646	0.003	0.549	103.5	10.349	-0.175

Chalcopyrite - CMC in buffer, pH 9, T = 25°C

Initial depressant concentration (mg/L)	Initial depressant mass (mg)	Sample mass (g)	Mineral surface area (m^2)	Absorbance				Actual Absorbance	Residual Concentration (mg/L)	Residual mass (mg)	Amount adsorbed (mg/m^2)
				1	2	Average	Std. deviation				
0	0	0	0	0.399	0.372	0.386	0.019	0.000	0.0	0.000	0.000
10	1.0	1.8808	2.0000	0.505	0.5	0.503	0.004	0.117	22.1	2.208	-0.604
15	1.5	1.8809	2.0001	0.525	0.519	0.522	0.004	0.137	25.8	2.575	-0.538
20	2.0	1.8808	2.0000	0.545	0.56	0.553	0.011	0.167	31.5	3.151	-0.575
25	2.5	1.8810	2.0003	0.592	0.576	0.584	0.011	0.199	37.5	3.745	-0.623
30	3.0	1.8810	2.0003	0.595	0.609	0.602	0.010	0.217	40.8	4.085	-0.542
40	4.0	1.8810	2.0003	0.635	0.649	0.642	0.010	0.257	48.4	4.840	-0.420
50	5.0	1.8810	2.0003	0.716	0.746	0.731	0.021	0.346	65.2	6.519	-0.759
60	6.0	1.8809	2.0001	0.759	0.796	0.778	0.026	0.392	74.0	7.396	-0.698
70	7.0	1.8809	2.0001	0.832	0.832	0.832	0.000	0.447	84.2	8.425	-0.712
80	8.0	1.8808	2.0000	0.945	0.913	0.929	0.023	0.544	102.5	10.255	-1.127
90	9.0	1.8808	2.0000	0.987	0.948	0.968	0.028	0.582	109.8	10.981	-0.991
100	10.0	1.8807	1.9999	0.991	1.025	1.008	0.024	0.623	117.5	11.745	-0.873

Initial depressant concentration (mg/L)	Initial depressant mass (mg)	Sample mass (g)	Mineral surface area (m^2)	Absorbance				Actual Absorbance	Residual Concentration (mg/L)	Residual mass (mg)	Amount adsorbed (mg/m^2)
				1	2	Average	Std. deviation				
0	0	0	0	0.382	0.375	0.379	0.005	0.000	0.0	0.000	0.000
10	1.0	1.8808	2.0000	0.469	0.472	0.471	0.002	0.092	17.4	1.736	-0.368
15	1.5	1.8810	2.0003	0.505	0.505	0.505	0.000	0.127	23.9	2.387	-0.443
20	2.0	1.8809	2.0001	0.549	0.542	0.546	0.005	0.167	31.5	3.151	-0.575
25	2.5	1.8808	2.0000	0.566	0.577	0.572	0.008	0.193	36.4	3.642	-0.571
30	3.0	1.8810	2.0003	0.581	0.594	0.588	0.009	0.209	39.4	3.943	-0.472
40	4.0	1.8809	2.0001	0.641	0.664	0.653	0.016	0.274	51.7	5.170	-0.585
50	5.0	1.8809	2.0001	0.692	0.689	0.691	0.002	0.312	58.9	5.887	-0.443
60	6.0	1.8809	2.0001	0.756	0.769	0.763	0.009	0.384	72.5	7.245	-0.623
70	7.0	1.8807	1.9999	0.824	0.816	0.820	0.006	0.442	83.3	8.330	-0.665
80	8.0	1.8808	2.0000	0.873	0.851	0.862	0.016	0.484	91.2	9.123	-0.561
90	9.0	1.8810	2.0003	0.944	0.918	0.931	0.018	0.553	104.2	10.425	-0.712
100	10.0	1.8810	2.0003	0.964	0.956	0.960	0.006	0.582	109.7	10.972	-0.486

Surface coverage – guar in buffer

Initial depressant concentration (mg/L)	Surface coverage - θ				
	talc	plagioclase	pyroxene	chromite	chalcopyrite
0	0	0	0	0	0
10	0.27	0.01	0.34	0.45	0.37
15	0.36	0.03	0.37	0.31	0.57
20	0.43	0.07	0.41	0.53	0.51
25	0.38	0.10	0.37	0.48	0.56
30	0.43	0.13	0.35	0.46	0.60
40	0.58	0.23	0.54	0.53	0.62
50	0.59	0.27	0.51	0.63	0.75
60	0.64	0.26	0.46	0.59	0.71
70	0.63	0.03	0.53	0.63	0.70
80	0.55	0.46	0.43	0.56	0.73
90	0.72	0.69	0.51	0.72	0.91
100	0.79		0.56	0.75	0.94

Surface coverage - guar in SPW

Initial depressant concentration (mg/L)	Surface coverage - θ				
	talc	plagioclase	pyroxene	chromite	chalcopyrite
0	0	0	0	0	0
10	0.35	0.08	0.29	0.32	0.60
15	0.47	0.12	0.28	0.13	0.76
20	0.63	0.10	0.16	0.38	0.88
25	0.43	0.18	0.13	0.32	0.88
30	0.51	0.20	0.14	0.39	0.97
40	0.63	0.20	0.24	0.36	0.89
50	0.66	0.30	0.30	0.45	0.76
60	0.67	0.27	0.37	0.55	1.11
70	0.68	0.27	0.36	0.57	1.17
80	0.97	0.22	0.44	0.54	1.32
90	0.78	0.25	0.42	0.65	1.28
100	0.79	0.34	0.55	0.62	1.34

Surface coverage – CMC in 10^{-2} IS $Ca(NO_3)_2$

Initial depressant concentration (mg/L)	Surface coverage - θ				
	talc	plagioclase	pyroxene	chromite	chalcopyrite
0	0	0	0	0	0
10	0.22		0.45	0.30	0.42
15	0.32	0.15	0.56	0.50	0.70
20	0.26	0.15	0.61	0.38	1.01
25	0.30	0.23	0.46	0.58	0.90
30	0.30	0.16	0.52	0.56	1.15
40	0.38	0.32	0.49	0.62	1.08
50	0.35	0.19	0.43	0.58	0.89
60	0.42	0.15	0.29	0.52	0.71
70	0.27	0.13	0.44	0.46	1.05
80	0.38	0.04	0.15	0.64	0.73
90	0.28	0.23	0.04	0.61	0.80
100	0.37	0.28	0.52	0.59	0.84

APPENDIX 8: MICROFLOTATION RAW DATA

Talc with no added mineral: 0.25 mg/L guar, pH 9

Run 1a

Minerals	Mass (g)	Time (mins)		Fp (g)	Fp+talc (g)	Talc (g)	% Recovery	% Cum. Recovery
talc	2.0001	0					0	0
		2	C1	0.3390	0.3735	0.0345	1.83	1.83
		6	C2	0.3327	0.3467	0.014	0.74	2.58
		12	C3	0.3333	0.351	0.0177	0.94	3.52
		20	C4	0.3354	0.3636	0.0282	1.50	5.02
			Tails	0.3311	2.1174	1.7863		
			Total			**1.8807**		

Run 1b

Minerals	Mass (g)	Time (mins)		Fp (g)	Fp+talc (g)	Talc (g)	% Recovery	% Cum. Recovery
talc	2.0000	0					0	0
		2	C1	0.3238	0.3864	0.0626	3.21	3.21
		6	C2	0.3244	0.3497	0.0253	1.30	4.50
		12	C3	0.3337	0.3533	0.0196	1.00	5.51
		20	C4	0.3348	0.3631	0.0283	1.45	6.95
			Tails	0.3313	2.1482	1.8169		
			Total			**1.9527**		

Talc with added chromite – 0.25 mg/L guar, pH 9

Run 1a

Minerals	Mass (g)	Time (mins)		Fp (g)	Fp+talc (g)	Talc (g)	% Recovery	% Cum. Recovery
talc	2.0001	0					0.00	0.00
chromite	2.3210	2	C1	0.3332	0.3881	0.0549	3.00	3.00
		6	C2	0.3293	0.383	0.0537	2.94	5.94
		12	C3	0.3254	0.3779	0.0525	2.87	8.82
		20	C4	0.3259	0.4096	0.0837	4.58	13.40
			Tails	0.3336	1.9159	1.5823		
			Total			1.8271		

Run 1b

Minerals	Mass (g)	Time (mins)		Fp (g)	Fp+talc (g)	Talc (g)	% Recovery	% Cum. Recovery
talc	2.0002	0					0.00	0.00
chromite	2.3206	2	C1	0.3358	0.4357	0.0999	5.42	5.42
		6	C2	0.3262	0.4786	0.1524	8.27	13.69
		12	C3	0.3321	0.4484	0.1163	6.31	19.99
		20	C4	0.3246	0.4484	0.1238	6.72	26.71
			Tails	0.3275	1.6786	1.3511		
			Total			1.8435		

Run 2a

Minerals	Mass (g)	Time (mins)		Fp (g)	Fp+talc (g)	Talc (g)	% Recovery	% Cum. Recovery
talc	2.0001	0					0.00	0.00
chromite	5.3675	2	C1	0.3235	0.4355	0.112	6.36	6.36
		6	C2	0.3181	0.4361	0.118	6.70	13.07
		12	C3	0.3257	0.4406	0.1149	6.53	19.60
		20	C4	0.3286	0.4274	0.0988	5.61	25.21
			Tails	0.3276	1.644	1.3164		
			Total			**1.7601**		

Run 2b

Minerals	Mass (g)	Time (mins)		Fp (g)	Fp+talc (g)	Talc (g)	% Recovery	% Cum. Recovery
talc	2.0002	0					0.00	0.00
chromite	5.3677	2	C1	0.3324	0.4336	0.1012	5.28	5.28
		6	C2	0.3242	0.4506	0.1264	6.60	11.88
		12	C3	0.3267	0.4545	0.1278	6.67	18.56
		20	C4	0.3261	0.4431	0.1170	6.11	24.67
			Tails	0.3246	1.7673	1.4427		
			Total			1.9151		

Run 3a

Minerals	Mass (g)	Time (mins)		Fp (g)	Fp+talc (g)	Talc (g)	% Recovery	% Cum. Recovery
talc	2.0001	0					0.00	0.00
chromite	6.9681	2	C1	0.3241	0.4529	0.1288	6.91	6.91
		6	C2	0.3221	0.4596	0.1375	7.38	14.28
		12	C3	0.3311	0.4545	0.1234	6.62	20.90
		20	C4	0.3274	0.4521	0.1247	6.69	27.59
			Tails	0.3321	1.6821	1.35		
			Total			**1.8644**		

Run 3b

Minerals	Mass (g)	Time (mins)		Fp (g)	Fp+talc (g)	Talc (g)	% Recovery	% Cum. Recovery
talc	2.0002						0.00	0.00
chromite	6.9683	0	C1	0.3305	0.4433	0.1128	6.04	6.04
		2	C2	0.329	0.4770	0.1480	7.92	13.95
		6	C3	0.3302	0.5150	0.1848	9.89	23.84
		12	C4	0.3227	0.4888	0.1661	8.89	32.73
		20	Tails	0.3253	1.5825	1.2572		
			Total			**1.8689**		

Talc with added plagioclase – 0.25 mg/L guar, pH 9

Run 1a

Minerals	Mass (g)	Time (mins)		Fp (g)	Fp+talc (g)	Talc (g)	% Recovery	% Cum. Recovery
talc	1.9999	0					0.00	0.00
plagioclaswe	1.6266	2	C1	0.3337	0.3554	0.0217	1.11	1.11
		6	C2	0.3310	0.3485	0.0175	0.90	2.01
		12	C3	0.3230	0.3477	0.0247	1.27	3.28
		20	C4	0.3275	0.3609	0.0334	1.71	4.99
			Tails	0.3383	2.1903	1.8520		
			Total			**1.9493**		

Run 1b

Minerals	Mass (g)	Time (mins)		Fp (g)	Fp+talc (g)	Talc (g)	% Recovery	% Cum. Recovery
talc	2.0001	0					0.00	0.00
plagioclase	1.6267	2	C1	0.3304	0.3714	0.0410	2.09	2.09
		6	C2	0.3322	0.3724	0.0402	2.05	4.14
		12	C3	0.3381	0.3924	0.0543	2.77	6.91
		20	C4	0.3304	0.3677	0.0373	1.90	8.81
			Tails	0.3266	2.1150	1.7884		
			Total			**1.9612**		

Run 2a

Minerals	Mass (g)	Time (mins)		Fp (g)	Fp+talc (g)	Talc (g)	% Recovery	% Cum. Recovery
talc	2.0002	0					0.00	0.00
plagioclase	3.9516	2	C1	0.3251	0.3751	0.05	2.63	2.63
		6	C2	0.3253	0.358	0.0327	1.72	4.35
		12	C3	0.3240	0.3617	0.0377	1.98	6.33
		20	C4	0.3155	0.3638	0.0483	2.54	8.87
			Tails	0.3161	2.0484	1.7323		
			Total			**1.9010**		

Run 2b

Minerals	Mass (g)	Time (mins)		Fp (g)	Fp+talc (g)	Talc (g)	% Recovery	% Cum. Recovery
talc	2.0003	0					0.00	0.00
plagioclase	3.9517	2	C1	0.3212	0.3783	0.0571	2.98	2.98
		6	C2	0.3219	0.3703	0.0484	2.52	5.50
		12	C3	0.3285	0.3844	0.0559	2.92	8.42
		20	C4	0.3244	0.4087	0.0843	4.40	12.81
			Tails	0.3348	2.0067	1.6719		
			Total			**1.9176**		

Run 3a

Minerals	Mass (g)	Time (mins)		Fp (g)	Fp+talc (g)	Talc (g)	% Recovery	% Cum. Recovery
talc	2.0000	0					0.00	0.00
plagioclase	4.8811	2	C1	0.3239	0.3556	0.0317	1.59	1.59
		6	C2	0.3357	0.3648	0.0291	1.46	3.04
		12	C3	0.3228	0.3663	0.0435	2.18	5.22
		20	C4	0.3309	0.3678	0.0369	1.85	7.07
			Tails	0.3345	2.1906	1.8561		
			Total			**1.9973**		

Run 3b

Minerals	Mass (g)	Time (mins)		Fp (g)	Fp+talc (g)	Talc (g)	% Recovery	% Cum. Recovery
talc	2.0002	0					0.00	0.00
plagioclase	4.8807	2	C1	0.3338	0.4102	0.0764	3.85	3.85
		6	C2	0.3256	0.3953	0.0697	3.51	7.36
		12	C3	0.3263	0.4027	0.0764	3.85	11.22
		20	C4	0.3308	0.4229	0.0921	4.64	15.86
			Tails	0.3306	1.9998	1.6692		
			Total			**1.9838**		

Talc with added pyroxene – 0.25 mg/L guar, pH 9

Run 1a

Minerals	Mass (g)	Time (mins)		Fp (g)	Fp+talc (g)	Talc (g)	% Recovery	% Cum. Recovery
talc	2.0002	0					0.00	0.00
pyroxene	1.5578	2	C1	0.3180	0.3997	0.0817	4.23	4.23
		6	C2	0.3215	0.3793	0.0578	3.00	7.23
		12	C3	0.3261	0.3875	0.0614	3.18	10.41
		20	C4	0.3180	0.3919	0.0739	3.83	14.24
			Tails	0.3194	1.9742	1.6548		
			Total			**1.9296**		

Run 1b

Minerals	Mass (g)	Time (mins)		Fp (g)	Fp+talc (g)	Talc (g)	% Recovery	% Cum. Recovery
talc	2.0001	0					0.00	0.00
pyroxene	1.5582	2	C1	0.3262	0.4647	0.1385	6.99	6.99
		6	C2	0.3183	0.4559	0.1376	6.94	13.93
		12	C3	0.3259	0.4517	0.1258	6.35	20.28
		20	C4	0.3259	0.4531	0.1272	6.42	26.70
			Tails	0.3276	1.7805	1.4529		
			Total			**1.9820**		

Run 2a

Minerals	Mass (g)	Time (mins)		Fp (g)	Fp+talc (g)	Talc (g)	% Recovery	% Cum. Recovery
talc	2.0002	0					0.00	0.00
pyroxene	3.7843	2	C1	0.3348	0.4625	0.1277	6.06	6.06
		6	C2	0.3341	0.4158	0.0817	3.88	9.94
		12	C3	0.3313	0.4848	0.1535	7.29	17.23
		20	C4	0.3309	0.4698	0.1389	6.60	23.83
			Tails	0.3276	1.9317	1.6041		
			Total			**2.1059**		

Run 2b

Minerals	Mass (g)	Time (mins)		Fp (g)	Fp+talc (g)	Talc (g)	% Recovery	% Cum. Recovery
talc	2.0003	0					0.00	0.00
pyroxene	3.7843	2	C1	0.3278	0.4961	0.1683	8.00	8.00
		6	C2	0.3278	0.489	0.1612	7.66	15.66
		12	C3	0.3286	0.5143	0.1857	8.82	24.48
		20	C4	0.3262	0.4474	0.1212	5.76	30.24
			Tails	0.3288	1.7971	1.4683		
			Total			**2.1047**		

Run 3a

Minerals	Mass (g)	Time (mins)		Fp (g)	Fp+talc (g)	Talc (g)	% Recovery	% Cum. Recovery
talc	1.9999	0					0.00	0.00
pyroxene	4.6743	2	C1	0.3313	0.4753	0.144	6.80	6.80
		6	C2	0.3255	0.4604	0.1349	6.37	13.18
		12	C3	0.3292	0.4969	0.1677	7.92	21.10
		20	C4	0.3295	0.4806	0.1511	7.14	28.24
			Tails	0.3307	1.8496	1.5189		
			Total			**2.1166**		

Run 3b

Minerals	Mass (g)	Time (mins)		Fp (g)	Fp+talc (g)	Talc (g)	% Recovery	% Cum. Recovery
talc	2.0001	0					0.00	0.00
pyroxene	4.6746	2	C1	0.3261	0.4694	0.1433	6.97	6.97
		6	C2	0.332	0.4585	0.1265	6.15	13.12
		12	C3	0.3348	0.5885	0.2537	12.34	25.46
		20	C4	0.3279	0.5527	0.2248	10.93	36.39
			Tails	0.3249	1.6331	1.3082		
			Total			**2.0565**		

Talc with added chalcopyrite – 0.25 mg/L guar, pH 9

Run 1a

Minerals	Mass (g)	Time (mins)		Fp (g)	Fp+talc (g)	Talc (g)	% Recovery	% Cum. Recovery
talc	1.9999	0					0.00	0.00
chalcopyrite	1.8809	2	C1	0.3286	0.4132	0.0846	4.40	4.40
		6	C2	0.3296	0.3937	0.0641	3.34	7.74
		12	C3	0.3254	0.4075	0.0821	4.27	12.02
		20	C4	0.3314	0.4385	0.1071	5.58	17.59
			Tails	0.3341	1.9171	1.5830		
			Total			**1.9209**		

Run 1b

Minerals	Mass (g)	Time (mins)		Fp (g)	Fp+talc (g)	Talc (g)	% Recovery	% Cum. Recovery
talc	2.0002	0					0.00	0.00
chalcopyrite	1.8810	2	C1	0.3285	0.4880	0.1595	8.43	8.43
		6	C2	0.3274	0.4911	0.1637	8.65	17.08
		12	C3	0.3288	0.5077	0.1789	9.46	26.54
		20	C4	0.3162	0.4748	0.1586	8.38	34.92
			Tails	0.3195	1.5508	1.2313		
			Total			**1.8920**		

Run 2a

Minerals	Mass (g)	Time (mins)		Fp (g)	Fp+talc (g)	Talc (g)	% Recovery	% Cum. Recovery
talc	2.0003	0					0.00	0.00
chalcopyrite	4.5682	2	C1	0.3258	0.4522	0.1264	6.79	6.79
		6	C2	0.3260	0.584	0.258	13.86	20.66
		12	C3	0.3210	0.4603	0.1393	7.49	28.14
		20	C4	0.3196	0.5308	0.2112	11.35	39.49
			Tails	0.3257	1.4517	1.126		
			Total			**1.8609**		

Run 2b

Minerals	Mass (g)	Time (mins)		Fp (g)	Fp+talc (g)	Talc (g)	% Recovery	% Cum. Recovery
talc	2.0000	0					0.00	0.00
chalcopyrite	4.5682	2	C1	0.3189	0.4385	0.1196	6.19	6.19
		6	C2	0.3244	0.4821	0.1577	8.16	14.36
		12	C3	0.3233	0.4653	0.1420	7.35	21.71
		20	C4	0.3264	0.5144	0.1880	9.73	31.44
			Tails	0.3255	1.6497	1.3242		
			Total			**1.9315**		

Run 3a

Minerals	Mass (g)	Time (mins)		Fp (g)	Fp+talc (g)	Talc (g)	% Recovery	% Cum. Recovery
talc	2.0003	0					0.00	0.00
chalcopyrite	5.6424	2	C1	0.3209	0.5803	0.2594	14.03	14.03
		6	C2	0.3193	0.4469	0.1276	6.90	20.93
		12	C3	0.3278	0.5680	0.2402	12.99	33.92
		20	C4	0.3237	0.5951	0.2714	14.68	48.60
			Tails	0.3191	1.2695	0.9504		
			Total			**1.849**		

Run 3b

Minerals	Mass (g)	Time (mins)		Fp (g)	Fp+talc (g)	Talc (g)	% Recovery	% Cum. Recovery
talc	1.9999	0					0.00	0.00
chalcopyrite	5.6425	2	C1	0.3223	0.5370	0.2147	12.95	12.95
		6	C2	0.3208	0.4552	0.1344	8.11	21.06
		12	C3	0.3301	0.6395	0.3094	18.66	39.72
		20	C4	0.3301	0.3944	0.0643	3.88	43.60
			Tails	0.3310	1.2659	0.9349		
			Total			**1.6577**		

Talc with added talc – 0.25 mg/L guar, pH 9

Run 1a

Minerals	Mass (g)	Time (mins)		Fp (g)	Fp+talc (g)	Talc (g)	% Recovery	% Cum. Recovery
talc	2.0002	0					0.00	0.00
talc	0.1452	2	C1	0.3267	0.3749	0.0482	2.63	2.63
		6	C2	0.3354	0.3811	0.0457	2.49	5.11
		12	C3	0.3200	0.3769	0.0569	3.10	8.21
		20	C4	0.3333	0.4329	0.0996	5.42	13.64
			Tails	0.3289	1.9146	1.5857		
			Total			**1.8361**		

Run 1b

Minerals	Mass (g)	Time (mins)		Fp (g)	Fp+talc (g)	Talc (g)	% Recovery	% Cum. Recovery
		0					0.00	0.00
talc	1.9999	2	C1	0.3260	0.3948	0.0688	3.56	3.56
talc	0.1449	6	C2	0.3279	0.4071	0.0792	4.10	7.65
		12	C3	0.3298	0.4080	0.0782	4.04	11.70
		20	C4	0.3302	0.4528	0.1226	6.34	18.04
			Tails	0.3289	1.9135	1.5846		
			Total			**1.9334**		

Run 2a

Minerals	Mass (g)	Time (mins)		Fp (g)	Fp+talc (g)	Talc (g)	% Recovery	% Cum. Recovery
talc	1.9998	0					0.00	0.00
talc	0.3522	2	C1	0.3276	0.4792	0.1516	7.92	7.92
		6	C2	0.3279	0.4394	0.1115	5.82	13.74
		12	C3	0.3268	0.4261	0.0993	5.19	18.93
		20	C4	0.3302	0.4209	0.0907	4.74	23.67
			Tails	0.3289	1.7902	1.4613		
			Total			**1.9144**		

Run 2b

Minerals	Mass (g)	Time (mins)		Fp (g)	Fp+talc (g)	Talc (g)	% Recovery	% Cum. Recovery
		0					0.00	0.00
talc	2.0001	2	C1	0.3216	0.4312	0.1096	5.53	5.53
talc	0.3521	6	C2	0.3295	0.4331	0.1036	5.23	10.76
		12	C3	0.3383	0.4701	0.1318	6.65	17.41
		20	C4	0.3271	0.4384	0.1113	5.62	23.03
			Tails	0.3200	1.8454	1.5254		
			Total			**1.9817**		

Run 3a

Minerals	Mass (g)	Time (mins)		Fp (g)	Fp+talc (g)	Talc (g)	% Recovery	% Cum. Recovery
talc	1.9999	0					0.00	0.00
talc	0.4349	2	C1	0.3213	0.4262	0.1049	5.52	5.52
		6	C2	0.3271	0.4555	0.1284	6.75	12.27
		12	C3	0.3206	0.4944	0.1738	9.14	21.41
		20	C4	0.3200	0.4647	0.1447	7.61	29.02
			Tails	0.3263	1.6761	1.3498		
			Total			1.9016		

Run 3b

Minerals	Mass (g)	Time (mins)		Fp (g)	Fp+talc (g)	Talc (g)	% Recovery	% Cum. Recovery
		0					0.00	0.00
talc	2.0001	2	C1	0.3173	0.4362	0.1189	6.14	6.14
talc	0.4349	6	C2	0.3273	0.4824	0.1551	8.01	14.14
		12	C3	0.3329	0.5027	0.1698	8.76	22.91
		20	C4	0.3294	0.495	0.1656	8.55	31.45
			Tails	0.3248	1.6528	1.328		
			Total			1.9374		

Talc with no added mineral: 0.25 mg/L CMC, pH 9

Run 1a

Minerals	Mass (g)	Time (mins)		Fp (g)	Fp+talc (g)	Talc (g)	% Recovery	% Cum. Recovery
talc	2.0000	0					0.00	0.00
		2	C1	0.3216	0.3610	0.0394	2.06	2.06
		6	C2	0.3303	0.3736	0.0433	2.27	4.33
		12	C3	0.3216	0.4258	0.1042	5.46	9.79
		20	C4	0.3277	0.3984	0.0707	3.70	13.50
			Tails	0.3292	1.9804	1.6512		
			Total			1.9088		

Run 1b

Minerals	Mass (g)	Time (mins)		Fp (g)	Fp+talc (g)	Talc (g)	% Recovery	% Cum. Recovery
talc	2.0000	0					0.00	0.00
		2	C1	0.3307	0.3694	0.0387	2.02	2.02
		6	C2	0.3288	0.4301	0.1013	5.30	7.32
		12	C3	0.3291	0.4320	0.1029	5.38	12.71
		20	C4	0.3217	0.4295	0.1078	5.64	18.35
			Tails	0.3167	1.8773	1.5606		
			Total			1.9113		

Talc with added chromite: 0.25 mg/L CMC, pH 9

Run 1a

Minerals	Mass (g)	Time (mins)		Fp (g)	Fp+talc (g)	Talc (g)	% Recovery	% Cum. Recovery
talc	1.9999	0					0.00	0.00
chromite	2.3211	2	C1	0.3247	0.3775	0.0528	2.84	2.84
		6	C2	0.3242	0.3408	0.0166	0.89	3.73
		12	C3	0.3289	0.3590	0.0301	1.62	5.35
		20	C4	0.3232	0.3713	0.0481	2.59	7.94
			Tails	0.3323	2.0440	1.7117		
			Total			**1.8593**		

Run 1b

Minerals	Mass (g)	Time (mins)		Fp (g)	Fp+talc (g)	Talc (g)	% Recovery	% Cum. Recovery
talc	2.0000	0					0.00	0.00
chromite	2.3212	2	C1	0.3358	0.4532	0.1174	6.12	6.12
		6	C2	0.3398	0.4402	0.1004	5.23	11.35
		12	C3	0.3300	0.4332	0.1032	5.38	16.73
		20	C4	0.3336	0.4565	0.1229	6.41	23.13
			Tails	0.3319	1.8068	1.4749		
			Total			**1.9188**		

Run 2a

Minerals	Mass (g)	Time (mins)		Fp (g)	Fp+talc (g)	Talc (g)	% Recovery	% Cum. Recovery
talc	1.9998	0					0.00	0.00
chromite	5.6378	2	C1	0.3270	0.4039	0.0769	4.21	4.21
		6	C2	0.3312	0.4402	0.1090	5.97	10.18
		12	C3	0.3288	0.4332	0.1044	5.72	15.90
		20	C4	0.3231	0.4365	0.1134	6.21	22.11
			Tails	0.3185	1.7410	1.4225		
			Total			**1.8262**		

Run 2b

Minerals	Mass (g)	Time (mins)		Fp (g)	Fp+talc (g)	Talc (g)	% Recovery	% Cum. Recovery
talc	2.0001	0					0.00	0.00
chromite	5.6376	2	C1	0.3248	0.4583	0.1335	7.38	7.38
		6	C2	0.3229	0.5203	0.1974	10.92	18.30
		12	C3	0.3247	0.4626	0.1379	7.63	25.92
		20	C4	0.3229	0.4460	0.1231	6.81	32.73
			Tails	0.3175	1.5339	1.2164		
			Total			**1.8083**		

Run 3a

Minerals	Mass (g)	Time (mins)		Fp (g)	Fp+talc (g)	Talc (g)	% Recovery	% Cum. Recovery
talc	2.0001	0					0.00	0.00
chromite	6.9632	2	C1	0.3269	0.4772	0.1503	7.84	7.84
		6	C2	0.3226	0.4902	0.1676	8.74	16.57
		12	C3	0.3249	0.4784	0.1535	8.00	24.58
		20	C4	0.3256	0.5410	0.2154	11.23	35.80
			Tails	0.3341	1.5655	1.2314		
			Total			**1.9182**		

Run 3b

Minerals	Mass (g)	Time (mins)		Fp (g)	Fp+talc (g)	Talc (g)	% Recovery	% Cum. Recovery
talc	2.0001	0					0.00	0.00
chromite	6.9683	2	C1	0.3230	0.5484	0.2254	12.00	12.00
		6	C2	0.3215	0.5233	0.2018	10.74	22.74
		12	C3	0.3232	0.5743	0.2511	13.37	36.11
		20	C4	0.3271	0.4776	0.1505	8.01	44.12
			Tails	0.3265	1.3763	1.0498		
			Total			**1.8786**		

Talc with added plagioclase: 0.25 mg/L CMC, pH 9

Run 1a

Minerals	Mass (g)	Time (mins)		Fp (g)	Fp+talc (g)	Talc (g)	% Recovery	% Cum. Recovery
talc	2.0002	0					0.00	0.00
plagioclase	1.6266	2	C1	0.3286	0.4796	0.1510	7.73	7.73
		6	C2	0.3293	0.4023	0.0730	3.74	11.47
		12	C3	0.3247	0.4092	0.0845	4.33	15.80
		20	C4	0.3285	0.4155	0.0870	4.46	20.26
			Tails	0.3222	1.8790	1.5568		
			Total			**1.9523**		

Run 1b

Minerals	Mass (g)	Time (mins)		Fp (g)	Fp+talc (g)	Talc (g)	% Recovery	% Cum. Recovery
talc	1.9998	0					0.00	0.00
plagioclase	1.6272	2	C1	0.3170	0.5128	0.1958	10.65	10.65
		6	C2	0.3215	0.4773	0.1558	8.48	19.13
		12	C3	0.3209	0.4883	0.1674	9.11	28.23
		20	C4	0.3255	0.4975	0.1720	9.36	37.59
			Tails	0.3245	1.4717	1.1472		
			Total			**1.8382**		

Run 2a

Minerals	Mass (g)	Time (mins)		Fp (g)	Fp+talc (g)	Talc (g)	% Recovery	% Cum. Recovery
talc	2.0003	0					0.00	0.00
plagioclase	3.9516	2	C1	0.3202	0.5282	0.2080	11.15	11.15
		6	C2	0.3262	0.5192	0.1930	10.35	21.50
		12	C3	0.3345	0.5263	0.1918	10.29	31.79
		20	C4	0.3244	0.5456	0.2212	11.86	43.65
			Tails	0.3154	1.3662	1.0508		
			Total			**1.8648**		

Run 2b

Minerals	Mass (g)	Time (mins)		Fp (g)	Fp+talc (g)	Talc (g)	% Recovery	% Cum. Recovery
talc	1.9999	0					0.00	0.00
plagioclase	3.9516	2	C1	0.3445	0.4946	0.1501	8.09	8.09
		6	C2	0.3188	0.4940	0.1752	9.44	17.52
		12	C3	0.3327	0.5323	0.1996	10.75	28.28
		20	C4	0.3369	0.4604	0.1235	6.65	34.93
			Tails	0.3197	1.5277	1.2080		
			Total			**1.8564**		

Run 3a

Minerals	Mass (g)	Time (mins)		Fp (g)	Fp+talc (g)	Talc (g)	% Recovery	% Cum. Recovery
talc	2.0002	0					0.00	0.00
plagioclase	4.8811	2	C1	0.3342	0.5282	0.1940	10.48	10.48
		6	C2	0.3281	0.5192	0.1911	10.32	20.80
		12	C3	0.3251	0.5263	0.2012	10.87	31.67
		20	C4	0.3226	0.5456	0.2230	12.04	43.71
			Tails	0.3240	1.3662	1.0422		
			Total			**1.8515**		

Run 3b

Minerals	Mass (g)	Time (mins)		Fp (g)	Fp+talc (g)	Talc (g)	% Recovery	% Cum. Recovery
talc	2.0002	0					0.00	0.00
plagioclase	4.8805	2	C1	0.3330	0.5166	0.1836	9.76	9.76
		6	C2	0.3200	0.5533	0.2333	12.41	22.17
		12	C3	0.3266	0.6095	0.2829	15.04	37.22
		20	C4	0.3251	0.5925	0.2674	14.22	51.44
			Tails	0.3301	1.2433	0.9132		
			Total			**1.8804**		

Talc with added pyroxene: 0.25 mg/L CMC, pH 9

Run 1a

Minerals	Mass (g)	Time (mins)		Fp (g)	Fp+talc (g)	Talc (g)	% Recovery	% Cum. Recovery
talc	2.0003	0					0.00	0.00
pyroxene	1.1632	2	C1	0.3304	0.4759	0.1455	7.46	7.46
		6	C2	0.3398	0.5466	0.2068	10.60	18.05
		12	C3	0.3357	0.5077	0.1720	8.81	26.87
		20	C4	0.3322	0.5402	0.2080	10.66	37.53
			Tails	0.3335	1.5525	1.2190		
			Total			**1.9513**		

Run 1b

Minerals	Mass (g)	Time (mins)		Fp (g)	Fp+talc (g)	Talc (g)	% Recovery	% Cum. Recovery
talc	2.0003	0					0.00	0.00
pyroxene	1.1633	2	C1	0.3242	0.4858	0.1616	8.50	8.50
		6	C2	0.3337	0.5197	0.1860	9.79	18.29
		12	C3	0.3286	0.4002	0.0716	3.77	22.06
		20	C4	0.3377	0.4289	0.0912	4.80	26.86
			Tails	0.3333	1.7234	1.3901		
			Total			**1.9005**		

Run 2a

Minerals	Mass (g)	Time (mins)		Fp (g)	Fp+talc (g)	Talc (g)	% Recovery	% Cum. Recovery
talc	2.0001	0					0.00	0.00
pyroxene	2.8258	2	C1	0.3304	0.6081	0.2777	14.23	14.23
		6	C2	0.3340	0.5667	0.2327	11.93	26.16
		12	C3	0.3364	0.5225	0.1861	9.54	35.69
		20	C4	0.3342	0.5261	0.1919	9.83	45.53
			Tails	0.3346	1.4863	1.1517		
			Total			**2.0401**		

Run 2b

Minerals	Mass (g)	Time (mins)		Fp (g)	Fp+talc (g)	Talc (g)	% Recovery	% Cum. Recovery
talc	2.0001	0					0.00	0.00
pyroxene	2.8256	2	C1	0.3240	0.4506	0.1266	6.66	6.66
		6	C2	0.3246	0.4783	0.1537	8.09	14.75
		12	C3	0.3242	0.5091	0.1849	9.73	24.48
		20	C4	0.3211	0.4903	0.1692	8.90	33.38
			Tails	0.3250	1.6592	1.3342		
			Total			**1.9686**		

Run 3a

Minerals	Mass (g)	Time (mins)		Fp (g)	Fp+talc (g)	Talc (g)	% Recovery	% Cum. Recovery
talc	2.0003	0					0.00	0.00
pyroxene	3.4901	2	C1	0.3258	0.5297	0.2039	10.44	10.44
		6	C2	0.3339	0.5396	0.2057	10.54	20.98
		12	C3	0.3243	0.5259	0.2016	10.33	31.31
		20	C4	0.3302	0.5124	0.1822	9.33	40.64
			Tails	0.3310	1.4899	1.1589		
			Total			**1.9523**		

Run 3b

Minerals	Mass (g)	Time (mins)		Fp (g)	Fp+talc (g)	Talc (g)	% Recovery	% Cum. Recovery
talc	2.0003	0					0.00	0.00
pyroxene	3.4900	2	C1	0.3245	0.5575	0.2330	11.59	11.59
		6	C2	0.3267	0.5095	0.1828	9.09	20.68
		12	C3	0.3262	0.4901	0.1639	8.15	28.84
		20	C4	0.3216	0.4958	0.1742	8.67	37.50
			Tails	0.3207	1.5770	1.2563		
			Total			**2.0102**		

Talc with added chalcopyrite: 0.25 mg/L CMC, pH 9

Run 1a

Minerals	Mass (g)	Time (mins)		Fp (g)	Fp+talc (g)	Talc (g)	% Recovery	% Cum. Recovery
talc	2.0000	0					0.00	0.00
chalcopyrite	1.8810	2	C1	0.3287	0.4034	0.0747	3.97	3.97
		6	C2	0.3261	0.3875	0.0614	3.27	7.24
		12	C3	0.3291	0.4379	0.1088	5.79	13.03
		20	C4	0.3265	0.4092	0.0827	4.40	17.43
			Tails	0.3373	1.8892	1.5519		
			Total			1.8795		

Run 2a

Minerals	Mass (g)	Time (mins)		Fp (g)	Fp+talc (g)	Talc (g)	% Recovery	% Cum. Recovery
talc	2.0002	0					0.00	0.00
chalcopyrite	4.8682	2	C1	0.3265	0.4657	0.1392	7.14	7.14
		6	C2	0.3213	0.5087	0.1874	9.61	16.75
		12	C3	0.3260	0.5055	0.1795	9.21	25.96
		20	C4	0.3271	0.5064	0.1793	9.20	35.16
			Tails	0.3297	1.5939	1.2642		
			Total			1.9496		

Run 2b

Minerals	Mass (g)	Time (mins)		Fp (g)	Fp+talc (g)	Talc (g)	% Recovery	% Cum. Recovery
talc	2.0001	0					0.00	0.00
chalcopyrite	4.8681	2	C1	0.3305	0.5481	0.2176	11.44	11.44
		6	C2	0.3193	0.4767	0.1574	8.27	19.71
		12	C3	0.3260	0.6654	0.3394	17.84	37.54
		20	C4	0.3271	0.4887	0.1616	8.49	46.04
			Tails	0.3297	1.3565	1.0268		
			Total			1.9028		

Run 3a

Minerals	Mass (g)	Time (mins)		Fp (g)	Fp+talc (g)	Talc (g)	% Recovery	% Cum. Recovery
talc	2.0002	0					0.00	0.00
chalcopyrite	5.6421	2	C1	0.3229	0.4633	0.1404	7.41	7.41
		6	C2	0.3388	0.5017	0.1629	8.60	16.01
		12	C3	0.3277	0.6390	0.3113	16.43	32.44
		20	C4	0.3332	0.4930	0.1598	8.44	40.88
			Tails	0.3406	1.4605	1.1199		
			Total			1.8943		

Run 3b

Minerals	Mass (g)	Time (mins)		Fp (g)	Fp+talc (g)	Talc (g)	% Recovery	% Cum. Recovery
talc	2.0001	0					0.00	0.00
chalcopyrite	5.6424	2	C1	0.3250	0.4581	0.1331	7.57	7.57
		6	C2	0.3282	0.5272	0.1990	11.32	18.88
		12	C3	0.3305	0.5889	0.2584	14.69	33.58
		20	C4	0.3370	0.5349	0.1979	11.25	44.83
			Tails	0.3388	1.3090	0.9702		
			Total			1.7586		

Talc with added talc: 0.25 mg/L CMC, pH 9

Run 1a

Minerals	Mass (g)	Time (mins)		Fp (g)	Fp+talc (g)	Talc (g)	% Recovery	% Cum. Recovery
talc	2.0001	0					0.00	0.00
talc	0.1453	2	C1	0.3251	0.3981	0.073	3.64	3.64
		6	C2	0.3227	0.4497	0.127	6.34	9.98
		12	C3	0.3296	0.4692	0.1396	6.97	16.95
		20	C4	0.3174	0.4283	0.1109	5.54	22.48
			Tails	0.3242	1.8773	1.5531		
			Total			2.0036		

Run 1b

Minerals	Mass (g)	Time (mins)		Fp (g)	Fp+talc (g)	Talc (g)	% Recovery	% Cum. Recovery
talc	2.0002	0					0.00	0.00
talc	0.1452	2	C1	0.3217	0.3981	0.0764	4.09	4.09
		6	C2	0.3197	0.4497	0.13	6.95	11.04
		12	C3	0.3224	0.4692	0.1468	7.85	18.89
		20	C4	0.3255	0.4283	0.1028	5.50	24.39
			Tails	0.3250	1.7387	1.4137		
			Total			1.8697		

Run 2a

Minerals	Mass (g)	Time (mins)		Fp (g)	Fp+talc (g)	Talc (g)	% Recovery	% Cum. Recovery
talc	1.9997	0					0.00	0.00
talc	0.3523	2	C1	0.3300	0.463	0.133	7.26	7.26
		6	C2	0.3266	0.6112	0.2846	15.53	22.79
		12	C3	0.3267	0.5994	0.2727	14.88	37.67
		20	C4	0.3213	0.4645	0.1432	7.81	45.48
			Tails	0.3277	1.3269	0.9992		
			Total			1.8327		

Run 2b

Minerals	Mass (g)	Time (mins)		Fp (g)	Fp+talc (g)	Talc (g)	% Recovery	% Cum. Recovery
talc	2.0002	0					0.00	0.00
talc	0.3522	2	C1	0.3278	0.522	0.1942	9.99	9.99
		6	C2	0.3237	0.6047	0.281	14.45	24.44
		12	C3	0.3264	0.5976	0.2712	13.95	38.39
		20	C4	0.3291	0.5596	0.2305	11.86	50.24
			Tails	0.3256	1.293	0.9674		
			Total			1.9443		

Run 3a

Minerals	Mass (g)	Time (mins)		Fp (g)	Fp+talc (g)	Talc (g)	% Recovery	% Cum. Recovery
talc	2.0001	0					0.00	0.00
talc	0.4352	2	C1	0.3454	0.4922	0.1468	7.78	7.78
		6	C2	0.3444	0.6238	0.2794	14.80	22.58
		12	C3	0.3378	0.6288	0.2910	15.42	37.99
		20	C4	0.3178	0.5953	0.2775	14.70	52.69
			Tails	0.3228	1.2158	0.8930		
			Total			1.8877		

Run 3b

Minerals	Mass (g)	Time (mins)		Fp (g)	Fp+talc (g)	Talc (g)	% Recovery	% Cum. Recovery
talc	2.002	0					0.00	0.00
talc	0.4350	2	C1	0.3366	0.6426	0.3060	17.18	17.18
		6	C2	0.3270	0.6166	0.2896	16.26	33.43
		12	C3	0.3459	0.5150	0.1691	9.49	42.92
		20	C4	0.3390	0.5839	0.2449	13.75	56.67
			Tails	0.3350	1.1070	0.7720		
			Total			1.7816		